

# **Comprehensive study on the synthesis and characterization of bio-based poly(farnesene) using controlled/radical polymerization**

Sharmaine Beatrice Luk

Department of Chemical Engineering

McGill University, Montreal

August 2021

A thesis submitted to McGill University in partial fulfillment of the requirements of the degree  
of Doctorate of Philosophy

© Sharmaine Beatrice Luk 2021

## Abstract

The goal of this doctoral thesis is to understand the polymerization of farnesene (Far) using nitroxide-mediated polymerization (NMP) in several modes of operation (bulk, solution, and aqueous dispersion). The copolymerization of Far with various functionalized methacrylates was investigated to make novel materials that could be used as alternative thermoplastic elastomers (TPEs), processing aids, and impact modifiers. In bulk, Far was statistically copolymerized with an epoxy functionalized methacrylate, glycidyl methacrylate (GMA), and showed that epoxy groups can be incorporated statistically throughout the polymer chain. The tendency to incorporate one monomer versus the other was expressed in their reactivity ratios ( $r_{\text{Far}} = 0.54 \pm 0.04$  and  $r_{\text{GMA}} = 0.24 \pm 0.02$ ). Furthermore, when Dispolreg 007 (D7) was used as the initiator, it possessed a greater ability in maintaining active polymer chain-ends compared to the conventional SG1-based initiator for chain-extension with GMA. In dispersed aqueous media, Far was polymerized by NMP in miniemulsion for the first time, to the best of our knowledge. Stable poly(Far) latex ( $M_n \sim 24$  to  $35 \text{ kg mol}^{-1}$ ) was formed using NMP with particle sizes around 300–400 nm, and successful chain-extension with both styrene and isobornyl methacrylate (iBOMA) indicated active chain-ends despite their high dispersities ( $\mathcal{D} > 2.2$ ). Diblock copolymers were made by solution homopolymerization of ethylene glycol dicyclopentenyl methacrylate (EGDEMA) and copolymerization of EGDEMA and iBOMA using D7, followed by chain-extension with Far. Both poly(EGDEMA-*b*-Far) and poly(EGDEMA-*co*-iBOMA-*b*-Far) successfully underwent thiol-ene clicking chemistry to attach thiol-POSS groups onto the polymer chain. Incorporation of POSS (<10 mol%), as well as copolymerization with iBOMA were shown to extend the linear viscoelastic regions and improve thermal stability. Lastly, high molecular weight poly(myrcene) and poly(Far) ( $M_n$  of 56 and  $62 \text{ kg mol}^{-1}$ , respectively) were synthesized by free radical polymerization. Almost complete hydrogenation of their double bonds was achieved by semi-batch chemical hydrogenation via diimide reduction. After saturation of the poly(dienes), the thermal stability and entanglement of polymer chains were greatly enhanced. Therefore, the work in this thesis shows that Far can be polymerized by NMP in a controlled fashion such that block copolymer synthesis was achieved in bulk, solution, and in emulsion. Furthermore, a wide range of novel materials were made with improved properties by several post-polymerization techniques.

## Résumé

L'objectif de cette thèse de doctorat est d'étudier la polymérisation de Farnésène (Far) en utilisant la polymérisation radicalaire médiée par le nitroxyde (NMP) dans plusieurs modes opératoires (en vrac, en solution et en dispersion aqueuse). La copolymérisation de Far avec divers méthacrylates fonctionnalisés a été étudiée pour préparer de nouveaux matériaux qui pourraient être utilisés comme élastomères thermoplastiques (TPEs) alternatifs, auxiliaires de traitement, et modificateurs d'impact. En vrac, Far a été copolymérisé statistiquement avec un méthacrylate ayant un groupe fonctionnel d'époxy : le méthacrylate de glycidyle (GMA), et a montré que les groupes d'époxy peuvent être incorporés statistiquement tout au long de la chaîne du polymère. La tendance à incorporer un monomère par rapport à l'autre a été exprimée par les rapports de réactivité ( $r_{\text{Far}} = 0.54 \pm 0.04$  and  $r_{\text{GMA}} = 0.24 \pm 0.02$ ). De plus, lorsque Dispolog 007 (D7) a été utilisé comme initiateur, il a montré une plus grande capacité à maintenir des extrémités de chaînes polymériques actives, par rapport à l'initiateur conventionnel à base de SG1, une fois appliqué à l'extension des chaînes avec GMA. En milieu aqueux dispersé, Far a été polymérisé par NMP en miniémulsion pour la première fois à notre connaissance. Un latex poly(Far) stable ( $M_n \sim 24$  à  $35 \text{ kg mol}^{-1}$ ) a été formé à l'aide de NMP avec des tailles de particules d'environ 300 à 400 nm, et une extension de chaîne réussie avec le styrène et le méthacrylate d'isobornyle (iBOMA) a indiqué des extrémités de chaîne actives malgré leur large dispersité ( $\mathcal{D} > 2,2$ ). Des copolymères diblocs ont été synthétisés par la homopolymérisation en solution de méthacrylate de dicyclopentényle d'éthylène glycol (EGDEMA) et la copolymérisation d'EGDEMA et d'iBOMA en utilisant D7 et suivie d'une extension de chaîne avec Far. Le poly(EGDEMA-*b*-Far) et le poly(EGDEMA-*co*-iBOMA-*b*-Far) ont subi avec succès une chimie de clic thiolène pour attacher des groupes de thiol-POSS sur la chaîne polymérique. Il a été démontré que l'incorporation de POSS (<10 mol%) ainsi que la copolymérisation avec iBOMA étendent les régions viscoélastiques linéaires et améliorent la stabilité thermique des polymères. Enfin, le poly(myrcène) et le poly(Far) de larges masses molaires moléculaires moyennes ( $M_n$  de 56 et  $62 \text{ kg mol}^{-1}$ , respectivement) ont été préparés par polymérisation radicalaire. Une hydrogénation presque complète de leurs doubles liaisons a été obtenue par hydrogénation chimique semi-continue via une réduction de diimide. Après saturation des poly(diènes), la stabilité thermique et l'enchevêtrement des chaînes polymériques ont été considérablement améliorés. Par conséquent, les travaux de cette thèse montrent que Far peut être

polymérisé de manière contrôlée à travers la méthode de NMP, de sorte que la synthèse de copolymère séquencé a été réalisée en vrac, en solution et en émulsion. En outre, une large gamme de nouveaux matériaux ont été fabriqués avec des propriétés améliorées par plusieurs techniques de post-polymérisation.

## Nomenclature

Acronym/symbol	Definition
AGET	Activators generated by electron transfer
AIBN	Azobisisobutyronitrile
AMS	$\alpha$ -Methyl- <i>p</i> -methylstyrene
AN	Acrylonitrile
ARGET	Activators regenerated by electron transfer
ATRP	Atom transfer radical polymerization
BD	Butadiene
BPO	Benzyl peroxide
CEF	Chain-end functionality
CRP	Controlled radical polymerization
CTA	Chain transfer agent
D7	Dispolreg 007
DCP	Dicumyl peroxide
DMTA	Dynamic mechanical thermal analysis
DP <sub>n</sub>	Degree of polymerization
DSC	Differential scanning calorimetry
EGDEMA	Ethylene glycol dicyclopentenyl methacrylate
Far	Farnesene
$f_i$	Monomer composition of $i$
$F_i$	Polymer composition of $i$
G'	Storage modulus
G''	Loss modulus
GMA	Glycidyl methacrylate
GPC	Gel permeation chromatography
iBOMA	Isobornyl methacrylate
ICAR	Initiators for continuous activator regeneration
IP	Isoprene

$K_{\text{act}}$	Reversible deactivation equilibrium constant
$k_c$	Recombination rate constant
$k_d$	Dissociation rate constant
$K_{\text{eq}}$	Activation-deactivation equilibrium constant
$k_p$	Propagation rate coefficient
$M_c$	Entanglement molecular weight
MMA	Methyl methacrylate
$M_n$	Number-average molecular weight
$M_{n,\text{target}}$	Target molecular weight
$M_w$	Weight-average molecular weight
MWD	Molecular weight distribution
Myr	Myrcene
NBR	Acrylonitrile butadiene rubber
NHS-BB	Succinimidyl-modified BlocBuilder
NMP	Nitroxide-mediated polymerization
NMR	Nuclear magnetic resonance
PEG-MA	Poly(ethylene glycol) methacrylate
PLA	Poly(lactic acid)
POSS	Polyhedral oligomeric silsesquioxane
PRE	Persistent radical effect
PSA	Pressure sensitive adhesives
QEC	Quasi-equilibrium condition
RAFT	Reversible addition-fragmentation transfer
RDRP	Reversible deactivation radical polymerization
$r_i$	Relative reactivity of monomer $i$
SARA	Supplemental activation reducing agent
SAXS	Small angle X-ray scattering
SBR	Styrene butadiene rubber
SBS	Poly(styrene- <i>b</i> -butadiene- <i>b</i> -styrene)
SET	Single electron transfer
SIS	Poly(styrene- <i>b</i> -isoprene- <i>b</i> -styrene)

SMS	Poly(styrene- <i>b</i> -myrcene- <i>b</i> -styrene)
St	Styrene
$T_{10\%}$	Decomposition temperature at 10 wt% loss
TBA	Tributylamine
$T_{\text{endset}}$	Endset decomposition temperature
$T_g$	Glass transition temperature
TGA	Thermogravimetric analysis
THF	Tetrahydrofuran
$T_{\text{onset}}$	Onset decomposition temperature
TPA	Tripropylamine
TPE	Thermoplastic elastomer
TSH	<i>p</i> -toluene sulfonyl hydrazide
VOC	Volatile organic compound
$X_i$	Conversion of <i>i</i>
$\bar{D}$	Dispersity ( $M_w/M_n$ )
$\tan\delta$	Damping factor ( $G''/G'$ )
$\chi$	Flory-Huggins enthalpic interaction parameter
$\delta_i$	Solubility parameter of monomer <i>i</i>

## Acknowledgements

Firstly, I would like to thank Prof. Milan Maric for his supervision, guidance, and support during my PhD, as he mentored me and gave me room to grow as a researcher and scientist in the last four years. I would also like to thank Dr. Robin Stein from the McGill Chemistry Characterization Facility for running countless NMR samples for me due to limited access during COVID. Also, I would like to thank Petr Fiurasek for his training and guidance in using the DSC and TGA instruments, and Dr. Hatem Titi for his help in running SAXS samples.

To my past and current colleagues in the Maric group, I want to thank you for the scientific discussions and non-scientific conversations in and out of the lab. I would like to thank Dr. Omar Garcia Valdez, a former post-doc and friend, for showing me the basics of nitroxide-mediated polymerization and the synthesis of Dispolreg 007 initiator. I think of our friendship fondly, which began when we attended a conference together in Hamburg, Germany before my PhD. Also, I would like to thank Dr. Adrien Metafiot, another former post-doc and friend, for his guidance and collaboration throughout my PhD. I am especially grateful for my friendship with Georges Younes as he provided constant emotional support and words of encouragement. You have become a confidante and much more than a colleague since we met during our master's degrees at Queen's University. I am also thankful for the friends I made throughout my time at McGill, some of which include Laura, Mike, Kelly, Christina, Matt, Farhad, and Mohammad. I would also like to thank the technical staff, Frank Caporuscio, Lou Cusmich, and Ranjan Roy, for their expertise that allowed me to do my research safely and effectively.

I want to thank my friends, Emily and Victor, who I have known since first year of university, and I am happy we remained friends as we navigate our different paths while living in different cities. I can finally be an adult with a job like you guys! I want to thank Xavier for his unwavering love, support, and words of encouragement. I am excited for our future as this chapter of my life comes to an end. Lastly, I want to thank my parents and brother for their continual support.

## **Contribution to original knowledge**

The study of the polymerization of farnesene using nitroxide-mediated polymerization and conventional radical polymerization is entirely original. The current literature for the synthesis of poly(farnesene) is limited to anionic polymerization and coordinative polymerization, and these studies have only emerged recently in the last four years [1-4]. There is a detailed study on the molecular dynamics of poly(farnesene) and several examples for the potential application of poly(farnesene) as adhesives or polyols (a precursor for polyurethane synthesis) [5-10]. Nitroxide-mediated polymerization of farnesene and its kinetics using conventional SG1-based BlocBuilder and novel Dispolreg 007 initiators in bulk, solution, and emulsion polymerization were investigated and discussed thoroughly for the first time in this doctoral thesis. Homopolymers, statistical copolymers, and block copolymers were synthesized, with a specific emphasis on the copolymerization with functionalized methacrylates (i.e. glycidyl methacrylate, isobornyl methacrylate, ethylene glycol dicyclopentenyl methacrylate) in order to synthesize materials with greater versatility. Furthermore, post-polymerization techniques were done via thiol-ene clicking chemistry and chemical hydrogenation using diimides, which were shown to improve the mechanical, thermal, and rheological properties of these novel polymers.

## Contribution of authors

Professor Milan Maric is a coauthor for every publication/submitted manuscript as the principle investigator, as he conceptualized the idea and advised the progress of research since the beginning. Lorena A. Azevedo, a coauthor on the review paper titled “Reversible Deactivation Radical Polymerization of Bio-based Dienes” published in *Reactive and Functional Polymers*, is a summer student from University of Toulouse who was remotely supervised by Prof. Maric and myself [11]. She helped with the literature search and organization of the review paper for publication. Adrien Metafiot, a former post-doc, along with a summer student from University of Toulouse, Judith Morize, and an undergraduate student, Emmanuel Edeh, are coauthors on the manuscript titled “Hydrogenation of poly(myrcene) and poly(farnesene) using diimide reduction at ambient pressure” submitted to *Journal of Polymer Science*. Adrien Metafiot designed and optimized the hydrogenation of poly(myrcene) with the help of Judith and Emmanuel, who also participated in the execution of the experiments and analysis of data. Based on their experiments, I used the optimized method to hydrogenate poly(farnesene) and acquired thermal and rheological data and wrote the manuscript as first author. I largely executed the studies on the copolymerization and polymerization kinetics of Far and GMA, polymerization of Far in miniemulsion, and block copolymer synthesis of Far and EGDEMA and subsequent thiol-ene clicking on my own.

# Table of Contents

<b>Abstract</b> .....	<b>i</b>
<b>Résumé</b> .....	<b>ii</b>
<b>Nomenclature</b> .....	<b>iv</b>
<b>Acknowledgements</b> .....	<b>vii</b>
<b>Contribution to original knowledge</b> .....	<b>viii</b>
<b>Contribution of authors</b> .....	<b>ix</b>
<b>1 Introduction</b> .....	<b>1</b>
<b>2 Literature review</b> .....	<b>4</b>
2.1 Abstract .....	6
2.2 Introduction .....	6
2.3 Synthesis of bio-based dienes .....	10
2.4 Ionic polymerization of dienes.....	12
2.5 Reversible deactivation radical polymerization of dienes.....	16
2.5.1 Nitroxide-mediated polymerization (NMP) .....	16
2.5.2 Atom transfer radical polymerization (ATRP).....	24
2.5.3 Reversible addition-fragmentation chain-transfer polymerization (RAFT).....	30
2.6 Outlook for bio-based poly(dienes) in real-world applications .....	35
2.7 References .....	38
<b>3 Nitroxide-mediated polymerization of bio-based farnesene with a functionalized methacrylate</b> .....	<b>59</b>
3.1 Abstract .....	60
3.2 Introduction .....	60
3.3 Experimental Section .....	63
3.3.1 Materials .....	63
3.3.2 Synthesis of Poly(Far- <i>stat</i> -GMA) Copolymers.....	64
3.3.3 Chain Extension of Poly(Far- <i>stat</i> -GMA) Macroinitiators .....	64
3.3.4 Synthesis of Poly(Far- <i>b</i> -GMA) Block Copolymers.....	65

3.3.5	Polymer Characterization .....	65
3.4	Results and Discussion.....	67
3.4.1	Statistical Copolymerization of Far/GMA Using NHS-BlocBuilder.....	67
3.4.2	Reactivity Ratios of Far/GMA Statistical Copolymerization.....	71
3.4.3	Chain Extension of Poly(Far- <i>stat</i> -GMA) Copolymers.....	74
3.4.4	Statistical Copolymerization of Far/GMA Using Dispolreg 007 .....	75
3.4.5	Block Copolymers Using NHS-BlocBuilder versus D7 .....	80
3.5	Conclusion.....	84
3.6	References .....	85
<b>4</b>	<b>Polymerization of bio-based farnesene in miniemulsions by nitroxide-mediated polymerization .....</b>	<b>92</b>
4.1	Abstract .....	94
4.2	Introduction .....	94
4.3	Results and discussion.....	97
4.3.1	Comparing surfactant loading in miniemulsions.....	97
4.3.2	Comparing target molecular weights in miniemulsions.....	101
4.3.3	Particle size of miniemulsions.....	103
4.3.4	Compartmentalization versus confined space effects.....	107
4.3.5	Molecular weight distributions of poly(Far) macroinitiators .....	109
4.3.6	All bio-sourced diblock copolymers .....	110
4.4	Conclusions .....	113
4.5	Experimental methods.....	113
4.5.1	Materials.....	113
4.5.2	Homopolymerization of farnesene in miniemulsions.....	114
4.5.3	Chain-extension of poly(Far) macroinitiator.....	114
4.5.4	Polymer characterization.....	115
4.5.5	Particle size characterization .....	115
4.6	References .....	117
<b>5</b>	<b>Farnesene and norbornenyl methacrylate block copolymers: application of thiol-ene clicking to improve thermal and mechanical properties .....</b>	<b>124</b>
5.1	Abstract .....	125

5.2	Introduction .....	125
5.3	Experimental Methods .....	129
5.3.1	Materials .....	129
5.3.2	Synthesis of poly(EGDEMA) or poly(EGDEMA-co-iBOMA) macroinitiator .....	130
5.3.3	Chain-extension of poly(EGDEMA) or poly(EGDEMA-co-iBOMA) with Far .....	131
5.3.4	Thiol-ene clicking of block copolymers with thiol-POSS .....	131
5.3.5	Polymer characterization .....	132
5.3.6	Thermogravimetric analysis and differential scanning calorimetry .....	133
5.3.7	Rheology.....	133
5.4	Results and discussion.....	134
5.4.1	Poly(EGDEMA- <i>b</i> -Far) block copolymers clicked with thiol-POSS.....	134
5.4.2	Poly(EGDEMA- <i>co</i> -iBOMA- <i>b</i> -Far) block copolymers clicked with thiol-POSS .....	138
5.4.3	Thermal stability of block copolymers with and without POSS .....	139
5.4.4	Rheology of block copolymers.....	143
5.4.5	Glass transition temperatures of block copolymers.....	146
5.5	Conclusions .....	153
5.6	References .....	155
<b>6</b>	<b>Hydrogenation of poly(myrcene) and poly(farnesene) using diimide reduction at ambient pressure.....</b>	<b>165</b>
6.1	Abstract .....	166
6.2	Introduction .....	166
6.3	Results and discussion.....	169
6.3.1	Hydrogenation of poly(Myrc) in batch mode .....	169
6.3.2	Hydrogenation of poly(Myrc) in semi-batch mode.....	172
6.3.3	Hydrogenation of poly(Far) in semi-batch mode .....	177
6.3.4	Thermal behaviour of hydrogenated poly(Myrc) and poly(Far).....	181
6.3.5	Rheology of hydrogenated poly(Myrc) and poly(Far).....	184
6.4	Conclusion.....	186
6.5	Experimental Section/Methods .....	187
6.6	References .....	192
<b>7</b>	<b>Conclusions and future work.....</b>	<b>198</b>

<b>8</b>	<b>References.....</b>	<b>200</b>
<b>9</b>	<b>Appendices .....</b>	<b>208</b>
9.1	Appendix A: Supporting Information for “Nitroxide-mediated polymerization of bio-based farnesene with incorporation of functional glycidyl methacrylate” .....	209
9.2	Appendix B: Supporting information for “Polymerization of bio-based farnesene in miniemulsions by nitroxide-mediated polymerization” .....	215
9.3	Appendix C: Supporting information for “Farnesene and norbornenyl methacrylate block copolymers: application of thiol-ene clicking to improve thermal and mechanical properties” .....	221
9.4	Appendix D: Supporting information for “Hydrogenation of poly(myrcene) and poly(farnesene) using diimide reduction at ambient pressure” .....	237

# 1 Introduction

Butadiene (BD) and isoprene (IP) dienes have been polymerized to make rubbery elastomers for many years, especially due to their abundance as olefin byproducts from crude oil cracking [12]. Once polymerized, these soft, rubbery polymers have low glass transition temperatures ( $T_g < \text{room temperature}$ ) and exhibit viscoelastic properties [13]. Like many synthetic materials, they are versatile and their properties are easily adjustable, therefore BD and IP are often copolymerized with other monomers to reinforce mechanical strength. Statistical copolymerization of BD with styrene (St) or acrylonitrile (AN) is done to make styrene butadiene rubber (SBR) or acrylonitrile butadiene rubber (NBR), respectively [14, 15]. Due to the nature of diene monomers, they can be polymerized by 1,4-addition, 1,2-addition, or 3,4-addition, hence a second double bond is available for further modification. For example, poly(BD) can be permanently crosslinked or vulcanized to form thermosets [16]. Conversely, BD and IP can be polymerized by advanced techniques to make block copolymers like poly(styrene-*b*-butadiene-*b*-styrene) (SBS) or poly(styrene-*b*-isoprene-*b*-styrene) (SIS), which are thermoplastic elastomers (TPEs) [17]. These materials are used in many industrial applications such as gaskets, sealants, automobile parts, and disposable gloves [18]. The polymerization and characterization of poly(BD) and poly(IP) homo- and copolymers are also well-studied in literature.

The emergence of bio-sourced monomers like myrcene (Myr) and farnesene (Far) have been shown to have great potential for replacing petroleum-derived monomers like BD and IP. Myr and Far are terpenes (hydrocarbons made of multiple units of isoprene) but also contain diene functionality that is accessible for polymerization. There is some literature on the homo- and copolymerization of Myr using different methods, but literature for Far is fairly limited [1-4, 19-24]. Therefore, there is still much to investigate in terms of the synthesis of poly(Far) and its characterization. Although the study of Myr and Far is attractive and relevant because they are bio-based [25, 26], it is important to note that their synthesis, polymerization, and purification processes may still not be sustainable. The advantages of these novel monomers encompass more than just being sustainably sourced. BD and IP are volatile organic compounds and have to be pressurized in specialized reactors for polymerization. Myr and Far have high boiling points,

therefore they are easily manipulated at ambient pressures, which is an added attribute in terms of green processing. More notably, the long side chains of Myr and Far can have improved viscoelastic properties due to their bottlebrush-like structure, which have been shown to have excellent rheological and viscoelastic properties [27].

This doctoral thesis investigates the synthesis of poly(Far) using predominantly nitroxide-mediated polymerization (NMP) in various mediums. Previous literature of poly(Far) employed anionic polymerization, however, NMP allows for the polymerization of monomers with functionalities, so the copolymerization of Far is not limited to St or AN like conventional SBR/NBR copolymers or SBS/SIS block copolymers. In this thesis, several functional methacrylates were copolymerized with Far to synthesize statistical and block copolymers. They were chosen because poly(methacrylates) have high  $T_g$ s ( $T_g >$  room temperature) [13], which would add mechanical strength, but specific functionalities can also improve polymer compatibility or allow for post-polymerization modification. The motivation for using NMP as opposed to other reversible deactivation radical polymerization (RDRP) techniques will be made apparent in the published review article in Chapter 2. Furthermore, the research findings are comprehensively discussed in the form of two published journal articles and two submitted manuscripts.

The first two journal articles focus on the synthesis of poly(Far) using NMP and understanding the kinetics of polymerizing this novel monomer using different initiators in bulk (Chapter 3) and in aqueous emulsion system (Chapter 4). Statistical copolymerization of Far with glycidyl methacrylate (GMA) showed that epoxy functional groups from GMA can be successfully incorporated throughout a poly(Far) chain. Synthesis of block copolymers showed that poly(Far) made by NMP had active chain-ends for re-initiation, which was done with both GMA and isobornyl methacrylate (iBOMA). The findings from the first two articles provided the optimal conditions for synthesis of block copolymers using Far and ethylene glycol dicyclopentenyl methacrylate (EGDEMA), and their post-polymerization modification via thiol-ene clicking (Chapter 5). In the last submitted manuscript, the post-polymerization modification of poly(My) and poly(Far) synthesized by free radical polymerization was done by chemical hydrogenation at ambient pressures, and efficient and complete hydrogenation was achieved (Chapter 6). In both

post-polymerization modification studies, an improvement in thermal and rheological properties were shown. Therefore, this thesis demonstrates a wide array of polymer materials made with Far using diverse synthesis and functionalization methods. Each chapter is a first look at the specific polymerization methods of Far and its properties and can certainly be further investigated, which will be summarized in Chapter 7.

## 2 Literature review

This chapter includes the literature review, which was published in *Reactive and Functional Polymers* in March 2021 (S.B. Luk, L.A. Azevedo, M. Maric, Reversible deactivation radical polymerization of bio-based dienes. *Reactive and Functional Polymers*. 162 (2021) 104871) [11]. It thoroughly summarizes the current progress in RDRP methods of mainly IP, Myr, and Far, and the methods discussed are nitroxide-mediated polymerization (NMP), atom transfer radical polymerization (ATRP), and reversible addition-fragmentation transfer (RAFT) polymerization. The various methods were compared in terms of their ability to control the rate of polymerization of bio-based dienes and maintain active chain-ends. In ionic polymerization and RDRP, the initiation step occurs simultaneously and only in beginning of the polymerization, therefore all polymer chains should propagate at the same rate and have the same chain length [28,29]. Polymer chain length is characterized by the number-average of the molecular weight distribution ( $M_n$ ), as well as the weight-average molecular weight ( $M_w$ ). Hence, polymerization is considered well-controlled when  $M_n$  increases linearly with conversion and the dispersity ( $\mathcal{D} = M_w/M_n$ ) is equal to one, which indicates a narrow distribution of polymer chains. Additionally, well-controlled polymerizations are suggested by the ability for the polymer chains to be re-initiated and undergo subsequent polymerization, or in other words, polymer chain-ends remain active and chain-end fidelity is maintained.

While conventional radical polymerization is widely used in industry, ionic polymerization and RDRP methods provide concisely controlled molecular architecture of polymer chains, therefore can produce high performance engineered materials. Homopolymers are polymer chains consisting of one monomer, while copolymers are made of two, which can be statistical, gradient, or block in composition [30]. Statistical and gradient copolymers can be synthesized by conventional radical copolymerization, where the comonomers are statistically added onto the polymer chain. If the comonomers have dissimilar reactivities, the polymerization will preferentially incorporate one monomer until its concentration becomes very low, then will eventually incorporate the other monomer, creating polymer chains that are gradient in composition. Due to the ability for polymer chains to be re-initiated using ionic polymerization or RDRP, block copolymers can be synthesized

with blocks of distinct monomer composition [28,29]. Therefore, block copolymers made of polymers of different solubilities can undergo microphase separation in a matrix, but still remain attached in the same polymer chain.

Ultimately, NMP was the RDRP method of choice in this thesis because it was the first RDRP method to successfully synthesize SBS and provided a good alternative to ionic polymerization [31]. Although a known disadvantage of NMP is its inability to homopolymerize methacrylates without controlling comonomer [32], the development of Dispolreg 007 alkoxyamine made it possible [31]. Therefore, it was thought to be suitable for the polymerization of Far and functionalized methacrylates to make block and statistical copolymers. ATRP is very efficient in polymerizing many functionalized vinyl monomers, but it lacked control when it came to polymerization of dienes until very recently [34, 35]. RAFT is also a good method for polymerizing a variety of vinyl monomers including dienes and methacrylates, however polymerization rates are slow and the use of free radical initiators can lead to gel formation, especially at higher temperatures [36, 37]. The review also includes a brief description on the synthesis of these terpene monomers, and some background on ionic polymerization and its disadvantages compared to RDRP. Furthermore, an outlook on the potential applications of these bio-based dienes is discussed as a result of the growing literature on their synthesis via RDRP.

## 2.1 Abstract

Dienes such as isoprene and butadiene have long been used to impart rubbery character into polymeric materials, often by homopolymerization as blends with stiffer polymers or by copolymerization with other monomers. Examples of such products are styrene-butadiene rubber (SBR), acrylonitrile-butadiene rubber (NBR) and the triblock copolymer families such as the various poly(styrene)-*b*-poly(isoprene)-*b*-poly(styrene) (SIS) thermoplastic elastomers (TPEs). Isoprene and butadiene are derived from petroleum-based resources and like other products, emphasis on their production has shifted towards using renewable resources. Consequently, bio-based monomers such as myrcene and farnesene have been targeted as replacements for petroleum-based dienes in polymeric products and have been polymerized to make polymers with controlled microstructures via traditional ionic polymerizations. More recently, alternatives to living polymerization such as reversible deactivation radical polymerization (RDRP) offer the advantages of conventional radical polymerization without the stringent requirements required of living polymerizations. The application of bio-based dienes to RDRP has only recently started to emerge and this review will summarize the current state of applying RDRP to make polymeric materials with controlled microstructure and chain length, as well as an outlook on potential applications of bio-based dienes.

## 2.2 Introduction

Dienes are conjugated hydrocarbons that contain two fixed double bonds (alkenes) and are typically byproducts, along with other olefins like ethylene and propylene, formed from steam cracking of crude oil [1]. These olefins are an integral part of the petrochemical industry as they can easily polymerize due to the double bond and enable production of polymeric materials at a large scale. Butadiene and isoprene are both dienes produced from the steam cracking process and are polymerized to make poly(diene) elastomers with viscoelastic properties and low glass transition temperature ( $T_g$ ),  $-100\text{ }^\circ\text{C}$  and  $-70\text{ }^\circ\text{C}$  for poly(butadiene) and poly(isoprene), respectively [2]. To improve the versatility and mechanical strength of these poly(diene) materials, they are often blended with thermoplastic polymers or copolymerized with styrene or acrylonitrile to make styrene-butadiene rubber (SBR) or nitrile-butadiene rubber (NBR) [3–5]. These added-

value engineered materials make them suitable for automotive parts, disposable gloves, footwear, asphalt modifiers, and sealants [6–9].

While SBR and NBR can be synthesized by conventional radical polymerization [10,11], which is straightforward and inexpensive, triblock copolymers like styrene-butadiene-styrene (SBS) and styrene-isoprene-styrene (SIS) are synthesized by anionic polymerization [12,13]. Living or ionic polymerization proceeds through a propagating site that is ionic in nature – it may be an anion or cation, depending on the initiator used. Employing typically strong bases (e.g. organo-lithium compounds like sec-butyl lithium), which ensure almost instantaneous initiation, and copiously purified reagents and air-free transfers, propagation ensues in a linear fashion (degree of polymerization linear with monomer conversion) without any chain transfer or termination, resulting in “living” polymers [14,15]. Ionic polymerizations can proficiently make polymers with narrow molecular weight distributions and precise microstructure. In fact, SBS, industrially known as Kraton™, is commercially produced by ionic polymerization [16].

However, due to the extremely high reactivity and sensitivity of the ionic groups to impurities, rigorous conditions must be met to achieve the desired polymer microstructure. It was long a goal to combine the control of microstructure obtained by living polymerizations and the simplicity and tolerance to impurities encountered with conventional radical polymerization. This was finally achieved with several landmark publications first reported in the early 1990s and generically referred to as controlled radical polymerization, more accurately termed by IUPAC as reversible deactivation radical polymerization (RDRP) [17]. In contrast to conventional free radical polymerization, concentration of radicals is controlled through a persistent radical effect (PRE), accomplished using reversible termination or chain transfer. Like living polymerizations, monomer can be added to an active propagating radical, approaching the linear degree of polymerization with monomer conversion and low dispersity, along with the ability to make block copolymers, as it would be in truly living polymerizations. Dispersity is much lower generally compared to conventional radical polymerizations but often are not as low as for living polymerizations, due to the inevitable irreversible radical associated reactions that are suppressed but not entirely eliminated.

Recently, great attention has been directed to the concept of sustainable development. The intensive use of non-renewable resources such as oil has a profound impact on the environment. This is an acute problem for the polymer industry as many commodity polymers and plastics are almost entirely based on fossil fuel sources and 4% of the world's consumption of fossil fuels are used for plastics [18,19]. Further, much publicity has focused on the effect on non-degradable plastics in the marine environment. Therefore, much research is increasingly working towards new ways to produce bio-based materials and which are readily biodegradable – this review will focus on the former. Several routes exist to create bio-based polymers. One method involves direct formation of polymers within the producing organisms (e.g. poly(hydroxyalkanoates) from microorganisms, algae, or plants), while others are manufactured from bio-based monomers, such as lactides or bio-based dienes [20,21].

As alluded to earlier, butadiene, isoprene, and styrene have long been used to produce polymers and copolymers with interesting properties such as SBR and natural rubber, which are known for excellent abrasion resistance and better aging characteristics, and consequently are used in tires and in footwear [6,8,22]. It has been found that it is possible to obtain bio-based terpene-derived monomers such as myrcene and farnesene, that are able to produce polymers and copolymers with similar properties to the conventional petroleum-derived polymers. These terpene-based polymers have been shown to have comparable elastomeric properties [23]. Poly(farnesene) exhibits low  $T_g$  ( $-85\text{ }^\circ\text{C}$ ) and has relatively low viscosity but a higher entanglement molecular weight ( $M_e \sim 50,000\text{ g mol}^{-1}$ ) when compared to poly(butadiene) and poly(isoprene) ( $M_e \sim 6000$  and  $13,000\text{ g mol}^{-1}$ , respectively) at the same molecular weight [24]. Poly(farnesene) finds uses in pressure sensitive adhesives, as an optically clear adhesive layer for touch screens on electronic devices, or can be converted to polyols to make polyurethanes [25–28]. Poly(myrcene) similarly has a low  $T_g$  ( $-73\text{ }^\circ\text{C}$ ) also with a comparatively higher entanglement molecular weight ( $M_e = 17,700\text{ g mol}^{-1}$ ), and therefore finds similar applications as adhesives and thermoplastic elastomers [29–33]. However, all these polymers are either synthesized by anionic polymerization or conventional radical polymerization. Alternatively, there have even been some examples of catalytic/coordination polymerization of myrcene and isoprene with high stereoselectivity for 1,4-*cis* or *trans* conformation [34–38].

Current advances have shown that these bio-based poly(diene) materials can be made by RDRP [39–44], which further simplifies the synthesis while still maintaining the precise molecular architecture of block copolymers for their applications. This review will introduce the different methods used currently while focusing particularly on three bio-based dienes: myrcene, farnesene and isoprene (which can be made from sources other petroleum). Specifically, the polymerization of bio-based dienes using the various RDRP methods will be reviewed: nitroxide-mediated polymerization (NMP), atom-transfer radical polymerization (ATRP), and reversible addition-fragmentation chain-transfer polymerization (RAFT) to achieve desirable (co)polymers with the requisite rubbery character. The general mechanisms of RDRP methods focused in this review are shown in Scheme 2-1. But first, the synthesis of the precursors for these materials will be briefly examined.

### Living/anionic polymerization



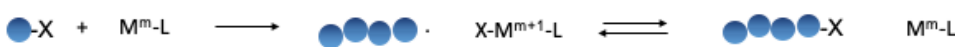
### This review

#### Reversible deactivation radical polymerization (RDRP)

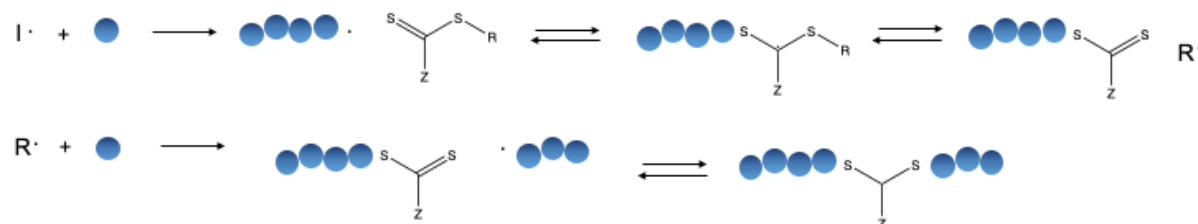
##### Nitroxide-mediated polymerization (NMP)



##### Atom transfer radical polymerization (ATRP)



##### Reversible addition-fragmentation chain-transfer (RAFT) polymerization

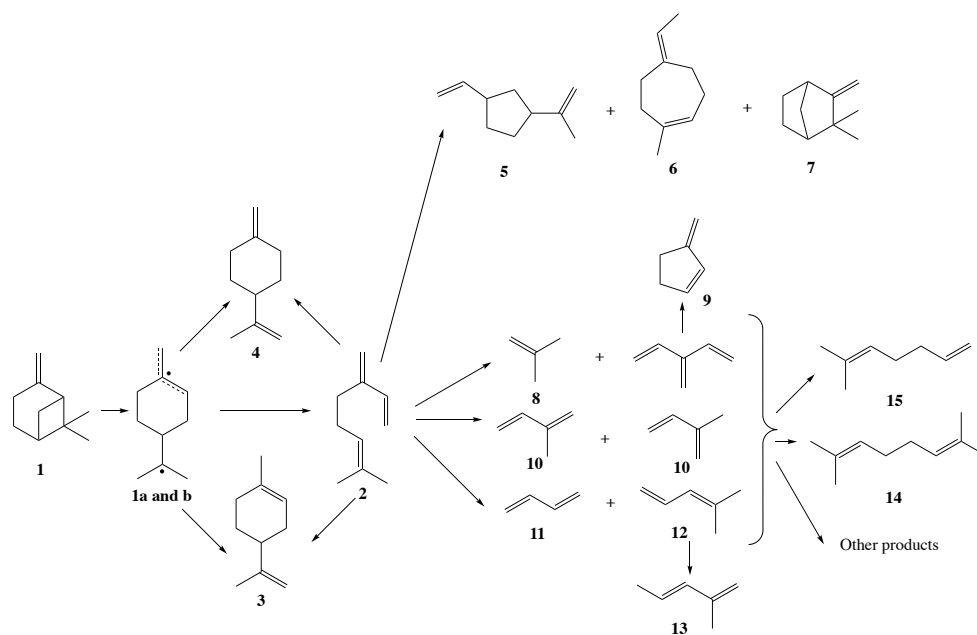


Scheme 2-1. General mechanisms for living/anionic polymerization, and different types of RDRP methods focused in this review (including NMP, ATRP, and RAFT polymerization)

### 2.3 Synthesis of bio-based dienes

Terpenes are hydrocarbons made of isoprene building blocks naturally found in trees, plants, and essential oils, as well as produced by insects as an alarm pheromone [45,46]. Because of their natural odors, they are often used in perfumes, cosmetics, aromatherapy, and food additives. Derivatives of terpenes that have hydroxyl functional groups are terpene alcohols, or terpenoids, that are used as building blocks for other chemicals [47]. For example, pinene is a cyclic terpene that is a major component of pine tree resin, as well as other coniferous trees [48,49], however it can also be made from sugars by using genetically-engineered microorganisms [50].

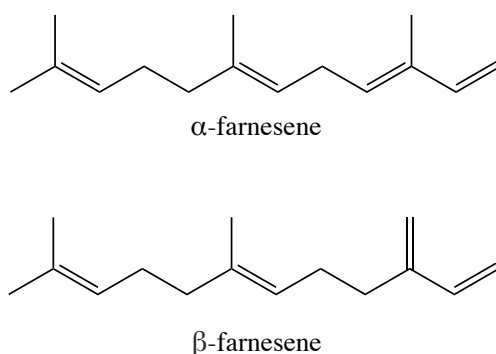
One of the monomers of interest in this review is myrcene and it can be obtained by the pyrolysis of  $\beta$ -pinene [51]. Very high temperatures of 998 K can yield about 85% of myrcene, however it was found that a residence time of  $0.4 \text{ s}^{-1}$  at 743 K was the optimal condition for the highest yield of myrcene [52]. The yield is not 100% due to the isomerization of  $\beta$ -pinene at high temperatures forming byproducts, which include limonene and  $\Psi$ -limonene as seen in Scheme 2-2. Furthermore, decomposition of these products would form smaller alkenes and dienes, including isoprene, another monomer of interest.



Scheme 2-2. Proposed products from the pyrolysis of  $\beta$ -pinene (1) to form isomers myrcene (2), limonene (3), and  $\Psi$ -limonene (4). The possible byproducts from decomposition reactions include 1-ethenyl-3-methylethenylcyclopentane (5), 5-ethylidene-1-methylcycloheptene (6), camphene (7), 2-methyl-1-propene (8), 3-methylenecyclopentene(9), isoprene (10), 4-methyl-1, 3-pen-tadiene (12), 2-methyl-1, 3-pentadiene (13), 2, 7-dimethyl-2, 6-octadiene (14) and 2-methyl-2, 6-heptadiene (15) [51].

Other novel methods of producing myrcene involve terpenoids like geraniol and linalool, that are also naturally found in essential oils [47]. Acid-catalyzed hydration of geraniol can be employed to form myrcene with the highest selectivity being 43.5% after optimizing the concentration of weak acid boron zeolite catalyst, temperature and nitrogen flow [53]. Other terpenoids like farnesol and nerolidol can be found in grapes and wines, along with small amounts of  $\alpha$ -farnesene isomers

[54]. The acid-catalyzed dehydration of both farnesol and nerolidol using  $\text{KHSO}_4$  at  $170\text{ }^\circ\text{C}$  can form trans- $\beta$ -farnesene, another monomer of interest in this review, along with other farnesene isomers (chemical structures are shown in Scheme 2-3) [55]. Base-catalyzed dehydration of farnesol using  $\text{KOH}$  at  $210\text{ }^\circ\text{C}$  gave a slightly higher yield of trans- $\beta$ -farnesene at 65%, which is similar to the catalytic dehydration using activated alumina which gave a yield of 65% as well [56]. Additionally, microbial pathways using genetically modified *Escherichia coli* can be employed to synthesize E- $\beta$ -farnesene (at high selectivity of up to 98% and small amounts of myrcene) and isoprene [57,58].

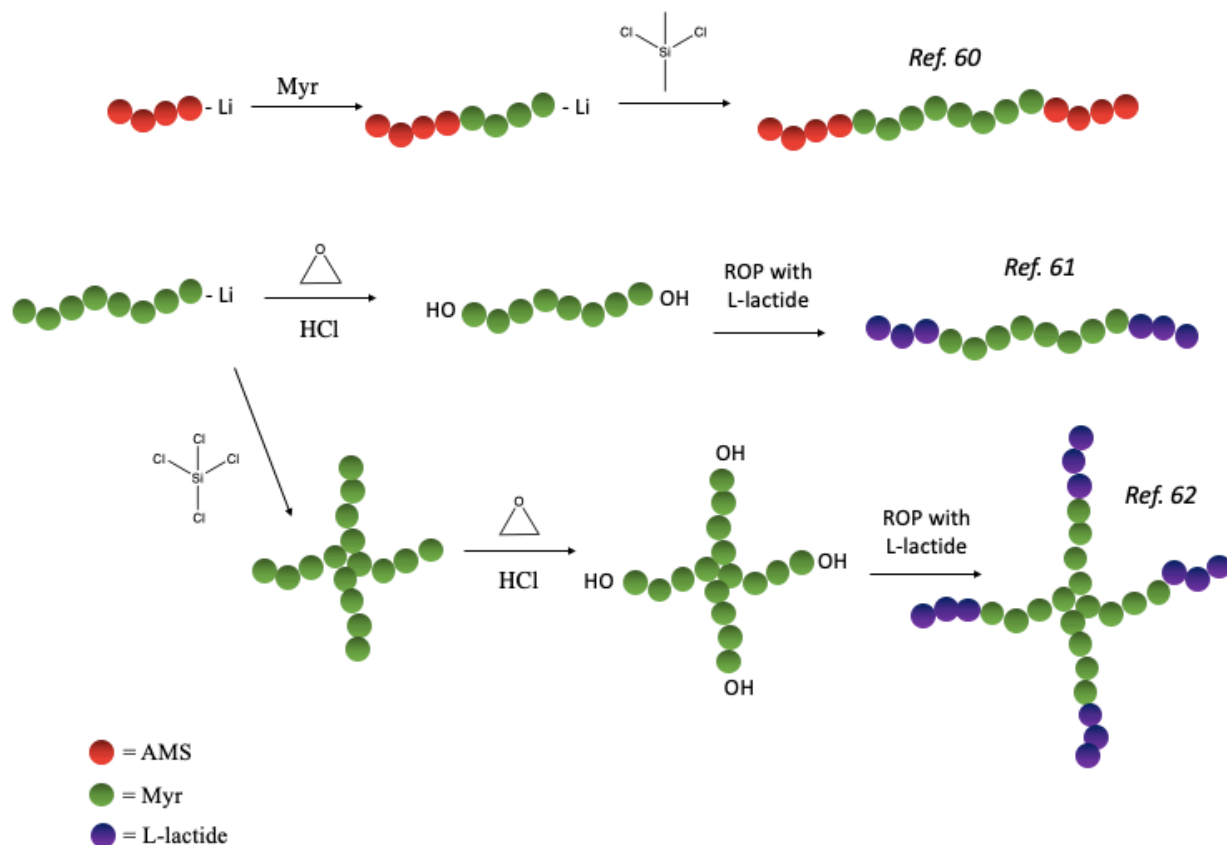


Scheme 2-3. Chemical structure of farnesene isomers.

#### 2.4 Ionic polymerization of dienes

The carbon-carbon double bond of dienes can be polymerized either by free radical, controlled radical and ionic polymerization methods. It is instructive to start this discussion regarding controlled polymerizations by examining ionic polymerizations of bio-based dienes. Recognizing the close similarity in structure to isoprene (IP) and butadiene (BD), myrcene (Myr) and farnesene (Far) were explicitly polymerized by living anionic polymerization using *sec*-butyl lithium (*sec*-BuLi) in cyclohexane at  $60\text{ }^\circ\text{C}$  [59]. However, the molecular weight distribution for poly(Myrcene) was broad ( $M_n = 87,000\text{ g mol}^{-1}$ ,  $M_w = 211,000\text{ g mol}^{-1}$ ) and was far above the expected  $M_n$  of  $46,000\text{ g mol}^{-1}$ . Using both  $^1\text{H}$  and  $^{13}\text{C}$  NMR, it was concluded that both poly(dienes) polymerized predominantly in a 1,4-*cis* configuration.

Later, polymerizations with myrcene proved more informative and successful (Scheme 2-4). Like IP or BD, Myr was targeted as the rubbery mid-block for bio-based thermoplastic elastomers. Instead of styrene (St),  $\alpha$ -methyl-*p*-methylstyrene (AMS) was polymerized as the hard segment using *sec*-BuLi in THF [60]. The resulting PAMS-Li was re-initiated to polymerize myrcene forming PAMS-PMyr-Li, then subsequently coupled using dichloromethylsilane to form PAMS-PMyr-PAMS triblock ABA copolymers. A slightly different approach was done as well by sandwiching the rubbery poly(Myrcene) between hard poly(L-lactide) end blocks [61]. In this case, myrcene was polymerized anionically, then the end group was reacted with ethylene oxide and small amounts of hydrochloric acid such that the poly(Myrcene) midblock was hydroxyl terminated on both ends. This was then used as a macroinitiator for the ring-opening polymerization of L-lactide. Similarly, poly(Myrcene) synthesized using *sec*-BuLi was combined using SiCl<sub>4</sub>, forming star-shaped poly(Myrcene), which was then hydroxylated for ring-opening polymerization of L-lactide. The result was a highly-branched poly(Myrcene)-*grafted*-poly(L-lactide) [62]. Furthermore, anionic polymerization of Myrcene followed by photo-initiated thiol-ene reactions was investigated to produce rubbery polyelectrolyte particles [63].



Scheme 2-4. Schematic of several syntheses of poly(Myrcene) block copolymers via anionic polymerization.

Statistical anionic copolymerization of myrcene with common monomers like IP, St and AMS has also been reported [64]. After co- and terpolymerization using *sec*-BuLi, all polymers achieved high  $M_n$  (up to  $161.5 \text{ kg mol}^{-1}$ ) and low dispersity ( $\mathcal{D} \leq 1.14$ ). The polymerization is therefore well controlled considering narrow molecular weight distribution and linear  $M_n$  versus conversion were obtained. Block-like copolymers were obtained by gradient copolymerization. Two glass transition temperatures were observed for every gradient copolymer, corresponding to the glass transition temperature of the two homopolymers. Noticeable was the steep gradients encountered, due to the disparate reactivity ratios of Myr with St and AMS ( $r_{\text{Myr}} = 36$ ,  $r_{\text{St}} = 0.028$ ;  $r_{\text{Myr}} = 140$ ,  $r_{\text{AMS}} = 0.0074$ ) which essentially allowed for block copolymers. These experiments demonstrate the high potential of the bio-based monomer myrcene for the anionic synthesis of block and gradient copolymers to impart bio-based character into thermoplastic elastomers.

Poly(Far) was prepared anionically in heptanes using n-butyl lithium as the initiator resulting in a wide range of molecular weights (3800 to 367,000 g mol<sup>-1</sup>) with narrow molecular weight distributions ( $\bar{D} = 1.1$  to 1.29) [24]. The polymerization was successfully conducted leading to poly(Far) of primarily 1,4-*cis* addition microstructure with  $T_{gs}$  around  $-73$  °C. At high molecular weights, polymers displayed a transition in the slope of zero shear viscosities ( $\eta_0$ ) from 1.2 to 3.1 at a critical entanglement molecular weight of  $M_e \sim 10^5$  g mol<sup>-1</sup>. This is considerably higher compared to other polydienes like poly(BD) ( $M_e \sim 6000$  g mol<sup>-1</sup>) and poly(IP) ( $M_e \sim 13,000$  g mol<sup>-1</sup>) as a function of weight average molecular weight ( $M_w$ ), indicative of the transition to entangled chain dynamics, which is responsible for high viscosities.

Emulsion cationic polymerization of Myr was done using Lewis acid surface combined complexes (LASC) [65]. The subsequent poly(Myr) present the highest molecular weights ( $M_n > 150,000$  g mol<sup>-1</sup>) ever reported in the cationic polymerization of 1,3-dienes, however very high  $\bar{D}$  (3.7–4.1) was also reported. The high  $\bar{D}$  was an indication quasi-livingness was not achieved, further supported by the plateauing of  $M_n$  versus conversion starting early in the reaction at  $X = 20\%$ . In addition, instantaneous initiation did not occur as there were long induction times of 10–14 h, which was explained by the hydrophobicity of myrcene that required considerable time for the LASC to enter the monomer droplets. Furthermore, short polymer chains were formed on the interface of the droplets and were quickly terminated due to chain-transfer of the polymer chains with water. These short chains stabilized the droplets while polymerization continued inside the droplets forming high molecular weight chains, hence the broad distribution of molecular weight. Nonetheless, linear poly(Myr) chains were formed with mostly 1,4-addition units (almost equal part *cis* and *trans*), and statistical copolymerization of Myr and St was performed as well, but with similar kinetics. Interestingly, the reactivity ratios of Myr and St ( $r_{Myr} = 1.14$  and  $r_{St} = 0.74$ ) were very similar to those obtained from free radical polymerization ( $r_{Myr} = 1.12$  and  $r_{St} = 0.87$ ) [66], but very different from those obtained from anionic polymerization as seen earlier [64].

Thus, ionic polymerizations of bio-based dienes (Far and Myr), like those of conventional dienes (IP and BD), are well-controlled, but this technique encounters some major drawbacks. As seen

with the anionic polymerization of Myr and AMS, crossover polymerization of the PAMS-PMyr-Li chains could not be done due to the ionic nature of the propagating chain, hence these polymer chains had to be coupled to form ABA block copolymers [60]. Emulsion cationic polymerization of Myr was attempted, but presence of water at the interface of the monomer droplets resulted in poor livingness of polymer chains [65]. Additionally, manipulation of IP and BD, being relatively volatile, requires some care when transferring reagents and solvents into the reactors. Therefore, some of these issues can be circumvented through the development of controlled radical polymerization for dienes that are essentially non-volatile, like Myr and Far.

## 2.5 *Reversible deactivation radical polymerization of dienes*

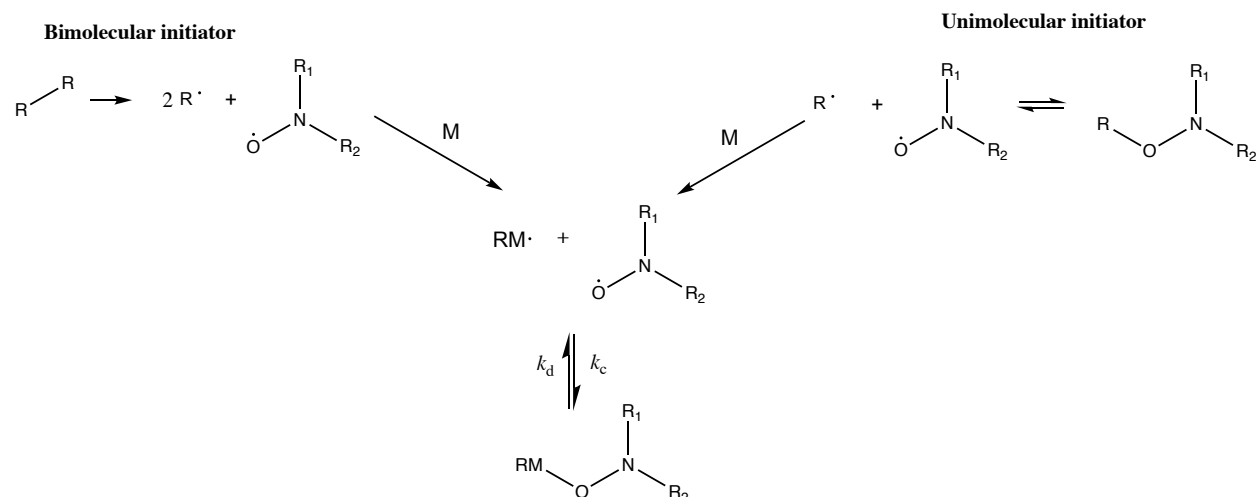
A “living” polymerization can be seen as a chain polymerization that proceeds without the occurrence of chain transfer and termination events, through the establishment of a dynamic equilibrium between active and dormant species [67]. This method opened the door to well-defined polymers with precise and predetermined molar masses, compositions, topologies, and functionalities. Until 30 years ago, living anionic and cationic polymerizations were the only available methods to reach a high degree of structural and compositional homogeneity of polymers. Controlled/living radical polymerization (CLRP) or reversible deactivation radical polymerization (RDRP) techniques enable a high degree of control to be reached [17]. RDRP differs from ionic polymerization by its relative ease-of-use (only dissolved oxygen has to be generally eliminated), the broad range of vinylic monomers which can be polymerized, and the numerous processes that can be implemented (bulk, solution, emulsion, dispersion, etc.) [68]. Among the most well-established methods deriving from this concept are nitroxide-mediated polymerization (NMP), atom-transfer radical polymerization (ATRP), and reversible addition-fragmentation chain transfer (RAFT).

### 2.5.1 Nitroxide-mediated polymerization (NMP)

NMP is often considered the oldest controlled radical polymerization technique [69,70]. Initial polymerizations employed (2,2,6,6-tetramethylpiperidin-1-yl)oxyl (TEMPO) as the persistent radical to mediate the radical concentrations by a reversible termination step due to the low bond dissociation energy of TEMPO [71]. These systems were initiated using a bicomponent pathway

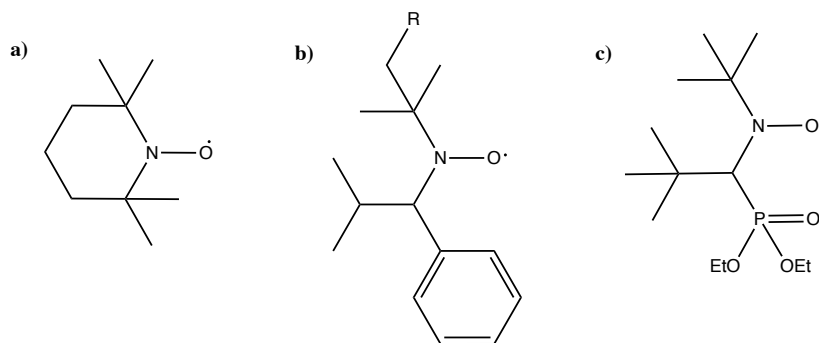
by combining a conventional thermal initiator such as azobisisobutyronitrile (AIBN) or benzoyl peroxide (BPO) with TEMPO. The free radical generated by the thermal initiator would initiate monomer propagation, while the free nitroxide, TEMPO, would deactivate the propagating macroradicals in an activation-deactivation equilibrium ( $K_{eq} = k_d/k_c$ ), where  $k_d$  is the dissociation rate constant and  $k_c$  is recombination rate constant. The equilibrium constant ( $K_{eq}$ ) remains sufficiently low such that the macroradical species are mostly dormant and termination events are suppressed, therefore approaching “living” polymerization kinetics. It was found that a higher TEMPO/BPO ratio of 3.0 led to lower dispersity (1.19) in the NMP of St, but the rate of polymerization was slower due to the excess of free nitroxide [70]. Furthermore, successful NMP synthesis of SBR was shown by chain-extending the poly(St) macroradical with BD, and then again with St to make triblock copolymers [72]. There were some reports of statistical and block copolymers using dienes, but most were limited to copolymerizations with styrene and several vinyl monomers and even crosslinking divinyl monomers [73–76].

Thermal initiators suffer from incomplete efficiency in forming primary radicals and they often undergo rearrangement and fragmentation. Therefore, unimolecular alkoxyamine initiators were developed so that it would dissociate into an initiating radical and a nitroxide at high temperatures, as opposed to a bimolecular system that required both thermal initiator and free nitroxide [77,78]. The initiation mechanisms using unimolecular and bimolecular initiators are shown in Scheme 2-5. It was found that  $\alpha$ -methyl groups were necessary for unimolecular initiators with benzylic derivatives to exhibit good control of polymerization [78]. Unimolecular initiators gave comparable low dispersity and molecular weight polymers to bimolecular systems, however unimolecular initiators were able to maintain good control even at higher degrees of polymerization. Both initiating systems still required high temperatures (120–125 °C) and long reaction times (~20 h) to reach high conversions.



Scheme 2-5. General mechanism for bimolecular and unimolecular initiation in nitroxide-mediated polymerization.  $\text{R}\cdot$  represents the initiating radical formed at high temperature from either the thermal initiator or the unimolecular initiator.  $\text{M}$  represents a single monomer unit that would become initiated by the radical.  $\text{R}_1\text{R}_2\text{NO}\cdot$  is the free nitroxide that would deactivate the propagating radical.

Hence, this led to further development to improve the cleavage of the nitroxide to carbon bond at lower temperatures. It was discovered that larger cyclic rings and acyclic nitroxides had lower bond dissociation energies, specifically referring to another widely used nitroxide, 2,2,5-trimethyl-4-phenyl-3-azahexane-3-oxyl (TIPNO) [79,80]. Soon after, it was found that  $\beta$ -phosphonylated nitroxides afforded stable nitroxides as well, which led to the synthesis of *N-tert*-butyl-*N*-[1-diethylphosphono-(2,2-dimethylpropyl)] nitroxide (SG1-based) initiators and the eventual commercialization of BlocBuilder™ by Arkema [81–83]. The chemical structures of the various commonly used commercially available nitroxides are shown in Scheme 2-6.

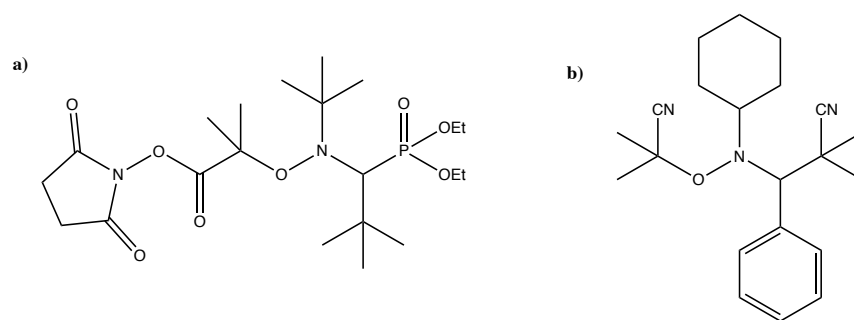


Scheme 2-6. Chemical structures of a) TEMPO, b) TIPNO, and c) SG1-based nitroxides.

Homopolymerization of 1,3-dienes including BD and IP using unimolecular TIPNO showed better control than using TEMPO, where poly(IP) reached an  $M_n$  of  $100,000 \text{ g mol}^{-1}$  and  $\text{Đ} < 1.20$  and poly(BD) had an  $M_n$  of  $5200 \text{ g mol}^{-1}$  and  $\text{Đ} = 1.14$  [84]. Random copolymerization of IP with various styrenic monomers and tert-butyl acrylate (tBA) also showed good control with low  $\text{Đ}$  all below 1.30. Block copolymers made of different monomer compositions such as poly(tBA-*b*-IP-*co*-tBA), poly(St-*b*-IP-*co*-St), and poly(IP-*b*-IP-*co*-St) all had low  $\text{Đ}$  values  $< 1.30$ . Random copolymerizations of IP with 1–10 wt% of glycidyl methacrylate (GMA) were done with unimolecular TIPNO, as well as with bimolecular OH-TEMPO and TIPNO [85]. The bimolecular polymerizations tended to yield higher  $\text{Đ} \sim 2\text{--}3.3$ , but copolymerizations with up to 10 wt% GMA using unimolecular TIPNO still gave reasonable  $\text{Đ}$  of 1.26 and  $M_n = 57,000 \text{ g mol}^{-1}$ . Similarly, NMP of IP was done with several SG1-based alkoxyamines and they showed low  $\text{Đ} \sim 1.10$  at high conversions [86]. Furthermore, difunctional TIPNO alkoxyamine was used to polymerize IP with dimethylacrylamide (DMA) and tBA and successfully synthesized ABA triblock copolymers, poly(IP-*b*-tBA-*b*-IP) and poly(DMA-*b*-IP-*b*-DMA) with  $\text{Đ} < 1.26$  [87].

Nitroxides such as TIPNO and SG1-based initiators were very effective when polymerizing functional monomers like acrylates and acrylamides, and also conventional dienes like BD and IP. However, one drawback of NMP is its inability to homopolymerize methacrylates while maintaining active chain-ends due to steric stability provided by the methacrylate propagating radical and steric hindrance from the bulky SG1-based nitroxide. This leads to a slow rate of recombination ( $k_c$ ) which leads to termination of the macroradicals by disproportionation [88,89]. One way to mitigate this problem is to add a small amount (5–10 mol%) of controlling comonomer

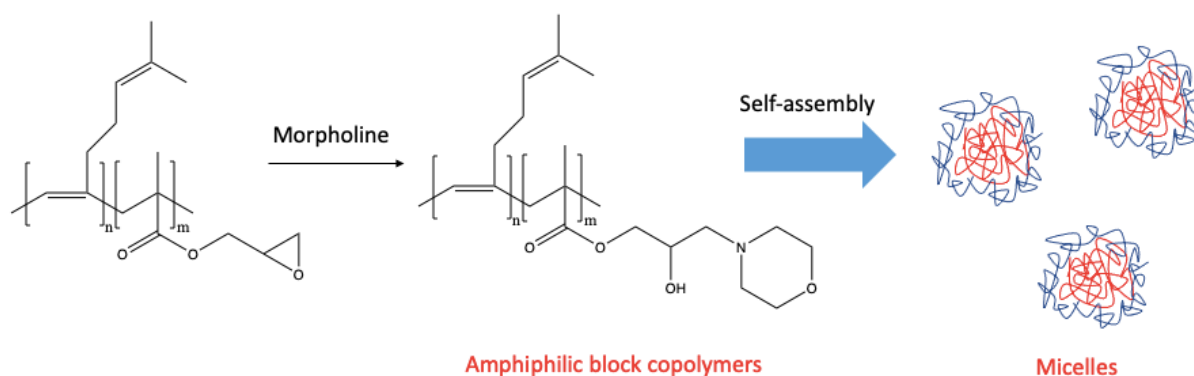
like St, acrylonitrile, or even IP to decrease the overall  $K_{eq}$  and better maintain active chain-ends [84,90–92]. The SG1-based BlocBuilder™ can be modified with a succinimidyl group (NHS-BB) to further improve the polymerization of methacrylates (since it does not rely on additional free nitroxide) but controlling comonomer is still needed [93]. More recently, a new alkoxyamine, Dispolreg 007 (D7), was developed that was able to homopolymerize methacrylates without controlling comonomer and could also be easily synthesized [94–96]. Chemical structures of the succinimidyl ester-modified BlocBuilder and Dispolreg 007 alkoxyamines are shown in Scheme 2-7.



Scheme 2-7. Chemical structures of a) succinimidyl-modified SG1-based BlocBuilder™ and b) Dispolreg 007 alkoxyamines.

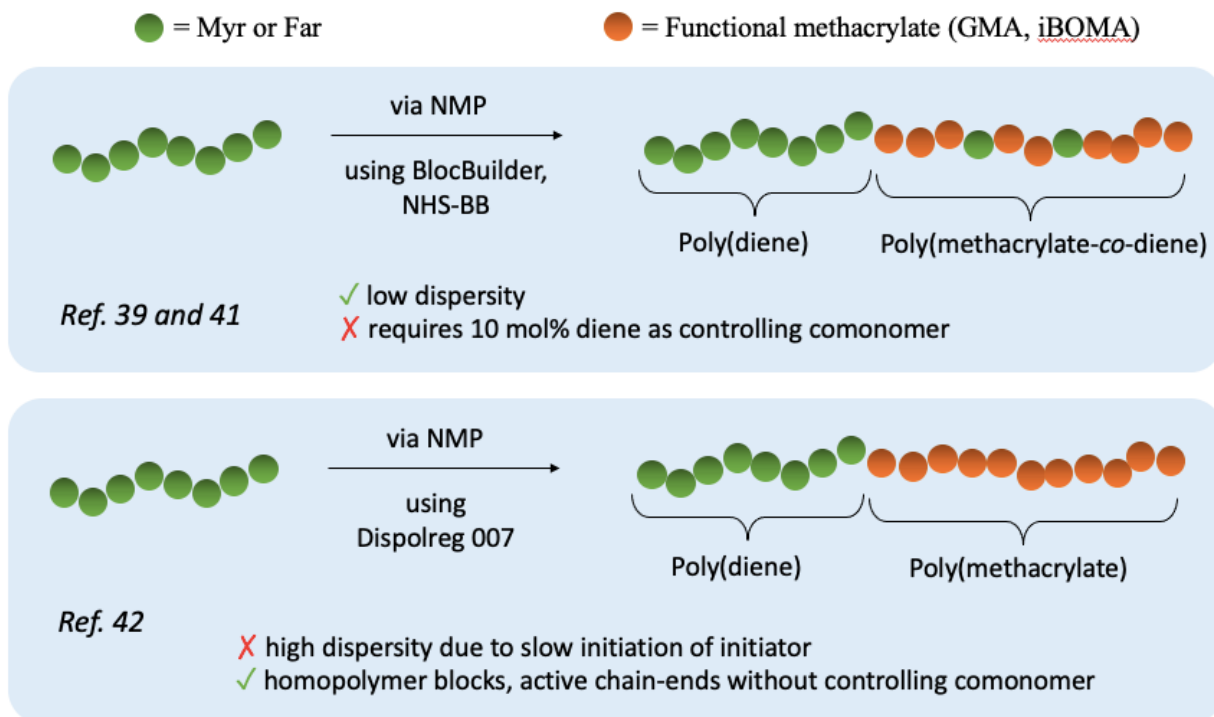
In an effort to synthesize a greener alternative to SBR, Myr was substituted in place of BD to make block and random copolymers with St using SG1-based NHS-BB initiator [40]. For the homopolymerization of Myr, well-defined polymers with  $M_n \sim 15,000 \text{ g mol}^{-1}$  were made with both BlocBuilder and NHS-BB, while NHS-BB resulted in lower  $\bar{D} = 1.26$  (versus  $\bar{D} = 1.45$  using BlocBuilder). Poly(Myrr) made with NHS-BB showed high SG1 chain-end fidelity and were successfully chain-extended with St making poly(Myrr-*b*-St) with two distinct  $T_g$ s of the two respective homopolymers. Statistical copolymerization of Myr and St by NMP gave similar reactivity ratios compared to free radical copolymerization ( $r_{Myr} = 1.88$  and  $r_{St} = 0.25$ ) [66]. Copolymers with high concentration of either Myr or St were successfully chain-extended, as well, with both Myr and St indicating good chain-end fidelity with final  $\bar{D} < 1.60$  [40].

Other examples of block and statistical copolymers with Myr and functional methacrylates like glycidyl methacrylate (GMA) and isobornyl methacrylate (iBOMA) have also been reported [39,41]. Statistical copolymerization of Myr and GMA using NHS-BB showed that at high concentrations of GMA ( $f_{\text{GMA}} < 0.50$ ),  $\bar{D}$  values became greater than 1.45 [39]. However, at low concentrations of GMA, the polymerization was better controlled with final  $\bar{D} \sim 1.30$  which indicates myrcene can also act as a controlling comonomer. The epoxy groups in the GMA block of poly(My**r**-*b*-GMA) (the chain-extension with GMA included 10 mol% of Myr as controlling comonomer) were modified with morpholine groups, and the diblock copolymers became amphiphilic and were able to self-assemble into aggregates in water at 45–65 °C (Scheme 2-8). Similarly, random copolymerization of Myr and iBOMA showed that myrcene could act as a controlling comonomer for NMP of iBOMA [41]. Furthermore, the reactivity ratios for iBOMA and Myr ( $r_{\text{Myr}} = 2.16$  and  $r_{\text{iBOMA}} = 0.07$ ) were quite different resulting in gradient-like copolymers. Poly(My**r**-*grad*-iBOMA), one rich in Myr and one rich in iBOMA, had  $\bar{D}$  of 1.32 and 1.51, respectively, and were chain-extended with Myr and iBOMA/Myr mixture with final  $\bar{D} \sim 1.60$ . Triblock copolymers, poly(iBOMA-*b*-Myr-*b*-iBOMA), were also synthesized using an SG1-terminated dialkoxamine ( $M_n = 51,000 \text{ g mol}^{-1}$  and  $\bar{D} = 1.91$ ) and two distinct  $T_g$ 's were shown at -51 and 181 °C.



Scheme 2-8. Schematic of poly(My**r**-*b*-Myr-*co*-GMA) modified with morpholine groups to make amphiphilic block copolymers that self-assembled into micelles in aqueous solution [39]. The red represents the hydrophobic poly(My**r**) block, and the blue represents the hydrophilic poly(GMA) block modified with morpholine, which acts as the steric stabilizer in aqueous solution.

Likewise, Far was polymerized using NHS-BB and D7 initiators to make block and statistical copolymers with GMA [42]. The reactivity ratios for Far and GMA ( $r_{\text{Far}} = 0.54$  and  $r_{\text{GMA}} = 0.25$ ) were very similar to Myr and GMA ( $r_{\text{Myr}} = 0.49$  and  $r_{\text{GMA}} = 0.50$ ) [39], where both systems resulted in essentially random copolymers. Poly(Far-*co*-GMA) rich in Far made with NHS-BB also showed lower  $\bar{D} = 1.33$  compared to a copolymer rich in GMA ( $\bar{D} = 1.63$ ) at similar  $M_n$  of  $\sim 20,000 \text{ g mol}^{-1}$ . In an equimolar statistical copolymerization of Far and GMA using D7, the resulting  $\bar{D}$  was high  $\sim 2.5$ , which was explained by both the great differences in rate of propagation between Far and GMA and the slow initiation of D7 (therefore not instantaneous initiation, a criteria for RDRP). Despite the homopolymerization of Far using D7 resulting in a high  $\bar{D}$  of 1.60, the chain-ends were still active and chain-extension with GMA was successful. Poly(Far) made with NHS-BB had a  $\bar{D}$  of 1.17, but required 10 mol% of Far as a controlling comonomer when chain-extended with GMA. Nonetheless, poly(Far-*b*-GMA) block copolymers were synthesized using both NHS-BB and D7 initiators. A schematic comparing the synthesis of poly(diene-*b*-methacrylate) block copolymers using SG1-based and D7 initiators is shown in Scheme 2-9.



Scheme 2-9. Schematic of chain-extension of poly(Myr) or poly(Far) with functional methacrylates using SG1-based (BlocBuilder and NHS-BB) and Dispolreg 007 initiators.

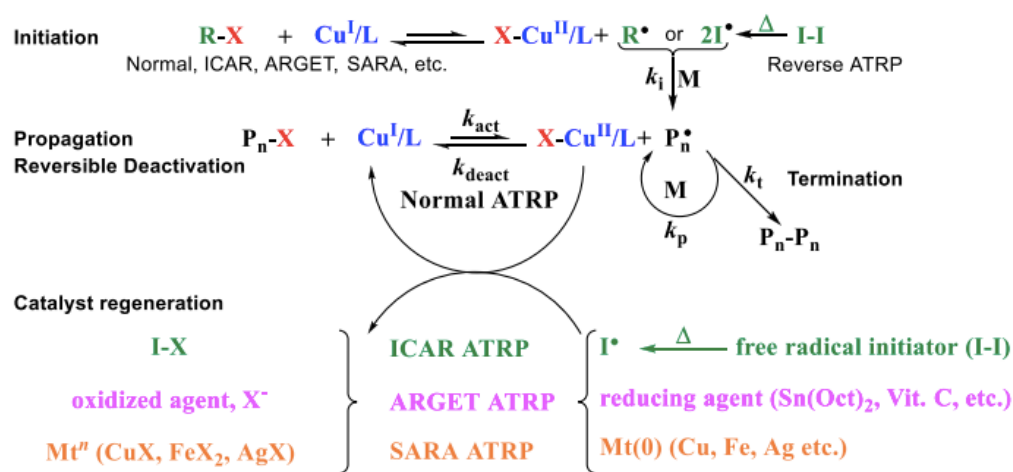
The synthesis of St-IP-St (SIS) copolymers was revisited by using a difunctionalized SG1-based alkoxyamine (PEG-SG12) [97]. The resulting poly(IP) midblocks had high molecular weight with  $M_n = 52\text{--}59 \text{ kg mol}^{-1}$  and  $\mathcal{D} \sim 1.5$ . Furthermore, they were able to be re-initiated after adding St monomer producing poly(St-*b*-IP-*b*-St) triblock copolymers. The polymers with higher composition of St ( $F_{St} = 0.49$ ) showed hard brittle behaviour, while the polymers with  $F_{St} = 0.30$  showed much better elongation and micro-phase separation into cylindrical/lamellar morphologies. The same method was used to produce an analogous poly(iBOMA-*b*-IP-*b*-iBOMA) triblock copolymer, where the chain-extension with iBOMA included 10 mol% of St. The final  $\mathcal{D}$ s of these polymers were lower (1.76) compared to the styrene analogous polymers ( $\mathcal{D} \sim 2.2$ ), and the increased hardness provided by the iBOMA segments improved the toughness and elongation at break of the final polymer.

The versatility of NMP has been shown from its initial conception for SBR synthesis using St and BD to adding functionality and polymerizing bio-based dienes through the development of next-

generation nitroxide initiators. Although  $\bar{D}$  values using NMP are typically higher than those achieved using ionic polymerization, chain-end activity was maintained, and block copolymers were successfully synthesized. Also, triblock copolymers were more efficiently synthesized by using difunctionalized alkoxyamines. The family of diene triblock copolymers has been extended by incorporating functionalized monomers like tBA, dimethylacrylamide [87], and iBOMA [41], the last case demonstrating improved mechanical strength of the material compared to styrene analogs.

### 2.5.2 Atom transfer radical polymerization (ATRP)

ATRP is one of the most efficient synthetic techniques allowing for controlled radical polymerizations with predetermined molecular weights, narrow molecular weight distributions, and high degrees of chain-end functionalities. Like other RDRP methods, ATRP utilizes the persistent radical effect (PRE) [98]. Primary radicals are formed when a transition metal complex ( $M^m-L$ ) abstracts the halogen atom from an alkyl halide ( $R-X$ ) to form an oxidized metal complex ( $X-M^{m+1}-L$ ), which acts as the radical deactivator. The radical  $R\cdot$  reacts with an alkene monomer and propagation proceeds, and termination of the propagating radical is suppressed by the reversible deactivation of  $X-M^{m+1}-L$  in an equilibrium process (characterized by  $K_{act}$ ). The general mechanism for ATRP using a copper metal catalyst is shown in Scheme 2-10. In the early conception of ATRP, several metallic catalysts were studied including ruthenium, copper, and nickel complexes and their ability to polymerize St and methacrylates resulted in low  $\bar{D}$  and linear  $M_n$  versus conversion [99–101].



Scheme 2-10. General mechanism for ATRP using copper as the metal catalyst. Catalyst regeneration mechanisms are included for ICAR, ARGET, and SARA. [143]

Typically, in all types of RDRP, every polymer chain is simultaneously initiated by an initiator, and hence the metal catalyst concentration in the final polymer for ATRP can be very high. As a result, there is discoloration and other negative effects possible with the metallic species, so catalyst removal is essential [102,103]. In order to minimize catalyst concentration to ppm amounts, methods have been developed to regenerate or lower the oxidation state of the metal catalyst such that less than the stoichiometric amount of catalyst is needed. Using activators generated by electron transfer (AGET) or activators regenerated by electron transfer (ARGET) methods, reducing agents are added to continually activate or regenerate the metal catalyst by electron transfer without initiating polymer chains on their own [104]. Some examples of reducing agents include FDA-approved tin(II) 2-hexanoate, ascorbic acid, glucose, silver metal, and hydrazine [105–109]. Another technique is the supplemental activation reducing agent (SARA) or single-electron transfer (SET), where a zero oxidation state metal (i.e. Cu(0) or Fe(0)) is utilized to reduce the activated catalyst concentration [110,111]. The proposed mechanisms for both SARA and SET include the same components and reactions, but differ in which competitive equilibria is responsible for activation and deactivation between oxidation states [112,113]. Alternatively, initiators for continuous activator regeneration (ICAR) employs free radical initiators to continuously reduce the oxidation state of the metal catalyst [114–116]. The different mechanisms for catalyst regeneration are also shown in Scheme 2-10.

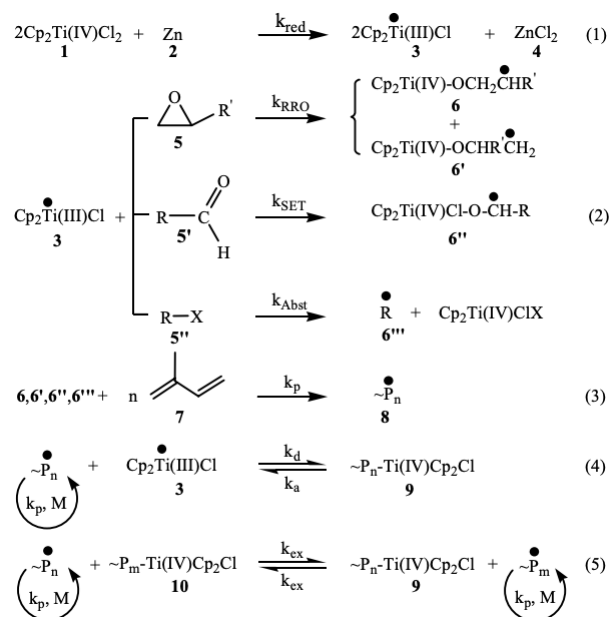
An advantage of using AGET/ARGET reducing agents is that it can also eliminate dissolved oxygen in the medium, so polymerizations can be done with a limited concentration of air [104–106]. As with most metal reducing agents, they can partake in competitive complexation with ligands, monomer, and polymer, or substitution/elimination of the halide chain-ends causing irreversible termination and poor livingness of polymer chains [117–119]. Therefore, it is common to add excess ligands in order to limit the complexation of monomer/solvent/reducing agent with the catalyst. As with the addition of free radical initiators, there will be a small portion of polymer chains that are initiated by free radicals, hence the rate of addition has to be slow in order to avoid rapid polymerization and loss of control [114,120].

ATRP has proven to be very effective in polymerizing vinylic monomers like St and (meth)acrylates using different catalyst regeneration techniques and in synthesizing various topologies including star, graft, and highly branched polymers [121]. However, ATRP of dienes using copper catalysts remains a challenge and it was believed to be due to the coordination of dienes to CuX, which is not observed with monomers like methyl (meth)acrylates or styrene [122–124]. Later on, it was discovered that the diene-copper complexes (i.e. BD and IP) were actually not very stable at common polymerization temperatures, especially compared to strong coordinating ligands like amines or phosphines [125–127]. In fact, it is the low bond dissociation energy of the poly(diene)-halide (PD-X) that leads to fast activation and slow deactivation of the propagating radical, and therefore loss of halide chain-end functionality (CEF) and loss of control [122].

Furthermore, polymerization temperatures are kept relatively low as BD and IP have low boiling points in addition to slow rates of propagation ( $k_p$ ) compared to methacrylates and St, both of which aid in loss of CEF [121]. The slow polymerization rate and slow deactivation of the propagating radical also lead to side reactions such as quaternization of diene with metal catalyst and Diels-Alder dimerization [128–131]. Indeed, in an attempt to polymerize isoprene using CuBr catalyst with *tris*-[2-(dimethylamino)ethyl] amine ligands (CuBr/Me<sub>6</sub>TREN) initiated by ethyl bromopropionate in bulk, very low yields <5% were obtained [132]. The lack of polymerization was mainly attributed to low solubility of CuBr/Me<sub>6</sub>TREN in the non-polar monomer, therefore methyl ethyl ketone was used as a solvent (up to 40 vol%) but yield did not improve. Some

progress was made in the ATRP of IP using copper halide and nitrogenous ligands (bipyridine and dinonyl bipyridine) due to a much lower rate of catalyst activity ( $k_{act}$ ) [133]. Much higher temperatures were used (100 °C, 130 °C, and 150 °C) to compensate for the low rate of propagation. As a result, low molecular weight poly(IP)s were synthesized ( $M_n < 10,000 \text{ g mol}^{-1}$ ) but high conversions were achieved ( $X = 88.8\%$  at 150 °C).

It was clear that conventional copper catalysts such as CuBr/Me6TREN was not sufficient in controlling the polymerization of dienes. The choice of metal catalyst, ligands, alkyl halide, temperature, reagent ratios, and ATRP method are all important factors to consider. There has been some success with the polymerization of IP using Ti-based catalysts (Cp<sub>2</sub>TiCl-catalyst). Titanocene dichloride, Cp<sub>2</sub>Ti(IV)Cl<sub>2</sub>, is often used in epoxide ring opening reactions, aldehyde reduction, and halide abstraction [134,135]. Cp<sub>2</sub>Ti(IV)Cl<sub>2</sub> is first reduced by Zn and undergoes radical ring opening, single electron transfer reduction, and halide abstraction with epoxides, aldehydes, and halides, respectively, to initiate CRP of IP (Scheme 2-11) [136–138]. It seemed the key to obtaining low Đ values was ensuring fast initiation by adding the initiator (e.g. epoxide, aldehyde, or halide) after most of the Cp<sub>2</sub>Ti(IV)Cl<sub>2</sub> had been reduced and having an excess of Ti to initiator. Aldehyde-initiated polymerizations of IP gave reasonable Đ values of 1.4–1.5 compared to epoxy-initiated polymerizations, and 110 °C was the optimal temperature compared to 90 or 130 °C [136]. However,  $M_n$  was typically low, being  $<10,000 \text{ g mol}^{-1}$ . Statistical and block copolymers of St and IP synthesized using Cp<sub>2</sub>TiCl-catalyst and epoxy initiator were reported, as well, but final polymer characteristics and synthesis of block copolymers were unclear [139].



Scheme 2-11. Cp<sub>2</sub>TiCl (3) initiated controlled radical polymerization of isoprene (7) using epoxides (5), aldehydes (5'), alkyl halides (5'') [138].

Some recent studies reported ATRP of BD using less conventional metal complexes like molybdenum, iron, nickel, palladium, and platinum [140–142]. One report used 1-octanol substituted MoCl<sub>5</sub> metal catalyst with triphenyl phosphine (PPh<sub>3</sub>) ligands to polymerize BD [140]. Although high conversions were achieved ( $X \sim 60\%$ ),  $\bar{D}$  remained at 1.7 throughout the reaction, which was attributed to the slow establishment of the equilibrium between active propagating radicals and dormant species using MoCl<sub>3</sub>(1-octanol)<sub>2</sub> catalyst.

Another study used iron metal complexed with a large series of ligands including carbon, nitrogen, halide, oxygen, and phosphorus-supported ligands [141]. It ultimately reported that one phosphorus-supported ligand, P[Ph(OMe)<sub>3</sub>]<sub>3</sub>, was far superior in controlling the polymerization of BD, and FeCl<sub>2</sub> and FeCl<sub>3</sub> provided much more stable PBD-X chain-ends and better deactivators than FeBr<sub>2</sub> and FeBr<sub>3</sub>. Furthermore, ICAR and photo-initiated ATRP using FeCl<sub>3</sub>/ P[Ph(OMe)<sub>3</sub>]<sub>3</sub> significantly increased the rate of polymerization compared to normal ATRP, where the rate of photo-initiated ATRP was 10 times that of normal ATRP and higher conversion ( $X = 70\%$  vs. 50%) and chain-end functionality (CEF = 0.9 vs. 0.65) were achieved.

Comparing between Ni, Pd, and Pt metal complexes and the effect of ligands initiated with bromoesters, it was found that ICAR-ATRP of BD using  $(\text{PPh}_3)\text{Ni}(\text{CO})_2$  and  $(\text{PPh}_3)\text{NiCl}_2$  resulted in better initiator efficiency, Br chain-end functionality, and higher conversion [142]. With the exception of Mo metal complex, phosphine-supported ligands seemed to be the most suitable for ATRP of BD as they were nucleophilic enough to reduce the metal catalyst but not too much that they would quaternize with PBD-X and lower CEF. Unlike the previous example of ATRP of IP [132], a non-polar solvent like toluene aided in the solubility of the metal catalyst in order to facilitate controlled polymerization.

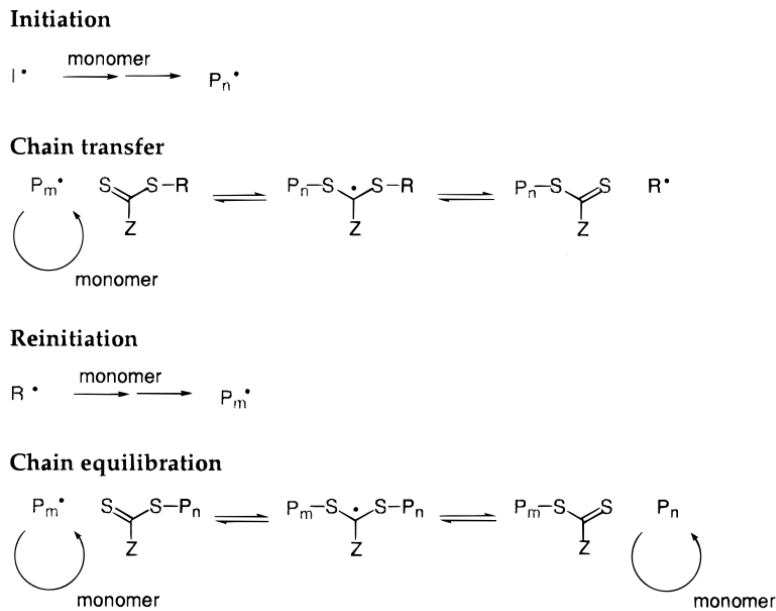
Moving towards conventional Cu-mediated ATRP of BD in the most recent study, similar conditions were found to lead to successful controlled polymerizations [143]. Tertiary bromoester (as opposed to benzyl) initiators combined with low nucleophilicity ligands and non-polar solvents resulted in poly(BD) with a wide range of  $M_n$  values (1000–100,000  $\text{g mol}^{-1}$ ) and low  $\text{Đ}$  of 1.2–1.5. Furthermore, ICAR-ATRP proved to be much more efficient at increasing the rate of polymerization and minimizing side reactions compared to normal, SARA, and ARGET ATRP. Triblock ABA copolymers were synthesized with St and MMA making poly(BD-*b*-St-*b*-BD) and poly(MMA-*b*-BD-*b*-MMA). Initially, a poly(St) midblock was made with a difunctional alkyl bromide initiator in normal ATRP, as St would make a more reactive propagating radical. Br-poly(St)-Br was then chain-extended with BD and the final CEF of the triblock polymer was ~40%. Therefore, poly(BD)-Br was shown to have a high enough CEF for subsequent chain-extension. A poly(BD) midblock was then synthesized with a CEF of ~90% and was successfully chain-extended with MMA with the final CEF being >50%. However, relatively short polymer chains were achieved for both triblock copolymers.  $M_n$  for poly(St) was 2000  $\text{g mol}^{-1}$  and increased to 13,000  $\text{g mol}^{-1}$  after chain-extension with BD, and  $M_n$  for poly(BD) was 4600  $\text{g mol}^{-1}$  and increased to 11,700  $\text{g mol}^{-1}$  after chain-extension with MMA.

Since successful studies for ATRP of BD were only very recently reported, it is understandable no reports of ATRP of bio-based dienes like Myr and Far were found. Even with studies of ATRP of BD using Mo, Fe, and Ni metal complexes, multi-block copolymers were not synthesized [140–142]. Triblock ABA copolymers were only reported in the latest Cu-mediated ATRP of BD [143]. By optimizing the selection of ligands, initiator, solvent, and metal catalyst, the control of ATRP

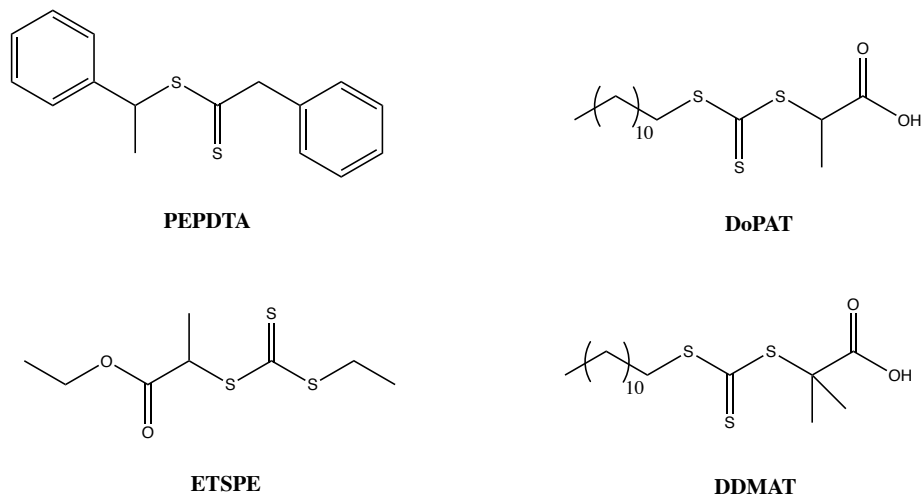
of dienes has improved greatly. This is hopeful for possible future studies for ATRP of Myr and Far, as both bio-based dienes have higher boiling points compared to IP and BD. Therefore, polymerization temperatures can be increased to further increase rate of initiation and rate of polymerization with hopefully an ability to minimize side reactions.

### 2.5.3 Reversible addition-fragmentation chain-transfer polymerization (RAFT)

The emergence of RAFT came shortly after NMP and ATRP, and is viewed as the most versatile among RDRP techniques [144]. Where NMP shows lack of control for polymerization of methacrylates and ATRP for dienes, RAFT is able to polymerize a diverse group of vinylic monomers including St, (meth)acrylates, and dienes [145–147]. The mechanism for RAFT differs slightly from NMP and ATRP and employs chain transfer agents (CTA) that reversibly react with propagating radicals instead of using radical deactivators. The CTA is often a dithioester with *Z* and *R* substituent groups. Polymerization begins with free radical initiation using common thermal initiators, which begins propagation of a polymer chain ( $P_n\cdot$ ). The CTA reversibly adds onto the propagating radical and subsequently through chain transfer would release the initiating radical  $R\cdot$ . The initiating radical would initiate propagation as well, forming another propagating polymer chain ( $P_m\cdot$ ). Finally, in the chain equilibration step, the CTA reversibly transfers between the two propagating polymer chains ( $P_n\cdot$  and  $P_m\cdot$ ) and irreversible termination is suppressed. The RAFT polymerization mechanism is shown in Scheme 2-12, along with chemical structures of common RAFT CTAs in Scheme 2-13.



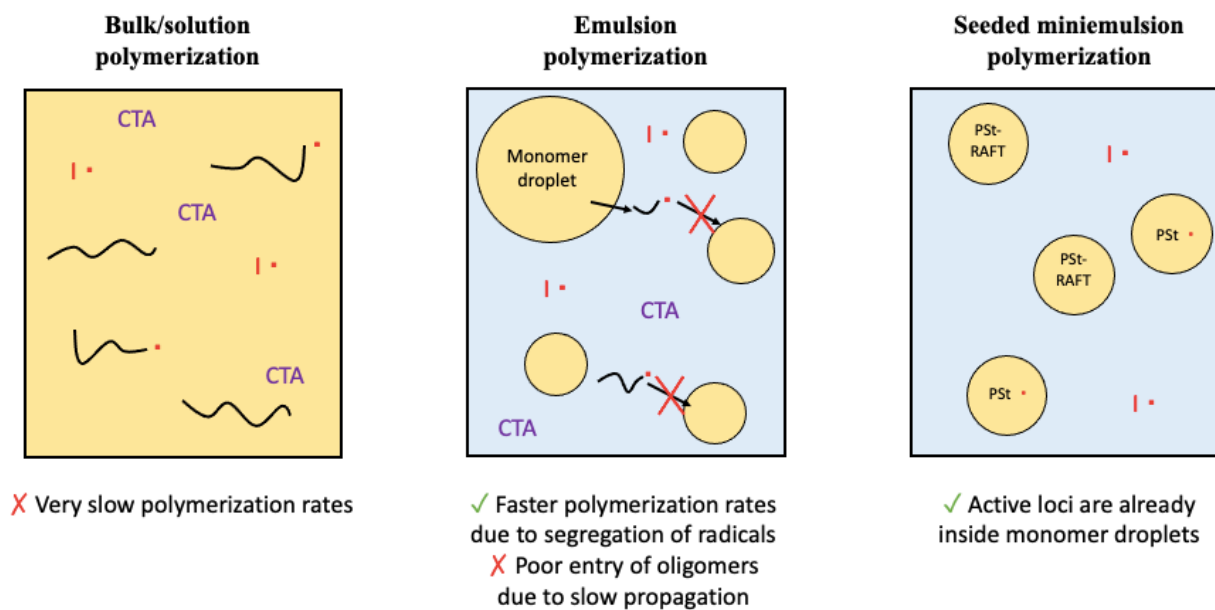
Scheme 2-12. General polymerization mechanism for RAFT using dithioester chain transfer agent [141].



Scheme 2-13. Chemical structures of common RAFT CTAs discussed in this review.

Early RAFT polymerizations of BD were mostly done in dispersed aqueous media as solution or bulk polymerizations yielded very slow rates (Scheme 2-14) [148,149]. Emulsion polymerization *ab initio* was employed in order to utilize compartmentalization effects (i.e. segregation of radicals such that every particle has either one or zero radicals) to increase polymerization rate. However, in conventional emulsion, the chain-extension of poly(St) using RAFT with BD was unsuccessful,

as the  $k_p$  of BD is very low and was unable to form hydrophobic oligomers in the aqueous phase to enter particles [148]. However, seeded miniemulsion showed much better success using 1-phenylethyl phenyl dithioacetate (PEPDTA), potassium persulfate (KPS) initiator, and SDS surfactant at 70 °C [149]. BD was added to the PSt-RAFT seed latex and continued to polymerize at 70 °C. Although gelation started to occur after 20% conversion of butadiene, poly(St-*b*-St-*co*-BD) copolymers were synthesized with varying compositions of BD ( $F_{BD} = 0.37$  to 0.92) and relatively low  $\bar{D}$  from 1.20–1.58. This work was expanded to synthesize triblock SBS copolymers by purging away BD and adding St again to make the third poly(St) block, although final  $\bar{D}$  were quite high ( $>2.2$ ) [150]. Another industrially relevant material, BD and acrylonitrile copolymer (NBR), was also successfully attained using RAFT in emulsion ab initio [151]. Polymerizations were done with 2-(((dodecylsulfanyl)carbonothioyl)sulfanyl)propanoic acid (DoPAT) and KPS, and showed good control up to 55% with  $M_n = 20,400 \text{ g mol}^{-1}$  and  $\bar{D} = 1.6$ . NBR copolymers were successfully chain-extended with St, as well, after re-initiation using AIBN.



Scheme 2-14. Schematic of RAFT polymerization of bio-based dienes in bulk/solution, conventional emulsion, and in seeded miniemulsion.

Following the success of RAFT polymerization of BD, there have been a few reports of RAFT polymerization of IP as well. One report used the RAFT CTA, 2-ethylsulfanylthiocarbonyl-

sulfanylpropionic acid ethyl ester (ETSPE) combined with thermal initiator dicumyl peroxide (DCP) for the polymerization of IP [152]. The optimal temperature of 115 °C was chosen to maintain reasonable polymerization rates without loss of control. Block copolymers were made by first synthesizing poly(St) and poly(tBA) via RAFT, then chain-extended with isoprene making poly(St-*b*-IP) with final  $M_n = 44,300 \text{ g mol}^{-1}$  and  $\bar{D} = 1.19$  and poly(tBA-*b*-IP) with final  $M_n = 21,500 \text{ g mol}^{-1}$  and  $\bar{D} = 1.20$ . Similarly, RAFT polymerization of IP was done using *S*-1-dodecyl-*S'*-(*r,r'*-dimethyl-*r''*-acetic acid)trithiocarbonate (DDMAT) and *t*-butyl peroxide at 125 °C [153]. Control of polymerization was shown by linear  $M_n$  versus conversion, and CTA-chain end was maintained by successful chain-extension of poly(IP) with St (final  $M_n = 15,600 \text{ g mol}^{-1}$  and  $\bar{D} = 1.28$ ). In both cases, increased thermal initiator helped to increase polymerization rate, as well as lower  $\bar{D}$ . These polymerizations were both done in bulk, and similar to BD, polymerization rates were very slow, where reaction times were at least 20 h.

Emulsion polymerization of IP using RAFT was also studied and much faster rates were achieved due to compartmentalization. In the same study that investigated ab initio emulsion polymerization of BD, IP was also added to poly(St) in emulsion [148]. Unlike the BD in emulsion, there was some St monomer left in the emulsion such that the  $k_p$  of copolymerization was increased to form oligomers that would eventually enter particles to continue polymerization. At the time of the study, there was no  $k_p$  data of IP and the authors speculated slow polymerization according to  $k_p$  of BD, and indeed  $k_p$  of IP is comparable and even lower than BD ( $k_{p,BD} = 135 \text{ L mol}^{-1} \text{ s}^{-1}$  and  $k_{p,IP} = 99 \text{ L mol}^{-1} \text{ s}^{-1}$  at 50 °C) [154,155]. However, the resulting copolymers included insoluble, crosslinked material. Seeded emulsion was done, where poly(St) particles were swollen with IP monomer before polymerization began. After 2 h of reaction, poly(AA<sub>10</sub>-St<sub>40</sub>-IP<sub>80</sub>) was synthesized reaching  $X = 58\%$  and showed two distinct  $T_g$ 's [148]. Poly(acrylic acid) (poly(AA)<sub>10</sub>) was the hydrophilic stabilizing block in the emulsion.

RAFT polymerization was then successfully applied to Myr. In a study also using ETSPE and AIBN, similar poly(My-*b*-St) block copolymers were made, where chain-extension of poly(My) with St increased from 2490 to 11,100  $\text{g mol}^{-1}$  and final  $\bar{D} = 1.40$  [43]. However, distinct  $T_g$ s of the two homopolymers were not obtained, likely due to the relatively short blocks in the polymer chain and thus phase separation was not achieved. A more recent study showed that

regioselectivity of poly(My) was affected by choice of thermal initiator more so than CTA [44]. In general, higher temperatures yielded lower percentage of 1,4-configuration, and dibenzoyl peroxide (DBPO) initiators yielded lower percentage of 1,4 configuration than AIBN. Since DBPO has a slower rate of dissociation than AIBN, the polymerization temperature was increased from 90 to 130 °C, and evidence of crosslinking started to occur. Furthermore, change in regioselectivity was plotted as a function of conversion for the first time, and it showed that the 1,4-configuration was initially favoured at 95% but decreased to 76% as 3,4-configuration increased by the end of the polymerization.

Although good chain end fidelity was achieved with RAFT of My, the polymerizations rates were very slow. Polymerizations of My were done at a low temperature of 65 °C and  $X \sim 50\%$  after 125 h, and even at a higher temperature of 130 °C conversion reached 50–60% after ~50 h [43,44]. Another example used UV instead of a thermal initiator to initiate RAFT polymerization of My in bulk and at room temperature [156]. Similarly, polymerization rate was slow reaching  $X = 20\%$  after 160 h with  $M_n$  of 12,000 g mol<sup>-1</sup> and  $\bar{D} \sim 1.6$ . However, triblock copolymers were synthesized with St and poly(ethylene glycol) methacrylate (PEG-MA). In a very recent study, ABA triblock poly(St-*b*-My-*b*-St) copolymers were made via a bifunctional RAFT CTA in aqueous dispersion [157]. High conversions ( $X > 68\%$ ) were achieved in 48 h at 75 °C, and the block copolymers had high  $M_n$  (>40,000 g mol<sup>-1</sup>) with relatively low  $\bar{D}$  (highest  $\bar{D}$  being 1.75) considering triblock copolymers were synthesized with vary compositions of St and My.

RAFT continues to show its versatility by successful synthesis of block copolymers made of IP with other monomers like *N*-vinyl pyrrolidinone and ethylene oxide [158,159], as well as statistical copolymerization with St and hydroxyl-functionalized (meth)acrylates and dienes [160–162]. Polymerization temperatures were generally kept relatively low to prevent crosslinking and loss of control, and therefore polymerization rates were very slow. Seeded emulsions and miniemulsions seemed to be a good solution as compartmentalization was achieved to increase polymerization rates and successful block copolymers were synthesized using isoprene and myrcene. However, examples of RAFT polymerization of Far were not found and can be further investigated, especially in dispersed aqueous media.

## 2.6 Outlook for bio-based poly(dienes) in real-world applications

Understandably, bio-based dienes find applications predominantly in the same sector as conventional dienes. They are used as feedstocks to impart rubbery character into polymers in the form of homopolymers, statistical, block and gradient copolymers. It is expected in the foreseeable future that monomers like Myr and Far will be touted as candidates for replacement of petroleum-based dienes and evidence suggests that these monomers can be readily adapted to various chemistries already established for dienes. Further, the key advantage of handling bio-based dienes like Myr and Far is their relatively lower volatility compared to IP or BD, which makes manipulation in polymerization processes much easier (for example, pressurized reactors are not required). However, like in other cases where a bio-based alternative is proposed (e.g. replacements for poly(ethylene terephthalate)) [163], there must be a compelling case for improvement or enhancement of properties in addition to a sound economic basis.

One major application for BD and IP is thermoplastic elastomers (TPEs) and many examples in this review showcased RDRP of Myr or Far with St to make block copolymers. In comparison, these Myr and Far analogous TPEs do not exhibit the same elongation to break properties due to the high hydrodynamic volume which requires high molecular weights for chains to entangle and form rubbery materials. However, using RDRP has allowed the hard segment (that would traditionally be made of St) to be replaced by functionalized methacrylates that introduced hydrophilicity (i.e. PEG-MA) [156], post-polymerization compatibilization and modification (i.e. GMA) [39], and increased thermal stability and hardness (i.e. iBOMA) [41].

Nonetheless, high entanglement molecular weights may be an advantage in low temperature applications. To take advantage of the low  $T_g$  of poly(My) and poly(Far), there have been several patents, as mentioned briefly in the introduction, that found new applications for these materials. Amyris Inc., filed a patent reporting the polymerization of Far to use in pressure sensitive adhesives (PSAs). Their patent describes the polymerization of Far using ionic polymerization or metal catalysts (Ziegler-Natta, Kaminsky, or metallocene) and copolymerization with other olefinic monomers to make statistical or block copolymers [25]. Poly(My) was copolymerized

with sulfur dioxide by free radical polymerization and showed good adhesion to various surfaces such as glass, wood, aluminum and copper [31].

Fina Technology Inc. owns several patents using poly(Far) in many applications. One patent describes the use of Friedel-Craft catalysts to make low molecular weight poly(Far) as tackifying resins to be blended with elastomers [26]. Another patent details anionic polymerization of Far with at least one hydroxyl-terminated chain-end for further modification such as hydrogenation or acrylation [28]. The resulting polymer is a liquid optically clear adhesive to use in laminated screen assemblies in electronic devices. Alternatively, Far can be modified with a terminal hydroxyl, amino, epoxy, isocyanato, or carboxylic acid group which can be reacted with a (meth)acrylate to make a macromonomer, and then be further polymerized radically [164]. This bottlebrush polymer can be used as an additive in lubricants, hydraulic fluids, cosmetics, or adhesives. Far homopolymer (or copolymer with other dienes or vinyl aromatics) with terminal hydroxyl groups (a Far polyol) can also be reacted with diisocyanates to make a polyurethane prepolymer, which can further react with polyols to lower the isocyanate content in the final polyurethane product while increasing molecular weight [27]. Such materials would find application in markets where polyurethanes are often used such as sealants, caulking, sponge, foam, coatings, and binders.

There is one example of RAFT polymerization of Myr used as an anti-fouling membrane for oil/water separation [165]. Cellulose membrane (CM) is modified with DoPAT RAFT agent via acid/hydroxyl esterification with a hydroxyl group on the cellulose. Subsequently, grafting-from polymerization of 3-(trimethoxysilyl)-propyl acrylate formed the first block, followed by polymerization of Myr to form the second block. The modified CMs showed exceptional hydrophobicity with a contact angle  $>160^\circ$  and was able to separate crude oil contaminants from water effectively. Odorous thiol contaminants can also be removed through their thiol-ene interactions with the double bonds in the poly(Myrr) block. These materials can find uses in many chemical processes and environmental remediation. Furthermore, they are made of mostly bio-derived sources, namely CM and Myr, and the cellulose component is bio-degradable.

This review highlights some of the particular advantages of using bio-based dienes in RDRP processes that have emerged over the past decade. Although many current applications using

poly(Far) and poly(Myrr) are synthesized via ionic, free radical, or catalytic polymerization, recent developments highlighted here can positively lead to more applications using RDRP. Continued activity is expected to concretely evaluate the merit of replacing petroleum-based dienes with their bio-based alternatives.

## 2.7 References

- [1] A. Chauvel, G. Lefebvre, L. Castex, Steam cracking, Petrochemicals processes, Editions Technip, Paris, 1989.
- [2] J. Brandrup, E.H. Immergut, E.A. Grulke, Polymer handbook, 4th ed. ed., Wiley, New York, 1999.
- [3] I. Kopal, P. Košťal, Z. Jančíková, J. Valíček, M. Harničárová, P. Hybler, M. Kušnerová, Modifications of Viscoelastic Properties of Natural Rubber/Styrene-Butadiene Rubber Blend by Electron Beam Irradiation, in: A. Öchsner, H. Altenbach (Eds.), Improved Performance of Materials: Design and Experimental Approaches, Springer International Publishing, Cham, 2018, pp. 219-229.
- [4] M.P. Bertin, G. Marin, J.P. Montfort, Viscoelastic properties of acrylonitrile-butadiene-styrene (ABS) polymers in the molten state, Polymer Engineering & Science 35(17) (1995) 1394-1406.
- [5] T. Masuda, A. Nakajima, M. Kitamura, Y. Aoki, N. Yamauchi, A. Yoshioka, Viscoelastic properties of rubber-modified polymeric materials at elevated temperatures, Pure and Applied Chemistry, 1984, p. 1457.
- [6] J.G. Drobny, 15 - Applications of Thermoplastic Elastomers, in: J.G. Drobny (Ed.), Handbook of Thermoplastic Elastomers, William Andrew Publishing, Norwich, NY, 2007, pp. 281-315.
- [7] J.M. Degrange, M. Thomine, P. Kapsa, J.M. Pelletier, L. Chazeau, G. Vigier, G. Dudragne, L. Guerbé, Influence of viscoelasticity on the tribological behaviour of carbon black filled nitrile rubber (NBR) for lip seal application, Wear 259(1) (2005) 684-692.

- [8] W.C. White, Butadiene production process overview, *Chemico-Biological Interactions* 166(1) (2007) 10-14.
- [9] R. Varma, H. Takeichi, J.E. Hall, Y.F. Ozawa, T. Kyu, Miscibility studies on blends of Kraton block copolymer and asphalt, *Polymer* 43(17) (2002) 4667-4671.
- [10] T.O. Broadhead, A.E. Hamielec, J.F. MacGregor, Dynamic modelling of the batch, semi-batch and continuous production of styrene/butadiene copolymers by emulsion polymerization, *Die Makromolekulare Chemie* 10(10-11) (1985) 105-128.
- [11] V.I. Rodríguez, D.A. Estenoz, L.M. Gugliotta, G.R. Meira, Emulsion copolymerization of acrylonitrile and butadiene. Calculation of the detailed macromolecular structure, *International Journal of Polymeric Materials and Polymeric Biomaterials* 51(6) (2002) 511-527.
- [12] A.F. Johnson, D.J. Worsfold, Anionic polymerization of butadiene and styrene, *Journal of Polymer Science Part A: General Papers* 3(2) (1965) 449-455.
- [13] A.F. Halasa, J.E. Hall, A. Para, Process for the preparation of block copolymers, U.S., 1980.
- [14] M. Morton, L.J. Fetters, E.E. Bostick, Mechanisms of homogeneous anionic polymerization by alkyllithium initiators, *Journal of Polymer Science Part C: Polymer Symposia* 1(1) (1963) 311-323.
- [15] M. Morton, L.J. Fetters, Homogeneous anionic polymerization of unsaturated monomers, *Journal of Polymer Science: Macromolecular Reviews* 2(1) (1967) 71-113.
- [16] R. Bening, D. Handlin, L. Sterna, C. Willis, Novel block copolymers and method for making same, Kraton Polymers US LLC, 2003.

- [17] D. Jenkins Aubrey, G. Jones Richard, G. Moad, Terminology for reversible-deactivation radical polymerization previously called "controlled" radical or "living" radical polymerization (IUPAC Recommendations 2010), *Pure and Applied Chemistry*, 2009, p. 483.
- [18] R.C. Thompson, C.J. Moore, F.S. vom Saal, S.H. Swan, Plastics, the environment and human health: current consensus and future trends, *Philosophical Transactions of the Royal Society B: Biological Sciences* 364(1526) (2009) 2153-2166.
- [19] Oil Consumption, 2019. [https://www.bpf.co.uk/Press/Oil\\_Consumption.aspx](https://www.bpf.co.uk/Press/Oil_Consumption.aspx). (Accessed November 26 2020).
- [20] T.A. Hottle, M.M. Bilec, A.E. Landis, Sustainability assessments of bio-based polymers, *Polymer Degradation and Stability* 98(9) (2013) 1898-1907.
- [21] K. Satoh, Controlled/living polymerization of renewable vinyl monomers into bio-based polymers, *Polymer Journal* 47(8) (2015) 527-536.
- [22] B. Davies, Natural rubber — Its engineering characteristics, *Materials & Design* 7(2) (1986) 68-74.
- [23] P. Sahu, A.K. Bhowmick, G. Kali, Terpene Based Elastomers: Synthesis, Properties, and Applications, *Processes* 8(5) (2020).
- [24] C. Iacob, T. Yoo, J. Runt, Molecular Dynamics of Polyfarnesene, *Macromolecules* 51(13) (2018) 4917-4922.
- [25] D.J. McPhee, M.J. Graham, Adhesives compositions comprising a polyfarnesene, Amyris Inc., United States, 2010.

- [26] K.A. Nelson, A. Pierre-Justin, N.P. Hansen, Farnesene-based tackifying resins and adhesive compositions containing the same, Fina Technology Inc., United States, 2018.
- [27] N. Tian, H. Chao, Polyols derived from farnesene for polyurethanes, Fina Technology Inc, United States, 2018.
- [28] T. Yoo, H. Chao, S.K. Henning, Farnesene-based polymers and liquid optically clear adhesive compositions incorporating the same, Fina Technology, United States, 2018.
- [29] P. Sarkar, A.K. Bhowmick, Synthesis, characterization and properties of a bio-based elastomer: polymyrcene, RSC Advances 4(106) (2014) 61343-61354.
- [30] R.P. Quirk, Triblock polymers of a monovinyl aromatic compound and myrcene, Michigan Molecular Institute, United States, 1981.
- [31] X. Guo, X. Liu, S. Shan, W. Zhao, H. Su, Q. Jia, Green approach toward sustainable adhesive: Synthesis and characterization of poly(myrcene sulfone), Journal of the Taiwan Institute of Chemical Engineers 95 (2019) 208-216.
- [32] C. Zhou, Z. Wei, C. Jin, Y. Wang, Y. Yu, X. Leng, Y. Li, Fully biobased thermoplastic elastomers: Synthesis of highly branched linear comb poly( $\beta$ -myrcene)-graft-poly(l-lactide) copolymers with tunable mechanical properties, Polymer 138 (2018) 57-64.
- [33] L.J. Fetters, D.J. Lohse, D. Richter, T.A. Witten, A. Zirkel, Connection between Polymer Molecular Weight, Density, Chain Dimensions, and Melt Viscoelastic Properties, Macromolecules 27(17) (1994) 4639-4647.
- [34] S. Loughmari, A. Hafid, A. Bouazza, A. El Bouadili, P. Zinck, M. Visseaux, Highly stereoselective coordination polymerization of  $\beta$ -myrcene from a lanthanide-based catalyst:

Access to bio-sourced elastomers, *Journal of Polymer Science Part A: Polymer Chemistry* 50(14) (2012) 2898-2905.

[35] B. Liu, D.T. Liu, S.H. Li, G.P. Sun, D.M. Cui, High trans-1,4 (co)polymerization of  $\beta$ -myrcene and isoprene with an iminophosphonamide lanthanum catalyst, *Chinese Journal of Polymer Science* 34(1) (2016) 104-110.

[36] S. Georges, M. Bria, P. Zinck, M. Visseaux, Polymyrcene microstructure revisited from precise high-field nuclear magnetic resonance analysis, *Polymer* 55(16) (2014) 3869-3878.

[37] S. Georges, A.O. Touré, M. Visseaux, P. Zinck, Coordinative Chain Transfer Copolymerization and Terpolymerization of Conjugated Dienes, *Macromolecules* 47(14) (2014) 4538-4547.

[38] S. Georges, O.H. Hashmi, M. Bria, P. Zinck, Y. Champouret, M. Visseaux, Efficient One-Pot Synthesis of End-Functionalized trans-Stereoregular Polydiene Macromonomers, *Macromolecules* 52(3) (2019) 1210-1219.

[39] A. Métafiot, J.F. Gérard, B. Defoort, M. Marić, Synthesis of  $\beta$ -myrcene/glycidyl methacrylate statistical and amphiphilic diblock copolymers by SG1 nitroxide-mediated controlled radical polymerization, *Journal of Polymer Science Part A: Polymer Chemistry* 56(8) (2018) 860-878.

[40] A. Métafiot, Y. Kanawati, J.F. Gérard, B. Defoort, M. Marić, Synthesis of  $\beta$ -Myrcene-Based Polymers and Styrene Block and Statistical Copolymers by SG1 Nitroxide-Mediated Controlled Radical Polymerization, *Macromolecules* 50(8) (2017) 3101-3120.

[41] A. Métafiot, L. Gagnon, S. Pruvost, P. Hubert, J.F. Gérard, B. Defoort, M. Marić,  $\beta$ -Myrcene/isobornyl methacrylate SG1 nitroxide-mediated controlled radical polymerization:

synthesis and characterization of gradient, diblock and triblock copolymers, *RSC Advances* 9(6) (2019) 3377-3395.

[42] S.B. Luk, M. Marić, Nitroxide-Mediated Polymerization of Bio-Based Farnesene with a Functionalized Methacrylate, *Macromolecular Reaction Engineering* 13(3) (2019) 1800080.

[43] J. Hilschmann, G. Kali, Bio-based polymyrcene with highly ordered structure via solvent free controlled radical polymerization, *European Polymer Journal* 73 (2015) 363-373.

[44] N. Bauer, J. Brunke, G. Kali, Controlled Radical Polymerization of Myrcene in Bulk: Mapping the Effect of Conditions on the System, *ACS Sustainable Chemistry & Engineering* 5(11) (2017) 10084-10092.

[45] E. Breitmaier, Terpenes: Importance, General Structure, and Biosynthesis, *Terpenes2006*, pp. 1-9.

[46] M.B. Isman, Plant essential oils for pest and disease management, *Crop Protection* 19(8) (2000) 603-608.

[47] W. Chen, A.M. Viljoen, Geraniol — A review of a commercially important fragrance material, *South African Journal of Botany* 76(4) (2010) 643-651.

[48] F. Englund, R.M. Nussbaum, Monoterpenes in Scots Pine and Norway Spruce and their Emission during Kiln Drying, *Holzforschung* 54(5) (2000) 449.

[49] L.L. Ingram, Jr., S. Rubin, A.T. Dalton, F.W. Taylor, M.C. Templeton, The measurement of volatile organic emissions from drying southern pine lumber in a laboratory-scale kiln, *Forest Products Journal* 50(4) (2000) 91-94.

- [50] S. Sarria, B. Wong, H.G. Martín, J.D. Keasling, P. Peralta-Yahya, Microbial Synthesis of Pinene, *ACS Synthetic Biology* 3(7) (2014) 466-475.
- [51] M.B. Kolicheski, L.C. Cocco, D.A. Mitchell, M. Kaminski, Synthesis of myrcene by pyrolysis of  $\beta$ -pinene: Analysis of decomposition reactions, *Journal of Analytical and Applied Pyrolysis* 80(1) (2007) 92-100.
- [52] H. Zheng, J. Chen, C. Li, J. Chen, Y. Wang, S. Zhao, Y. Zeng, Mechanism and kinetics of the pyrolysis of  $\beta$ -pinene to myrcene, *Journal of Analytical and Applied Pyrolysis* 123 (2017) 99-106.
- [53] M. Eisenacher, S. Beschnitt, W. Hölderich, Novel route to a fruitful mixture of terpene fragrances in particular phellandrene starting from natural feedstock geraniol using weak acidic boron based catalyst, *Catalysis Communications* 26 (2012) 214-217.
- [54] Z. Li, K. Howell, Z. Fang, P. Zhang, Sesquiterpenes in grapes and wines: Occurrence, biosynthesis, functionality, and influence of winemaking processes, *Comprehensive Reviews in Food Science and Food Safety* 19(1) (2020) 247-281.
- [55] G. Brieger, T.J. Nestrick, C. McKenna, Synthesis of trans, trans- $\alpha$ -farnesene, *The Journal of Organic Chemistry* 34(12) (1969) 3789-3791.
- [56] G. Brieger, Convenient preparation of trans- $\beta$ -farnesene, *The Journal of Organic Chemistry* 32(11) (1967) 3720-3720.
- [57] J. Crock, M. Wildung, R. Croteau, Isolation and bacterial expression of a sesquiterpene synthase cDNA clone from peppermint (*Mentha X Piperita* L.) that produces the aphid alarm pheromone (E)- $\beta$ -farnesene, *Proceedings of the National Academy of Sciences* 94(24) (1997) 12833.

- [58] R.C. Morais, S. Dworakowska, A. Reis, L. Gouveia, C.T. Matos, D. Bogdał, R. Bogel-Łukasik, Chemical and biological-based isoprene production: Green metrics, *Catalysis Today* 239 (2015) 38-43.
- [59] R.A. Newmark, R.N. Majumdar, <sup>13</sup>C-NMR spectra of cis-polymyrcene and cis-polyfarnesene, *Journal of Polymer Science Part A: Polymer Chemistry* 26(1) (1988) 71-77.
- [60] J.M. Bolton, M.A. Hillmyer, T.R. Hoye, Sustainable Thermoplastic Elastomers from Terpene-Derived Monomers, *ACS Macro Letters* 3(8) (2014) 717-720.
- [61] C. Zhou, Z. Wei, X. Lei, Y. Li, Fully biobased thermoplastic elastomers: synthesis and characterization of poly(l-lactide)-b-polymyrcene-b-poly(l-lactide) triblock copolymers, *RSC Advances* 6(68) (2016) 63508-63514.
- [62] C. Zhou, Z. Wei, Y. Wang, Y. Yu, X. Leng, Y. Li, Fully biobased thermoplastic elastomers: Synthesis of highly branched star comb poly( $\beta$ -myrcene)-graft-poly(l-lactide) copolymers with tunable mechanical properties, *European Polymer Journal* 99 (2018) 477-484.
- [63] A. Matic, H. Schlaad, Thiol-ene photofunctionalization of 1,4-polymyrcene, *Polymer International* 67(5) (2018) 500-505.
- [64] E. Grune, J. Bareuther, J. Blankenburg, M. Appold, L. Shaw, A.H.E. Müller, G. Floudas, L.R. Hutchings, M. Gallei, H. Frey, Towards bio-based tapered block copolymers: the behaviour of myrcene in the statistical anionic copolymerisation, *Polymer Chemistry* 10(10) (2019) 1213-1220.
- [65] M.I. Hulnik, I.V. Vasilenko, A.V. Radchenko, F. Peruch, F. Ganachaud, S.V. Kostjuk, Aqueous cationic homo- and co-polymerizations of  $\beta$ -myrcene and styrene: a green route toward terpene-based rubbery polymers, *Polymer Chemistry* 9(48) (2018) 5690-5700.

- [66] P. Sarkar, A.K. Bhowmick, Terpene Based Sustainable Elastomer for Low Rolling Resistance and Improved Wet Grip Application: Synthesis, Characterization and Properties of Poly(styrene-co-myrcene), *ACS Sustainable Chemistry & Engineering* 4(10) (2016) 5462-5474.
- [67] M. Szwarc, *Living Polymers*, *Nature* 178(4543) (1956) 1168-1169.
- [68] D.A. Shipp, *Living Radical Polymerization: Controlling Molecular Size and Chemical Functionality in Vinyl Polymers*, *Journal of Macromolecular Science, Part C* 45(2) (2005) 171-194.
- [69] D.H. Solomon, E. Rizzardo, P. Cacioli, *Polymerization process and polymers produced thereby*, Google Patents, 1986.
- [70] M.K. Georges, R.P.N. Veregin, P.M. Kazmaier, G.K. Hamer, *Narrow molecular weight resins by a free-radical polymerization process*, *Macromolecules* 26(11) (1993) 2987-2988.
- [71] P.M. Kazmaier, K.A. Moffat, M.K. Georges, R.P.N. Veregin, G.K. Hamer, *Free-Radical Polymerization for Narrow-Polydispersity Resins. Semiempirical Molecular Orbital Calculations as a Criterion for Selecting Stable Free-Radical Reversible Terminators*, *Macromolecules* 28(6) (1995) 1841-1846.
- [72] M.K. Georges, G.K. Hamer, N.A. Listigovers, *Block Copolymer Synthesis by a Nitroxide-Mediated Living Free Radical Polymerization Process*, *Macromolecules* 31(25) (1998) 9087-9089.
- [73] C. Burguière, M.-A. Dourges, B. Charleux, J.-P. Vairon, *Synthesis and Characterization of  $\omega$ -Unsaturated Poly(styrene-*b*-*n*-butyl methacrylate) Block Copolymers Using TEMPO-Mediated Controlled Radical Polymerization*, *Macromolecules* 32(12) (1999) 3883-3890.

- [74] T. Fukuda, T. Terauchi, A. Goto, Y. Tsujii, T. Miyamoto, Y. Shimizu, Well-Defined Block Copolymers Comprising Styrene–Acrylonitrile Random Copolymer Sequences Synthesized by “Living” Radical Polymerization, *Macromolecules* 29(8) (1996) 3050-3052.
- [75] M. Baumert, J. Fröhlich, M. Stieger, H. Frey, R. Mülhaupt, H. Plenio, Styrene-vinylferrocene random and block copolymers by TEMPO-mediated radical polymerization, *Macromolecular Rapid Communications* 20(4) (1999) 203-209.
- [76] E. Tuinman, N.T. McManus, M. Roa-Luna, E. Vivaldo-Lima †, L.M.F. Lona, A. Penlidis, Controlled Free-Radical Copolymerization Kinetics of Styrene and Divinylbenzene by Bimolecular NMRP using TEMPO and Dibenzoyl Peroxide, *Journal of Macromolecular Science, Part A* 43(7) (2006) 995-1011.
- [77] C.J. Hawker, Molecular Weight Control by a "Living" Free-Radical Polymerization Process, *Journal of the American Chemical Society* 116(24) (1994) 11185-11186.
- [78] C.J. Hawker, G.G. Barclay, A. Orellana, J. Dao, W. Devonport, Initiating Systems for Nitroxide-Mediated “Living” Free Radical Polymerizations: Synthesis and Evaluation, *Macromolecules* 29(16) (1996) 5245-5254.
- [79] G. Moad, E. Rizzardo, Alkoxyamine-Initiated Living Radical Polymerization: Factors Affecting Alkoxyamine Homolysis Rates, *Macromolecules* 28(26) (1995) 8722-8728.
- [80] D. Benoit, V. Chaplinski, R. Braslau, C.J. Hawker, Development of a Universal Alkoxyamine for “Living” Free Radical Polymerizations, *Journal of the American Chemical Society* 121(16) (1999) 3904-3920.
- [81] S. Grimaldi, J.P. Finet, F. Le Moigne, A. Zeghdaoui, P. Tordo, D. Benoit, M. Fontanille, Y. Gnanou, Acyclic  $\beta$ -Phosphonylated Nitroxides: A New Series of Counter-Radicals for “Living”/Controlled Free Radical Polymerization, *Macromolecules* 33(4) (2000) 1141-1147.

- [82] D. Bertin, F. Chauvin, J.L. Couturier, P.E. Dufils, D. Gigmes, O. Guerret, S. Marque, P. Tordo, Alkoxyamines originating from beta-phosphorylated nitroxides and use thereof in radical polymerisation, Google Patents, 2005.
- [83] F. Chauvin, J.L. Couturier, P.-E. Dufils, P. Gérard, D. Gigmes, O. Guerret, Y. Guillaneuf, S.R.A. Marque, D. Bertin, P. Tordo, Crowded Phosphonylated Alkoxyamines with Low Dissociation Temperatures: A Milestone in Nitroxide-Mediated Polymerization, Controlled/Living Radical Polymerization, American Chemical Society 2006, pp. 326-341.
- [84] D. Benoit, E. Harth, P. Fox, R.M. Waymouth, C.J. Hawker, Accurate Structural Control and Block Formation in the Living Polymerization of 1,3-Dienes by Nitroxide-Mediated Procedures, *Macromolecules* 33(2) (2000) 363-370.
- [85] D. Contreras-López, M. Albores-Velasco, E. Saldívar-Guerra, Isoprene (co)polymers with glycidyl methacrylate via bimolecular and unimolecular nitroxide mediated radical polymerization, *Journal of Applied Polymer Science* 134(29) (2017) 45108.
- [86] S. Harrisson, P. Couvreur, J. Nicolas, SG1 Nitroxide-Mediated Polymerization of Isoprene: Alkoxyamine Structure/Control Relationship and  $\alpha,\omega$ -Chain-End Functionalization, *Macromolecules* 44(23) (2011) 9230-9238.
- [87] J. Ruehl, A. Nilsen, S. Born, P. Thoniyot, L.-p. Xu, S. Chen, R. Braslau, Nitroxide-mediated polymerization to form symmetrical ABA triblock copolymers from a bidirectional alkoxyamine initiator, *Polymer* 48(9) (2007) 2564-2571.
- [88] C. Dire, J. Belleney, J. Nicolas, D. Bertin, S. Magnet, B. Charleux,  $\beta$ -Hydrogen transfer from poly(methyl methacrylate) propagating radicals to the nitroxide SG1: Analysis of the chain-end and determination of the rate constant, *Journal of Polymer Science Part A: Polymer Chemistry* 46(18) (2008) 6333-6345.

- [89] Y. Guillaneuf, D. Gigmes, S.R.A. Marque, P. Tordo, D. Bertin, Nitroxide-Mediated Polymerization of Methyl Methacrylate Using an SG1-Based Alkoxyamine: How the Penultimate Effect Could Lead to Uncontrolled and Unliving Polymerization, *Macromolecular Chemistry and Physics* 207(14) (2006) 1278-1288.
- [90] E. Guégain, Y. Guillaneuf, J. Nicolas, Nitroxide-Mediated Polymerization of Methacrylic Esters: Insights and Solutions to a Long-Standing Problem, *Macromolecular Rapid Communications* 36(13) (2015) 1227-1247.
- [91] B. Charleux, J. Nicolas, O. Guerret, Theoretical Expression of the Average Activation–Deactivation Equilibrium Constant in Controlled/Living Free-Radical Copolymerization Operating via Reversible Termination. Application to a Strongly Improved Control in Nitroxide-Mediated Polymerization of Methyl Methacrylate, *Macromolecules* 38(13) (2005) 5485-5492.
- [92] J. Nicolas, C. Dire, L. Mueller, J. Belleney, B. Charleux, S.R.A. Marque, D. Bertin, S. Magnet, L. Couvreur, Living Character of Polymer Chains Prepared via Nitroxide-Mediated Controlled Free-Radical Polymerization of Methyl Methacrylate in the Presence of a Small Amount of Styrene at Low Temperature, *Macromolecules* 39(24) (2006) 8274-8282.
- [93] J. Vinas, N. Chagneux, D. Gigmes, T. Trimaille, A. Favier, D. Bertin, SG1-based alkoxyamine bearing a N-succinimidyl ester: A versatile tool for advanced polymer synthesis, *Polymer* 49(17) (2008) 3639-3647.
- [94] N. Ballard, M. Aguirre, A. Simula, A. Agirre, J.R. Leiza, J.M. Asua, S. van Es, New Class of Alkoxyamines for Efficient Controlled Homopolymerization of Methacrylates, *ACS Macro Letters* 5(9) (2016) 1019-1022.

- [95] N. Ballard, M. Aguirre, A. Simula, J.R. Leiza, S. van Es, J.M. Asua, High solids content nitroxide mediated miniemulsion polymerization of n-butyl methacrylate, *Polymer Chemistry* 8(10) (2017) 1628-1635.
- [96] N. Ballard, A. Simula, M. Aguirre, J.R. Leiza, S. van Es, J.M. Asua, Synthesis of poly(methyl methacrylate) and block copolymers by semi-batch nitroxide mediated polymerization, *Polymer Chemistry* 7(45) (2016) 6964-6972.
- [97] A. Métafiot, S. Pruvost, J.F. Gérard, B. Defoort, M. Marić, Synthesis of isoprene-based triblock copolymers by nitroxide-mediated polymerization, *European Polymer Journal* 134 (2020) 109798.
- [98] K. Matyjaszewski, J. Xia, Atom Transfer Radical Polymerization, *Chemical Reviews* 101(9) (2001) 2921-2990.
- [99] M. Kato, M. Kamigaito, M. Sawamoto, T. Higashimura, Polymerization of Methyl Methacrylate with the Carbon Tetrachloride/Dichlorotris-(triphenylphosphine)ruthenium(II)/Methylaluminum Bis(2,6-di-tert-butylphenoxide) Initiating System: Possibility of Living Radical Polymerization, *Macromolecules* 28(5) (1995) 1721-1723.
- [100] J.S. Wang, K. Matyjaszewski, Controlled/"living" radical polymerization. atom transfer radical polymerization in the presence of transition-metal complexes, *Journal of the American Chemical Society* 117(20) (1995) 5614-5615.
- [101] C. Granel, P. Dubois, R. Jérôme, P. Teyssié, Controlled Radical Polymerization of Methacrylic Monomers in the Presence of a Bis(ortho-chelated) Arylnickel(II) Complex and Different Activated Alkyl Halides, *Macromolecules* 29(27) (1996) 8576-8582.
- [102] Y. Shen, H. Tang, S. Ding, Catalyst separation in atom transfer radical polymerization, *Progress in Polymer Science* 29(10) (2004) 1053-1078.

- [103] K. Matyjaszewski, T. Pintauer, S. Gaynor, Removal of Copper-Based Catalyst in Atom Transfer Radical Polymerization Using Ion Exchange Resins, *Macromolecules* 33(4) (2000) 1476-1478.
- [104] W. Jakubowski, K. Matyjaszewski, Activator Generated by Electron Transfer for Atom Transfer Radical Polymerization, *Macromolecules* 38(10) (2005) 4139-4146.
- [105] W. Jakubowski, K. Min, K. Matyjaszewski, Activators Regenerated by Electron Transfer for Atom Transfer Radical Polymerization of Styrene, *Macromolecules* 39(1) (2006) 39-45.
- [106] W. Jakubowski, K. Matyjaszewski, Activators Regenerated by Electron Transfer for Atom-Transfer Radical Polymerization of (Meth)acrylates and Related Block Copolymers, *Angewandte Chemie International Edition* 45(27) (2006) 4482-4486.
- [107] K. Min, H. Gao, K. Matyjaszewski, Use of Ascorbic Acid as Reducing Agent for Synthesis of Well-Defined Polymers by ARGET ATRP, *Macromolecules* 40(6) (2007) 1789-1791.
- [108] V.A. Williams, K. Matyjaszewski, Expanding the ATRP Toolbox: Methacrylate Polymerization with an Elemental Silver Reducing Agent, *Macromolecules* 48(18) (2015) 6457-6464.
- [109] K. Matyjaszewski, W. Jakubowski, K. Min, W. Tang, J. Huang, W.A. Braunecker, N.V. Tsarevsky, Diminishing catalyst concentration in atom transfer radical polymerization with reducing agents, *Proceedings of the National Academy of Sciences* 103(42) (2006) 15309.
- [110] K. Matyjaszewski, S. Coca, S.G. Gaynor, M. Wei, B.E. Woodworth, Zerovalent Metals in Controlled/"Living" Radical Polymerization, *Macromolecules* 30(23) (1997) 7348-7350.
- [111] V. Percec, T. Guliashvili, J.S. Ladislaw, A. Wistrand, A. Stjerndahl, M.J. Sienkowska, M.J. Monteiro, S. Sahoo, Ultrafast Synthesis of Ultrahigh Molar Mass Polymers by Metal-Catalyzed

Living Radical Polymerization of Acrylates, Methacrylates, and Vinyl Chloride Mediated by SET at 25 °C, *Journal of the American Chemical Society* 128(43) (2006) 14156-14165.

[112] K. Matyjaszewski, N.V. Tsarevsky, W.A. Braunecker, H. Dong, J. Huang, W. Jakubowski, Y. Kwak, R. Nicolay, W. Tang, J.A. Yoon, Role of Cu<sup>0</sup> in Controlled/"Living" Radical Polymerization, *Macromolecules* 40(22) (2007) 7795-7806.

[113] B.M. Rosen, V. Percec, Single-Electron Transfer and Single-Electron Transfer Degenerative Chain Transfer Living Radical Polymerization, *Chemical Reviews* 109(11) (2009) 5069-5119.

[114] M. Zhong, K. Matyjaszewski, How Fast Can a CRP Be Conducted with Preserved Chain End Functionality?, *Macromolecules* 44(8) (2011) 2668-2677.

[115] A. Plichta, W. Li, K. Matyjaszewski, ICAR ATRP of Styrene and Methyl Methacrylate with Ru(Cp\*)Cl(PPh<sub>3</sub>)<sub>2</sub>, *Macromolecules* 42(7) (2009) 2330-2332.

[116] S. Okada, S. Park, K. Matyjaszewski, Initiators for Continuous Activator Regeneration Atom Transfer Radical Polymerization of Methyl Methacrylate and Styrene with N-Heterocyclic Carbene as Ligands for Fe-Based Catalysts, *ACS Macro Letters* 3(9) (2014) 944-947.

[117] A. Simakova, S.E. Averick, D. Konkolewicz, K. Matyjaszewski, Aqueous ARGET ATRP, *Macromolecules* 45(16) (2012) 6371-6379.

[118] S.R. Woodruff, B.J. Davis, N.V. Tsarevsky, Selecting the Optimal Reaction Conditions for Copper-Mediated Atom Transfer Radical Polymerization at Low Catalyst Concentration, *Progress in Controlled Radical Polymerization: Mechanisms and Techniques*, American Chemical Society 2012, pp. 99-113.

- [119] N.V. Tsarevsky, W. Jakubowski, Atom transfer radical polymerization of functional monomers employing Cu-based catalysts at low concentration: Polymerization of glycidyl methacrylate, *Journal of Polymer Science Part A: Polymer Chemistry* 49(4) (2011) 918-925.
- [120] W. Jakubowski, Adapting Atom Transfer Radical Polymerization to Industrial Scale Production: The Ultimate ATRP<sub>SM</sub> Technology, *Progress in Controlled Radical Polymerization: Mechanisms and Techniques*, American Chemical Society 2012, pp. 203-216.
- [121] K. Matyjaszewski, Atom Transfer Radical Polymerization (ATRP): Current Status and Future Perspectives, *Macromolecules* 45(10) (2012) 4015-4039.
- [122] M.B. Gillies, K. Matyjaszewski, P.-O. Norrby, T. Pintauer, R. Poli, P. Richard, A DFT Study of R–X Bond Dissociation Enthalpies of Relevance to the Initiation Process of Atom Transfer Radical Polymerization, *Macromolecules* 36(22) (2003) 8551-8559.
- [123] W.A. Braunecker, T. Pintauer, N.V. Tsarevsky, G. Kickelbick, M. Krzysztow, Towards understanding monomer coordination in atom transfer radical polymerization: synthesis of [CuI(PMDETA)( $\pi$ -M)][BPh<sub>4</sub>] (M=methyl acrylate, styrene, 1-octene, and methyl methacrylate) and structural studies by FT-IR and <sup>1</sup>H NMR spectroscopy and X-ray crystallography, *Journal of Organometallic Chemistry* 690(4) (2005) 916-924.
- [124] W.A. Braunecker, N.V. Tsarevsky, T. Pintauer, R.R. Gil, K. Matyjaszewski, Quantifying Vinyl Monomer Coordination to CuI in Solution and the Effect of Coordination on Monomer Reactivity in Radical Copolymerization, *Macromolecules* 38(10) (2005) 4081-4088.
- [125] J. Hendra, D.B. Powell, Co-ordination complexes of butadiene with platinum-II, palladium-II and copper-I, *Spectrochimica Acta* 18(9) (1962) 1195-1199.
- [126] M. Håkansson, K. Brantin, S. Jagner, Copper(I) complexes with conjugated dienes, *Journal of Organometallic Chemistry* 602(1) (2000) 5-14.

- [127] M. Haakansson, S. Jagner, D. Walther, A complex between isoprene and copper(I) chloride: synthesis and structural characterization, *Organometallics* 10(5) (1991) 1317-1319.
- [128] W.v.E. Doering, M. Franck-Neumann, D. Hasselmann, R.L. Kaye, Mechanism of a Diels-Alder reaction. Butadiene and its dimers, *Journal of the American Chemical Society* 94(11) (1972) 3833-3844.
- [129] G. Huybrechts, L. Luyckx, T. Vandenboom, B. Van Mele, Thermal dimerization of 1,3-butadiene: Kinetics of the formation of cis, cis-cycloocta-1,5-diene, *International Journal of Chemical Kinetics* 9(2) (1977) 283-293.
- [130] E.C.F. Ko, K.T. Leffek, Studies on the Decomposition of Tetra-alkylammonium Salts in Solution. V. Rates and Activation Parameters of Salts Containing Substituted-benzyl or Other Active Groups, *Canadian Journal of Chemistry* 50(9) (1972) 1297-1302.
- [131] A. Anastasaki, C. Waldron, P. Wilson, R. McHale, D.M. Haddleton, The importance of ligand reactions in Cu(0)-mediated living radical polymerisation of acrylates, *Polymer Chemistry* 4(9) (2013) 2672-2675.
- [132] J. Wootthikanokkhan, M. Peesan, P. Phinyocheep, Atom transfer radical polymerizations of (meth)acrylic monomers and isoprene, *European Polymer Journal* 37(10) (2001) 2063-2071.
- [133] Y.-F. Zhu, F.-J. Jiang, P.-P. Zhang, J. Luo, H.-D. Tang, Atom transfer radical polymerization and copolymerization of isoprene catalyzed by copper bromide/2,2'-bipyridine, *Chinese Chemical Letters* 27(6) (2016) 910-914.
- [134] T.V. RajanBabu, W.A. Nugent, Selective Generation of Free Radicals from Epoxides Using a Transition-Metal Radical. A Powerful New Tool for Organic Synthesis, *Journal of the American Chemical Society* 116(3) (1994) 986-997.

- [135] R.J. Enemærke, J. Larsen, T. Skrydstrup, K. Daasbjerg, Revelation of the Nature of the Reducing Species in Titanocene Halide-Promoted Reductions, *Journal of the American Chemical Society* 126(25) (2004) 7853-7864.
- [136] A.D. Asandei, G. Saha, Toward Cp<sub>2</sub>TiCl-Catalyzed Living Radical Polymerization of Isoprene, *Polym. Prepr* 46(2) (2005) 474-475.
- [137] A.D. Asandei, O. Adebolu, H.S. Yu, C.P. Simpson, M. Gilbert, Carbonyl initiated Cp<sub>2</sub>TiCl-catalyzed controlled radical polymerization of isoprene, *Polymer Preprints* 50(1) (2009) 177.
- [138] A.D. Asandei, C.P. Simpson, H.S. Yu, Cp<sub>2</sub>TiCl-catalyzed controlled radical polymerization of isoprene initiated from epoxides, aldehydes and halides, *Polym. Prepr. Am. Chem. Soc* 49 (2008) 73-74.
- [139] A.D. Asandei, C.P. Simpson, Cp<sub>2</sub>TiCl-catalyzed synthesis of styrene/isoprene copolymers by controlled radical polymerization, *Polym. Prepr. Am. Chem. Soc* 49 (2008) 75-76.
- [140] J. Hua, H. Xu, J. Geng, Z. Deng, L. Xu, Y.I. Yu, Atom transfer radical polymerizations of styrene and butadiene as well as their copolymerization initiated by benzyl chloride / 1-octanol-substituted MoCl<sub>5</sub> / PPh<sub>3</sub>, *Journal of Polymer Research* 18(1) (2011) 41-48.
- [141] V. Vasu, J.S. Kim, H.S. Yu, W.I. Bannerman, M.E. Johnson, A.D. Asandei, Normal, ICAR and photomediated butadiene-ATRP with iron complexes, *Polymer Chemistry* 9(18) (2018) 2389-2406.
- [142] V. Vasu, J.S. Kim, H.S. Yu, W.I. Bannerman, M.E. Johnson, A.D. Asandei, Toward Butadiene-ATRP with Group 10 (Ni, Pd, Pt) Metal Complexes, *Reversible Deactivation Radical Polymerization: Mechanisms and Synthetic Methodologies*, American Chemical Society 2018, pp. 205-225.

- [143] H.S. Yu, J.S. Kim, V. Vasu, C.P. Simpson, A.D. Asandei, Cu-Mediated Butadiene ATRP, *ACS Catalysis* 10(12) (2020) 6645-6663.
- [144] T. Le, G. Moad, E. Rizzardo, S. Thang, PCT Int. Appl. Number PCT/US/97/12540. Int. Publ. Number WO 98/01478. Al. 15 January, (1998).
- [145] J. Chiefari, Y.K. Chong, F. Ercole, J. Krstina, J. Jeffery, T.P.T. Le, R.T.A. Mayadunne, G.F. Meijs, C.L. Moad, G. Moad, E. Rizzardo, S.H. Thang, Living Free-Radical Polymerization by Reversible Addition–Fragmentation Chain Transfer: The RAFT Process, *Macromolecules* 31(16) (1998) 5559-5562.
- [146] Y.K. Chong, T.P.T. Le, G. Moad, E. Rizzardo, S.H. Thang, A More Versatile Route to Block Copolymers and Other Polymers of Complex Architecture by Living Radical Polymerization: The RAFT Process, *Macromolecules* 32(6) (1999) 2071-2074.
- [147] G. Moad, Reversible addition–fragmentation chain transfer (co)polymerization of conjugated diene monomers: butadiene, isoprene and chloroprene, *Polymer International* 66(1) (2017) 26-41.
- [148] G. Bar-Nes, R. Hall, V. Sharma, M. Gaborieau, D. Lucas, P. Castignolles, R.G. Gilbert, Controlled/living radical polymerization of isoprene and butadiene in emulsion, *European Polymer Journal* 45(11) (2009) 3149-3163.
- [149] R. Wei, Y. Luo, Z. Li, Synthesis of structured nanoparticles of styrene/butadiene block copolymers via RAFT seeded emulsion polymerization, *Polymer* 51(17) (2010) 3879-3886.
- [150] R. Wei, Y. Luo, W. Zeng, F. Wang, S. Xu, Styrene–Butadiene–Styrene Triblock Copolymer Latex via Reversible Addition–Fragmentation Chain Transfer Miniemulsion Polymerization, *Industrial & Engineering Chemistry Research* 51(47) (2012) 15530-15535.

- [151] L. Hlalele, D.R. D'hooge, C.J. Dürr, A. Kaiser, S. Brandau, C. Barner-Kowollik, RAFT-Mediated *ab Initio* Emulsion Copolymerization of 1,3-Butadiene with Acrylonitrile, *Macromolecules* 47(9) (2014) 2820-2829.
- [152] V. Jitchum, S. Perrier, Living Radical Polymerization of Isoprene via the RAFT Process, *Macromolecules* 40(5) (2007) 1408-1412.
- [153] D.S. Germack, K.L. Wooley, Isoprene polymerization via reversible addition fragmentation chain transfer polymerization, *Journal of Polymer Science Part A: Polymer Chemistry* 45(17) (2007) 4100-4108.
- [154] S. Deibert, F. Bandermann, Rate coefficients of the free-radical polymerization of 1,3-butadiene, *Die Makromolekulare Chemie* 194(12) (1993) 3287-3299.
- [155] B. van Büren, F. Brandl, S. Beuermann, Propagation Kinetics of Isoprene Radical Homopolymerization Derived from Pulsed Laser Initiated Polymerizations, *Macromolecular Reaction Engineering* 14(1) (2020) 1900030.
- [156] L. Niedner, G. Kali, Green Engineered Polymers: Solvent Free, Room-Temperature Polymerization of Monomer From a Renewable Resource, Without Utilizing Initiator, *ChemistrySelect* 4(12) (2019) 3495-3499.
- [157] U. Kalita, S. Samanta, S.L. Banerjee, N.C. Das, N.K. Singha, Biobased Thermoplastic Elastomer Based on an SMS Triblock Copolymer Prepared via RAFT Polymerization in Aqueous Medium, *Macromolecules* (2021).
- [158] J.W. Bartels, P.L. Billings, B. Ghosh, M.W. Urban, C.M. Greenlief, K.L. Wooley, Amphiphilic Cross-Linked Networks Produced from the Vulcanization of Nanodomains within Thin Films of Poly(N-vinylpyrrolidinone)-*b*-Poly(isoprene), *Langmuir* 25(16) (2009) 9535-9544.

- [159] J.W. Bartels, S.I. Cauët, P.L. Billings, L.Y. Lin, J. Zhu, C. Fidge, D.J. Pochan, K.L. Wooley, Evaluation of Isoprene Chain Extension from PEO Macromolecular Chain Transfer Agents for the Preparation of Dual, Invertible Block Copolymer Nanoassemblies, *Macromolecules* 43(17) (2010) 7128-7138.
- [160] M. Langer, J. Brandt, A. Lederer, A.S. Goldmann, F.H. Schacher, C. Barner-Kowollik, Amphiphilic block copolymers featuring a reversible hetero Diels-Alder linkage, *Polymer Chemistry* 5(18) (2014) 5330-5338.
- [161] M. Langer, J.O. Mueller, A.S. Goldmann, F.H. Schacher, C. Barner-Kowollik,  $\alpha,\omega$ -Reactive Building Blocks Based on a Dual Functional RAFT Agent for Thermal and Light-Induced Ligation, *ACS Macro Letters* 5(5) (2016) 597-601.
- [162] W.M. Gramlich, G. Theyo, M.A. Hillmyer, Copolymerization of isoprene and hydroxyl containing monomers by controlled radical and emulsion methods, *Polymer Chemistry* 3(6) (2012) 1510-1516.
- [163] X. Fei, J. Wang, J. Zhu, X. Wang, X. Liu, Biobased Poly(ethylene 2,5-furancarboxate): No Longer an Alternative, but an Irreplaceable Polyester in the Polymer Industry, *ACS Sustainable Chemistry & Engineering* 8(23) (2020) 8471-8485.
- [164] S.K. Henning, T. Yoo, H.S. Chao, Farnesene-based macromonomers and methods of making and using the same, Google Patents, 2020.
- [165] R.H. Kollarigowda, S. Abraham, C.D. Montemagno, Antifouling Cellulose Hybrid Biomembrane for Effective Oil/Water Separation, *ACS Applied Materials & Interfaces* 9(35) (2017) 29812-29819.

### 3 Nitroxide-mediated polymerization of bio-based farnesene with a functionalized methacrylate

The manuscript in this chapter was published in *Macromolecular Reaction Engineering* in 2019 (S.B. Luk, M. Maric, Nitroxide-mediated polymerization of bio-based farnesene with a functionalized methacrylate, *Macromolecular Reaction Engineering* 13 (2019) 1800080) [38]. This was the first study on the NMP of farnesene using a succinimidyl-modified commercial BlocBuilder initiator (NHS-BB) and a newly developed alkoxyamine named Dispolreg 007 (D7). Successful statistical copolymerizations of Far and an epoxy-functionalized glycidyl methacrylate (GMA) were done at varying molar compositions using NHS-BB at 120 °C, and their reactivity ratios were determined using the Mayo-Lewis equation ( $r_{\text{Far}} = 0.54 \pm 0.04$  and  $r_{\text{GMA}} = 0.24 \pm 0.02$ ). Nevertheless, there are several key takeaways from this chapter. Copolymerizations using NHS-BB showed lack of control at high compositions of GMA resulting in high dispersity of polymer chains and poor chain-end fidelity. An equimolar copolymerization of Far and GMA done with D7 showed good control but led to broad and bimodal molecular weight distribution, which was attributed the large difference in propagation rates of the respective monomers and slow initiation of D7. Homopolymerization of Far was successfully done using both NHS-BB and D7, but chain-extension with GMA using macroinitiators made with D7 showed better linear polymer chain growth despite having higher dispersity, whereas macroinitiators made with NHS-BB still required 10 mol% Far and had some irreversible termination. This publication concludes that D7 is not ideal for statistical copolymerization of monomers with such diverse kinetics such as Far and GMA and leads to polymer chains with non-homogeneous composition, but it is more suitable for homopolymerization and block copolymer synthesis. The supporting information of this publication is included in Appendix A, and the figures and tables included in Appendix A are referred to as Figure A-X and Table A-X in this chapter.

### 3.1 Abstract

Farnesene (Far) is a bio-based terpene monomer that is similar in structure to commercially used dienes like butadiene and isoprene. Nitroxide-mediated polymerization (NMP) is adept for the polymerization of dienes, but not particularly effective at controlling the polymerization of methacrylates using commercial nitroxides. In this study, Far is statistically copolymerized with a functional methacrylate, glycidyl methacrylate (GMA), by NMP using *N*-succinimidyl modified commercial BlocBuilder (NHS-BB) initiator. Reactivity ratios are determined to be  $r_{\text{Far}} = 0.54 \pm 0.04$  and  $r_{\text{GMA}} = 0.24 \pm 0.02$ . The ability of the poly(Far-*stat*-GMA) chains to reinitiate for chain extension with styrene showed a clear shift in molecular weight and monomodal distribution. Copolymerizations using a new alkoxyamine, Dispolreg 007 (D7), is explored as it is shown to homopolymerize methacrylates, but not yet reported for statistical copolymerizations. Bimodal molecular weight distributions are observed when an equimolar ratio of Far and GMA is copolymerized with D7 due to slow decomposition of the initiator, but chain ends are active as shown by successful chain extension with styrene. Both NHS-BB and D7 initiators are used to synthesize poly[Far-*b*-(GMA-*stat*-Far)] and poly(Far-*b*-GMA) diblock copolymers. While the NHS-BB initiated polymer chains have lower dispersity, D7 exhibits more linear polymerization kinetics and maintains more active chain ends.

### 3.2 Introduction

Dienes (e.g., butadiene and isoprene) are industrially important monomers in making rubbery materials for applications like gasket and automotive parts, gloves and footwear, sealants, impact modifiers, and asphalt modifiers [1-4]. Poly(butadiene) and poly(isoprene) have low glass transition temperatures ( $T_g$ ) of  $-100$  and  $-70$  °C, respectively [5], and are copolymerized with monomers or blended with thermoplastic resins based on styrene and/or acrylonitrile to impart viscoelastic properties to the material [6-8]. Styrene-butadiene rubber (SBR) and acrylonitrile-butadiene rubber (NBR) are typically synthesized industrially by emulsion conventional radical polymerization using redox catalysts or free radical initiators [9, 10], but there are also cases of living/controlled radical polymerization (LRP/CRP) of SBR and NBR that provide polymers with controlled architectures [11, 12]. Styrene-butadiene-styrene (SBS) and styrene-isoprene-styrene

(SIS) triblock copolymers have long been commercialized too, such as the Kraton family of thermoplastic elastomers, which are made by anionic polymerization [13, 14].

While many industrial applications use free radical polymerization, CRP precisely controls the molecular architecture of polymer chains, therefore making homopolymers, diblock and triblock copolymers with narrow molecular weight distributions (MWDs) and low dispersity [15]. Ionic polymerization is a truly “living” method, but it is intolerant to functional monomers and impurities [16]. CRP, more properly defined as reversible deactivation radical polymerization (RDRP), is a newer, more versatile technique to control the polymerization of free radicals. It utilizes activation–deactivation equilibrium or reversible chain transfer to suppress irreversible termination such that the propagating radical is primarily in its dormant state [17]. Amongst the several types of RDRP, atom transfer radical polymerization (ATRP) [18-20] and reversible addition–fragmentation transfer (RAFT) [21-23] can polymerize a wide variety of functional monomers like vinyl esters and (meth)acrylates. This study will focus on nitroxide-mediated polymerization (NMP) as it is particularly adept for polymerization of styrene-diene systems [24-26].

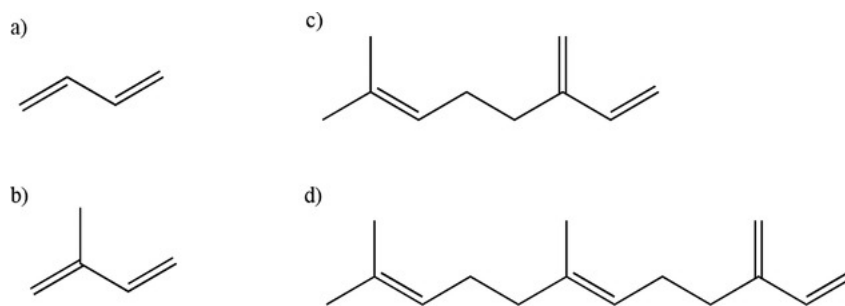
NMP is able to polymerize functionalized styrene and acrylate monomers successfully [27], however it is limited in its ability to maintain active chain ends in the polymerization of methacrylates [28, 29]. It was discovered that the rate of dissociation ( $k_d$ ) is very large because of steric stabilization of the propagating methacrylate radical, and the rate of combination ( $k_c$ ) is very low due to steric hindrance provided by the bulky SG1-nitroxide (*N-tert-butyl-N*-[1-diethylphosphono-(2,2-dimethylpropyl)] nitroxide). Consequently, the activation–deactivation equilibrium ( $K_{eq} = k_d/k_c$ ) is high, resulting in termination by disproportionation [30]. To overcome this, small amounts of controlling comonomer like styrene or acrylonitrile can be added to effectively lower  $K_{eq}$  [28, 31]. Furthermore, the SG1-based nitroxide, BlocBuilder, can be modified with an *N*-succinimidyl ester group (*N*-succinimidyl modified commercial BlocBuilder [NHS-BB]) to better control the polymerization of methacrylates [32], and successful polymerization of various methacrylates was done using SG1-nitroxides with 5–10 mol% of styrene [33-35].

Several alternative initiators have been investigated for the homopolymerization of methacrylates as well. 2,2-Diphenyl-3-phenylimino-2,3-dihydroindol-1-yloxy nitroxide (DPAIO)-based alkoxyamine was able to homopolymerize methyl methacrylate (MMA) to high conversion with low dispersity, but was not able to polymerize acrylates or styrene in ensuing chain extensions [36]. An *N*-phenylalkoxyamine initiator (*N*-(1-methyl-(1-(4-nitrophenoxy)carbonyl) ethoxy)-*N*-(1-methyl-(1-(4-nitrophenoxy)carbonyl)ethyl)benzenamine) was also able to homopolymerize MMA but only to low conversion ( $X < 50\%$ ) [37]. More recently, a new class of alkoxyamines was developed that is able to homopolymerize methacrylates without using controlling comonomer in solution and miniemulsion polymerization [38-40]. This new alkoxyamine, 3-(((2-cyanopropan-2-yl)oxy)(cyclohexyl)amino)-2,2-dimethyl-3-phenylpropanenitrile, which the authors have named Dispolreg 007 (D7), has a higher  $k_c$ , therefore exhibiting better control of the polymerization of methacrylates with minimal irreversible termination and successful chain extension with *n*-butyl acrylate.

It is advantageous to incorporate methacrylates into poly(diene) materials because methacrylates can have a broad range of  $T_g$ s—for example, poly(isobornyl methacrylate) has  $T_g \approx 190$  °C [41] and poly(glycidyl methacrylate) has a  $T_g$  of 80 °C, while poly(butyl methacrylate) has  $T_g = 20$  °C [42]. Additionally, many methacrylates possess functional groups which can be incorporated into such hybrid materials. For example, they can act as compatibilizers for polymer blending. Glycidyl methacrylate (GMA) has been used to functionalize polymers (either by peroxide grafting or by a priori copolymerization) which can then be used to compatibilize immiscible polymer blends by grafting or reactive extrusion, where the epoxy group of GMA reacts with the carboxyl or hydroxyl groups of the immiscible polymer to form an in situ copolymer preventing phase separation [43-45].

Moreover, there is increasing interest in replacing petroleum-derived monomers with renewable sources. Terpene-based monomers such as myrcene and farnesene (Far) have emerged as one possible source providing an alternative to traditionally petroleum-derived butadiene and isoprene monomers (Scheme 3-1). Myrcene and Far are both found in nature, but can also be produced by pyrolysis of  $\beta$ -pinene [46] and microbial pathways from glucose [47], respectively. Although, there are new bio-based pathways to synthesize butadiene and isoprene [48-50], myrcene and Far are

made up of multiple isoprene units, which can provide different rheological properties. It was shown that bottlebrush polymers with densely packed, long side chains improve elastic properties [51, 52]. Furthermore, myrcene and Far are nonvolatile compounds so they can be polymerized in atmospheric conditions without using pressurized vessels as would be necessary for isoprene or butadiene.



Scheme 3-1. Chemical structures of a) 1,3-butadiene, b) isoprene, c) myrcene, and d) farnesene.

Myrcene has been copolymerized with monomers typically used for thermoplastics like  $\alpha$ -methyl-*p*-methylstyrene [53] and poly(lactic acid) [54] by anionic polymerization, and more recently copolymerized with GMA and styrene by NMP [55, 56]. Far has been homopolymerized by ionic polymerization [57], but polymerization by RDRP has not yet been reported. This study investigates NMP of bio-based Far with incorporation of functional GMA. The homopolymerization of Far and copolymerization with GMA using NHS-BB were done to determine reactivity ratios and hence expected microstructure. The ability of the D7 to control the copolymerization of Far and GMA was also examined, and the kinetics were thoroughly discussed and contrasted with SG1-nitroxides. Poly(Far-*b*-GMA) diblock copolymers were made using both NHS-BB and D7, and discussions regarding the important parameters governing microstructural control (e.g., molecular weight vs conversion, dispersity, and chain-end fidelity) were compared.

### 3.3 Experimental Section

#### 3.3.1 Materials

Trans- $\beta$ -Far, known as Biofene (Far,  $\geq 95\%$ ) was obtained from Amyris. GMA (97%) and styrene (St,  $\geq 99\%$ ) monomers were purchased from Millipore Sigma. Monomers were purified using 1.0

g of aluminum oxide (basic Al<sub>2</sub>O<sub>3</sub>, activated, Brockmann I) and 0.05 g calcium hydride (CaH<sub>2</sub>, ≥90%) per 50 mL of monomer, which were used as purchased from Millipore Sigma. 2-([tert-Butyl[1-(diethoxy-phosphoryl)-2,2-dimethylpropyl]amino]oxy)-2-methylpropionic acid or BlocBuilder was purchased from Arkema and modified with an *N*-succinimidyl ester group following a method used in the literature to synthesize 2-methyl-2-[*N*-tert-butyl-*N*-(1-diethoxyphosphoryl-2,2-dimethylpropyl)-aminoxy]-*N*-propionyloxysuccinimide or NHS-BlocBuilder (NHS-BB) [58]. 3-(((2-Cyanopropan-2-yl)oxy)(cyclohexyl)amino)-2,2-dimethyl-3-phenylpropanenitrile, D7, was synthesized according to the method described by Ballard et al [38]. Toluene (≥99%), methanol (MeOH, ≥99%), and tetrahydrofuran (THF, 99.9% HPLC grade) were obtained from Fisher Scientific and used as received. Deuterated chloroform (CDCl<sub>3</sub>, 99.9% D) was purchased from Cambridge Isotope Laboratories, USA and used as received.

### 3.3.2 Synthesis of Poly(*Far-stat*-GMA) Copolymers

Statistical copolymers of *Far* and GMA were synthesized via NMP using NHS-BB and D7 initiators. Experiments for various molar ratios of *Far* and GMA were done in bulk and the amount of initiator was calculated based on a target molecular weight of 30 000 g mol<sup>-1</sup>. See Table A-1, Appendix A for quantities of initiator and monomers for *Far*/GMA copolymerizations. Reaction mixtures were prepared in a 10 mL three-neck round-bottom flask, stirred, and bubbled with N<sub>2</sub> for 30 min. They were heated up to reaction temperature on a heating mantle with N<sub>2</sub> bubbling on top to ensure an oxygen-free environment with continuous stirring throughout the reaction. Samples were taken at various time points using a 1 mL syringe for conversion and molecular weight analysis. Polymers were purified by precipitation using methanol and dried in the vacuum oven at room temperature overnight.

### 3.3.3 Chain Extension of Poly(*Far-stat*-GMA) Macroinitiators

Several poly(*Far-stat*-GMA) macroinitiators were used for chain extension: *Far*-rich and GMA-rich macroinitiators—both synthesized using NHS-BB, and equimolar poly(*Far-stat*-GMA) synthesized using D7. The syntheses of the macroinitiators were described previously for *Far*/GMA random copolymers. After purification, the macroinitiators were dissolved in toluene and 3:1 mass ratio of styrene to macroinitiator was added to the solution (50 wt% monomer in toluene). The reaction mixture was bubbled with N<sub>2</sub> for 30 min and remained under N<sub>2</sub> atmosphere

throughout the reaction with stirring. The chain-extension reaction was done at 110 °C and samples were taken at various time points using a 1 mL syringe for conversion and molecular weight analysis. The final polymer was precipitated again using methanol and dried in the vacuum oven at room temperature overnight.

### 3.3.4 Synthesis of Poly(Far-*b*-GMA) Block Copolymers

Block copolymers were made by first synthesizing the Far homopolymer block using NHS-BB or D7 initiators in bulk at 120 °C. The polymerization was typically stopped at a conversion of <50% to ensure high chain-end fidelity for chain extension. The polymer was purified by precipitation in methanol and dried in a vacuum oven at room temperature overnight. The poly(Far) macroinitiator was dissolved in toluene and chain extended with GMA or monomer mixture of 90 mol% GMA and 10 mol% Far (50 wt% monomer in toluene) at 110 °C. Reaction mixtures were bubbled with N<sub>2</sub> for 30 min and remained under N<sub>2</sub> atmosphere throughout the reaction with stirring. Samples were taken using a 1 mL syringe for conversion and molecular weight analysis. The final polymer was precipitated again using methanol and dried in the vacuum oven at room temperature overnight.

### 3.3.5 Polymer Characterization

Overall monomer conversion was determined by proton nuclear magnetic resonance (<sup>1</sup>H NMR, 16 scans) using a Varian/Agilent 500 MHz spectrometer. All NMR samples were prepared in deuterated chloroform (CDCl<sub>3</sub>). Homopolymerization of Far was mostly by 1,4 addition with ≈3 mol% of 1,2 addition as seen in Figure A-1, Supporting Information. The conversion of Far ( $X_{\text{Far}}$ ) was calculated using Equation 1 and  $A_{\delta}$  is the area of proton peak integration. The Far monomer proton at  $\delta = 6.4$  ppm and the two singlets (three methyl groups, 9H) at  $\delta = 1.65$  ppm were used to determine  $X_{\text{Far}}$ . Conversion of GMA ( $X_{\text{GMA}}$ ) was calculated using Equation 2 using the two vinyl GMA monomer protons at  $\delta = 6.2$  and 5.6 ppm, and the peaks at  $\delta = 4.4, 3.9, 2.8, 2.6$  ppm, which include both monomer and polymer protons each. The overall conversion ( $X$ ) for copolymerization of Far and GMA calculated using Equation 3 was an average of the two monomer conversions based on the initial monomer compositions ( $f_{\text{Far},0}$  and  $f_{\text{GMA},0}$ ). See Figure A-2, Supporting Information for the NMR spectra of Far/GMA copolymerization.

$$X_{Far} = 1 - \frac{A_{6.4}}{\frac{A_{1.65}}{9}} \quad (1)$$

$$X_{GMA} = 1 - \frac{\frac{A_{6.2} + A_{5.6}}{2}}{\frac{A_{4.4} + A_{3.9} + A_{2.8} + A_{2.6}}{4}} \quad (2)$$

$$X = f_{Far,0}X_{Far} + f_{GMA,0}X_{GMA} \quad (3)$$

Monomer conversion of styrene ( $X_{St}$ ) for chain extension of poly(Far-*ran*-GMA) macroinitiators were determined by  $^1\text{H}$  NMR as shown in Figure A-3, Supporting Information. The vinyl protons of styrene were at  $\delta = 5.3$  and  $5.8$  ppm. For the conversion calculation, the vinyl proton at  $\delta = 5.8$  ppm was set to an normalized area of 1. Because the chain-extension reactions were done in toluene, the aromatic protons of toluene and styrene overlap in the  $\delta = 7-7.5$  ppm region and the polymer protons were also in the range of  $\delta = 6-7.5$  ppm. Therefore, the singlet at  $\delta = 2.4$  ppm (toluene methyl group, 3H) was accounted for and subtracted from the total number of protons contributed by toluene and styrene ( $\delta = 6.8$  ppm, 1H) to determine the conversion as shown in Equation 4.

$$X_{St} = 1 - \frac{\frac{A_{5.8} + A_{5.3}}{2}}{\frac{(A_{6-7.6} - 1 - \frac{A_{2.4}}{3} \times 5)}{5}} \quad (4)$$

Number average molecular weight ( $M_n$ ) and dispersity ( $\mathcal{D} = M_w/M_n$ ) of polymer samples were measured using gel permeation chromatography (GPC, Water Breeze) with HPLC grade THF as an eluent at a flow rate of  $0.3 \text{ mL min}^{-1}$ . The GPC has three Waters Styragel HR columns (HR1 with a molecular weight measurement range of  $10^2$  to  $5 \times 10^3 \text{ g mol}^{-1}$ , HR2 with a molecular weight measurement range of  $5 \times 10^2$  to  $2 \times 10^4 \text{ g mol}^{-1}$ , and HR4 with a molecular weight measurement range of  $5 \times 10^3$  to  $6 \times 10^5 \text{ g mol}^{-1}$ ), a guard column, and a refractive index (RI 2414) detector. The columns were heated to  $40 \text{ }^\circ\text{C}$  during analysis. The molecular weights were determined relative to poly(methyl methacrylate) (PMMA) calibration standards from Varian Inc.

(ranging from 875 to 1677 000 g mol<sup>-1</sup>). The reported molecular weights were all relative to the PMMA standards and not adjusted with Mark–Houwink parameters.

### 3.4 Results and Discussion

#### 3.4.1 Statistical Copolymerization of Far/GMA Using NHS-BlocBuilder

The homopolymerization of methacrylates by NMP is generally done at 90–100 °C due to the slow rate of recombination ( $k_c$ ) between the nitroxide and methacrylate radical and fast propagation rate ( $k_p$ ) [28, 29, 31]. Lower temperature is ideal for limiting the formation of inactive chain ends by irreversible termination. However, the homopolymerization of Far is much slower in comparison, and showed signs of chain transfer below 120 °C. The statistical copolymerizations of Far and GMA were all done at 120 °C initially at seven different monomer compositions ( $f_{\text{Far},0} = 0.1\text{--}0.9$ ) in bulk using NHS-BB. In GMA-rich compositions ( $f_{\text{Far},0} = 0.1$  and  $0.2$ ), the conversion versus time and the number average molecular weight ( $M_n$ ) versus conversion plots were not linear, and dispersity was high ( $\mathcal{D} > 1.6$ ) as shown in Figures A-4 and A-5, Supporting Information. This indicated the polymerizations were not well controlled by the nitroxide, and polymer chains were not propagating after a certain conversion because the chain ends were no longer active. The increase in dispersity was further indication that the chains have been irreversibly terminated.

The GMA-rich copolymerizations were repeated at 90 °C, and were much more controlled than at 120 °C. As seen in Figure 3-1a, the conversion versus time plots for the GMA-rich copolymerizations at 90 °C show a linear correlation with reaction time. The GMA-rich polymerizations at high conversion ( $\approx 80\%$ ) became very viscous and accelerated the reaction, therefore the last conversion data did not follow the linear trend and was not included in Figure 3-1a. However, the  $M_n$  versus conversion plots in Figure 3-2a including the high conversion data points were linear. The more Far-rich copolymerizations done at 120 °C are shown in Figure 3-1b and also show linear correlations. The linearity of these copolymerizations show that the majority of the polymer chains remained active throughout the reaction even to higher conversions, as the solid trend line was extended to the end of the reactions.

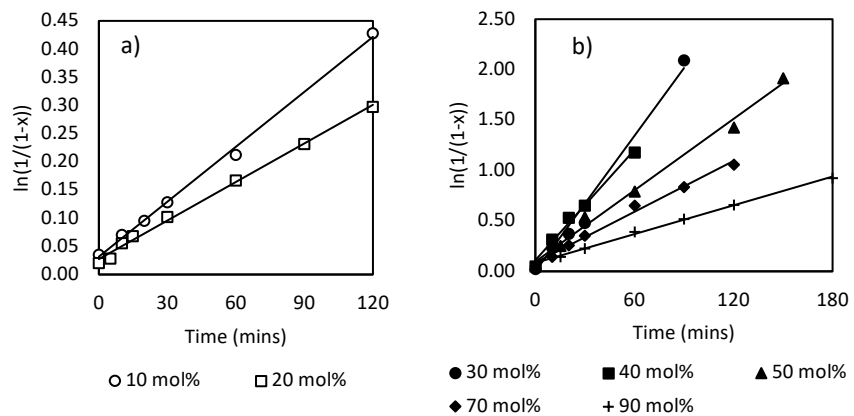


Figure 3-1. Linearized conversion as a function of reaction time for the random copolymerizations of Far/GMA at various Far compositions at a) 90 and b) 120 °C in bulk using NHS-BB.

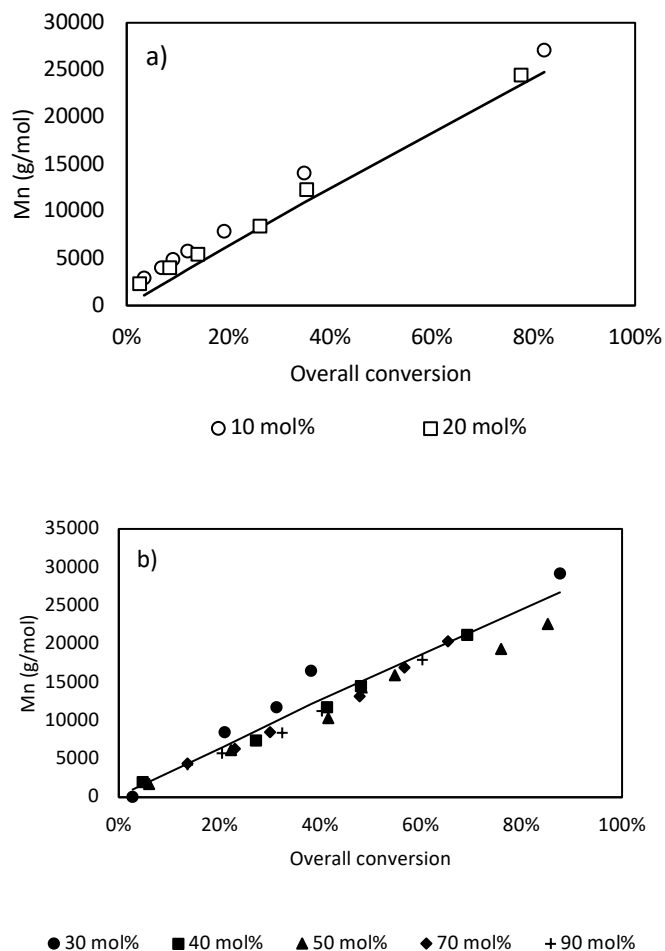


Figure 3-2. Number averaged molecular weight ( $M_n$ ) as a function of conversion for random copolymerizations of Far/GMA at various Far compositions at a) 90 and b) 120 °C in bulk using NHS-BB. The solid lines represent the theoretical molecular weight calculated from the conversion based on a target molecular weight of 30 000 g mol<sup>-1</sup>.

Molecular weight of the Far/GMA copolymerizations increased linearly with conversion as well, as shown in Figure 3-2. The fast increase of  $\bar{D}$  in Figure 3-3a suggests low initiator efficiency as the initial high  $\bar{D}$  means not all chains were initiated at the same time. The final dispersity at  $f_{\text{far},0} = 0.1$  and 90 °C in Figure 3-3a was quite high ( $\approx 1.8$ ) likely due to the high viscosity at the end of the reaction leading to irreversible termination. At 120 °C, the  $M_n$  values were all very close to the theoretical  $M_n$  values with the exception of  $f_{\text{far},0} = 0.3$ , where the growth of polymer chains slightly deviated from linearity. However, looking at the  $\bar{D}$  values in Figure 3-3b, the highest  $\bar{D}$  was  $\approx 1.5$ .

Linear increase in molecular weight and low  $\bar{D}$  suggest that most chains have active chain ends and are growing simultaneously at a controlled rate.

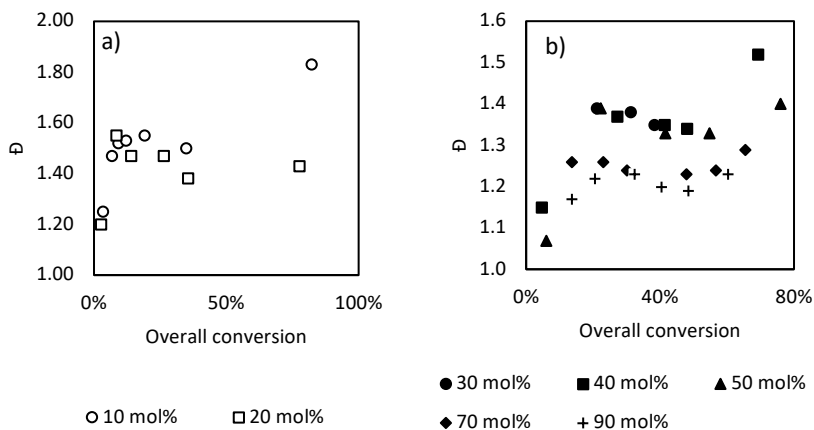


Figure 3-3. Dispersity ( $\bar{D}$ ) as a function of overall conversion for random copolymerization of Far/GMA at various Far compositions in bulk at a) 90 and b) 120 °C using NHS-BB.

A limitation of NMP is that the homopolymerization of methacrylates using SG1-based initiators requires 5–10 mol% of controlling comonomer to maintain high chain-end fidelity [32, 34, 35, 59]. Styrene is most commonly used as a controlling comonomer because it effectively lowers the activation–deactivation equilibrium ( $\langle K \rangle$ ) of the nitroxide by penultimate effects [60]. In these statistical Far/GMA copolymerizations, it seems that Far can act as a controlling comonomer for the homopolymerization of GMA by adding 10 mol% of Far at 90 °C, similar to isoprene when randomly copolymerized with methacrylates by NMP [61]. However, further decreasing to 5 mol% Far, the Far/GMA copolymerization resulted in a high fraction of dead chains and high dispersity ( $\approx 1.8$ ).

The apparent rate constant of Far/GMA copolymerization by NMP is proportional to  $\langle k_p \rangle \langle K \rangle$ , which is the product of the average propagation rate coefficient and average activation–deactivation equilibrium constant for Far and GMA. From the slopes of the linearized conversion versus time plots in Figure 3-1,  $\langle k_p \rangle \langle K \rangle$  values can be determined from the theoretical expression for the activation–deactivation equilibrium expression shown in Equation 5, where  $C_0$  is initial concentration of alkoxyamine initiator and  $[N]_0$  is initial concentration of free nitroxide [31].

$$\frac{d\left(\ln\left(\frac{1}{1-X}\right)\right)}{dt} = \langle k_p \rangle \langle K \rangle \frac{C_0}{[N]_0} \quad (5)$$

The concentration of nitroxide can only be assumed to remain constant at low conversion,  $[N]_0 = [N]$ , because of possible irreversible termination of the nitroxide in the latter stages of the polymerization. Therefore, the  $\langle k_p \rangle \langle K \rangle$  values were calculated from the slope determined at  $X < 60\%$ . Furthermore, there was no excess free nitroxide added, so  $C_0/[N]_0 = 1$ . The  $\langle k_p \rangle \langle K \rangle$  values at different initial Far monomer fractions is shown in Figure 3-4 and it is evident that the rate of Far/GMA copolymerization was slowed down by increasing Far content. The  $\langle k_p \rangle \langle K \rangle$  values were also found to significantly decrease when isoprene and myrcene were copolymerized with methacrylates [55, 61]. Because  $\langle k_p \rangle \langle K \rangle$  is a lumped term, the decrease in value can indicate a decrease in the averaged copolymerization propagation rate  $\langle k_p \rangle$  and/or a decrease in the activation–deactivation equilibrium constant  $\langle K \rangle$  depending on the terminal radical unit (Far or GMA).

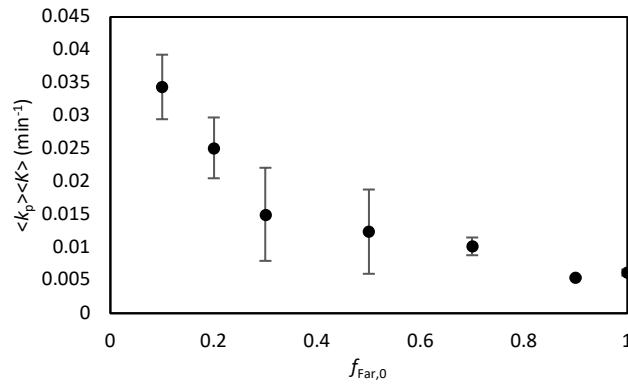


Figure 3-4: Average  $\langle k_p \rangle \langle K \rangle$  as a function of initial Far monomer fraction for Far/GMA statistical copolymerizations using NHS-BB at 120 °C in bulk. The error bars represent 95% confidence intervals.

### 3.4.2 Reactivity Ratios of Far/GMA Statistical Copolymerization

Culminating all the statistical copolymerizations of Far and GMA at different monomer compositions at 120 °C, a Mayo–Lewis plot was made as shown in Figure 3-5. The Mayo–Lewis equation (Equation 6) correlates instantaneous copolymer composition ( $F_i$ ) as a function of comonomer feed composition ( $f_i$ ) to infer the relative reactivity ratios ( $r_i$ ) of species  $i$  [62]. This

assumes the terminal model, meaning the reactivity of the propagating radical is only dependent on the terminal radical unit. If the reactivity ratios are at unity ( $r_1 = r_2 = 1$ ), it indicates that the propagating radical is equally likely to add on the same monomer as the propagating radical (homopropagation) or the other monomer (cross-propagation).

$$F_1 = \frac{r_1 f_1^2 + f_1 f_2}{r_1 f_1^2 + 2f_1 f_2 + r_2 f_2^2} \quad (6)$$

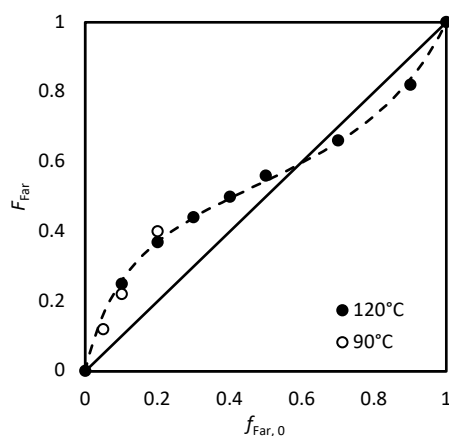


Figure 3-5. Mayo–Lewis plot for random copolymerization of farnesene and GMA in bulk at 120 and 90 °C using NHS-BB. The dashed line is the Mayo–Lewis curve calculated using relative reactivity ratios  $r_{\text{Far}} = 0.54$  and  $r_{\text{GMA}} = 0.24$ . The solid line represents the relative reactivity ratios at unity.

The relative reactivity ratios of Far/GMA copolymerization were estimated by fitting the  $F_{\text{Far}}$  versus  $f_{\text{Far},0}$  data at 120 °C using the Mayo–Lewis equation in MATLAB. The reactivity ratios were determined with 95% confidence intervals to be  $r_{\text{Far}} = 0.54 \pm 0.04$  and  $r_{\text{GMA}} = 0.24 \pm 0.02$ . The cumulative polymer compositions were measured at low conversion ( $X < 15\%$ ) (see Table A-2 in Appendix A) to apply the Mayo–Lewis equation. Both reactivity ratios are  $< 1$ , therefore both Far and GMA have higher cross-propagation rate coefficients than homopropagation. However,  $r_{\text{Far}}$  is about two times higher than  $r_{\text{GMA}}$ , so Far is slightly more preferentially incorporated into the copolymer. The Mayo–Lewis curve has an azeotrope at  $f_{\text{Far},0} \approx 0.62$  and both ratios are  $< 1$ , so the polymer composition is essentially random. Three data points from the 90 °C experiments were included in the Mayo–Lewis plot as well. They were close to the estimated Mayo–Lewis curve

determined at 120 °C, which suggests that reactivity ratios were not greatly affected by temperature.

Other diene/GMA statistical copolymerizations like isoprene/GMA and myrcene/GMA have similar reactivity ratios estimated assuming the terminal model and are summarized in Table 3-1. Interestingly, as the terpene monomer side chains get longer, their reactivity ratios relative to GMA increase. In other words, their homopropagation rate coefficients increase relative to cross-propagation. Myrcene/GMA have almost identical reactivity ratios, and isoprene is less reactive than GMA, whereas Far is more reactive than GMA. However, looking at the diene/MMA systems, dienes are consistently more reactive than MMA.

Table 3-1. Summary of reactivity ratios for butadiene (BD)/MMA, isoprene (IP)/MMA, myrcene (Myr)/MMA, IP/GMA, Myr/GMA, and Far/GMA copolymerizations

	$r_{\text{diene}}$	$r_{\text{MMA}}$
<b>BD/MMA [63]</b>	0.75 ± 0.05	0.25 ± 0.03
<b>IP/MMA [64]</b>	0.78 ± 0.13	0.4 ± 0.1
<b>Myr/MMA [65]</b>	0.44	0.27
	$r_{\text{diene}}$	$r_{\text{GMA}}$
<b>IP/GMA [42]</b>	0.119 ± 0.048	0.248 ± 0.161
<b>Myr/GMA [55]</b>	0.49 ± 0.13	0.50 ± 0.13
<b>Far/GMA</b>	0.54 ± 0.04	0.25 ± 0.02

In copolymerizations of St/GMA and St/MMA, it was concluded that GMA was more preferentially incorporated relative to alkyl methacrylates like MMA due to polarity of the epoxy ester [66]. The polar ester decreases electron density of the double bond, therefore increasing the incorporation of functional methacrylate, which was also observed in the copolymerization of St and 2-hydroxyethyl methacrylate [67]. Nonetheless, all the diene/GMA systems have reactivity ratios <1, so these copolymers are random in composition which indicates the functionality in GMA is well distributed throughout the polymer chain. The statistical copolymerization of Far/GMA using NHS-BB gave insight regarding composition of the polymer chains, chain-end

moiety (Far in Far-rich compositions, and GMA in GMA-rich compositions), and would allow us to compare it to copolymerization with the new alkoxyamine (D7) later.

### 3.4.3 Chain Extension of Poly(Far-*stat*-GMA) Copolymers

To investigate whether the poly(Far-*stat*-GMA) copolymers made with NHS-BB have active chain ends, they were chain extended with styrene at 110 °C in 50 wt% toluene. Two different macroinitiators were synthesized, GMA rich and Far rich, to compare the ability for the macroinitiators of different compositions to be reinitiated for polymerization. The compositions and properties of the macroinitiators are summarized in Table 3-2. The GMA-rich and Far-rich macroinitiators were synthesized with initial monomer fractions  $f_{\text{Far},0} = 0.2$  and 0.8, respectively. After polymerization at  $X < 60\%$ , the actual polymer compositions were  $F_{\text{Far}} = 0.24$  and 0.74, respectively.

Table 3-2. GMA- and Far-rich macroinitiators synthesized in bulk at 120 °C using NHS-BB

Macro-initiator	$f_{\text{Far},0}$	$f_{\text{GMA},0}$	$X$ (%)	$M_n$ (kg/mol)	$\bar{D}$	$F_{\text{Far}}$	$F_{\text{GMA}}$
<b>GMA-rich</b>	0.2	0.8	58.2	23.0	1.63	0.24	0.76
<b>Far-rich</b>	0.8	0.2	56.9	19.2	1.33	0.74	0.26

The  $\bar{D}$  of GMA-rich macroinitiator was fairly high (1.63), because it was synthesized at 120 °C and polymerization of GMA is not as well controlled at high temperatures. After 60 min of chain extension, the molecular weight did not increase very much in the next hour and the  $\bar{D}$  increased to 1.77 as seen in Table A-3, Supporting Information. The high  $\bar{D}$  suggests a significant fraction of the polymer chains were terminated and could not continue to polymerize. This was expected as the GMA-rich macroinitiator started with a high  $\bar{D}$ , with some of the chains already dead, but it was still able to chain extend showing some pseudo-livingness.

The Far-rich macroinitiator had a lower  $\bar{M}_n$  of 1.33, as anticipated, because Far-rich copolymerizations had much better control with the majority of the chains remaining active. The chain-extension reaction with styrene also increased linearly after 2 h, while the  $\bar{M}_n$  remained low with a final  $\bar{M}_n$  of 1.34 shown in Table A-4, Supporting Information. Far-rich macroinitiators were mostly active and chain extended successfully due to high chain-end fidelity.

The MWDs for the chain-extension reactions are shown in Figure 3-6 and there was a clear shift/increase in molecular weight for both GMA- and Far-rich macroinitiators. Both sets of GPC traces showed a small low molecular weight tail, indicating some macroinitiator chains did not chain extend. Nonetheless, both macroinitiators were reinitiated to a high level and continued to polymerize with styrene showing effective chain extension with significant amount of active chain ends.

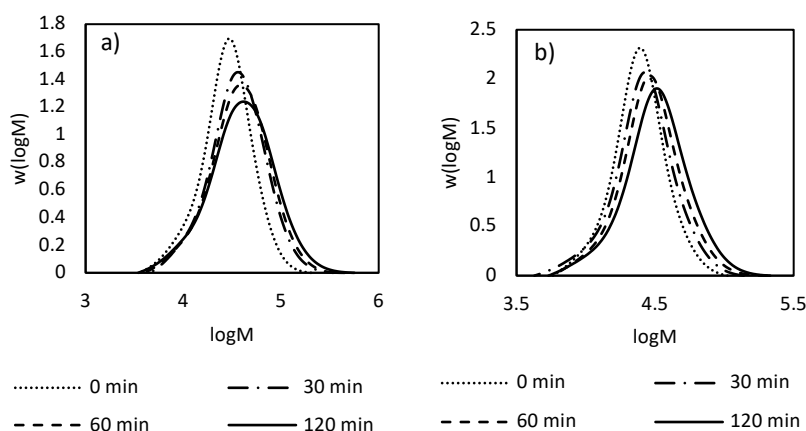
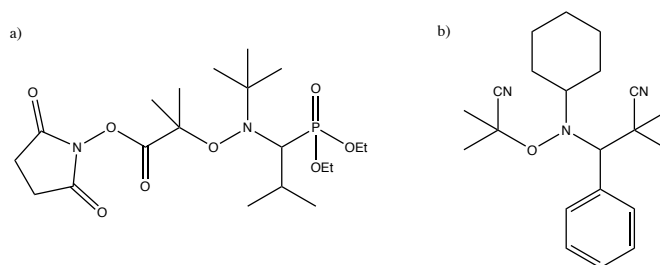


Figure 3-6. GPC traces of chain-extension reactions of a) GMA-rich and b) Far-rich macroinitiators with styrene in 50 wt% toluene at 110 °C.

#### 3.4.4 Statistical Copolymerization of Far/GMA Using Dispolreg 007

NMP of methacrylates using conventional BlocBuilder or NHS-BB is improved by adding a small portion of controlling comonomer [29, 60], and recently a new class of alkoxyamines was developed via a readily scalable process that was able to homopolymerize methacrylates by NMP [38-40]. One alkoxyamine in particular, D7, showed good control over the polymerization of MMA with a fast rate of polymerization, and can be easily synthesized from readily available

reagents [38]. The chemical structures of the two initiators in this study are shown in Scheme 3-2. D7 has a higher  $k_c$  because the steric hindrance provided by the tert-butyl and dimethyl groups on the nitroxide of NHS-BB is replaced with the cyclohexyl and benzyl groups on D7. This new alkoxyamine has not yet been reported for the copolymerization of methacrylates with other types of monomers, therefore it was directly applied to this study for the copolymerization of Far and GMA.



Scheme 3-2. Chemical structures of a) NHS modified BlocBuilder (NHS-BB) and b) D7 alkoxyamine.

Copolymerization of equimolar Far and GMA was done using D7 as the alkoxyamine initiator in bulk at 120 and 90 °C. The GPC traces of the copolymers synthesized using D7 at both temperatures showed a hint of a shoulder in the MWD (Figure 3-7), and increased the  $\bar{D}$  as a result (Figure 3-8). Especially at 120 °C, the  $\bar{D}$  and  $M_n$  were initially high, indicating slow decomposition of the alkoxyamine, which is consistent with the literature [38-40]. As the polymerization progressed, new chains continue to be initiated slowly until the chain lengths approached the theoretical  $M_n$  and consequently  $\bar{D}$  decreased [68]. In previous studies, the slow decomposition was suppressed by increasing the temperature, however, the dispersity at 120 °C was higher than at 90 °C. It is likely that the temperature was too high at 120 °C for the polymerization to remain well controlled, creating more dead chains.

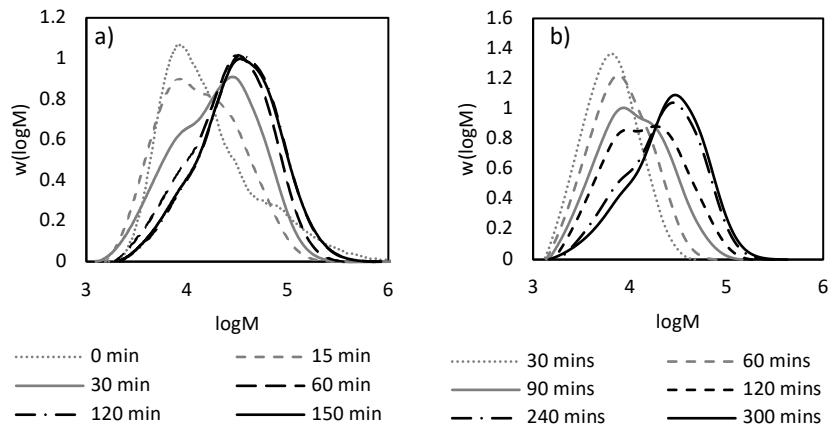


Figure 3-7. GPC traces of 50/50 molar ratio of Far/GMA random copolymerizations in bulk using D7 at a) 120 and b) 90 °C.

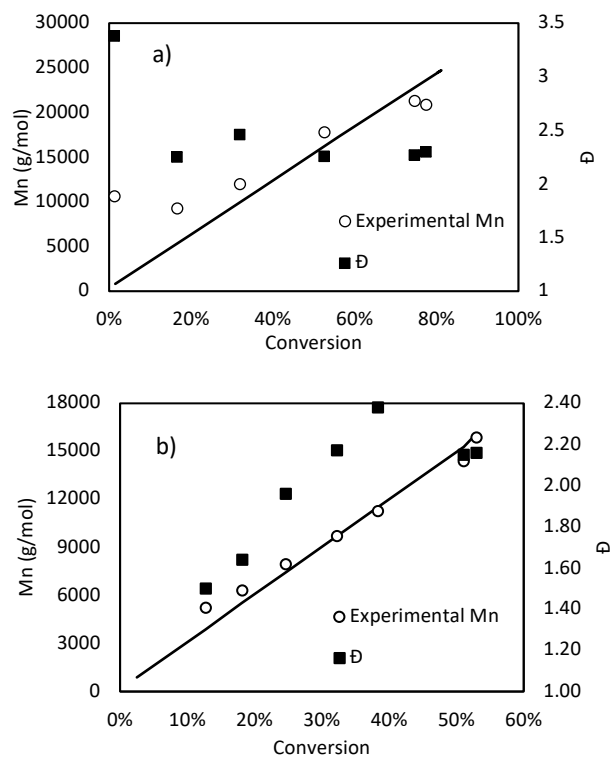


Figure 3-8. Number average molecular weights ( $M_n$ ) and dispersity ( $\bar{D}$ ) plotted as a function of conversion for 50/50 molar ratio of Far/GMA random copolymerizations with D7 in bulk at a) 120 and b) 90 °C. The solid line is the theoretical  $M_n$  calculated from the conversion based on a target molecular weight of 30 000 g mol<sup>-1</sup>.

Despite the slow decomposition, homopolymerization of MMA and n-butyl methacrylate using D7 did not result in a shoulder in the MWD, only increasing the  $\bar{M}_w$  [39, 40]. Furthermore, irreversible termination of chains in copolymerizations of Far and GMA using NHS-BB in GMA-rich compositions broadened the MWD and created a low molecular weight tail, but not a shoulder. The Far/GMA copolymers synthesized using D7 had more of a shoulder at 90 °C than at 120 °C, so the apparent shoulder in the MWD is not due to irreversible termination, which should be more prominent at higher temperatures. The shoulder in the MWD (or bimodal distribution) suggests there are two populations of polymer chains that are distinctly different in chain length, which was not seen in homopolymerizations using D7 or copolymerizations using NHS-BB.

In Figure 3-9, the MWD for 50/50 Far/GMA copolymer is overlaid with the MWDs of Far and GMA homopolymers all synthesized using D7 at 90 °C. The shoulder of the copolymer matches the peak of the Far homopolymer, and the taller peak of the copolymer matches the peak of the GMA homopolymer. This seems to suggest that the two populations of polymer chains are different in length and in composition, where the shorter chains are Far rich and the longer chains are GMA rich.

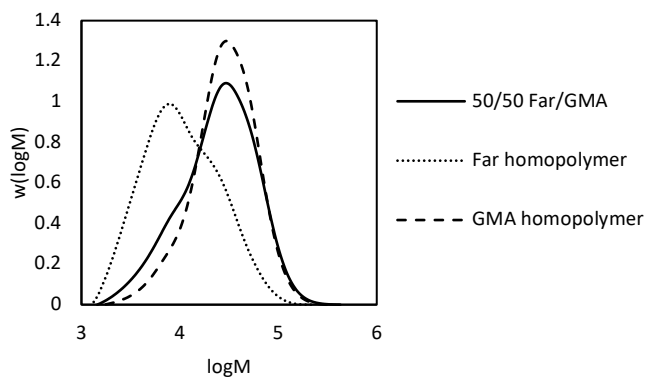


Figure 3-9. GPC traces of 50/50 molar ratio of Far/GMA random copolymer, farnesene homopolymer, and GMA homopolymer at 90 °C in bulk using D7.

In a study investigating nitroxide-mediated copolymerization, copolymer composition was found to deviate from the terminal model largely due to asymmetry of the copolymerization parameters. This is especially evident before the activation–deactivation equilibrium (quasi-equilibrium

condition or QEC) is established [69]. The rate at which the QEC is established relative to cross-propagation is important to consider in all types of RDRP including ATRP [70, 71] and RAFT polymerizations [72].

The Far and GMA reactivity ratios obtained earlier, using NHS-BB initiator and assuming a terminal model, were  $r_{\text{Far}} = 0.54$  and  $r_{\text{GMA}} = 0.24$ , which means the cross-propagation coefficients are two and four times higher than the homopropagation coefficients for Far and GMA, respectively. Furthermore, the rate of decomposition for D7 ( $k_{\text{d},90\text{C}} = 0.001 \text{ s}^{-1}$ ) is much slower than BlocBuilder ( $k_{\text{d},90\text{C}} = 0.046 \text{ s}^{-1}$ ) [38]. The slow rate of decomposition limits the source of radicals, which delays the rate at which QEC is established. Before QEC is established, the radical populations are predetermined by the cross-propagation kinetics [69]. Because D7 has a slow rate of decomposition and both Far and GMA tend to cross-propagate, these Far/GMA copolymers synthesized using D7 do not have good chain-to-chain compositional homogeneity.

The averaged propagation rate coefficient for isoprene and GMA copolymerization was slowed down significantly compared to the homopolymerization of GMA by free radical polymerization ( $k_{\text{pcop}} = 42 \text{ L mol}^{-1} \text{ s}^{-1}$  at  $f_{\text{GMA},0} = 0.24$  versus  $k_{\text{p,GMA}} = 600 \text{ L mol}^{-1} \text{ s}^{-1}$  at  $25 \text{ }^\circ\text{C}$ ) [73]. Propagation coefficients were not obtained for Far/GMA, but as seen previously the  $\langle k_{\text{p}} \rangle \langle K \rangle$  values decreased significantly by increasing Far monomer composition. This suggests that the homopropagation of Far is much slower than GMA, and Far is slightly more prone to homopropagation than GMA according to their reactivity ratios.

Therefore, several factors can be used to rationalize the bimodal distribution of the Far/GMA copolymers with D7. Far monomers were initiated, and when they did homopropagate, they grew very slowly into short, Far-rich chains. GMA monomers were also initiated, and although they did not homopropagate as much, the homopropagation was very fast and grew into long, GMA-rich chains. Both of these populations were established pre-QEC, and continued to polymerize in a controlled fashion once the nitroxide population has stabilized. The bimodal distribution could also be due to a difference in initiation rate for Far and GMA monomers and/or a large difference in equilibrium constants for Far and GMA propagating radicals ( $K_{\text{Far}}$  and  $K_{\text{GMA}}$ ). However, further kinetic studies will need to be done to verify these justifications.

Nonetheless, poly(Far-*stat*-GMA) copolymer made with D7 was successfully chain extended with styrene at 110 °C in 50 wt% toluene. This further indicates the shorter chains were not formed due to irreversible termination, because they were reinitiated and continued to polymerize with styrene. In fact, the dispersity decreased from 2.07 initially to 1.80 after 3 h, as  $M_n$  increased from 19 to 30 kg mol<sup>-1</sup>. It is evident from the GPC traces in Figure 3-10 that the shoulder eventually disappeared, and the  $\bar{M}$  became lower.

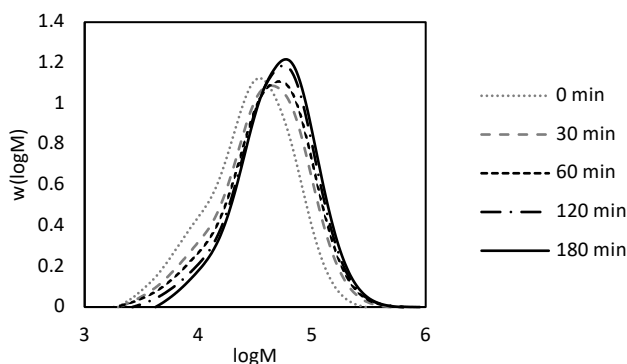


Figure 3-10. GPC traces for chain extension of 50/50 molar ratio of Far/GMA macroinitiator using D7 with styrene in 50 wt% toluene at 110 °C.

### 3.4.5 Block Copolymers Using NHS-BlocBuilder versus D7

CRP is well known to tightly control chain-to-chain composition and molecular structure of polymer chains. Styrene-*b*-acrylic acid (PS-*b*-PAA) block copolymers were made by NMP with precisely controlled dispersity and block lengths to use as stabilizers in emulsion polymerization [74]. It was also shown that these surfactants do not require low dispersity to create a stable emulsion [75]. Therefore, the synthesis of Far-*b*-GMA diblock copolymers was investigated using both NHS-BB and D7 initiators. First, the Far homopolymer block was synthesized using NHS-BB in bulk at 120 °C, and the Far-NHS macroinitiator was used for two different chain-extension reactions with GMA. Another Far homopolymer macroinitiator was synthesized using D7 (Far-D7) in the same conditions for chain extension with GMA. The properties of the two poly(Far) macroinitiators are summarized in Table 3-3. The homopolymerization of Far using NHS-BB was well controlled as seen in Figure A-6, Supporting Information resulting in a low  $\bar{D}$  of 1.17. The homopolymerization of Far using D7 also showed linear chain growth with conversion as seen in

Figure A-7, Supporting Information, but is higher in  $\bar{D}$  and molecular weight due to the slow initiation of D7.

Table 3-3. Summary of poly(Far) macroinitiators using NHS-BB and D7 synthesized in bulk at 120 °C

Macroinitiator	X (%)	$M_n$ (g/mol)	$\bar{D}$
Far-NHS	38	9100	1.17
Far-D7	45	18900	1.60

Far-NHS was first chain extended with GMA without any controlling comonomer at 110 °C in 50 wt% toluene. The polymerization rate was fast and molecular weight increased quickly after 90 min. When Far-NHS was chain extended with GMA and 10 mol% Far (acting controlling comonomer), the final  $\bar{D}$  is slightly lower than without Far, suggesting less irreversible termination. The dispersity of the Far-NHS chain extensions with and without Far are 1.50 and 1.80 (Table 3-4), respectively, so adding 10 mol% Far did aid in controlling the polymerization of GMA. The GPC traces for both chain extensions of Far-NHS in Figure 3-11 show that most chains were able to reinitiate and continued to polymerize throughout the reaction.

Table 3-4. Chain extension of poly(Far) macroinitiators to make Far-*b*-GMA diblock copolymers. Cumulative polymer composition ( $F_{Far}$  and  $F_{GMA}$ ) were determined by  $^1H$  NMR

Macroinitiator	$f_{Far,0}$	$f_{GMA,0}$	$M_n$ (g/mol)	$\bar{D}$	$F_{Far}$	$F_{GMA}$
Far-NHS	0	1	48100	1.80	0.38	0.62
Far-NHS	0.1	0.9	35100	1.50	0.63	0.37
Far-D7	0	1	44756	3.07	0.35	0.65

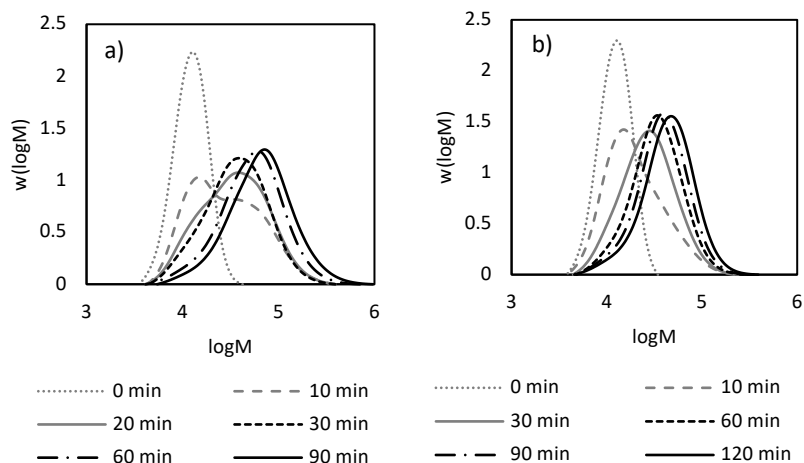


Figure 3-11. GPC traces of Far-NHS macroinitiator chain extension with a) GMA and b) 10 mol% Far and 90 mol% GMA in 50 wt% toluene at 110 °C.

A poly(Far) macroinitiator was synthesized with D7 initiator to examine whether it would also chain extend with GMA. Similarly, it was done in 50 wt% toluene at 110 °C. Looking at the GPC traces in Figure 3-12, the majority of the chains did chain extend as seen by the shift in the MWDs. There is a more evident high molecular weight tail compared to the chain extensions using Far-NHS macroinitiator resulting in a very high final  $\bar{M}_w$  of 3.07 as seen in Table 3-4. The dispersity of Far-D7 was high to begin with because of the slow initiation of D7, however, it seems the reinitiation of Far-D7 macroinitiator is also slow therefore further increasing the dispersity.

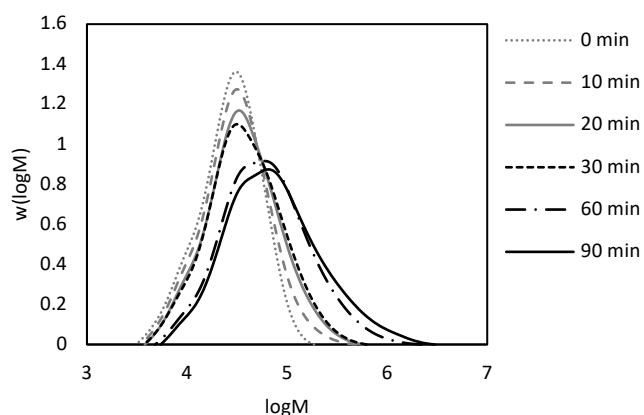


Figure 3-12. GPC traces of Far-D7 macroinitiator chain extension with GMA in 50 wt% toluene at 90 °C.

It may appear that chain extension using D7 resulted in less active chain ends because of the high final  $\bar{D}$  compared to chain extensions done with NHS-BB. However, looking at the increase of molecular weight with conversion in Figure 3-13, the chain extensions of Far-NHS deviated more from linearity than chain extension of Far-D7. With Far-NHS, molecular weight did not increase as linearly, indicating some degree of irreversible termination, whereas Far-D7 increased linearly in molecular weight meaning most of the chains continued to polymerize.

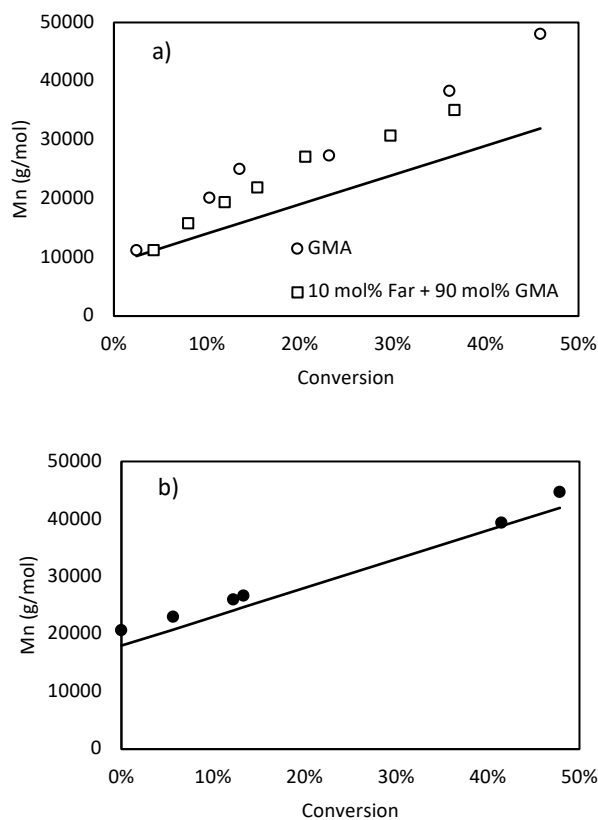


Figure 3-13. Molecular weight ( $M_n$ ) and dispersity ( $\bar{D}$ ) versus conversion plots for chain extension of a) Far-NHS with GMA with and without 10 mol% Far and b) chain extension of Far-D7 with GMA at 110 °C and 50 wt% toluene.

The new alkoxyamine, D7, was designed to better control the polymerization of methacrylates. In the chain extension of Far-D7, it did exhibit better control over the polymerization of GMA as most chain ends remained active. The chain extensions done with NHS-BB was not as well controlled and adding 10 mol% of Far in the feed improved the chain extension with GMA slightly. The diblock Far-*b*-GMA copolymers made with D7 vary greatly in chain length for the respective

Far and GMA blocks as shown by the high  $\bar{D}$ . However, the polymer chains have distinct homogeneous blocks of Far and GMA while maintaining active chain ends for perhaps another chain extension, which is an advantage over NHS-BB.

### 3.5 Conclusion

The bio-based monomer, Far, was successfully statistically copolymerized with epoxy-functional GMA by NMP. Although conventional SG1-based initiators are known to not control the polymerization of methacrylates well, statistical copolymerization of Far/GMA with NHS-BB showed that Far can act as a controlling comonomer at 10 mol% and 90 °C. Furthermore, the low conversion data of Far/GMA copolymerizations were used to determine reactivity ratios ( $r_{\text{Far}} = 0.54 \pm 0.04$  and  $r_{\text{GMA}} = 0.24 \pm 0.02$ ) indicating that the copolymers were essentially random in composition similar to isoprene/GMA and myrcene/GMA. The Far/GMA copolymers had active chain ends as shown by successful chain extension, although Far-rich macroinitiators exhibited better control than GMA-rich macroinitiators.

The statistical copolymerization using NHS-BB provided a good basis for assessment of the new alkoxyamine, D7, which was shown to improve homopolymerization of methacrylates but not yet used in copolymerizations. The resulting Far/GMA copolymers synthesized with D7 had bimodal MWDs due to the slow decomposition of the initiator and asymmetry of the cross-propagation kinetics, which resulted in high dispersity but active chain ends. Synthesis of diblock poly(Far-*b*-GMA) and poly[Far-*b*-(GMA-*stat*-Far)] copolymers using NHS-BB and poly(Far-*b*-GMA) using D7 were compared. Chain extension of Far-NHS with GMA was better controlled with 10 mol% Far added, but chain extension of Far-D7 with only GMA had more active chain ends. However, the slow initiation of D7 was still apparent in the chain extension with GMA resulting in high dispersity. This study showed that Far can be polymerized by NMP for the first time, and copolymerization (statistical and block) with a functionalized GMA was done with both NHS-BB and D7, however, the copolymerization kinetics of the new alkoxyamine needs to be further investigated.

### 3.6 References

- [1] J. G. Drobny, "15 - Applications of Thermoplastic Elastomers", in Handbook of Thermoplastic Elastomers, J.G. Drobny, Ed., William Andrew Publishing, Norwich, NY, 2007, p. 281.
- [2] J. M. Degrange, M. Thomine, P. Kapsa, J. M. Pelletier, L. Chazeau, G. Vigier, G. Dudragne, L. Guerbé, *Wear* 2005, 259, 684.
- [3] S. Wang, Q. Wang, X. Wu, Y. Zhang, *Construction and Building Materials* 2015, 93, 678.
- [4] W. C. White, *Chemico-Biological Interactions* 2007, 166, 10.
- [5] J. Brandrup, E. H. Immergut, E. A. Grulke, "Polymer handbook", 4th ed. edition, Wiley, New York, 1999.
- [6] M. P. Bertin, G. Marin, J. P. Montfort, *Polymer Engineering & Science* 1995, 35, 1394.
- [7] I. Kopal, P. Košťial, Z. Jančíková, J. Valíček, M. Harničárová, P. Hybler, M. Kušnerová, "Modifications of Viscoelastic Properties of Natural Rubber/Styrene-Butadiene Rubber Blend by Electron Beam Irradiation", in *Improved Performance of Materials: Design and Experimental Approaches*, A. Öchsner and H. Altenbach, Eds., Springer International Publishing, Cham, 2018, p. 219.
- [8] T. Masuda, A. Nakajima, M. Kitamura, Y. Aoki, N. Yamauchi, A. Yoshioka, "Viscoelastic properties of rubber-modified polymeric materials at elevated temperatures", in *Pure and Applied Chemistry*, 1984, p. 56/1457.
- [9] T. O. Broadhead, A. E. Hamielec, J. F. MacGregor, *Die Makromolekulare Chemie* 1985, 10, 105.

- [10] V. I. Rodríguez, D. A. Estenoz, L. M. Gugliotta, G. R. Meira, *International Journal of Polymeric Materials and Polymeric Biomaterials* 2002, 51, 511.
- [11] M. Abbasian, H. Namazi, A. A. Entezami, *Polymers for Advanced Technologies* 2004, 15, 606.
- [12] A. Kaiser, S. Brandau, M. Klimpel, C. Barner-Kowollik, *Macromolecular Rapid Communications* 2010, 31, 1616.
- [13] A. F. Johnson, D. J. Worsfold, *Journal of Polymer Science Part A: General Papers* 1965, 3, 449.
- [14] U.S. US4219627A (1980), *invs.:* A. F. Halasa, J. E. Hall, A. Para;
- [15] M. F. Cunningham, R. Hutchinson, "Industrial Applications and Processes", in *Handbook of Radical Polymerization*, John Wiley & Sons, Inc., 2003, p. 333.
- [16] M. Szwarc, *Nature* 1956, 178, 1168.
- [17] D. Jenkins Aubrey, G. Jones Richard, G. Moad, "Terminology for reversible-deactivation radical polymerization previously called "controlled" radical or "living" radical polymerization (IUPAC Recommendations 2010)", in *Pure and Applied Chemistry*, 2009, p. 82/483.
- [18] N. Chan, M. F. Cunningham, R. A. Hutchinson, *Macromolecular Chemistry and Physics* 2008, 209, 1797.
- [19] M. Li, N. M. Jahed, K. Min, K. Matyjaszewski, *Macromolecules* 2004, 37, 2434.
- [20] P. Raffa, M. C. A. Stuart, A. A. Broekhuis, F. Picchioni, *Journal of Colloid and Interface Science* 2014, 428, 152.

- [21] S. Harrisson, X. Liu, J. N. Ollagnier, O. Coutelier, J. D. Marty, M. Destarac, *Polymers* 2014, 6, 1437.
- [22] G. Moad, Y. K. Chong, A. Postma, E. Rizzardo, S. H. Thang, *Polymer* 2005, 46, 8458.
- [23] K. Satoh, D. H. Lee, K. Nagai, M. Kamigaito, *Macromolecular Rapid Communications* 2014, 35, 161.
- [24] M. K. Georges, G. K. Hamer, N. A. Listigovers, *Macromolecules* 1998, 31, 9087.
- [25] C. Detrembleur, V. Sciannamea, C. Koulic, M. Claes, M. Hoebeke, R. Jérôme, *Macromolecules* 2002, 35, 7214.
- [26] J. K. Wegrzyn, T. Stephan, R. Lau, R. B. Grubbs, *Journal of Polymer Science Part A: Polymer Chemistry* 2005, 43, 2977.
- [27] C. J. Hawker, A. W. Bosman, E. Harth, *Chemical Reviews* 2001, 101, 3661.
- [28] Y. Guillaneuf, D. Gigmes, S. R. A. Marque, P. Tordo, D. Bertin, *Macromolecular Chemistry and Physics* 2006, 207, 1278.
- [29] E. Guégain, Y. Guillaneuf, J. Nicolas, *Macromolecular Rapid Communications* 2015, 36, 1227.
- [30] C. Dire, J. Belleney, J. Nicolas, D. Bertin, S. Magnet, B. Charleux, *Journal of Polymer Science Part A: Polymer Chemistry* 2008, 46, 6333.
- [31] B. Charleux, J. Nicolas, O. Guerret, *Macromolecules* 2005, 38, 5485.

- [32] A. Moayeri, B. Lessard, M. Maric, *Polymer Chemistry* 2011, 2, 2084.
- [33] A. Darabi, P. G. Jessop, M. F. Cunningham, *Macromolecules* 2015, 48, 1952.
- [34] B. Lessard, M. Marić, *Journal of Polymer Science Part A: Polymer Chemistry* 2009, 47, 2574.
- [35] C. Zhang, B. Lessard, M. Maric, *Macromolecular Reaction Engineering* 2010, 4, 415.
- [36] Y. Guillaneuf, D. Gigmes, S. R. A. Marque, P. Astolfi, L. Greci, P. Tordo, D. Bertin, *Macromolecules* 2007, 40, 3108.
- [37] A. C. Greene, R. B. Grubbs, *Macromolecules* 2010, 43, 10320.
- [38] N. Ballard, M. Aguirre, A. Simula, A. Agirre, J. R. Leiza, J. M. Asua, S. van Es, *ACS Macro Letters* 2016, 5, 1019.
- [39] N. Ballard, M. Aguirre, A. Simula, J. R. Leiza, S. van Es, J. M. Asua, *Polymer Chemistry* 2017, 8, 1628.
- [40] N. Ballard, A. Simula, M. Aguirre, J. R. Leiza, S. van Es, J. M. Asua, *Polymer Chemistry* 2016, 7, 6964.
- [41] J. M. Yu, P. Dubois, R. Jérôme, *Macromolecules* 1996, 29, 7316.
- [42] D. Contreras-López, E. Saldívar-Guerra, G. Luna-Bárcenas, *European Polymer Journal* 2013, 49, 1760.

- [43] P. Juntuek, C. Ruksakulpiwat, P. Chumsamrong, Y. Ruksakulpiwat, *Journal of Applied Polymer Science* 2011, 122, 3152.
- [44] Z. Su, Q. Li, Y. Liu, G. H. Hu, C. Wu, *European Polymer Journal* 2009, 45, 2428.
- [45] N. Zhang, Q. Wang, J. Ren, L. Wang, *Journal of Materials Science* 2009, 44, 250.
- [46] A. Behr, L. Johnen, *ChemSusChem* 2009, 2, 1072.
- [47] M. A. Rude, A. Schirmer, *Current Opinion in Microbiology* 2009, 12, 274.
- [48] O. A. Abdelrahman, D. S. Park, K. P. Vinter, C. S. Spanjers, L. Ren, H. J. Cho, D. G. Vlachos, W. Fan, M. Tsapatsis, P. J. Dauenhauer, *ACS Sustainable Chemistry & Engineering* 2017, 5, 3732.
- [49] O. A. Abdelrahman, D. S. Park, K. P. Vinter, C. S. Spanjers, L. Ren, H. J. Cho, K. Zhang, W. Fan, M. Tsapatsis, P. J. Dauenhauer, *ACS Catalysis* 2017, 7, 1428.
- [50] M. D. Kumbhalkar, J. S. Buchanan, G. W. Huber, J. A. Dumesic, *ACS Catalysis* 2017, 7, 5248.
- [51] S. J. Dalsin, M. A. Hillmyer, F. S. Bates, *Macromolecules* 2015, 48, 4680.
- [52] W. F. M. Daniel, J. Burdyńska, M. Vatankhah-Varnoosfaderani, K. Matyjaszewski, J. Paturej, M. Rubinstein, A. V. Dobrynin, S. S. Sheiko, *Nature Materials* 2015, 15, 183.
- [53] J. M. Bolton, M. A. Hillmyer, T. R. Hoye, *ACS Macro Letters* 2014, 3, 717.
- [54] C. Zhou, Z. Wei, X. Lei, Y. Li, *RSC Advances* 2016, 6, 63508.

- [55] A. Métafiot, J. F. Gérard, B. Defoort, M. Marić, *Journal of Polymer Science Part A: Polymer Chemistry* 2018, 56, 860.
- [56] A. Métafiot, Y. Kanawati, J. F. Gérard, B. Defoort, M. Marić, *Macromolecules* 2017, 50, 3101.
- [57] T. Yoo, S. K. Henning, *Rubber Chemistry and Technology* 2017, 90, 308.
- [58] J. Vinas, N. Chagneux, D. Gigmes, T. Trimaille, A. Favier, D. Bertin, *Polymer* 2008, 49, 3639.
- [59] A. Darabi, A. R. Shirin-Abadi, P. G. Jessop, M. F. Cunningham, *Macromolecules* 2015, 48, 72.
- [60] J. Nicolas, C. Dire, L. Mueller, J. Belleney, B. Charleux, S. R. A. Marque, D. Bertin, S. Magnet, L. Couvreur, *Macromolecules* 2006, 39, 8274.
- [61] D. Benoit, E. Harth, P. Fox, R. M. Waymouth, C. J. Hawker, *Macromolecules* 2000, 33, 363.
- [62] F. R. Mayo, F. M. Lewis, *Journal of the American Chemical Society* 1944, 66, 1594.
- [63] F. M. Lewis, C. Walling, W. Cummings, E. R. Briggs, W. J. Wensch, *Journal of the American Chemical Society* 1948, 70, 1527.
- [64] E. Oikawa, K. i. Yamamoto, *Polymer Journal* 1970, 1, 669.
- [65] D. L. Trumbo, *Polymer Bulletin* 1993, 31, 629.

- [66] W. Wang, R. A. Hutchinson, *Macromolecules* 2008, 41, 9011.
- [67] K. Liang, M. Dossi, D. Moscatelli, R. A. Hutchinson, *Macromolecules* 2009, 42, 7736.
- [68] F. Chauvin, P. E. Dufils, D. Gigmes, Y. Guillaneuf, S. R. A. Marque, P. Tordo, D. Bertin, *Macromolecules* 2006, 39, 5238.
- [69] I. Zapata-González, R. A. Hutchinson, K. Matyjaszewski, E. Saldívar-Guerra, J. Ortiz-Cisneros, *Macromolecular Theory and Simulations* 2014, 23, 245.
- [70] B. Klumperman, G. Chambard, R. H. G. Brinkhuis, "Peculiarities in Atom Transfer Radical Copolymerization", in *Advances in Controlled/Living Radical Polymerization*, American Chemical Society, 2003, p. 180.
- [71] K. Matyjaszewski, *Macromolecules* 2002, 35, 6773.
- [72] A. Feldermann, A. Ah Toy, H. Phan, M. H. Stenzel, T. P. Davis, C. Barner-Kowollik, *Polymer* 2004, 45, 3997.
- [73] F. Brandl, M. Drache, J. E. S. Schier, T. Nentwig, D. Contreras-López, E. Saldívar-Guerra, R. A. Hutchinson, S. Beuermann, *Macromolecular Rapid Communications* 2017, 38, 1700105.
- [74] C. Burguière, S. Pascual, C. Bui, J.-P. Vairon, B. Charleux, K. A. Davis, K. Matyjaszewski, I. Bétremieux, *Macromolecules* 2001, 34, 4439.
- [75] S. George, R. Champagne-Hartley, G. Deeter, D. Campbell, B. Reck, D. Urban, M. Cunningham, *Macromolecules* 2015, 48, 8913.

## 4 Polymerization of bio-based farnesene in miniemulsions by nitroxide-mediated polymerization

After successful NMP of Far was done in bulk, the logical next step was to perform the polymerization in aqueous dispersion. One benefit of polymerization in emulsion systems is eliminating volatile organic compound solvents, while maintaining low viscosity of the reaction mixture. Furthermore, the initial intent on synthesizing poly(Far) in emulsion systems was to utilize compartmentalization effects to achieve high molecular weights, therefore surpassing the entanglement molecular of poly(Far) in order to exhibit viscoelastic properties. There are several examples of emulsion polymerization of Myr done by redox polymerization and RAFT [39-41], but Far had not been polymerized in emulsion until now. This chapter demonstrates the NMP of Far in miniemulsion for the first time and the article was published in *ACS Omega* in 2021 (S.B. Luk, M. Maric, Polymerization of bio-based farnesene in miniemulsions by nitroxide-mediated polymerization, *ACS Omega* 6(7) (2021) 4939-4949) [42].

Similar to the polymerizations of Far done in bulk, the kinetics were compared between NHS-BB and D7 initiators. Surprisingly, particle size of these miniemulsion systems were not as affected by surfactant concentration, although chain-end activity was better when more surfactant was used. Smaller particles were observed when using NHS-BB (~300 nm) compared to D7 initiator (~400 nm), therefore there was a higher number of particles, which led to faster polymerization rate and higher conversion. Unfortunately, compartmentalization did not occur, but confined space effects were observed, even though particle size was larger than typical NMP miniemulsions [43, 44]. This was due to the slow activation of D7 initiator effectively lowering the average concentration of radicals per particle such that the overall polymerization rate was decreased. Nonetheless, poly(Far) macroinitiators synthesized in miniemulsion were able to be chain-extended with St, suggesting active chain-ends, and successfully formed diblock copolymers. Poly(Far) macroinitiators were also chain-extended with iBOMA making an all bio-sourced diblock copolymer. However, poly(Far) made with D7 showed better chain-extension with iBOMA compared to NHS-BB as seen by an obvious shift in molecular weight distribution. The supporting information of this publication is included in Appendix B, and the supporting figures and tables

are referred to as Figure B-X and Table B-X in this chapter. There is also a correction in this publication regarding the reference to Table 4-2 on page 105, which should be Table 4-1.

#### 4.1 Abstract

Biobased farnesene (Far) was polymerized by nitroxide-mediated polymerization in miniemulsions using two different alkoxyamine initiators, the SG1-based and succinimidyl-modified BlocBuilder (NHS-BB) and Dispolreg 007 (D7). Stable emulsions were observed after 30 h of reaction at 90 °C, where NHS-BB-initiated systems resulted in smaller particles (~300 nm) than using D7 (~400 nm). Successful chain extension of the poly(Far) macroinitiators (24,500–39,700 g mol<sup>-1</sup>) with styrene were achieved using 15 wt % surfactant relative to monomer concentration. Compartmentalization effects were not observed in these emulsions as the polymerization rate was still much slower compared to the bulk, even though *Z*-averaged particle sizes were around 300–400 nm. Finally, all biobased diblock copolymers were synthesized by chain-extending poly(Far) macroinitiators with isobornyl methacrylate (iBOMA), where the D7 initiator showed more effective chain extension (less unreacted macroinitiator) than NHS-BB.

#### 4.2 Introduction

There is increasing incentive to create materials from biorenewable resources, as well as modifying the processes in creating these materials to become greener. One such industrially relevant material is poly(styrene-block-butadiene-block-styrene) (SBS), which is a triblock copolymer used as a thermoplastic elastomer (TPE) [1]. This material can be processed at high temperatures such as thermoplastics and also have elastic properties without being chemically cross-linked, therefore making it a versatile material that is used in automotive parts, rubber soles for shoes, and asphalt modifiers [2–4]. The elastomeric segment is made of a poly(diene) (i.e., butadiene or isoprene [5]) sandwiched between thermoplastic segments made of poly(styrene). Traditionally, SBS is synthesized via anionic polymerization, which is done in organic solvents, and butadiene and styrene, which are both petroleum-derived monomers [6]. Moreover, anionic polymerization is intolerant to functional groups and cannot be done in water. Although there have been recently reported methods to produce butadiene and isoprene from biorenewable resources, these monomers are still volatile and nevertheless require pressurized vessels for polymerizations to occur [7,8].

Controlled radical polymerization, or more properly known as reversible deactivation radical polymerization (RDRP), combines the specificity of anionic/living polymerization to control the molecular architecture of polymer chains and the simplicity of radical chemistry that is robust and less stringent reactions conditions in comparison [9,10]. There are several types of RDRP: atom transfer radical polymerization [11], reversible addition–fragmentation transfer polymerization (RAFT) [12], and nitroxide-mediated polymerization (NMP) [13]. All these methods are able to incorporate functional groups into a polymer chain largely without need for protecting group strategies, and therefore, the resulting materials can be easily tailored to improve compatibilization and performance.

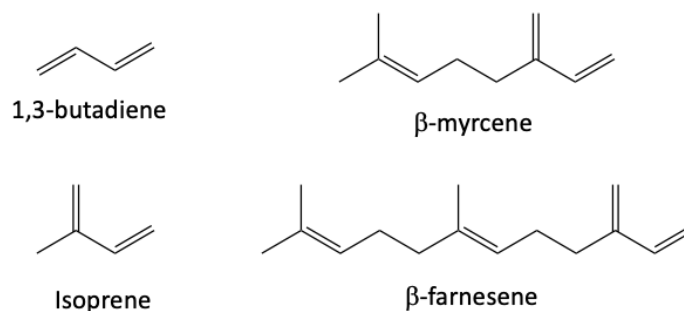
An added advantage of RDRP is its ability to be done in dispersed aqueous media (e.g., emulsion, miniemulsion, or dispersion polymerization), as well as in solution and bulk [14]. This reduces the use of volatile organic compounds (VOCs) and lowers emissions while maintaining low viscosity, which can be important for latex coatings [15]. Furthermore, depending on the particle size, there can be compartmentalization of the radicals, which could help attain higher polymer molecular weight and/or rate of polymerization compared to in bulk [16–18]. For RDRP, partitioning of the chain-transfer agent between the organic and aqueous phase is another significant factor to consider [19–21].

The polymerization of butadiene and isoprene has been explored by RAFT [22,23] and NMP in solution/bulk polymerization, and NMP generally resulted in poly(dienes) that were lower in dispersity [24]. Emulsion polymerization of butadiene and isoprene were mainly done by RAFT, and the resulting diblock copolymers consisting of poly(isoprene-*b*-styrene) showed micro-phase separation, as in differential scanning calorimetry, an important property for thermoplastic elastomers [25,26]. Triblock SBS polymer latex was successfully synthesized by RAFT in miniemulsions and showed comparable mechanical properties to conventional SBS made by anionic polymerization [27].

Initially, NMP in emulsion proved to be difficult using a TEMPO alkoxyamine initiator as the polymerization loci would occur in the large monomer droplets, causing coagulation and emulsion instability [28]. Additionally, TEMPO is hydrophobic and requires high temperatures for

activation ( $\sim 135$  °C). A second-generation alkoxyamine, the SG1-based BlocBuilder, is water-soluble when neutralized and has a higher rate of activation and allowed for NMP in emulsions [29]. Even more recently, a newly developed alkoxyamine, Dispolreg 007 (D7), that is tailored for nitroxide-mediated homopolymerization of methacrylates, has been applied successfully in miniemulsions as well [30–32].

In an effort to replace petroleum-derived materials, farnesene (Far) and myrcene (Myr) have been investigated as biosourced dienes that are similar to butadiene and isoprene (see Scheme 4-1) [33,34]. Myr has been polymerized by conventional free radical polymerization and RAFT, [35,36], and Far has been polymerized by anionic polymerization and redox free-radical polymerization in emulsion [37,38]. Both Myr and Far have also been successfully polymerized by NMP in bulk for making thermoplastic elastomers with functionalized methacrylates (e.g., glycidyl methacrylate (GMA) and isobornyl methacrylate (iBOMA)) [39–41]. Statistical copolymers were also made using either Myr or Far with GMA and iBOMA to incorporate functional groups throughout the poly(diene) chain. Poly(Far-*stat*-GMA) and poly(Far-*b*-GMA) were made with succinimidyl-modified BlocBuilder (NHS-BB) and D7 initiators, which are both used to better control polymerization of methacrylates [41]. NHS-BB requires a small amount of the controlling comonomer, while D7 can homopolymerize methacrylates. Furthermore, Myr and Far are less volatile than butadiene and isoprene and therefore can be polymerized at atmospheric pressure, further simplifying the process and avoiding the use of more costly pressurized reactors. However, due to the long side chains of Myr and Far increasing their hydrodynamic volumes, higher molecular weights are required in order for the polymer chains to entangle and provide sufficient elastomeric properties. The entanglement molecular weight ( $M_e$ ) for poly(Myr) and poly(Far) are 17,700 and  $\sim 50,000$  g mol<sup>-1</sup>, respectively, whereas  $M_e$  for poly(butadiene) and poly(isoprene) are 1800 and 5400 g mol<sup>-1</sup>, respectively [42,43].



Scheme 4-1. Chemical Structures of Petroleum-Derived Dienes, Butadiene, and Isoprene, and Biosourced Dienes, Myrcene and Farnesene

In this study, biosourced Far was polymerized by NMP using both NHS-BB and D7 initiators in miniemulsions for the first time. The sustainable aspect of this investigation is threefold: using a biosourced monomer to replace petroleum-derived monomers, performing the polymerization in aqueous media, eliminating VOCs, as well as performing the polymerization at atmospheric pressure, given the lower volatility of Far. Additionally, the goal was to utilize the compartmentalization effect in miniemulsions to lead to higher-molecular weight poly(Far) segments and improve the elastomeric properties by far exceeding the entanglement molecular weight of the rubbery block segment, which is the general approach applied for most TPEs (i.e., 10–20,000 g mol<sup>-1</sup> for poly(styrene) block and 40–80,000 g mol<sup>-1</sup> for poly(butadiene) block for SBS) [1]. The chain-end activity of the poly(Far) macroinitiators was investigated by chain extension with St to synthesize poly(Far-*b*-St) and with iBOMA to synthesize a completely biosourced poly(Far-*b*-iBOMA). The kinetics of nitroxide-mediated polymerizations in miniemulsions were also compared between the NHS-BB and D7 initiators. Furthermore, surfactant loading, particle size, and compartmentalization were comprehensively studied to understand how these factors affected the chain-end fidelity and molecular weight of poly(Far).

### 4.3 Results and discussion

#### 4.3.1 Comparing surfactant loading in miniemulsions

Initially, the first two miniemulsion experiments were done with 5 wt % surfactant relative to the monomer using both initiators: D7 and NHS-BB. While both experiments showed linear kinetics

in the  $\ln(1/(1 - X))$  versus time plots after 30 h of reaction (shown in Figure B-1 in Appendix B), the poly(Far) macroinitiators did not chain-extend when polymerized with styrene (St) afterward. The dispersed particles appeared to remain stable at the end of the reaction as the particles did not coagulate and settle to the bottom; however, 5 wt % surfactant was not sufficient to maintain active chain ends of the polymer chains as the molecular weight distributions did not shift to higher molecular weights after the intended chain extension with St (Figure B-2). The final conversion of these two experiments initiated by D7 and NHS-BB were 28 and 40%, respectively. The final properties of all poly(Far) made by miniemulsions in this study are summarized in Table 4-1.

Table 4-1. Table of Poly(Far) Properties from Miniemulsion Polymerization Summarizing Final Conversion, Final Molecular Weight, Dispersity, Z-Averaged Particle Size, and Polydispersity Index of Particles<sup>a</sup>

Experiment	Initiator	$M_{n,target}$ (g mol <sup>-1</sup> )	Surfactant loading (wt%)	Final Conversion (%)	Final $M_n$ (g mol <sup>-1</sup> )	Final $\bar{D}$	Final Z- averaged particle size (nm)	Poly- dispersity index
Exp 1	D7	50,000	5	27.7	22,800	2.31	425	0.287
Exp 2	NHS-BB	50,000	5	39.7	49,300	2.23	298	0.297
Exp 3	D7	50,000	15	27.7	24,500	2.22	362	0.386
Exp 4	D7	30,000	15	29.4	13,900	2.38	310	0.286
Exp 5	NHS-BB	50,000	15	32.7	39,700	1.67	336	0.286

a) Final measurements were taken after 30 h of reaction.

The remaining miniemulsion experiments were done with 15 wt % surfactant using different initiators and different target molecular weights ( $M_{n,target}$ ). First, the experiments done using the D7 initiator and 5 versus 15 wt % surfactant (Exp 1 vs Exp 3) were compared. The  $\ln(1/(1 - X))$  with time followed a linear trend in both cases, as seen in Figure 4-1, which shows good simultaneous chain growth for most polymer chains. The rates of polymerization in both cases were also the same, so it was not affected by increasing the surfactant loading. Similarly, the molecular weight and dispersity versus conversion plots were not affected by surfactant loading, as shown in Figure 4-2. Molecular weights also increased linearly with conversion, further indicating steady growth, suggestive of a controlled polymerization. Dispersities remained high, typically  $\sim 2$ , likely due to the slow rate of propagation and initiation at a relatively low

polymerization temperature of 90 °C. However, polymer chains continued to grow, and dispersity decreased at  $X > 10\%$ , as seen in Figure 4-2b, so the high dispersity can also be due to the polymerization being in the early stages with the low conversions reported. Perhaps, dispersity could continue to decrease as the conversion increases (until irreversible termination occurs).

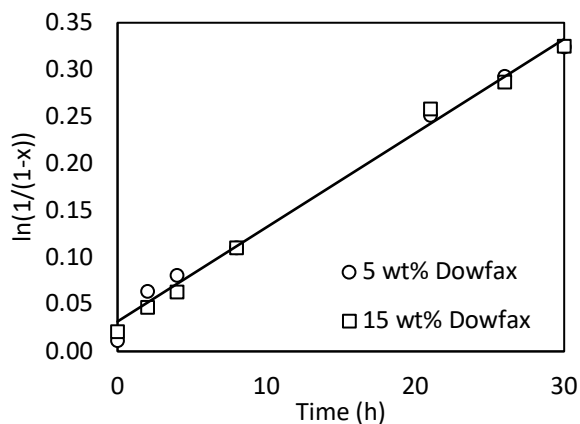


Figure 4-1. Linearized conversion vs time plot for the homopolymerization of farnesene in miniemulsions using D7 at 90 °C in 20 wt % monomer with 5 and 15 wt % surfactant and a  $M_{n,target} = 50,000 \text{ g mol}^{-1}$ .

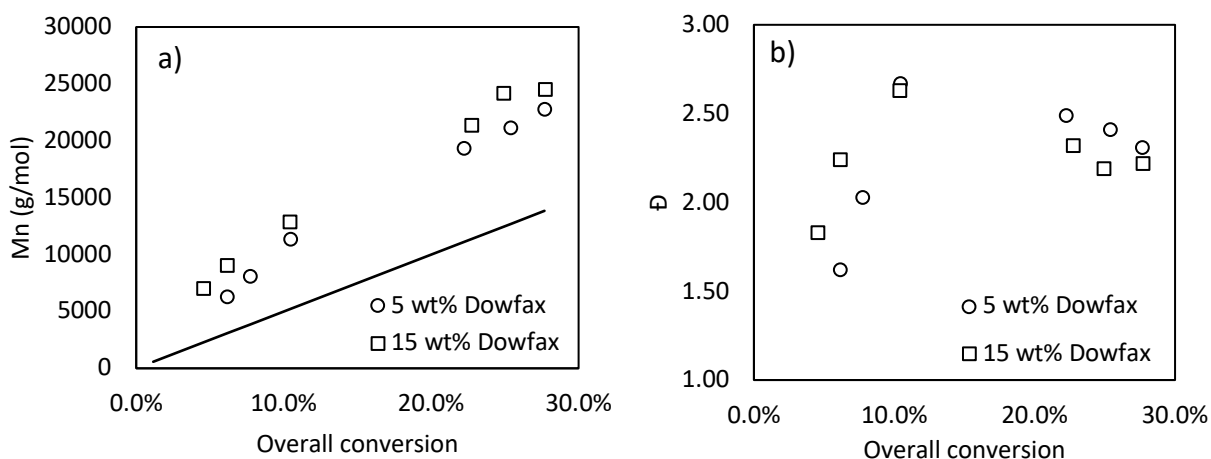


Figure 4-2. (a) Molecular weight and (b) dispersity vs conversion plots for the homopolymerization of farnesene in miniemulsions using D7 at 90 °C in 20 wt % monomer with 5 and 15 wt % surfactant and  $M_{n,target} = 50,000 \text{ g mol}^{-1}$ .

The experimental  $M_n$  values were consistently higher than the theoretical  $M_n$  values, which is expected as D7 has a slower rate of activation ( $k_{act}$ ) compared to TEMPO and SG1-based initiators and is known to create longer polymer chains due to fewer alkoxyamines initiating chain growth

from the beginning [30,31]. This also explains the higher dispersity values of  $\sim 2.3$ , although they are considerably higher than previously reported for polymerization of Far using D7 in bulk [41]. Despite the high dispersity, which should indicate a significant concentration of inactive chain ends, poly(Far) synthesized using 15 wt % surfactant successfully chain-extended with styrene, as opposed to poly(Far) made using 5 wt % surfactant. In Figure 4-3, the molecular weight distributions (MWDs) shifted to the right as the molecular weights increased with reaction time after 120 min of chain extension from 24,500 to 35,100  $\text{g mol}^{-1}$ . The resulting poly(Far-*b*-St) diblock copolymer had a dispersity of 2.20. Final copolymer composition along with other block copolymer properties are summarized in Table 4-2. The kinetics of the two miniemulsions were very similar, but increasing the surfactant loading maintained more active chain ends. This will be discussed more fully in a later section.

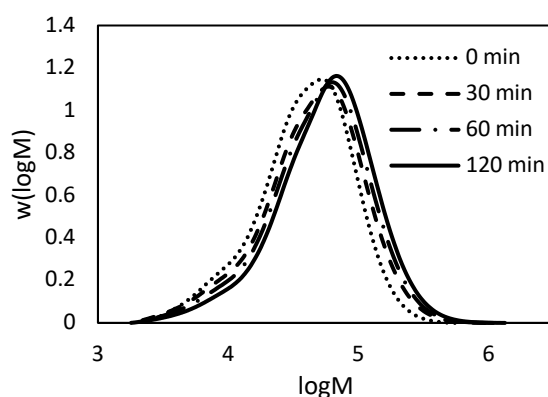


Figure 4-3. MWD of poly(Far-*b*-St) after 120 min of chain extension of poly(Far) made with 15 wt % surfactant and  $M_{n,target} = 50,000 \text{ g mol}^{-1}$ .

Table 4-2. Summary of Poly(Far) Macroinitiators Made with D7 and NHS-BB Initiators and Chain-Extended with St and iBOMA at 120 and 90 °C, Respectively, in 50 wt % Toluene<sup>a</sup>

Chain-extension	Macroinitiator alkoxyamine	Poly(Far) macroinitiator $M_n$ ( $\text{g mol}^{-1}$ )	$f_{St}$	$f_{iBOMA}$	Final $M_n$ ( $\text{g mol}^{-1}$ ) <sup>b</sup>	Final $\bar{D}$	$F_{Far}$ estimated by NMR
CX-1	D7	24,500	1.0	0	35,100	2.20	0.38
CX-2	D7	13,900	1.0	0	28,900	2.22	0.27
CX-3	NHS-BB	39,700	1.0	0	70,400	2.15	0.31
CX-4	D7	24,500	0	1.0	30,645	3.19	0.30

CX-5	NHS-BB	39,700	0.1	0.9	44,300	2.24	N/A
------	--------	--------	-----	-----	--------	------	-----

<sup>a)</sup> Final copolymer compositions were estimated by <sup>1</sup>H NMR; <sup>b)</sup> Final  $M_n$  of the diblock copolymers were estimated by GPC and are relative values using PMMA standards; therefore, copolymer compositions were more accurately estimated using <sup>1</sup>H NMR.

All the miniemulsion experiments were analyzed after 30 h of reaction and achieved relatively low conversions of ~30–40%. One miniemulsion study was done with 15 wt % surfactant using the D7 initiator, and the reaction time was extended to 72 h. The conversion achieved was not much higher and the final  $M_n$  and  $\bar{D}$  were 32,300 g mol<sup>-1</sup> and 2.19 (Figure B-3), respectively. Therefore, the reaction time was chosen to be 30 h in this study for convenience. However, the 72 h emulsion reaction remained visibly stable without coagulation and chain extension with St was successful, indicating high chain-end fidelity (Figure B-4). The low conversions from the 30 h reaction were also ideal as most polymer chain ends would remain active for chain extension, with the long-term goal of deriving high-molecular weight block copolymers.

#### 4.3.2 Comparing target molecular weights in miniemulsions

The effect of changing  $M_{n,target}$  of the farnesene homopolymerizations in miniemulsions was studied as well using the D7 alkoxyamine. By varying  $M_{n,target}$ , it effectively varies the monomer-to-nitroxide ratio in the system. The  $\ln(1/(1 - X))$  versus time plots of the miniemulsions done with  $M_{n,target} = 30,000$  versus 50,000 g mol<sup>-1</sup> (Exp 3 vs Exp 4) are shown in Figure 4-4. With  $M_{n,target} = 30,000$  g mol<sup>-1</sup>, the plot showed linear kinetics in the range studied, which indicate that most polymer chains were growing simultaneously at the same rate, similar to the previous experiment with  $M_{n,target} = 50,000$  g mol<sup>-1</sup>. The molecular weight also increased linearly with conversion, as seen in Figure 4-5, as the final molecular weight was 13,900 g mol<sup>-1</sup> and the final  $\bar{D} = 2.38$ .

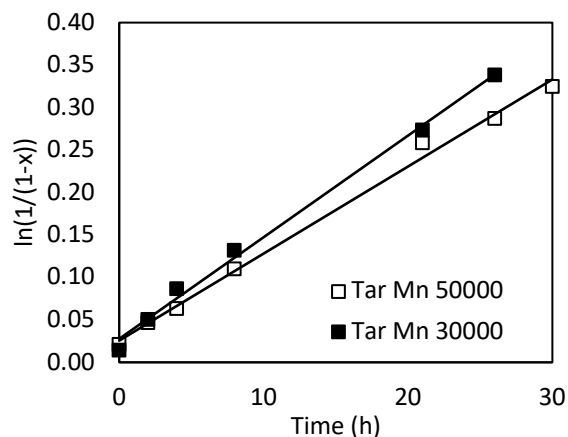


Figure 4-4. Linearized conversion vs time plot for the homopolymerization of farnesene in miniemulsions using D7 at 90 °C in 20 wt % monomer with 15 wt % surfactant and  $M_{n,target} = 30,000$  and  $50,000 \text{ g mol}^{-1}$ .

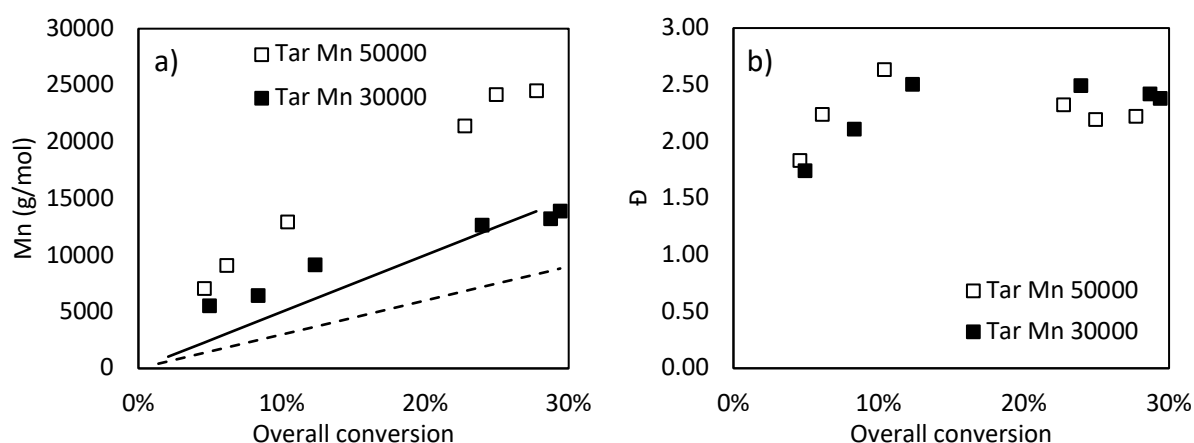


Figure 4-5. (a) Molecular weight and (b) dispersity vs conversion plots for the homopolymerization of farnesene in miniemulsions using D7 at 90 °C in 20 wt % monomer with 15 wt % surfactant and  $M_{n,target} = 30,000$  and  $50,000 \text{ g mol}^{-1}$ . The solid line in (a) represents the theoretical  $M_n$  for  $M_{n,target} = 50,000 \text{ g mol}^{-1}$ , and the dashed line represents the theoretical  $M_n$  for  $M_{n,target} = 30,000 \text{ g mol}^{-1}$ .

The experimental  $M_n$  for  $M_{n,target} = 30,000 \text{ g mol}^{-1}$  was also significantly higher than the theoretical  $M_n$  but not as significant compared to  $M_{n,target} = 50,000 \text{ g mol}^{-1}$ . Furthermore, the rate of polymerization for  $M_{n,target} = 30,000$  was faster than  $M_{n,target} 50,000$ , as seen in Figure 4-4, although in bulk or solution polymerization, the rate of polymerization would be slower when the target molecular weight is lower. This is due to the lower monomer-to-nitroxide ratio, which means a higher concentration of nitroxides to deactivate the propagating polymer chains, thereby decreasing the rate of polymerization. However, the faster rate of polymerization is likely due to

the smaller particle size in the emulsion, which is discussed in a later section. Additionally, the dispersity was not affected by the change in  $M_{n,target}$ , even though higher concentration of nitroxides should maintain more active chain ends and effectively lower the dispersity.

The chain-end activity of poly(Far) made with  $M_{n,target} = 30,000 \text{ g mol}^{-1}$  was investigated by doing a chain extension with styrene. The MWD is shown in Figure 4-6, and an increase in molecular weight is seen as the distribution shifted to the right with reaction time. The molecular weight increased from 13,900 to 28,900  $\text{g mol}^{-1}$ , indicating most of the polymer chains remained active. There is also a clear disappearance of the slightly low molecular weight shoulder from 0 to 120 min, therefore decreasing the  $\bar{D}$  from 2.38 to 2.22. Block copolymer properties are summarized in Table 4-2.

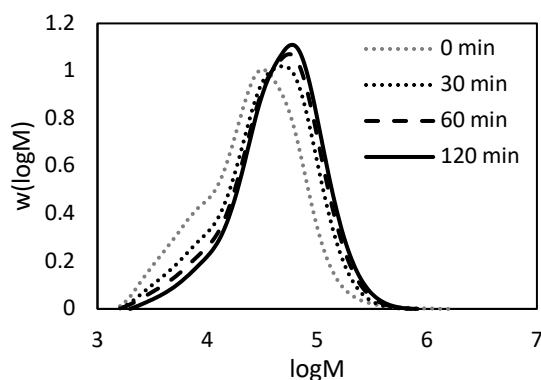


Figure 4-6. MWD of poly(Far-*b*-St) after 120 min of chain extension of poly(Far) made with 15 wt % surfactant and  $M_{n,target} = 30,000 \text{ g mol}^{-1}$ .

#### 4.3.3 Particle size of miniemulsions

Particle size and distribution is an important variable in miniemulsion polymerizations as it is affected by solubility of the monomer, surfactant, and costabilizer concentration.(14,45) Consequently, the particle size and number of particles would affect rate of polymerization and therefore, molecular weight of the polymer chains. Furthermore, in nitroxide-mediated polymerization, the partition of nitroxides in the oil and aqueous phases have to be considered as well, which would affect the chain-end fidelity of the polymer chains [17,20].

Because the polymerizations were done in miniemulsions, the oil phase was dispersed in the water phase using ultrasonication to form small micron-sized droplets stabilized by the surfactant. Theoretically, each droplet is its own batch reactor containing the oil-soluble initiator, as opposed to having large monomer reservoirs and small monomer-swollen micelles such as in conventional emulsions (Scheme 4-2). In the DLS analysis, there was evidence of a low fraction of larger droplets (103 nm) likely due to the high hydrophobicity of farnesene, but the majority of the droplets were  $\sim 102$  nm (Figures B-5 and B-6). The emulsions appeared to remain stable without obvious visible coagulation (even after 72 h of reaction). At above the critical micelle concentration (CMC) of DOWFAX 8390 (3 mM) [46], there is likely the presence of small micelle-sized ( $<100$  nm) droplets even though it was not observed from DLS analysis. There is also likely excess surfactant at the interface. The Z-averaged particle sizes for the homopolymerizations with  $M_{n,target} = 50,000$  g mol<sup>-1</sup> are shown in Figure 4-7. The particle sizes mostly remained constant and slightly decreased after 30 h. This was more evident with NHS-BB experiments, which could indicate some homogeneous nucleation of new particles in the aqueous phase.

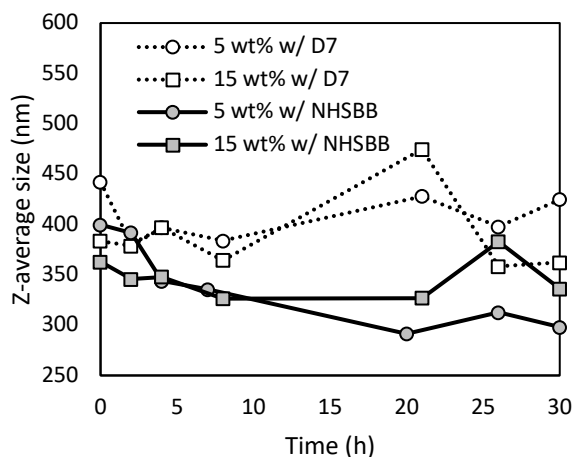
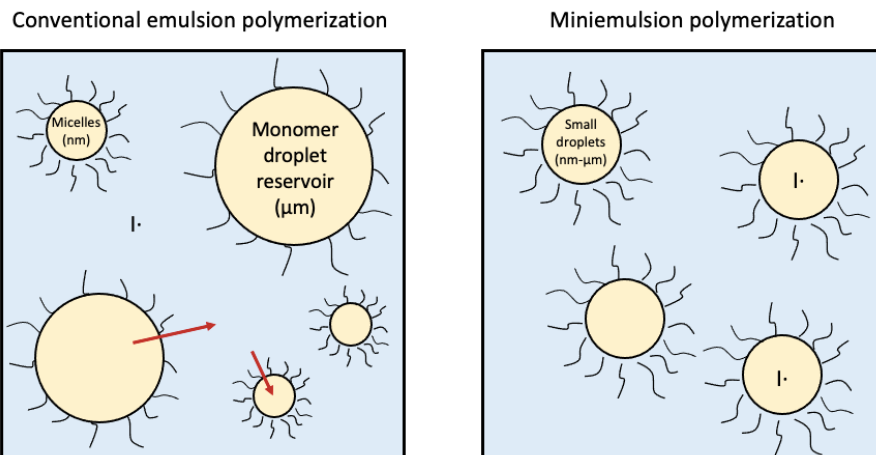


Figure 4-7. Z-averaged particle size of miniemulsions for homopolymerizations of farnesene in 5 and 15 wt % surfactant using D7 and NHS-BB initiators at 90 °C with a  $M_{n,target} = 50,000$  g mol<sup>-1</sup>.



Scheme 4-2. Diagram of Conventional Emulsion Polymerization (Left) vs Miniemulsion Polymerization (Right)<sup>a</sup>

- a) Droplets are stabilized by surfactants, and the red arrows in the right show mass transfer of monomer from monomer reservoir into the aqueous phase and then into the micelles for polymerization to occur. Initiator is represented by  $I\bullet$  either in the aqueous or oil phase.

The original intent on increasing surfactant concentration was to decrease particle size, which would help with maintaining active chain ends and perhaps lead to compartmentalization, therefore enabling higher molecular weights to be achieved. It is evident in Figure 4-7 that surfactant loading did not quite have an effect on the particle size and polymerization rate, and final  $M_n$  also did not increase as discussed previously. However, using NHS-BB initiator led to smaller particles than using D7, which led to faster rates of polymerization and higher final  $M_n$ . Final particle sizes and polydispersity index are summarized in Table 4-2.

Increasing surfactant loading from 5 to 15 wt % did not significantly decrease the Z-averaged particle size for both D7 and NHS-BB miniemulsions, but as seen previously, it improved chain-end fidelity of the poly(Far) macroinitiators for chain extension. Looking at the particle size distributions more closely, specifically the volume-averaged distributions, there was a higher percentage of large droplets (103 nm in size) nearing the end of the reaction when there was only 5 wt % surfactant compared to 15 wt % surfactant (Figure 4-8). Although the difference is not obvious, there seems to be a smaller left-hand side shoulder at higher surfactant concentration.

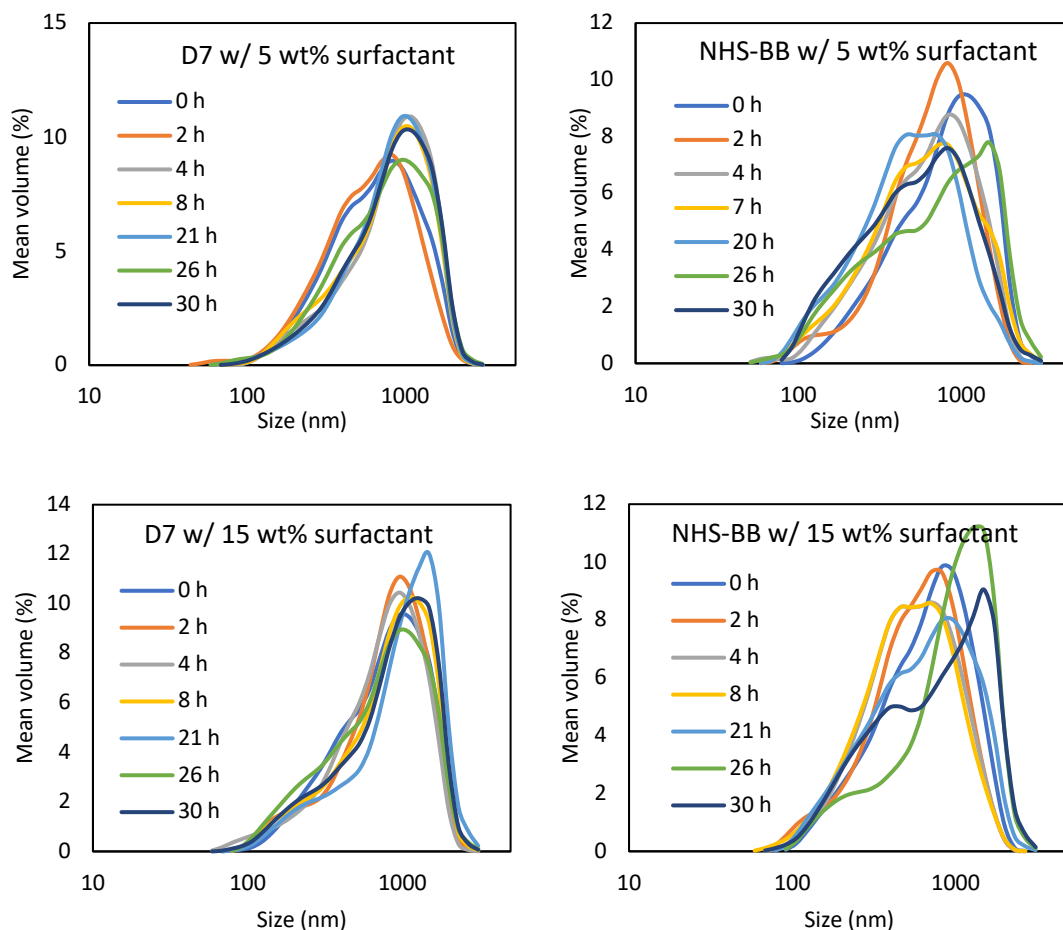


Figure 4-8. Volume-averaged particle size from DLS for homopolymerizations of Far in miniemulsions in 20 wt % monomer using D7 and NHS-BB initiators at 120 °C.

Nitroxides partition between the aqueous and oil phases in an equilibrium and continuously enter and exit the particles [20]. When there is a distribution of particle sizes, nitroxides are much more likely to enter smaller micron-sized droplets than larger droplets due to the higher surface area-to-volume ratio. Therefore, there is a lower concentration of nitroxides in the larger droplets such that the likelihood of irreversible termination is increased when there is only 5 wt % surfactant present, which perhaps lowered the overall chain-end fidelity in the system. However, a faster rate of nitroxide entry also means a faster rate of nitroxide exit. Nonetheless, it is uncertain what phenomena caused increased livingness at increased surfactant concentration, and more studies would need to be done to conclusively determine the cause for better chain end fidelity at such conditions.

Although surfactant concentration did not have a significant effect on particle size, alkoxyamine concentration did. In the miniemulsion using D7 and  $M_{n,target} = 30,000 \text{ g mol}^{-1}$ , the particle size was consistently smaller than the miniemulsion with  $M_{n,target} = 50,000 \text{ g mol}^{-1}$  and it was similar to the particle size achieved using NHS-BB. In Figure 4-9, the particle size with conversion is plotted for both experiments using different  $M_{n,target}$ . Because the particle size was smaller with  $M_{n,target}$  of  $30,000 \text{ g mol}^{-1}$ , the rate of polymerization was more rapid as a result, as seen earlier in Figure 4-4.

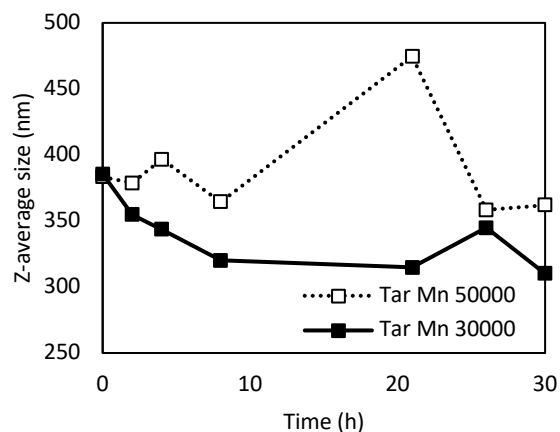


Figure 4-9. Z-averaged particle size of miniemulsions for homopolymerizations of farnesene in 15 wt % surfactant using D7 at 90 °C with  $M_{n,target} = 30,000$  and  $50,000 \text{ g mol}^{-1}$ .

#### 4.3.4 Compartmentalization versus confined space effects

It was estimated that for NMP in dispersed systems, compartmentalization occurs when particles are <110 nm in diameter, and a confined space effect was observed when particles are <60 nm diameter [17]. Compartmentalization is observed when particle size is in a range where each particle has an average radical concentration of 0.5, where the propagating radicals are segregated from one another and irreversible termination is minimized. Therefore, the rate of polymerization is increased, leading to higher conversions and degrees of polymerization. However, any type of RDRP and specifically NMP, the partition of nitroxides between the aqueous and the oil phase is also very important. When the particle size is further decreased, then the rate at which nitroxides enter the particle is much faster and more effectively deactivates the propagating radicals, such

that rate of polymerization is decreased [20]. In this case, the confined space effect is observed when the polymerization rate is slower than that in bulk.

Once again, it is interesting that increasing the surfactant concentration had a minimal effect on *Z*-averaged particle size unlike what is observed in conventional free radical miniemulsions [47]. This was supported by the polymerization rates and  $M_n$  versus conversion results that remained the same after increasing surfactant concentration. In a miniemulsion study for NMP of styrene using TEMPO, where surfactant concentration ranged from below to above CMC, the polymerization rate and  $M_n$  also remained the same [48]. The initial particle size ranged from 40–100 nm by decreasing the surfactant concentration from 15 to 1.25 mM. This was justified by the fact that the average number of radicals per particle is much lower than 0.5 due to the high concentration of nitroxides that are present per particle. Therefore, the rate of polymerization is dominated by the deactivation of propagating chains from the nitroxides, such that even with smaller particles, the rate did not increase, and compartmentalization was not achieved. Even with particle sizes up to 180 nm, compartmentalization was not observed [49]. Similarly, much larger particle size was required for compartmentalization in particles with low macroinitiator concentration [50]. Furthermore, it has been simulated that with a lower  $k_{act}$ , which is the case for the D7 initiator, larger particle sizes are required for compartmentalization to occur [20]. This is because radical concentration is decreased at lower  $k_{act}$ .

Hence, in nitroxide-mediated polymerizations combined with a lower  $k_{act}$ , the particle size would have to be larger to increase the average radical concentration per particle to 0.5 and allow for compartmentalization. Although the *Z*-average particle sizes in this study were ~300–400 nm, the number-averaged particle sizes showed that the majority of the particles were ~150–200 nm in size. However, the rate of polymerization was still much slower than compared to bulk, ( $X_{bulk} = 85\%$  after 4 h [41] vs  $X_{miniemulsion} = 28\%$  after 30 h both using D7 initiator). Similar to previous studies, not only is compartmentalization not observed but also the confined space effect seems to be in effect even with relatively large particle sizes, partly due to the slower activation of D7 and the presence of nitroxides in these miniemulsions.

#### 4.3.5 Molecular weight distributions of poly(Far) macroinitiators

The molecular weight distributions (MWDs) of the miniemulsion homopolymerizations of Far done with  $M_{n,target} = 50,000 \text{ g mol}^{-1}$  are shown in Figure 4-10. As discussed earlier, the  $\mathcal{D}$  of the experiments done with the D7 initiator are high ( $\sim 2.3$ ). Looking at the MWDs in Figure 4-10a,b, there is a slight low molecular weight shoulder, which is expected as the activation of D7 is slow and not all polymer chains were initiated in the beginning of the polymerization, leading to shorter chains that were formed later. The low molecular weight shoulder was also seen in homopolymerization of Far using D7 in bulk [41]. Moreover, comparing to MWDs of the experiments done with NHS-BB in Figure 4-10c and d, they are narrower and more monomodal, which indicate all polymer chains were initiated simultaneously.

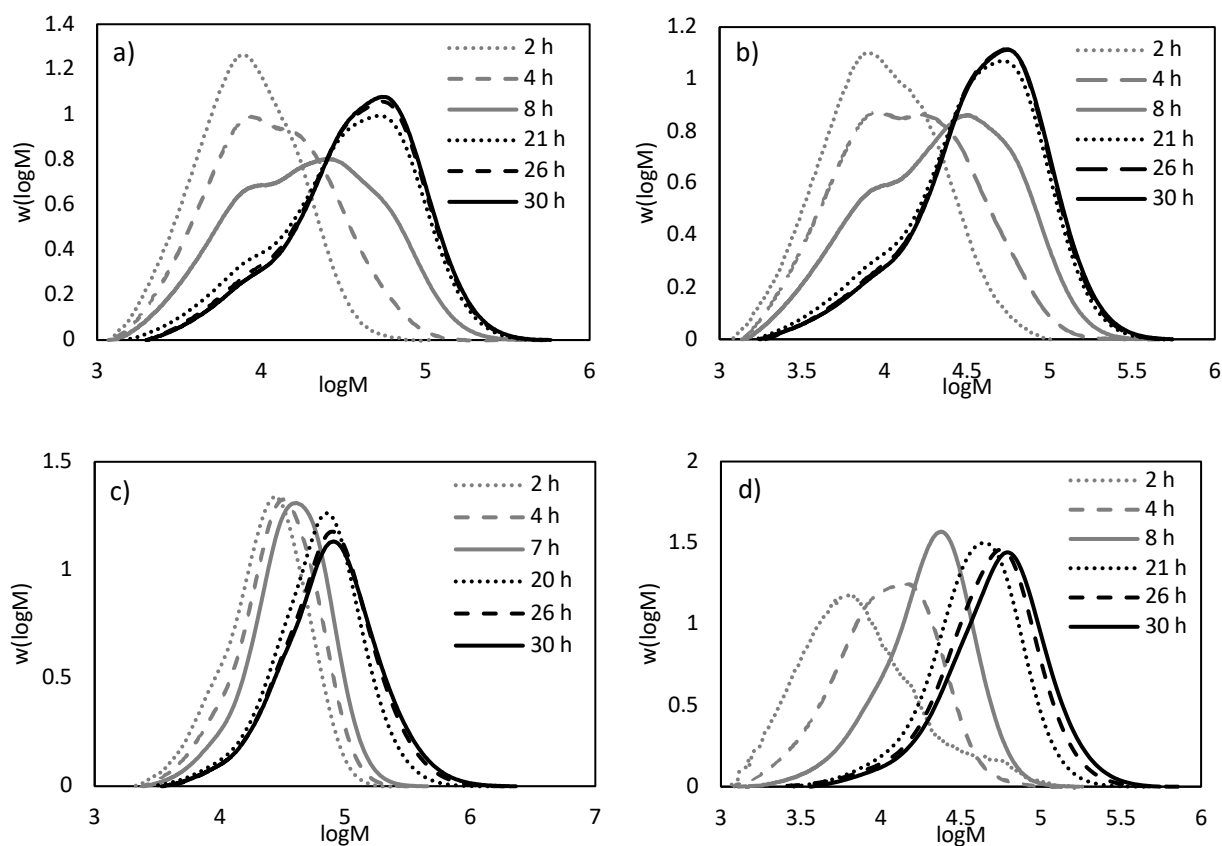


Figure 4-10. Molecular weight distributions of homopolymerizations of Far in miniemulsions and  $M_{n,target}$  of 50,000  $\text{g mol}^{-1}$  using D7 and (a) 5 wt % and (b) 15 wt % surfactant, and using NHS-BB and (c) 5 wt % and (d) 15 wt % surfactant.

Figure 4-11 is the MWD of the miniemulsion homopolymerization of Far done with  $M_{n,target} = 30,000 \text{ g mol}^{-1}$ . The dispersities are slightly higher compared to  $M_{n,target} = 50,000 \text{ g mol}^{-1}$  (2.38 vs 2.22, respectively), and this is evident from the more apparent low molecular weight shoulder in the MWD. Although a lower  $M_{n,target}$  should mean better control of polymerization (as there is a higher concentration of nitroxides), in this case it is likely due to the delay in initiation of polymer chains that is more apparent at a higher concentration of D7. As a result, there is a higher number of short polymer chains being formed.

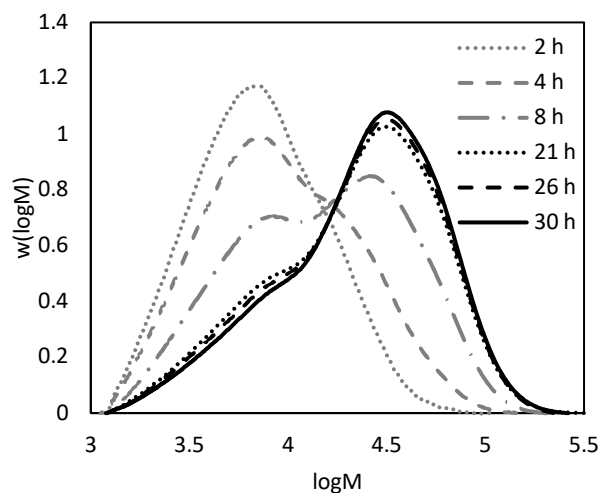


Figure 4-11. Molecular weight distributions of homopolymerizations of Far in the miniemulsion with 20 wt % monomer loading and  $M_{n,target}$  of  $30,000 \text{ g mol}^{-1}$  using D7 and 15 wt % surfactant.

#### 4.3.6 All bio-sourced diblock copolymers

It has been shown in this study that farnesene, a biosourced monomer, can be polymerized in dispersed aqueous media by nitroxide-mediated polymerization. These poly(Far) materials were chain-extended earlier with styrene to make diblock copolymers (somewhat resembling SBS materials which are triblock copolymers), and now they are chain-extended with another biosourced monomer, iBOMA, to make an virtually all-biosourced and more sustainable material compared to SBS. Poly(Far) made with both D7 and NHS-BB initiators, 15 wt % surfactant, and  $M_{n,target} = 50,000 \text{ g mol}^{-1}$  was used as the macroinitiator (poly(Far)-D7 and poly(Far)-NHS-BB, respectively).

Poly(Far)-NHS-BB was chain-extended with an iBOMA/Far mixture (10 mol % Far relative to iBOMA) as NHS-BB requires a small amount of the controlling comonomer to control the polymerization of a methacrylate [51]. Dienes such as isoprene, myrcene, and farnesene have been shown to be effective controlling comonomers in nitroxide-mediated polymerizations of methacrylates [24,39,41]. The resulting poly(Far-*b*-iBOMA-*ran*-Far) was essentially a diblock copolymer, where the molecular weight increased from 38,900 to 44,300 g mol<sup>-1</sup> and  $\bar{D}$  increased from 1.83 to 2.24. The MWDs of the chain extension is shown in Figure 4-12. As seen in the MWD, the shift in molecular weight was not significant and  $\bar{D}$  increased slightly, indicating some irreversible termination in the chain extension with iBOMA even with 10 mol % of Far as the controlling comonomer. This is consistent with poly(Far) made in bulk with NHS-BB when chain-extended with glycidyl methacrylate and 10 mol % Far [41].

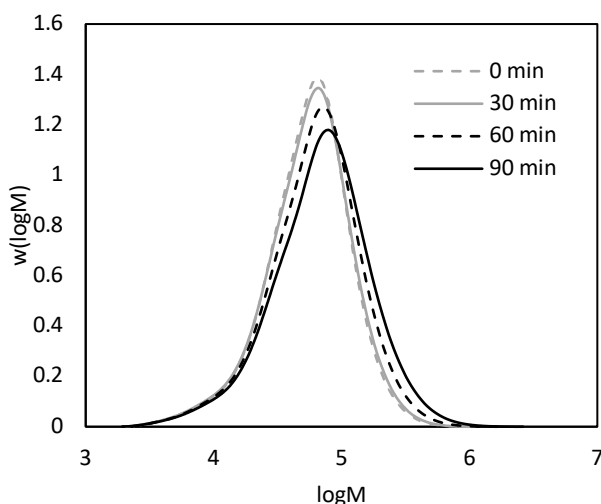


Figure 4-12. MWD of poly(Far-*b*-iBOMA-*ran*-Far) after 90 min of chain extension of poly(Far) made with NHS-BB, 15 wt % surfactant, and  $M_{n,target} = 50,000$  g mol<sup>-1</sup>.

Next, poly(Far)-D7 was also chain-extended with iBOMA for comparison, and no controlling comonomer was added with this macroinitiator as D7 does not require a controlling comonomer. The final poly(Far-*b*-iBOMA) polymer properties can be found in Table 4-3. The molecular weight increased from 15,400 to 30,600 g mol<sup>-1</sup>,  $\bar{D}$  decreased from 4.90 to 3.19, and the shift in MWD is seen in Figure 4-13. It is unclear why the initial  $\bar{D}$  was so high as the poly(Far)-D7 macroinitiator had a  $\bar{D}$  of 2.08. This chain extension was done twice and similar high  $\bar{D}$  was observed, but chain

extension did continue to proceed. As seen in Figure 4-13, the initial MWD had a low molecular weight shoulder. Perhaps the chain extension started with very fast polymerization of iBOMA, and only a portion of the macroinitiators were initiated. However, despite the high  $\bar{D}$ , the polymer chains continued to grow and eventually  $\bar{D}$  decreased with the disappearance of the low molecular weight shoulder. In fact, poly(Far)-D7 showed better chain extension compared to poly(Far)-NHS-BB as expected as there was a significant increase in molecular weight in the same reaction time without controlling comonomer despite the high dispersity. Furthermore, chain extension of poly(Far) made with D7 after 72 h of reaction was also successful, as shown in Figure B-7.

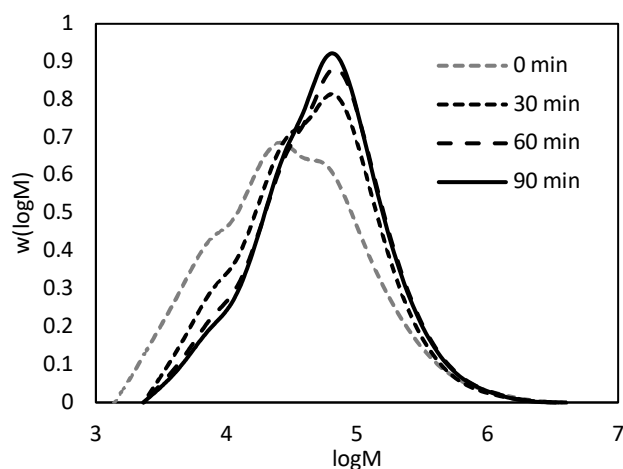


Figure 4-13. MWD of poly(Far-*b*-iBOMA) after 90 min of chain extension of poly(Far) made with D7, 15 wt % surfactant, and  $M_{n,target} = 50,000 \text{ g mol}^{-1}$ .

Table 4-3. Table of Miniemulsion Experiments with Different Initiators, Target Molecular Weights, and Surfactant Loading (Based on Monomer Content)

Experiment	Initiator	Target $M_n$ (g $\text{mol}^{-1}$ ) <sup>a</sup>	Surfactant loading (wt%) <sup>b</sup>	Oil phase			Water phase	
				$m_{\text{initiator}}$ (g)	$m_{\text{Far}}$ (g)	$m_{\text{co-stabilizer}}$ (g) <sup>c</sup>	$m_{\text{water}}$ (g)	$m_{\text{surfactant}}$ (g)
Exp 1	D7	50000	5	0.10	14.77	0.12	59.09	0.74
Exp 2	NHS-BB	50000	5	0.10	13.12	0.10	52.49	0.66
Exp 3	D7	50000	15	0.10	14.77	0.12	59.09	2.22
Exp 4	D7	30000	15	0.10	8.86	0.07	35.45	1.33
Exp 5	NHS-BB	50000	15	0.10	13.12	0.10	52.49	1.97

a) Target  $M_n$  is determined based on the initial monomer-to-alkoxyamine concentration ratio; b) Surfactant loading amounts are relative to monomer amounts; c) Costabilizer amounts were added at 0.8 wt % relative to the monomer.

#### 4.4 Conclusions

Farnesene, a biobased diene monomer, was successfully polymerized for the first time in miniemulsions via nitroxide-mediated polymerization. Although there was evidence of large oil droplets present, stable emulsions were achieved after 30 h, reaching a final conversion of ~30–40%. The resulting poly(Far) made with both D7 and NHS-BB initiators had active chain ends when 15 wt % surfactant was added to the system. This was attributed to a higher fraction of micron-sized droplets present in the emulsion. Particle size had an effect on the rates of polymerization, but they were still slow compared to rates in bulk, and so compartmentalization was still not achieved. Therefore, the molecular weights of poly(Far) homopolymers did not exceed the entanglement molecular weight to create sufficiently elastomeric materials. However, entirely biosourced diblock copolymers were synthesized by chain-extending poly(Far) macroinitiators with iBOMA, where macroinitiators made with D7 showed better chain-end fidelity than NHS-BB. This study showed that farnesene and iBOMA can be biobased alternatives to butadiene and styrene in making similar materials to SBS, as well as utilizing an aqueous dispersed system at ambient pressures to make the process more sustainable. Future works include optimizing the molecular weight and composition of the poly(Far-*b*-iBOMA) polymers to obtain more desirable rheological properties for TPEs.

#### 4.5 Experimental methods

##### 4.5.1 Materials

Trans- $\beta$ -farnesene, known as Biofene (Far,  $\geq 95\%$ ) was obtained from Amyris. Styrene (St,  $\geq 99\%$ ) monomer was purchased from Millipore Sigma. Isobornyl methacrylate (VISIOMER Terra iBOMA) was obtained from Evonik. Monomers were purified using 1.0 g of aluminum oxide (basic  $\text{Al}_2\text{O}_3$ , activated, Brockmann I) and 0.05 g of calcium hydride ( $\text{CaH}_2$ ,  $\geq 90\%$ ) per 50 mL of

the monomer, which were used as purchased from Millipore Sigma. 2-([*tert*-Butyl[1-(diethoxyphosphoryl)-2,2-dimethylpropyl]amino]oxy)-2-methylpropionic acid or BlocBuilder was kindly provided by Arkema and modified with an *N*-succinimidyl ester group by following a method used in literature to synthesize 2-methyl-2-[*N-tert*-butyl-*N*-(1-diethoxyphosphoryl)-2,2-dimethylpropyl]-aminoxy]-*N*-propionyloxysuccinimide or NHS-BlocBuilder (NHS-BB) [44]. 3-(((2-Cyanopropan-2-yl)oxy) (cyclohexyl)amino)-2,2-dimethyl-3-phenylpropanenitrile, Dispolreg 007 (D7) was synthesized according to the method described by Ballard et al [30]. Toluene ( $\geq 99\%$ ), methanol (MeOH,  $\geq 99\%$ ), and tetrahydrofuran (THF, 99.9% HPLC grade) were obtained from Fisher Scientific and used as received. Deuterated chloroform ( $\text{CDCl}_3$ , 99.9% D) was purchased from Cambridge Isotope Laboratories, USA, and used as received. DOWFAX 8390 was purchased for The Dow Chemical Company and used as purchased. Hexadecane (99%) was used as purchased from Millipore Sigma.

#### 4.5.2 Homopolymerization of farnesene in miniemulsions

The miniemulsions were done with 20 wt % monomer in water (20% solids content) purified by reverse osmosis (RO) (see Table 4-3 for miniemulsion recipes). DOWFAX 8390 surfactant was dissolved in water and stirred for 10 min in a 100 mL glass beaker. The Far monomer, initiator, and hexadecane (used as the costabilizer) were dissolved and stirred separately in a 20 mL vial for 10 min. The oil phase was added to the aqueous phase and stirred with a magnetic stir bar for another 15 min before being sonicated for 10 min at 70% amplitude and 0.50 duty cycle using the Hielscher sonicator UP200S. The milky emulsified mixture was added into a 100 mL three-neck round-bottom flask and purged with nitrogen for 30 min before being heated up to 90 °C with stirring for polymerization to occur for 30 h. A reflux condenser was attached to the reactor to ensure all volatile components remain in the reactor. Samples were taken intermittently for gravimetric conversion calculation and molecular weight analysis.

#### 4.5.3 Chain-extension of poly(Far) macroinitiator

Purified poly(Far) macroinitiators (~0.5–0.75 g) were dissolved in toluene with either St and/or iBOMA monomer added to the solution (50 wt % monomer and macroinitiator in toluene). The reaction mixture was added to a 10 mL three-neck round-bottom flask and purged with nitrogen for 30 min with stirring. The chain-extension reactions were done at 120 °C for 90–120 min with

a reflux condenser attached. Similarly, samples were taken intermittently for gravimetric or  $^1\text{H}$  NMR conversion calculation and molecular weight analysis.

#### 4.5.4 Polymer characterization

Monomer conversion was determined gravimetrically. The samples ( $\sim 3$  mL) taken from the miniemulsions were weighed and dried under air for 24 h to remove most of the water and then placed in the vacuum oven at room temperature to ensure residual water was removed. Afterward, the polymer/monomer mixture was redissolved again in small amounts of toluene ( $\sim 2$  mL) and precipitated in excess methanol. The polymer samples were then dried under air for several hours before being dried in the vacuum oven completely at room temperature overnight. The final dried polymers were weighed and used to determine the conversion. The conversion calculations of the chain-extension reactions with St and iBOMA were done by  $^1\text{H}$  NMR (see Figures B-8 and B-9 in Appendix B). Copolymer compositions were analyzed by  $^1\text{H}$  NMR as well (Figure B-10).

Number-average molecular weight ( $M_n$ ) and dispersity ( $\mathcal{D} = M_w/M_n$ ) of polymer samples were measured using gel permeation chromatography (GPC, Water Breeze) with HPLC-grade THF as an eluent at a flow rate of  $0.3 \text{ mL min}^{-1}$ . The GPC has three Waters Styragel HR columns (HR1 with a molecular weight measurement range of  $10^2$  to  $5 \times 10^3 \text{ g mol}^{-1}$ , HR2 with a molecular weight measurement range of  $5 \times 10^2$  to  $2 \times 10^4 \text{ g mol}^{-1}$ , and HR4 with a molecular weight measurement range of  $5 \times 10^3$  to  $6 \times 10^5 \text{ g mol}^{-1}$ ), a guard column, and a refractive index (RI 2414) detector. The columns were heated to  $40 \text{ }^\circ\text{C}$  during analysis. The molecular weights were determined relative to poly(methyl methacrylate) (PMMA) calibration standards from Varian Inc. (ranging from 875 to  $1,677,000 \text{ g mol}^{-1}$ ). The reported molecular weights were all relative to the PMMA standards and not adjusted with Mark–Houwink parameters.

#### 4.5.5 Particle size characterization

Particle size distributions of the miniemulsion experiments were measured by dynamic light scattering (DLS) using the Malvern Zetasizer Nano-ZS. The instrument has a 4 mW He–Ne laser at 633 nm and an avalanche photodiode detector. The original dispersed samples were further diluted with water ( $0.01$ – $1000 \text{ mg ml}^{-1}$ ) for analysis. Samples were analyzed with a measurement angle of  $173^\circ$  at  $25 \text{ }^\circ\text{C}$ , and each sample measurement was repeated five times.



#### 4.6 References

- [1] Morton, M.; McGrath, J. E.; Juliano, P. C., Structure-property relationships for styrene-diene thermoplastic elastomers. *J. Polym. Sci., Part C: Polym. Symp.* 1969, 26 (1), 99-115.
- [2] Drobny, J. G., 15 - Applications of Thermoplastic Elastomers. In *Handbook of Thermoplastic Elastomers*, Drobny, J. G., Ed. William Andrew Publishing: Norwich, NY, 2007; pp 281-315.
- [3] Wang, S.; Wang, Q.; Wu, X.; Zhang, Y., Asphalt modified by thermoplastic elastomer based on recycled rubber. *Constr. Build. Mater.* 2015, 93, 678-684.
- [4] White, W. C., Butadiene production process overview. *Chem.-Bio. Interact.* 2007, 166 (1), 10-14.
- [5] Custro, S.; Zazzetta, A. Styrene-isoprene block copolymers. US5284915A, 1994.
- [6] Johnson, A. F.; Worsfold, D. J., Anionic polymerization of butadiene and styrene. *J. Polym. Sci., Part A: Gen. Pap.* 1965, 3 (2), 449-455.
- [7] Abdelrahman, O. A.; Park, D. S.; Vinter, K. P.; Spanjers, C. S.; Ren, L.; Cho, H. J.; Vlachos, D. G.; Fan, W.; Tsapatsis, M.; Dauenhauer, P. J., Biomass-Derived Butadiene by Dehydro-Decyclization of Tetrahydrofuran. *ACS Sustainable Chem. Eng.* 2017, 5 (5), 3732-3736.
- [8] Abdelrahman, O. A.; Park, D. S.; Vinter, K. P.; Spanjers, C. S.; Ren, L.; Cho, H. J.; Zhang, K.; Fan, W.; Tsapatsis, M.; Dauenhauer, P. J., Renewable Isoprene by Sequential Hydrogenation of Itaconic Acid and Dehydro-Decyclization of 3-Methyl-Tetrahydrofuran. *ACS Catal.* 2017, 7 (2), 1428-1431.

- [9] Jenkins Aubrey, D.; Jones Richard, G.; Moad, G., Terminology for reversible-deactivation radical polymerization previously called "controlled" radical or "living" radical polymerization (IUPAC Recommendations 2010). In *Pure and Applied Chemistry*, 2009; Vol. 82, p 483.
- [10] Shipp, D. A., Reversible-Deactivation Radical Polymerizations. *Polym. Rev.* 2011, 51 (2), 99-103.
- [11] Matyjaszewski, K.; Xia, J., Atom Transfer Radical Polymerization. *Chem. Rev.* 2001, 101 (9), 2921-2990.
- [12] Chiefari, J.; Chong, Y. K.; Ercole, F.; Krstina, J.; Jeffery, J.; Le, T. P. T.; Mayadunne, R. T. A.; Meijs, G. F.; Moad, C. L.; Moad, G.; Rizzardo, E.; Thang, S. H., Living Free-Radical Polymerization by Reversible Addition–Fragmentation Chain Transfer: The RAFT Process. *Macromol.* 1998, 31 (16), 5559-5562.
- [13] Georges, M. K.; Veregin, R. P. N.; Kazmaier, P. M.; Hamer, G. K., Narrow molecular weight resins by a free-radical polymerization process. *Macromol.* 1993, 26 (11), 2987-2988.
- [14]. Cunningham, M. F., Controlled/living radical polymerization in aqueous dispersed systems. *Prog. Polym. Sci.* 2008, 33 (4), 365-398.
- [15] Schneider, M.; Claverie, J.; Graillat, C.; McKenna, T. F., High solids content emulsions. I. A study of the influence of the particle size distribution and polymer concentration on viscosity. *J. Appl. Polym. Sci.* 2002, 84 (10), 1878-1896.
- [16] Kagawa, Y.; Zetterlund, P. B.; Minami, H.; Okubo, M., Compartmentalization in Atom Transfer Radical Polymerization (ATRP) in Dispersed Systems. *Macromol. Theory Simul.* 2006, 15 (8), 608-613.

- [17] Zetterlund, P. B.; Okubo, M., Compartmentalization in Nitroxide-Mediated Radical Polymerization in Dispersed Systems. *Macromol.* 2006, 39 (26), 8959-8967.
- [18] Suzuki, K.; Nishimura, Y.; Kanematsu, Y.; Masuda, Y.; Satoh, S.; Tobita, H., Experimental Validation of Intermediate Termination in RAFT Polymerization with Dithiobenzoate via Comparison of Miniemulsion and Bulk Polymerization Rates. *Macromol. React. Eng.* 2012, 6 (1), 17-23.
- [19] Qiu, J.; Pintauer, T.; Gaynor, S. G.; Matyjaszewski, K.; Charleux, B.; Vairon, J.-P., Mechanistic Aspect of Reverse Atom Transfer Radical Polymerization of n-Butyl Methacrylate in Aqueous Dispersed System. *Macromol.* 2000, 33 (20), 7310-7320.
- [20] Zetterlund, P. B., Nitroxide-Mediated Radical Polymerization in Dispersed Systems: Compartmentalization and Nitroxide Partitioning. *Macromol. Theory Simul.* 2010, 19 (1), 11-23.
- [21] Moad, G.; Mayadunne, R. T. A.; Rizzardo, E.; Skidmore, M.; Thang, S. H., Kinetics and Mechanism of RAFT Polymerization. In *Advances in Controlled/Living Radical Polymerization*, American Chemical Society: 2003; Vol. 854, pp 520-535.
- [22] Jitchum, V.; Perrier, S., Living Radical Polymerization of Isoprene via the RAFT Process. *Macromol.* 2007, 40 (5), 1408-1412.
- [23] Moad, G., Reversible addition–fragmentation chain transfer (co)polymerization of conjugated diene monomers: butadiene, isoprene and chloroprene. *Polym. Int.* 2017, 66 (1), 26-41.
- [24] Benoit, D.; Harth, E.; Fox, P.; Waymouth, R. M.; Hawker, C. J., Accurate Structural Control and Block Formation in the Living Polymerization of 1,3-Dienes by Nitroxide-Mediated Procedures. *Macromol.* 2000, 33 (2), 363-370.

- [25] Bar-Nes, G.; Hall, R.; Sharma, V.; Gaborieau, M.; Lucas, D.; Castignolles, P.; Gilbert, R. G., Controlled/living radical polymerization of isoprene and butadiene in emulsion. *Europ. Polym. J.* 2009, 45 (11), 3149-3163.
- [26] Gramlich, W. M.; Theryo, G.; Hillmyer, M. A., Copolymerization of isoprene and hydroxyl containing monomers by controlled radical and emulsion methods. *Polym. Chem.* 2012, 3 (6), 1510-1516.
- [27] Wei, R.; Luo, Y.; Zeng, W.; Wang, F.; Xu, S., Styrene–Butadiene–Styrene Triblock Copolymer Latex via Reversible Addition–Fragmentation Chain Transfer Miniemulsion Polymerization. *Ind. Eng. Chem. Res.* 2012, 51 (47), 15530-15535.
- [28] Maehata, H.; Liu, X.; Cunningham, M.; Keoshkerian, B., TEMPO-Mediated Emulsion Polymerization. *Macromol. Rapid Commun.* 2008, 29 (6), 479-484.
- [29] Charleux, B.; Nicolas, J., Water-soluble SG1-based alkoxyamines: A breakthrough in controlled/living free-radical polymerization in aqueous dispersed media. *Polym.* 2007, 48 (20), 5813-5833.
- [30] Ballard, N.; Aguirre, M.; Simula, A.; Agirre, A.; Leiza, J. R.; Asua, J. M.; van Es, S., New Class of Alkoxyamines for Efficient Controlled Homopolymerization of Methacrylates. *ACS Macro Lett.* 2016, 5 (9), 1019-1022.
- [31] Ballard, N.; Aguirre, M.; Simula, A.; Leiza, J. R.; van Es, S.; Asua, J. M., High solids content nitroxide mediated miniemulsion polymerization of n-butyl methacrylate. *Polym. Chem.* 2017, 8 (10), 1628-1635.
- [32] Noppalit, S.; Simula, A.; Billon, L.; Asua, J. M., On the nitroxide mediated polymerization of methacrylates derived from bio-sourced terpenes in miniemulsion, a step towards sustainable products. *Polym. Chem.* 2020, 11 (6), 1151-1160.

- [33] Behr, A.; Johnen, L., Myrcene as a Natural Base Chemical in Sustainable Chemistry: A Critical Review. *ChemSusChem* 2009, 2 (12), 1072-1095.
- [34] Rude, M. A.; Schirmer, A., New microbial fuels: a biotech perspective. *Curr. Opin. Microbiol.* 2009, 12 (3), 274-281.
- [35] Bauer, N.; Brunke, J.; Kali, G., Controlled Radical Polymerization of Myrcene in Bulk: Mapping the Effect of Conditions on the System. *ACS Sustainable Chem. Eng.* 2017, 5 (11), 10084-10092.
- [36] Sarkar, P.; Bhowmick, A. K., Synthesis, characterization and properties of a bio-based elastomer: polymyrcene. *RSC Adv.* 2014, 4 (106), 61343-61354.
- [37] Yoo, T.; Henning, S. K., Synthesis and Characterization of Farnesene-based Polymers. *Rubber Chem. Technol.* 2017, 90 (2), 308-324.
- [38] Sahu, P.; Bhowmick, A. K., Redox Emulsion Polymerization of Terpenes: Mapping the Effect of the System, Structure, and Reactivity. *Ind. Eng. Chem. Res.* 2019, 58 (46), 20946-20960.
- [39] Métafiot, A.; Gérard, J. F.; Defoort, B.; Marić, M., Synthesis of  $\beta$ -myrcene/glycidyl methacrylate statistical and amphiphilic diblock copolymers by SG1 nitroxide-mediated controlled radical polymerization. *J. Polym. Sci., Part A: Polym. Chem.* 2018, 56 (8), 860-878.
- [40] Métafiot, A.; Kanawati, Y.; Gérard, J. F.; Defoort, B.; Marić, M., Synthesis of  $\beta$ -Myrcene-Based Polymers and Styrene Block and Statistical Copolymers by SG1 Nitroxide-Mediated Controlled Radical Polymerization. *Macromol.* 2017, 50 (8), 3101-3120.
- [41] Luk, S. B.; Marić, M., Nitroxide-Mediated Polymerization of Bio-Based Farnesene with a Functionalized Methacrylate. *Macromol. React. Eng.* 2019, 13 (3), 1800080.

- [42] Fetters, L. J.; Lohse, D. J.; Richter, D.; Witten, T. A.; Zirkel, A., Connection between Polymer Molecular Weight, Density, Chain Dimensions, and Melt Viscoelastic Properties. *Macromol.* 1994, 27 (17), 4639-4647.
- [43] Iacob, C.; Yoo, T.; Runt, J., Molecular Dynamics of Polyfarnesene. *Macromol.* 2018, 51 (13), 4917-4922.
- [44] Vinas, J.; Chagneux, N.; Gignes, D.; Trimaille, T.; Favier, A.; Bertin, D., SG1-based alkoxyamine bearing a N-succinimidyl ester: A versatile tool for advanced polymer synthesis. *Polym.* 2008, 49 (17), 3639-3647.
- [45] Cunningham, M. F., Recent progress in nitroxide-mediated polymerizations in miniemulsion. *C. R. Chim.* 2003, 6 (11), 1351-1374.
- [46] DOWFAX, Anionic Surfactants. Dow Company Co.: Midland, MI, 48641-1206, 1991.
- [47] Gilbert, R. G., Emulsion polymerization: a mechanistic approach. Academic Pr: 1995.
- [48] Pan, G.; Sudol, E. D.; Dimonie, V. L.; El-Aasser, M. S., Surfactant Concentration Effects on Nitroxide-Mediated Living Free Radical Miniemulsion Polymerization of Styrene. *Macromol.* 2002, 35 (18), 6915-6919.
- [49] Maehata, H.; Buragina, C.; Cunningham, M.; Keoshkerian, B., Compartmentalization in TEMPO-Mediated Styrene Miniemulsion Polymerization. *Macromol.* 2007, 40 (20), 7126-7131.
- [50] Zetterlund, P. B.; Okubo, M., Compartmentalization in TEMPO-Mediated Radical Polymerization in Dispersed Systems: Effects of Macroinitiator Concentration. *Macromol. Theory Simul.* 2007, 16 (3), 221-226.

[51] Charleux, B.; Nicolas, J.; Guerret, O., Theoretical Expression of the Average Activation–Deactivation Equilibrium Constant in Controlled/Living Free-Radical Copolymerization Operating via Reversible Termination. Application to a Strongly Improved Control in Nitroxide-Mediated Polymerization of Methyl Methacrylate. *Macromol.* 2005, 38 (13), 5485-5492.

## 5 Farnesene and norbornenyl methacrylate block copolymers: application of thiol-ene clicking to improve thermal and mechanical properties

The synthesis of block copolymers using D7 is now better understood, therefore the optimization of mechanical and rheological properties are investigated. The polymerization of ethylene glycol dicyclopentenyl methacrylate (EGDEMA) followed by chain-extension with Far was explored in this chapter. EGDEMA is interesting because it is another functionalized methacrylate with a norbornene group containing a second double bond. Furthermore, poly(EGDEMA) is relatively “soft” due to its flexible ether linkages and modest  $T_g$  of 28°C [45]. Poly(EGDEMA) was mostly studied for its antibacterial properties in applications such as coatings and barriers, however their polymerization kinetics were not described [43-45]. EGDEMA was previously polymerized using conventional SG1-based initiators, but required small amounts of controlling comonomer [49], however this chapter showed that D7 can successfully control the homopolymerization of EGDEMA and demonstrated linear polymer chain growth and active chain-ends for re-initiation. Both poly(EGDEMA) and poly(EGDEMA-*co*-iBOMA) were synthesized using D7 and then chain-extended with Far to make various block copolymers of different block lengths. The second double bond of EGDEMA units were exploited using thiol-ene click chemistry to attach thiol-POSS units. The small amounts of POSS incorporated (<10 mol%) into the polymer chains were able to enhance thermal stability by decreasing the depolymerization of Far units, cyclization between side chains, as well as the release of isobornyl units. The mechanical strength of the poly(EGDEMA-*b*-Far) was reinforced by the POSS functionalization, as well as the addition of iBOMA in poly(EGDEMA-*co*-iBOMA-*b*-Far). Therefore, the use of EGDEMA in block copolymer synthesis with post-polymerization modification and potential application as TPEs is entirely novel. This work is described in more detail in this chapter, and it is currently under review at *Polymer* (S. B. Luk, M. Marić. POLYMER-21-1277, submitted: June 2021). The supporting information of this manuscript is in Appendix C, and the supporting figures and tables are referred to as Figure C-X and Table C-X in this chapter.

## 5.1 Abstract

Novel block copolymers were synthesized for the first time via nitroxide-mediated polymerization (NMP) using ethylene glycol dicyclopentenyl methacrylate (EGDEMA), which has a pendent double bond in the norbornene group, and farnesene (Far), a terpene-based diene. Homo poly(EGDEMA) was synthesized successfully using Dispolreg 007 initiator without any co-monomer as typically required of NMP, and the macroinitiator was chain-extended with Far making poly(EGDEMA-*b*-Far) diblock copolymers. Due to the relatively low glass transition temperature ( $T_g$ ) of poly(EGDEMA), the methacrylate block was also copolymerized statistically with isobornyl methacrylate (iBOMA) to add stiffness, then chain-extended with Far. Additionally, the pendent double bond of EGDEMA allowed for thiol-ene clicking of POSS units for further functionalization of these block copolymers. However, the conjugation efficiency of the thermally initiated thiol-ene clicking was low and resulted in low POSS incorporation (1.6 – 10 mol%), especially for block copolymers that included iBOMA due to its increased stiffness and steric hindrance. Nonetheless, the added POSS improved the thermal stability by minimizing the degradation of the 1,4-addition Far units, as well as the degradation of isobornyl units of iBOMA. The mechanical strength was also increased as POSS units reinforced the physical crosslinks of these block copolymers as shown by an increase in linear viscoelastic regions. Distinct  $T_g$ s were observed for the respective elastomeric poly(Far) block (~70°C) and thermoplastic block (30°C for poly(EGDEMA) and 110°C for poly(EGDEMA-*co*-iBOMA)), therefore suggesting microphase separation. An increase in  $T_g$  was also observed in all polymers with added POSS, further confirming the added stiffness provided by POSS. These poly(EGDEMA-*b*-Far) and poly(EGDEMA-*co*-iBOMA-*b*-Far) show great versatility as alternative TPE materials, with improved mechanical and thermal properties added by functionalization of POSS.

## 5.2 Introduction

Thermoplastic elastomers (TPEs) are very industrially relevant as they exhibit rubbery properties at usage temperatures but can still be processed at high temperatures like thermoplastics. Unlike vulcanized or chemically crosslinked elastomers (i.e. thermosets), TPEs are made of hard thermoplastics with high glass transition temperatures ( $T_g$  above ambient temperature) that act as

physical crosslinks and soft elastomers serving as a matrix with low  $T_g$  [1]. Due to the immiscibility of the respective polymers, these polymers undergo phase separation, which is important for providing mechanical strength in the material. Block or grafted copolymer TPEs differ from melt-blended TPEs as they are synthesized by more sophisticated methods like ionic polymerization and therefore do not require post-polymerization blending [2]. Furthermore, melt-blended polymers exhibit macrophase separation, as opposed to block copolymers which exhibit microphase separation and can lead to various morphologies of the dispersed domains such as spheres, cylinders, or lamellae [1].

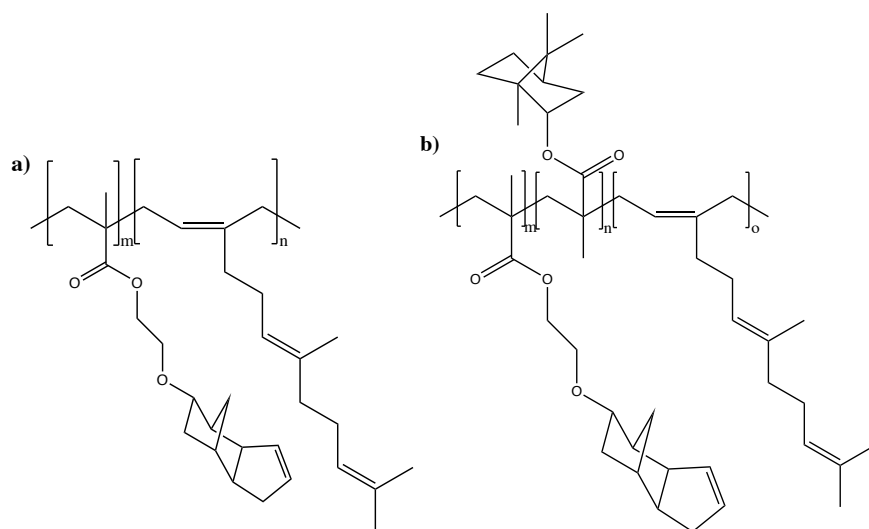
Examples of TPEs like poly(styrene-*b*-butadiene-*b*-styrene) (SBS) and poly(styrene-*b*-(ethylene-*co*-butadiene)-*b*-styrene) (SEBS) are typically synthesized via ionic polymerization [3, 4]. Ionic polymerization applies the ionic nature of the active polymerization site and can produce polymers with precise molecular architecture, like block copolymers, with low dispersity [5, 6]. However, this method requires stringent conditions (i.e. no impurities, absence of water) and is intolerant to functional monomers, thereby necessitating the use of protecting groups in some cases. Reversible deactivation radical polymerization (RDRP) employs the simplicity of radical polymerization, but it is also able to make block copolymers with low dispersity via the persistent radical effect (PRE) or reversible chain transfer [7]. In this method, the active polymerization site is a radical that is suppressed with a radical deactivator or chain transfer agent in an equilibrium such that irreversible termination is suppressed. In addition, RDRP is able to polymerize a wide variety of functional monomers derived from (meth)acrylates, styrenics, and (meth)acrylamides, not only in bulk or solution, but in aqueous dispersions, as well [8]. Among the different types of RDRP, nitroxide-mediated polymerization (NMP) was the first RDRP method used to polymerize styrene and then successfully used to synthesize SBS, which demonstrated that NMP was a viable alternative to ionic polymerization to produce TPEs [9]. Therefore, NMP was the chosen method to make alternative block copolymers with potential applications as TPEs in this study.

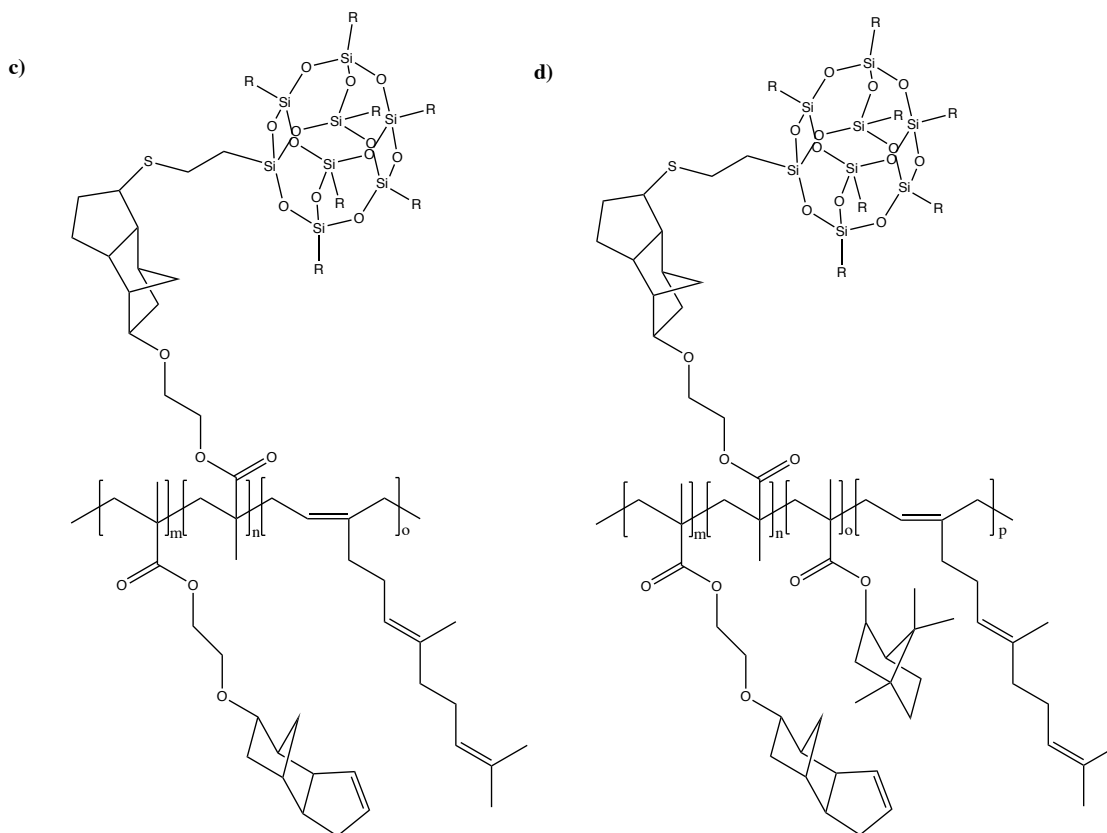
Recently, it has become apparent that movement towards bio-sourced materials is important towards lessening the impact on the environment, amid other initiatives. Myrcene is a terpene-based diene that is formed from the pyrolysis of  $\beta$ -pinene, which is found in tree sap [10, 11]. Farnesene is a similar monomer that is derived from terpenoids but can be produced by

microorganisms [12-14]. Myrcene and farnesene are bio-based alternatives to petroleum-derived butadiene or isoprene and have been successfully polymerized ionically or using RDRP to make rubbery materials similar to poly(butadiene) and poly(isoprene) [15-19]. They also have low  $T_g$ s ( $T_g \sim -70^\circ\text{C}$  for both poly(myrcene) and poly(farnesene), similar to  $T_g = -100^\circ\text{C}$  for poly(butadiene)) with the potential of improved viscoelastic properties due to their bottlebrush-like structure making them good candidates for TPEs [20, 21]. Farnesene (Far) has also been polymerized via NMP using SG1-based and Dispolreg 007 initiators, and copolymerized with functionalized methacrylates such as glycidyl methacrylate and isobornyl methacrylate (iBOMA) [22, 23]. Similarly, myrcene has been polymerized with NMP and block copolymers made with myrcene and iBOMA showed increased thermal stability and mechanical properties, which suggests that polymers synthesized with bio-based dienes and functionalized methacrylates have potential to be effective, versatile TPEs [24].

One methacrylic comonomer of interest that has not been widely studied is ethylene glycol dicyclopentenyl ether methacrylate (EGDEMA), which contains a norbornene group with a pendent double bond. Poly(EGDEMA) was shown to be resistant to bacterial attachment and has been studied mainly for applications such as anti-bacterial films and coatings [25-27]. The polymerization of EGDEMA was previously reported for NMP, however using the conventional SG1-based initiator led to high dispersity ( $\text{Đ} \sim 1.56 - 1.74$ ) and irreversibly terminated polymer chains without copolymerizing with styrene comonomer [28]. SG1-based initiators often require controlling comonomer when polymerizing methacrylates due to slow deactivation between the radical centre and nitroxide [29-31]. Consequently, Dispolreg 007 (D7) initiator was developed to be able to homopolymerize methacrylates with active chain-ends and does not require controlling comonomer [32, 33]. D7 initiator has a faster rate of combination between the nitroxide and the active methacrylate radical such that the homopolymerization of methacrylates is much better controlled compared to SG1-based initiators. Poly(EGDEMA) homopolymer and triblock copolymers were also successfully synthesized by ATRP [34, 35]. It was discovered that poly(EGDEMA) has a relatively low  $T_g$  ( $28^\circ\text{C}$ ) compared to other poly(methacrylates) due to the chain mobility provided by the ethylene glycol ether bonds. Comparatively, poly(iBOMA) also contains a norbornyl group but has a very high  $T_g$  (up to  $190^\circ\text{C}$ ) due to the much more rigid bond between the methacrylate and norbornyl group [34, 36].

Post-polymerization methods are commonly done to add functionality in order to reinforce material properties or improve compatibility. Polyhedral oligomeric silsesquioxanes (POSS) is a bulky inorganic-organic cage-like molecule that has been copolymerized or used as an additive to improve mechanical properties, thermal stability, and anti-flammability in polymer materials [37-40]. POSS has been successfully clicked onto azido-functionalized SEBS to reinforce the TPE material [41]. Furthermore, poly(EGDEMA) was also successfully modified by thiol-ene click chemistry to add hydrophilicity and improve adhesion properties [34, 35]. In this study, the synthesis of poly(EGDEMA-*b*-Far) diblock copolymers by NMP was investigated using D7 initiator for the first time. Post-polymerization via thiol-ene click chemistry of the resulting block copolymers was done with a thiol-containing POSS (thiol-POSS) (Scheme 5-1a and c). The EGDEMA methacrylate block was also copolymerized with iBOMA to increase the  $T_g$  of the methacrylate block, then chain-extended with Far, in addition to thiol-ene clicking with thiol-POSS (Scheme 5-1b and d). The thermal properties and rheology of the block copolymers were studied to compare between different concentrations of thiol-POSS added, block copolymer compositions, and with and without copolymerization with iBOMA. The aim of this study is to show these poly(methacrylate-*b*-farnesene) block copolymers with the addition of POSS groups could potentially be an alternative TPE with improved thermal properties.





Scheme 5-1: Chemical structures of a) poly(EGDEMA-*b*-Far) and b) poly(EGDEMA-*co*-iBOMA-*b*-Far) block copolymers synthesized via NMP using D7 initiators. These block copolymers then underwent thiol-ene clicking with thiol-POSS and the proposed chemical structures are shown in c) and d). The *R* groups on the POSS units represent isobutyl groups.

### 5.3 Experimental Methods

#### 5.3.1 Materials

Ethylene glycol dicyclopentenyl ether methacrylate (EGDEMA  $\geq 90\%$ ) was purchased from Millipore Sigma. Isobornyl methacrylate (VISIOMER®, Terra iBOMA) monomer was obtained from Evonik. Trans- $\beta$ -farnesene, or Biofene (Far  $\geq 95\%$ ), was obtained from Amyris. Monomers were purified using 1.0 g of aluminum oxide (basic Al<sub>2</sub>O<sub>3</sub>, activated, Brockmann I) and 0.05 g calcium hydride (CaH<sub>2</sub>,  $\geq 90\%$ ) per 50 mL of monomer, which were used as purchased from

Millipore Sigma. Mercaptopropyl isobutyl polyhedral oligomeric silsesquioxanes (thiol-POSS, 100%) was purchased from Hybrid Plastics Inc, and used as received. Azobisisobutyronitrile (AIBN, 98%) radical initiator was used as received from Millipore Sigma. Toluene ( $\geq 99.5\%$ ), xylene ( $\geq 98.5\%$ ), methanol (MeOH,  $\geq 99.8\%$ ), and tetrahydrofuran (THF, 99.9% HPLC grade) were purchased from Fisher Chemicals and used as received. Deuterated chloroform ( $\text{CDCl}_3$ , 99.9% D) was purchased from Cambridge Isotope Laboratories, USA and used as received. Dispolreg 007 initiator was synthesized according to the procedure described by Ballard *et al* [32].

### 5.3.2 Synthesis of poly(EGDEMA) or poly(EGDEMA-co-iBOMA) macroinitiator

A typical formulation for the synthesis of poly(EGDEMA) macroinitiator was 0.3 g (0.89 mmol) of D7, 8.86 g (33.8 mmol) of EGDEMA monomer, and 8.86 g (96.2 mmol) of toluene solvent added into a 50 mL three-neck round bottom flask. The reactor was attached to a condenser to prevent evaporation of solvent and monomer. For the poly(EGDEMA-co-iBOMA) macroinitiators, 0.30 g of D7 was added, along with an equimolar mixture of EGDEMA (4.07 g, 18.3 mmol) and iBOMA (4.80 g, 18.3 mmol) monomers and 8.86 g (96.2 mmol) of toluene. Detailed formulations for macroinitiator synthesis are shown in Table 5-1. The mixture was then purged with nitrogen for 30 mins and reaction would proceed under nitrogen atmosphere at  $90^\circ\text{C}$  with stirring. The reaction time would vary between 60 to 120 min depending on the desired chain length for the macroinitiators. The resulting polymers were precipitated with methanol, then dried under air overnight and in a vacuum oven at room temperature for a day, and they are characterized in Table 5-1.

Table 5-1. Formulations for poly(EGDEMA) and poly(EGDEMA-co-iBOMA) macroinitiator synthesis at  $90^\circ\text{C}$  and polymer characterization.

Macroinitiator ID	$m_{\text{D7}}$ (g mL <sup>-1</sup> )	$m_{\text{EGDEMA}}$ (g mL <sup>-1</sup> )	$m_{\text{iBOMA}}$ (g mL <sup>-1</sup> )	$m_{\text{toluene}}$ (g mL <sup>-1</sup> )	$X$	$M_n$ of			
						macroinitiat or (g mol <sup>-1</sup> )	$\bar{D}$	$F_{\text{EGDEMA}}$	$F_{\text{iBOMA}}$
EG1	0.0161	0.477	-	0.477	32.0% <sup>a</sup>	7,500	1.57	1.00	-
EG2	0.00538	0.477	-	0.477	46.7% <sup>a</sup>	15,700	1.64	1.00	-
EGiB1	0.0158	0.215	0.253	0.467	36.0% <sup>b</sup>	7,700	1.58	0.49	0.51
EGiB2	0.00527	0.214	0.253	0.467	42.2% <sup>b</sup>	15,600	1.59	0.50	0.50

a) Conversion of the homopolymerization of EGDEMA monomer was calculated using  $^1\text{H}$  NMR relative to inert  $\text{CH}_2$  ether protons of EGDEMA (see Figure C-1 and C-2); b) Average conversion of the equimolar copolymerization of EGDEMA and iBOMA, where conversion of EGDEMA was calculated using  $^1\text{H}$  NMR relative to inert  $\text{CH}_2$  ether protons (see Figure C-3 and C-4).

### 5.3.3 Chain-extension of poly(EGDEMA) or poly(EGDEMA-*co*-iBOMA) with Far

The dried poly(EGDEMA) or poly(EGDEMA-*co*-iBOMA) macroinitiators were dissolved in xylene in a 100 mL round-bottom flask and Far monomer was added. The formulations used for chain-extension with Far monomer to synthesize diblock copolymers are shown in Table 5-2. Similarly, reaction mixtures were purged with nitrogen for 30 mins, and reactions proceeded at  $120^\circ\text{C}$  for 120 to 300 mins depending on the desired final polymer chain length. Final block copolymers were precipitated using methanol, then dried in air overnight and in a vacuum oven at room temperature for a day.

Table 5-2. Recipes for poly(EGDEMA) and poly(EGDEMA-*co*-iBOMA) macroinitiator chain-extensions with Far at  $120^\circ\text{C}$  and polymer characterization.

Block copolymer ID	$m_{\text{macroinitiator}}$ (wt%)	$m_{\text{Far}}$ (wt%)	$m_{\text{xylene}}$ (wt%)	$X_{\text{Far}}^a$	Final $M_n$ (g mol $^{-1}$ )	Final $\bar{D}$
EG1-Far	7.14	42.9	50.0	35.0%	19,000	1.86
EG2-Far	22.0	28.0	50.0	23.0%	25,300	1.77
EGiB1-Far	8.00	42.0	50.0	32.0%	22,700	1.84
EGiB2-Far	11.9	38.1	50.0	33.0%	29,700	1.87

a) Conversion of Far monomer in the chain-extensions of macroinitiators for synthesis of block copolymers.

### 5.3.4 Thiol-ene clicking of block copolymers with thiol-POSS

Thiol-ene clicking of the poly(methacrylate-*b*-Far) block copolymers were done with mercaptopropyl isobutyl POSS (thiol-POSS) in 30 wt% polymer and POSS in toluene. About 2 g of polymer was dissolved in toluene, then either 10 or 20 molar equivalent of thiol-POSS to polymer chains was added with 0.5 wt% (relative to polymer and POSS) of AIBN initiator. Molar amounts of polymer were estimated using relative  $M_n$  values obtained from gel permeation

chromatography (GPC) described in a later section. The mixture was purged with nitrogen for 30 mins and the reaction proceeded under nitrogen atmosphere with stirring at 80°C for 4 h. The final polymer was precipitated with methanol several times to remove unreacted POSS, then dried in air overnight and in a vacuum oven at room temperature for a day. The remaining double bonds of EGDEMA and Far after thiol-ene clicking were quantified using <sup>1</sup>H NMR. A summary of the characterized block copolymers after thiol-ene clicking is shown in Table 5-3.

Table 5-3. Summary of poly(methacrylate-*b*-Far) block copolymers after thiol-ene clicking with thiol-POSS.

<b>Block copolymer ID</b>	<b>Molar equivalent of POSS<sup>a</sup></b>	<b>Remaining EGDEMA C=C bonds</b>	<b>Remaining Far C=C bonds</b>	<b>Final <math>M_n</math> after clicking (g mol<sup>-1</sup>)</b>	<b>Final <math>\bar{D}</math> after clicking</b>
EG1-Far POSS1	10	54%	93%	25,900	1.52
EG1-Far POSS2	20	46%	94%	25,300	1.51
EG2-Far POSS1	10	46%	97%	38,500	1.39
EG2-Far POSS2	20	74%	97%	41,700	1.83
EGiB1-Far POSS	10	75%	90%	24,900	1.67
EGiB2-Far POSS	10	59%	95%	34,200	1.76

<sup>a</sup>) Amount of POSS added for thiol-ene clicking reactions were measured based on molar ratio of thiol:polymer chain and the moles of polymer were estimated using  $M_n$  from GPC analysis of the block copolymers.

### 5.3.5 Polymer characterization

Polymer samples (~0.15 mL) taken from the reaction mixtures for <sup>1</sup>H NMR and molecular weight analysis. Monomer conversion, copolymer composition, and amount of POSS clicked onto the polymer chains were determined from the NMR spectra, which are shown in Figure C-1 to C-9 in Appendix C. Conversions of EGDEMA were calculated relative to inert CH<sub>2</sub> ether protons of EGDEMA, as well as the pendent double bond protons assuming they were also inert in the polymerization as seen in Figure C-10 and Table C-1. NMR samples were dissolved in CDCl<sub>3</sub> and were analyzed using the Bruker AVIIIHD 500 MHz spectrometer (16 scans). The final purified polymers after thiol-ene clicking showed that there was no residual unclicked POSS as indicated

by the disappearance of the S-H proton at 1.3 ppm in the  $^1\text{H}$  NMR spectra in Figure C-8 and C-9 and verified by the absence of POSS peak in the GPC chromatogram (Figure C-10).

Number average molecular weight ( $M_n$ ) and dispersity ( $\mathcal{D} = M_w/M_n$ ) of polymer samples were measured using gel permeation chromatography (GPC, Water Breeze) with HPLC grade THF as an eluent at a flow rate of  $0.3 \text{ mL min}^{-1}$ . The GPC has three Waters Styragel HR columns (HR1 with a molecular weight measurement range of  $10^2$  to  $5 \times 10^3 \text{ g mol}^{-1}$ , HR2 with a molecular weight measurement range of  $5 \times 10^2$  to  $2 \times 10^4 \text{ g mol}^{-1}$ , and HR4 with a molecular weight measurement range of  $5 \times 10^3$  to  $6 \times 10^5 \text{ g mol}^{-1}$ ), a guard column, and a refractive index (RI 2414) detector. The columns were heated to  $40^\circ\text{C}$  during analysis. The molecular weights were determined relative to poly(methyl methacrylate) (PMMA) calibration standards from Varian Inc. (ranging from 875 to  $1,677,000 \text{ g mol}^{-1}$ ). The reported molecular weights were all relative to the PMMA standards and not adjusted with Mark–Houwink parameters.

### 5.3.6 Thermogravimetric analysis and differential scanning calorimetry

Thermogravimetric analysis (TGA) was done to determine thermal stability of the block copolymers with and without POSS using a Discovery 5500 TGA (TA Instruments). Polymer samples weighing between 5 – 10 mg were placed in platinum pans, and they were analyzed from room temperature to  $500^\circ\text{C}$  under nitrogen flow, then switched to air flow from 500 to  $700^\circ\text{C}$  at a rate of  $10^\circ\text{C min}^{-1}$ .

Glass transition temperatures ( $T_g$ ) were determined using differential scanning calorimetry (DSC) Discovery 2500 from TA instruments. Polymer samples were heated up from room temperature to  $200^\circ\text{C}$  to remove any thermal history, then cooled to  $-90^\circ\text{C}$ , then heated up to  $200^\circ\text{C}$  again to determine  $T_g$ . The heating rate used for all three cycles was  $10^\circ\text{C min}^{-1}$ .

### 5.3.7 Rheology

Rheological properties of the polymers were measured using the MCR302 rheometer (Anton Paar Instruments). The samples were placed between parallel plates with a gap of 1 mm, and storage ( $G'$ ) and loss ( $G''$ ) moduli were measured at an increasing shear strain from 0.01 to 100% using 25 measurements at room temperature. Amplitude sweeps were also done to determine the shear

strain range needed eventually for dynamic mechanical thermal analysis (DMTA). DMTA was done at a constant shear strain of 0.1% and frequency of 10 Hz from room temperature to 150°C at a rate of 10°C min<sup>-1</sup> using the same parallel plate setup. Storage and loss moduli ( $G'$  and  $G''$ ) and damping factor ( $\tan\delta = G''/G'$ ) were measured accordingly using DMTA.

## 5.4 Results and discussion

### 5.4.1 Poly(EGDEMA-*b*-Far) block copolymers clicked with thiol-POSS

Initially, two poly(EGDEMA-*b*-Far) block copolymers (EG1-Far and EG2-Far) were synthesized, then clicked with thiol-POSS. The synthesis of the block copolymers began with the polymerization of EGDEMA to make macroinitiators. From literature, EGDEMA was not able to polymerize using SG1-based BlocBuilder or succinimidyl-modified BlocBuilder without the addition of 10 mol% of styrene [28]. The polymerization of EGDEMA using D7 initiator and no controlling comonomer showed linear kinetics (semi-logarithmic plots of conversion versus time) and molecular weight increased linearly with conversion as shown in Figure C-11. Molecular weights of up to 15,700 g mol<sup>-1</sup> at low conversions ( $X \sim 30\text{-}46\%$ ) were obtained with a  $\bar{D}$  of  $\sim 1.5\text{-}1.6$ . Experimental  $M_n$  was consistently higher than the theoretical  $M_n$ , which indicates slow initiation but this was expected with D7 initiators, and is reflected in the higher  $\bar{D}$  [32]. Nonetheless, the polymerization kinetic studies indicate adequate control of the homopolymerization of EGDEMA similar to other studies of homopolymerization of methacrylates using D7 [42, 43]. Conversions of EGDEMA polymerizations were calculated relative to the inert CH<sub>2</sub> ether protons as shown in Table 5-1. To confirm that the pendent double bonds did not participate in the polymerization, conversions were also calculated relative to the pendent protons assuming they are inert. Both methods gave similar conversions as shown in Table C-1, therefore the pendent double bonds are shown to not participate in the polymerization via NMP. Furthermore, the resulting poly(EGDEMA) and poly(EGDEMA-*co*-iBOMA) macroinitiators were completely soluble in THF, indicating there was no crosslinked material despite having a pendent norbornene double bond.

To further demonstrate effective control of the polymerization of EGDEMA using D7, the resulting macroinitiators were successfully chain-extended with Far to make diblock copolymers.

The  $M_n$  increased from 7,700 and 15,700 g mol<sup>-1</sup> for EG1 and EG2, respectively, to 19,000 and 25,300 g mol<sup>-1</sup> after chain-extension as shown in Table 5-2. There was a clear shift in molecular weight distribution (MWD) from the blue MWD of the poly(EGDEMA) block to the green MWD of the poly(EGDEMA-*b*-Far) after chain-extension as shown in Figure 5-1. This indicates that all of the poly(EGDEMA) macroinitiators remained active and were able to re-initiate and polymerize the Far block. Although,  $\bar{M}_w$  did increase after chain-extension with Far as seen in Table 5-1 and Table 5-2, which suggests that there was some irreversible termination of polymer chains during chain-extension.

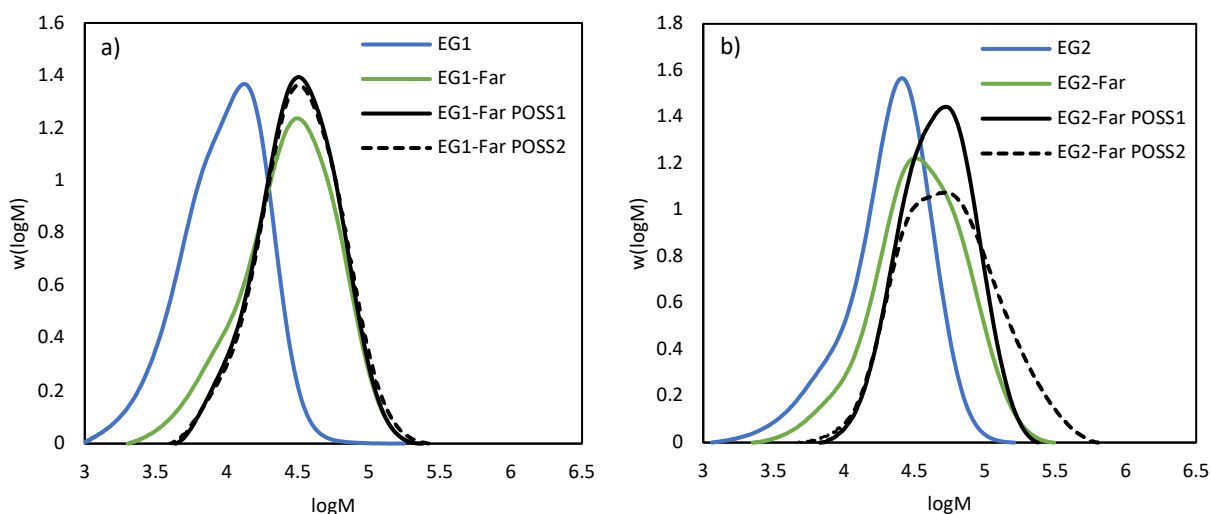


Figure 5-1. GPC traces of a) EG1-Far and b) EG2-Far block copolymers. The blue curves represent the poly(EGDEMA) macroinitiators, the green curves represent the chain-extended poly(EGDEMA-*b*-Far) block copolymers, and the black curves represent the block copolymers thiol-ene clicked with 10 and 20 molar equivalent of thiol-POSS.

Next, thiol-ene clicking was done on the block copolymers, where 10 and 20 molar equivalents of thiol-POSS to polymer chain was added to the reaction mixture dissolved in toluene. Thiol-ene clicking was done using thermally initiated radicals from AIBN decomposition at 80°C for 4 h. Afterwards, the final polymers were carefully purified to remove unreacted thiol-POSS by dissolving in small amount of THF and precipitated with minimal methanol until the solution was cloudy, indicating the start of phase separation. <sup>1</sup>H NMR showed the disappearance of S-H proton at 1.3 ppm and presence of the isobutyl groups from thiol-POSS in the final polymer at 0.6 ppm

(Figure C-8 and C-9), therefore showing the POSS groups were successfully attached to the polymer chains. Absence of unreacted POSS after purification was also confirmed from GPC spectra (Figure C-10), therefore the presence of POSS in the  $^1\text{H}$  NMR spectra confirm attachment of POSS onto the polymer chain. The molecular weights of EG1-Far and EG2-Far increased to  $\sim 25,000$  and  $40,000 \text{ g mol}^{-1}$ , respectively, and the molecular weight distributions shifted slightly as seen in Figure 5-1.

It is important to note that GPC traces reported in this study are relative molecular weights, therefore they actually represent the change in hydrodynamic volumes of the polymer chains after thiol-ene clicking. GPC traces obtained may not reflect the true change in molecular weight or molecular weight distribution, especially because the block copolymers were qualitatively measured according to the homopolymer calibrations [44]. The decrease in  $\bar{M}_w$  of polymer chains after thiol-ene clicking as shown in Table 5-3 may be explained by the increase in entanglement of polymer chains after the incorporation of POSS. Therefore, the hydrodynamic volume of the polymer chains is effectively reduced and may be reflected in the narrowing of the MWD in GPC analysis [45]. It is also possible the unreacted and dead polymer chains were removed after purification following thiol-ene clicking, therefore narrowing the MWD.

Nonetheless, the percentage of remaining double bonds as reported in Table 5-3 suggest higher degree of functionalization, when indeed, the  $^1\text{H}$  NMR spectra (Figure C-8 and C-9) show much lower POSS functionalization and conjugation efficiency (defined here as percentage of thiol functionalization versus percentage of disappeared alkenes). The copolymer composition of POSS as determined from  $^1\text{H}$  NMR using the isobutyl protons of POSS at 0.6 ppm and are summarized in Table 5-4. The low conjugation efficiency was consistent with previous studies of functionalization of poly(butadiene)-*co*-poly(ethylene oxide), which was attributed to cyclization of the thiol radical with the neighbouring pendent butadiene double bond via hydrogen abstraction [46, 47]. However, cyclization is very unlikely in this case because very large-membered rings would be formed between neighbouring EGDEMA units.

Table 5-4. Summary of block copolymer compositions after thiol-ene clicking from  $^1\text{H}$  NMR.

Block copolymer ID	$F_{\text{Far}}$	$F_{\text{iBOMA}}$	$F_{\text{EGDEMA}}$	$F_{\text{POSS}}$
EG1-Far POSS1	0.775	-	0.192	0.033
EG1-Far POSS2	0.757	-	0.218	0.025
EG2-Far POSS1	0.770	-	0.122	0.103
EG2-Far POSS2	0.551	-	0.431	0.018
EGiB1-Far POSS	0.689	0.296	0.270	0.041
EGiB2-Far POSS	0.559	0.486	0.425	0.016

Many thiol-ene addition examples between small molecules, polymer-polymer conjugations, or functionalization of polymers with thiol molecules have shown that photo-initiated reactions exhibit higher conjugation efficiency and conversion with shorter reaction times compared to thermally initiated systems [48-51]. The general limitation to thiol-ene additions with thermally initiated radicals is the side reactions that occur, such as bimolecular radical termination. However, the low efficiency of thermally initiated systems was explained by the faster addition of initiator fragments onto the alkene relative to the abstraction of hydrogen from the thiol-radical [51]. Therefore, the conjugation efficiency is decreased due to the addition of initiator fragments as opposed to thiol functionalization. These side reactions can be alleviated by decreasing initiator concentration, which would slow down the rate of reaction, or increasing the thiol:ene ratio. Most thiol-ene functionalization of polymers utilize a 10:1 thiol:ene ratio, but this study used a 10:1 thiol:polymer chain ratio [46, 47, 52]. Notably, increasing the thiol-POSS:polymer ratio from 10 to 20 mol eq. did not increase functionalization significantly. Moreover, increasing the thiol-POSS:polymer ratio beyond 20 mol eq. was attempted, but due to the low thiol-ene clicking efficiency, it became difficult to separate unreacted POSS from the polymer. Therefore, photo-initiated thiol-ene clicking would have likely improved the efficiency of POSS functionalization in this study. Moreover, the bulky thiol-POSS groups likely provided extra steric hindrance, which further decreased conjugation efficiency.

Nonetheless, higher conversion of EGDEMA alkene bonds over Far alkene bonds suggest preferential clicking of thiol-POSS with EGDEMA over Far units. It was shown that terminal alkenes undergo thiol-ene clicking much more efficiently than internal *cis* alkenes and cyclic

alkenes [53]. The functionalization of poly(1,2-butadiene) was much more efficient due to the 1,2-addition of butadiene, which ensures the double bond is at the end of the side groups [46, 47, 52]. Similarly, thiol-ene clicking of 1,2-addition isoprene units were much higher than 1,4-addition units [54, 55]. In this study, farnesene was polymerized mostly by 1,4-addition with the two other double bonds located internally on the pendent side chains, therefore the clicking of alkenes on poly(Far) was unlikely. Furthermore, thiol-ene reactions for norbornene have been shown to be very effective because the transition from a ring-strained alkene to a more flexible cyclic alkane is highly favoured [56, 57].

#### 5.4.2 Poly(EGDEMA-*co*-iBOMA-*b*-Far) block copolymers clicked with thiol-POSS

Since most of the double bonds in the EGDEMA units were not able to click with thiol-POSS units, the unused EGDEMA units were then replaced with iBOMA units. There are several motivations for this: 1) poly(iBOMA) will add stiffness and mechanical strength to the block copolymers, and 2) iBOMA is also bio-sourced and may contribute from a sustainability viewpoint (however merely replacing a monomer feedstock with a renewable alternative should not be considered a sole sufficient criteria for making a process greener) [58]. Therefore, the poly(methacrylate) macroinitiators were synthesized by copolymerizing equimolar parts of EGDEMA and iBOMA monomers. The kinetics of the EGDEMA and iBOMA copolymerization were similar to the homopolymerization of EGDEMA, producing polymers of similar  $M_n$  and  $\bar{D}$  at the same conditions as seen in Table 5-1. Additionally, the copolymer compositions of EGDEMA and iBOMA remained relatively constant and equal to the initial monomer composition throughout polymerization, which suggests the copolymerization is near the azeotropic composition, where there is negligible compositional drift. The copolymerization of EGDEMA and iBOMA also showed linear increase of  $M_n$  with conversion, suggesting good control of polymerization (Figure C-12).

The poly(EGDEMA-*co*-iBOMA) macroinitiators were successfully chain-extended with Far, indicating most polymer chains had active chain-ends. As seen in Figure 5-2, the molecular weight distributions of EGiB1 and EGiB2 clearly shifted after chain-extension with Far. However, after clicking EGiB1-Far and EGiB2-Far with 10 molar equivalents of thiol-POSS, not many POSS units were apparently added to the polymer chains as shown by the modest increase in molecular

weight. This could have been due to the added steric hindrance from the iBOMA units, impeding POSS units from clicking with the double bonds of EGDEMA. Furthermore, adding iBOMA units also increase the stiffness of the polymer (discussed in a later section), which likely decreased polymer chain mobility and further impeded thiol-ene clicking of POSS. The final  $M_n$  after thiol-ene clicking with 10 mol eq. thiol-POSS for EGiB1-Far and EGiB2-Far were 24,900 and 34,200  $\text{g mol}^{-1}$ , respectively. Similarly, the POSS functionalization of EGiB1-Far and EGiB2-Far block copolymers after thiol-ene clicking were fairly low compared to the remaining double bonds as seen from  $^1\text{H NMR}$  shown in Table 5-4.

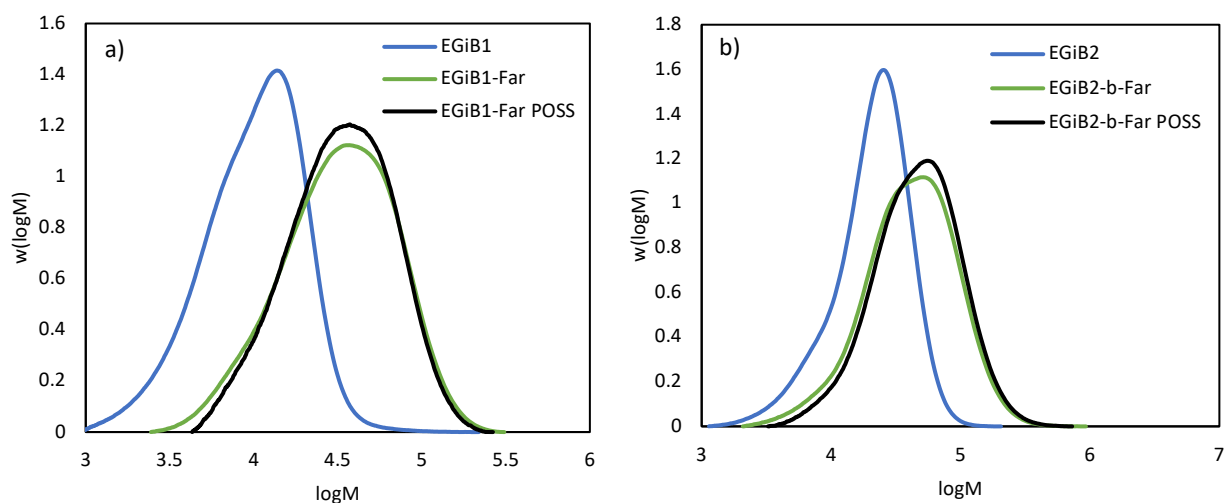


Figure 5.2. GPC traces of a) EGiB1-Far and b) EGiB2-Far block copolymers. The blue curves represent the poly(EGDEMA-co-iBOMA) macroinitiators, the green curves represent the chain-extended poly(EGDEMA-co-iBOMA-b-Far) block copolymers, and the black curves represent the block copolymers thiol-ene clicked with 10 molar equivalent of thiol-POSS.

#### 5.4.3 Thermal stability of block copolymers with and without POSS

As thermoplastic elastomers are processible at high temperatures, it is important to understand their thermal stability and determine the processing temperature while avoiding decomposition of the material. TGA plots showing the decrease in weight with increasing temperature for poly(EGDEMA-*b*-Far) with and without POSS are shown in Figure 5-3. The decomposition temperature, or onset temperature ( $T_{\text{onset}}$ ), is the temperature at which the mass of the polymer sample starts to decrease after a plateau. The endset temperature ( $T_{\text{endset}}$ ) is the temperature at

which the mass of polymer sample has reached close to zero. The  $T_{\text{onset}}$  and  $T_{\text{endset}}$  for all polymer samples are summarized in Table 5-5.

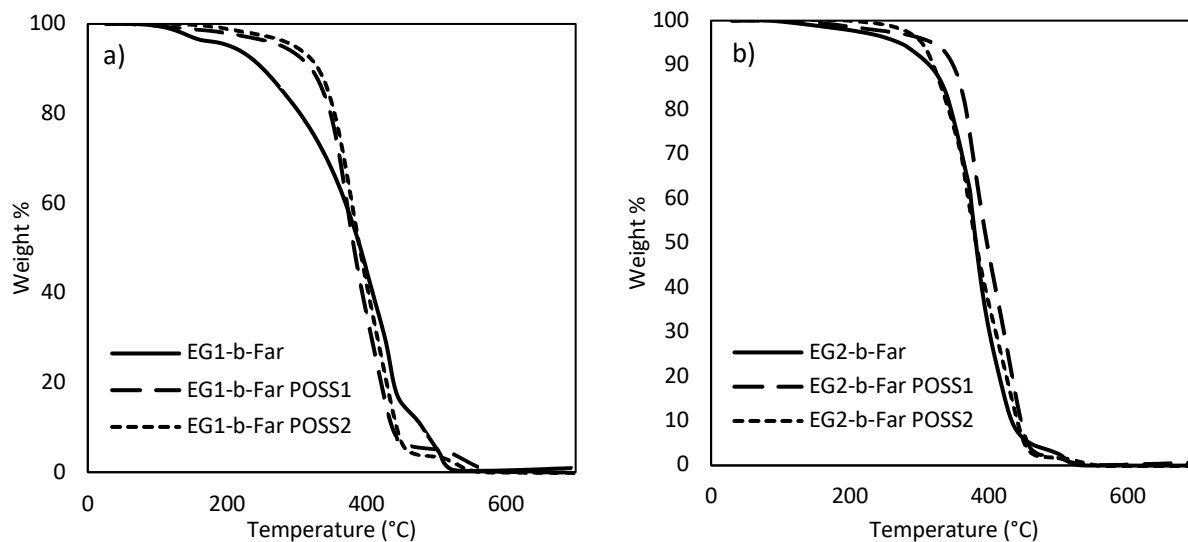


Figure 5-3. TGA plots of a) EG1-Far and b) EG2-Far block copolymers with and without POSS showing decrease in weight% with increasing temperature.

Table 5-5. TGA results of poly(methacrylate-b-Far) block copolymers with and without added POSS.

	EG1-Far			EG2-Far			EGiB1-Far		EGiB2-Far	
	EG1-Far <sup>a</sup>	EG1-Far POSS1	EG1-Far POSS2	EG2-Far	EG2-Far POSS1	EG2-Far POSS2	EGiB1-Far	EGiB1-Far POSS	EGiB2-Far	EGiB2-Far POSS
$T_{\text{onset}}$ (°C)	120 298.2	335.2	335.5	351.2	351.1	334.0	315.0	310.2	301.0	315.6
$T_{\text{endset}}$ (°C)	442.0	441.8	449.9	436.6	455.5	452.7	449.6	455.4	442.4	468.8

<sup>a)</sup> EG1-Far block copolymer with no POSS exhibited two-step degradation, therefore two  $T_{\text{onset}}$  values were reported.

Firstly, it is evident that the degradation curve for EG1-Far without POSS was a two-step degradation, whereas none of the other polymers exhibited the same behaviour. The first degradation step for EG1-Far began at around 120°C, then the second degradation occurred when

the weight % decreased rapidly at around 298°C. Recall that EG1-Far has a very short poly(EGDEMA) block and mostly composed of poly(Far). This two-step degradation has been seen before with poly(myrcene), first at ~250°C which then decomposes quickly at ~425°C [20]. It was also observed with poly(styrene-*b*-myrcene-*b*-styrene) (SMS) triblock copolymer synthesized via RAFT, and the initial degradation was attributed to the depolymerization of poly(myrcene) with 1,4-addition, similar to poly(butadiene) with 1,4-conformation [59, 60]. However, in the cases for SMS block copolymers with longer poly(styrene) blocks, the initial degradation step was no longer evident. Furthermore, the thermal degradation of all block copolymers had 5-10 weight % of residual char until the nitrogen flow was switched to air flow at 500°C to completely decompose the residual mass. The residual char is typical of the decomposition of poly(butadiene) due to the depolymerization and thermally-induced crosslinking during degradation [61]. Both the poly(EGDEMA) and poly(Far) blocks in this study have remaining double bonds, therefore crosslinked residue is very likely. The residual char could be due to the decomposition of POSS as well [62].

It is apparent that by having a longer poly(EGDEMA) block (i.e. EG2-Far) or by linking the POSS moieties to EG1-Far (i.e. EG1-Far POSS1 and EG1-Far POSS2), the TGA curves only showed one degradation step. Interestingly, the degradation temperature of poly(EGDEMA) homopolymer synthesized by ATRP was reported to be 237°C, which is lower than what is observed for poly(EGDEMA-*b*-Far) in this study [34]. There seems to be a synergistic effect, where block copolymers help to minimize the initial degradation of poly(dienes) but also increase the thermal stability of poly(EGDEMA). This was also observed in a study examining the thermal degradation of poly(styrene-*b*-butadiene) diblock copolymers, where the block copolymers had a stabilization effect such that thermal stability is improved compared to a blend of the respective homopolymers [63]. This finding was explained by the delay of poly(styrene) degradation into toluene and styrene by-products due to the volatilization of poly(butadiene) into 1,3-butadiene and vinylcyclohexene, with the addition of methane and hydrogen. Perhaps, the degradation of EGDEMA was slowed down by decomposition of farnesene in this study.

For the block copolymers where the methacrylate blocks consisted of EGDEMA/iBOMA units, the addition of iBOMA also improved the thermal stability of the poly(Far) block such that the

initial degradation is eliminated. EGiB1-Far and EG1-Far are similar in composition, where they have very short methacrylate blocks. As seen in Figure 5-4a for EGiB1-Far without POSS compared to EG1-Far without POSS, the addition of iBOMA units increased the initial thermal degradation from 120 to 315°C. However, there is a weak indicator of a second degradation around 350°C for EGiB1-Far, which suggests some decomposition and release of the isobornyl group from the methacrylate backbone [36]. With POSS added to EGiB1-Far, the second decomposition of the isobornyl group was minimized. Similarly, in Figure 5-4b the degradation of EGiB2-Far shows as slight indication of the release of isobornyl groups at 350°C but was minimized with the addition of POSS.

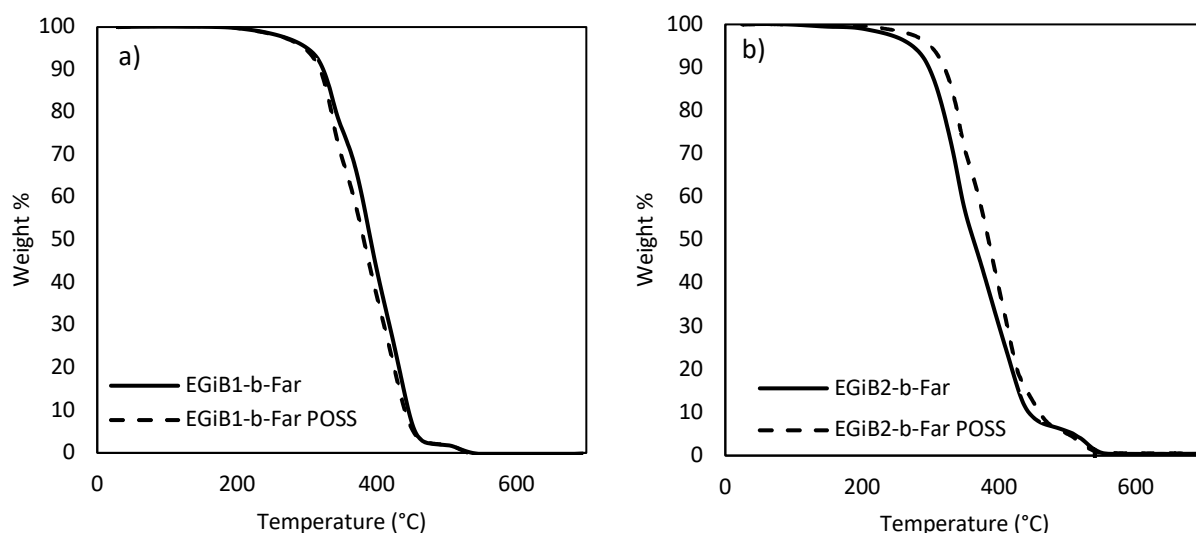


Figure 5-4. TGA plots of a) EGiB1-Far and b) EGiB2-Far block copolymers with and without POSS showing decrease in weight% with increasing temperature.

Otherwise, the decomposition temperature ( $T_{\text{onset}}$ ) appeared to show negligible increase for block copolymers with added POSS compared to without (except for EG1-Far). This is likely due to the very low concentration of POSS that was added onto the polymer chains (1.6 to 10 mol%). In a study investigating the thermal stability of POSS-functionalized poly(ethylene), the increase in decomposition temperature depended on the substituents of the POSS units, as well as the type of bond that attaches the POSS to the polymer chain, but generally showed an improvement in thermal stability [40]. However, poly(ethylene) functionalized with POSS containing isobutyl R-groups and attached by a C<sub>4</sub>H<sub>8</sub> alkyl chain did not show a significant increase in temperature at

5% weight loss ( $T_{5\%}$ ). One study copolymerized styrene with POSS-functionalized styrene ( $F_{\text{POSS}} = 0.36\text{-}3.2$  mol%) and reported an increase of  $10^{\circ}\text{C}$  in decomposition temperature at 10% weight loss ( $T_{10\%}$ ) [64]. Conversely, in another study where poly(styrene) was functionalized with POSS groups ( $F_{\text{POSS}} = 1.1\text{-}1.4$  mol%) post-polymerization showed negligible change in  $T_{10\%}$  [65]. In an example most similar to our study, SEBS was functionalized with POSS via an azido group, and at most where there were 35 units of grafted POSS, the decomposition temperature increased  $\sim 20^{\circ}\text{C}$  [41]. Therefore, it is difficult to conclude whether polymers functionalized with POSS would have a significant effect on overall thermal stability at such low concentrations. Nonetheless, the addition of POSS improved the thermal degradation of Far diene units for EG1-Far block copolymers, as well as preventing the release of isobornyl groups for EG1B1-Far and EG1B2-Far block copolymers.

#### 5.4.4 Rheology of block copolymers

Rheological tests were done to characterize viscoelastic properties of the block copolymers. Amplitude tests were performed at room temperature, where the polymer samples were placed between parallel plates, and the storage ( $G'$ ) and loss ( $G''$ ) moduli were measured with increasing shear strain. The  $G'$  and  $G''$  versus shear strain plots for the poly(EGDEMA-*b*-Far) block copolymers are compared in Figure 5-5.

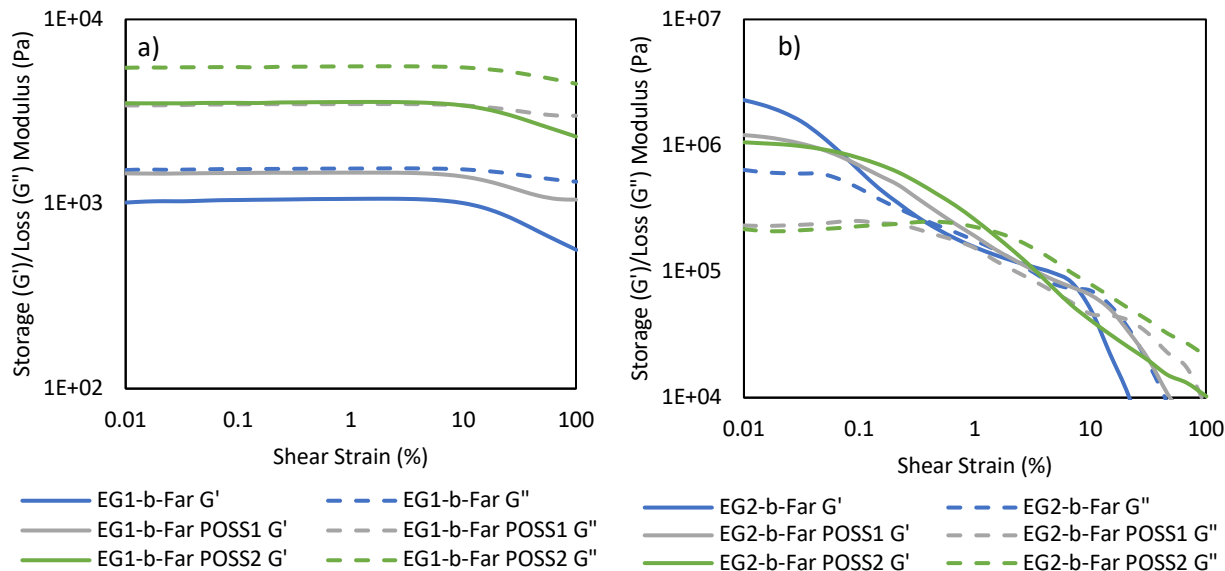


Figure 5-5. Storage ( $G'$ ) and loss ( $G''$ ) moduli versus shear strain plots for a) EG1-Far and b) EG2-Far block copolymers with and without POSS.

Since EG1-Far has a very short poly(EGDEMA) block, and the length of the poly(Far) block is well below its entanglement molecular weight of  $50,000 \text{ g mol}^{-1}$  [17], the block copolymer behaved like a very viscous liquid, even with added POSS. Furthermore, poly(EGDEMA) is a relatively soft polymer in comparison to other poly(methacrylates) as suggested by its  $T_g = 28^\circ\text{C}$  [34]. As seen in Figure 5-5a,  $G''$  is consistently higher than  $G'$  for all EG1-Far samples indicating the polymers were indeed liquid-like. However, EG1-Far samples with added POSS show an increase in both storage and loss moduli, which indicates the mechanical strength of the block copolymers is increased even with low loadings of POSS. Furthermore, the linear viscoelastic (LVE) region was demonstrated by the plateau of  $G'$  and  $G''$  values up to a shear strain of 10%.

For the block copolymers with a longer poly(EGDEMA) block ( $M_n$  of poly(EGDEMA) macroinitiator was  $15,700 \text{ g mol}^{-1}$  versus  $7,500 \text{ g mol}^{-1}$ ), EG2-Far, the polymer samples were solid at room temperature as they were able to be hot-pressed into disks of 1 mm thickness. In this case,  $G'$  was greater than  $G''$  at low shear strain as shown in Figure 5-5b, which indicate these polymers were more solid/gel-like. As shear strain increased,  $G'$  crossed over with  $G''$ , suggesting flow and more liquid-like behaviour. A LVE region of  $G'$  over a limited shear strain range was noticed for EG2-Far. This region became more noticeable and sharper with increasing POSS as seen for EG2-

Far POSS1 and EG2-Far POSS2 and spanned over a wider shear strain range. The LVE regions exhibited by the EG2-Far polymers with and without POSS suggest the polymers behaved like a cross-linked material, but at higher shear strains, they flowed. This is indicative of a thermoplastic elastomer, which should behave like physically crosslinked polymer at ambient conditions but processible at high temperatures and/or shear. Furthermore, improved viscoelastic properties suggest that POSS was able to reinforce the physical crosslinks in these block copolymers, which is consistent with other thermoplastic elastomers either blended or functionalized with POSS [66, 67].

The EGiB1-Far and EGiB2-Far block copolymers, which include iBOMA units in the methacrylate block, display a LVE plateau region over an even wider range of shear strains compared to the EG2-Far block copolymers as seen in Figure 5-6. Similarly,  $G'$  was greater than  $G''$  indicating elastic solid-like materials, as EGiB1-Far and EGiB2-Far polymer samples were able to be hot pressed into solid discs as well. At higher shear strains  $> 1\%$ ,  $G'$  crosses over with  $G''$  and the polymers flowed. The broader plateaus were attributed to the more rigid isobornyl groups and higher  $T_g$  of poly(iBOMA) ( $190^\circ\text{C}$ ) that further reinforced the hard segments of the block copolymers [36]. However, there is negligible difference in the plateau regions for EGiB1-Far and EGiB2-Far with and without POSS since there was very little POSS added.

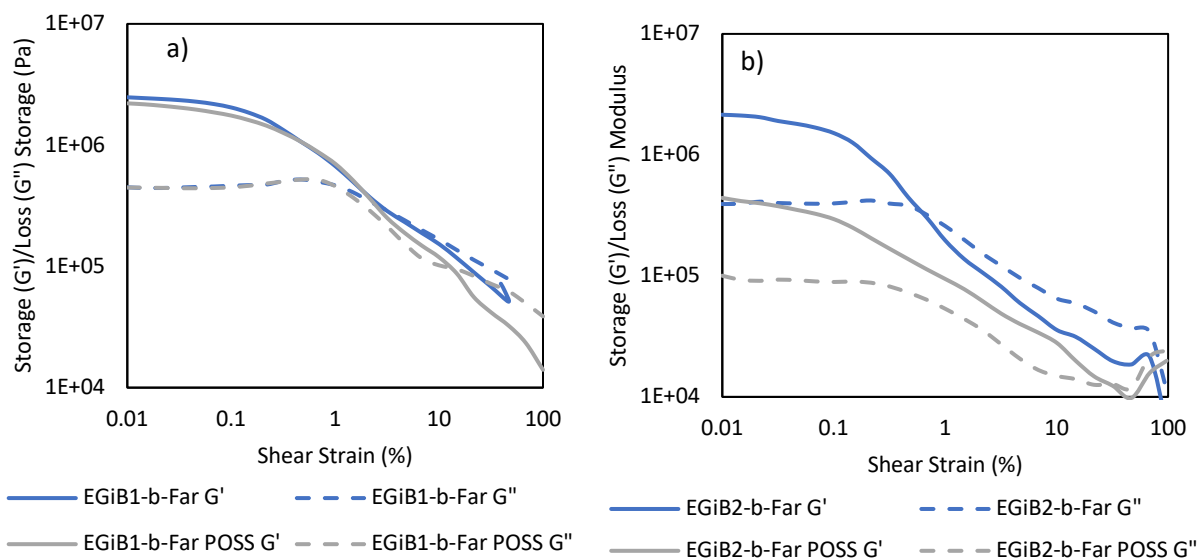


Figure 5-6. Storage ( $G'$ ) and loss ( $G''$ ) moduli versus shear strain plots for a) EG1B1-Far and b) EG1B2-Far block copolymers with and without POSS.

The addition of POSS made a significant improvement in viscoelastic properties for EG1-Far and EG2-Far block copolymers by providing mechanical strength in the poly(EGDEMA) segments and reinforcing the physical crosslinks. As for EG1B1-Far and EG1B2-Far, which have iBOMA copolymerized with EGDEMA statistically, the addition of POSS was very limited and therefore the mechanical properties remained relatively the same. Nonetheless, the addition of iBOMA did improve mechanical properties in comparison to EG1-Far and EG2-Far due to the rigid isobornyl groups of iBOMA. Furthermore, all block copolymers demonstrate glassy regions, which suggest the presence of physical crosslinks until higher shear strains were applied.

#### 5.4.5 Glass transition temperatures of block copolymers

Glass transition temperatures of the block copolymers were determined thermally using DSC, as well as rheologically using DMTA. As the chiller for the rheometer could not reach below  $0^{\circ}\text{C}$ , sub-zero  $T_g$ s were not determined using DMTA. A summary of  $T_g$ s obtained are shown in Table 5-6. For all DSC endotherms, see Figure C-13 to C-16 in Appendix C.

Table 5-6. Glass transition temperatures of block copolymers measured using DSC and DMTA.

<b>Differential Scanning Calorimetry (DSC)</b>										
	<b>EG1-Far</b>			<b>EG2-Far</b>			<b>EGiB1-Far</b>		<b>EGiB2-Far</b>	
	<b>EG1-Far</b>	<b>EG1-Far</b>	<b>EG1-Far</b>	<b>EG2-Far</b>	<b>EG2-Far</b>	<b>EG2-Far</b>	<b>EGiB1-Far</b>	<b>EGiB1-Far</b>	<b>EGiB2-Far</b>	<b>EGiB2-Far</b>
	<b>Far</b>	<b>Far</b>	<b>Far</b>	<b>Far</b>						
		<b>POSS1</b>	<b>POSS2</b>		<b>POSS1</b>	<b>POSS2</b>		<b>POSS</b>		<b>POSS</b>
$T_g$	-71.6	-66.2	-64.2	-76.8	-70.5	-63.1	-72.0	-71.6	-67.8	-67.5
(°C)				30.6	31.3	49.8			91.3	87.8
<b>Dynamic Mechanical Temperature Analysis (DMTA)<sup>a</sup></b>										
$T_g$	-	-	-	63.3	72.2	71.2	109	115	123	123
(°C)										

a)  $T_g$ s reported using DMTA method in this table were obtained from the peak of  $\tan\delta$  versus temperature plots.

Examination of the DSC results indicated a distinct change in heat flow around  $-70^\circ\text{C}$  for all block copolymers. This low  $T_g$  corresponds with the  $T_g$  of poly(Far) homopolymer in agreement with the literature value of  $-73^\circ\text{C}$  [17]. The low  $T_g$  is also indicative of the soft, elastomeric segments of the block copolymers. However, a second  $T_g$  was not observed for the block copolymers with short poly(methacrylate) blocks (EG1-Far and EGiB1-Far), likely because the hard segments were not long enough to display a distinct second  $T_g$  and suggests some miscibility with the elastomeric phase. The block copolymers with longer poly(methacrylate) blocks exhibited two  $T_g$ s. The second  $T_g$  for EG2-Far with no POSS was observed at  $30.6^\circ\text{C}$  and corresponds to the  $T_g$  of poly(EGDEMA) homopolymer ( $T_g = 28^\circ\text{C}$ ) [34]. With the good agreement of the two  $T_g$ s ( $-76.8^\circ\text{C}$  and  $30.6^\circ\text{C}$ ) observed for EG2-Far with the  $T_g$ s of the homopolymers, it indicates possible microphase separation of the block copolymer.

The  $T_g$  from DMTA was obtained by determining the temperature at which  $\tan\delta = G''/G'$  reaches its peak. Since EG1-Far block copolymers were already liquid-like at room temperature, the DMTA revealed only a continual decrease in  $G'$  and  $G''$  with temperature. According to the  $\tan\delta$

versus temperature plot in Figure 5-7a, there was a peak observed for all EG2-Far block copolymers above room temperature, which reconfirmed the second  $T_g$ s observed using DSC. Since sub-zero  $T_g$ s could not be measured with the rheometer, the first  $T_g$ s observed by DSC were not validated.

Nonetheless,  $T_g$ s acquired using DMTA were about 20°C higher than the second  $T_g$  values obtained from DSC for EG2-Far block copolymers. This discrepancy can be explained by the heterogeneity of the overall block copolymers that resulted in a distribution of relaxation times [68]. This was also observed with SBS polymers blended with POSS fillers, where there was a broadening of the  $\tan\delta$  peak [66]. The increase in POSS fillers increased the breadth of the peak due to the segmental constraints and interactions between polymer chains and POSS additives. Furthermore, the block copolymers in this study have fairly high  $\bar{D}$  especially compared to commercially available SBS, which usually have  $\bar{D}$ s closer to 1.1. Higher  $\bar{D}$  indicates that not all polymer segments are the same length, which would also contribute to the distribution of relaxation times. Conversely, homopolymers show excellent agreement of  $T_g$ s between DSC and DMTA methods as seen for poly(Far) [17].

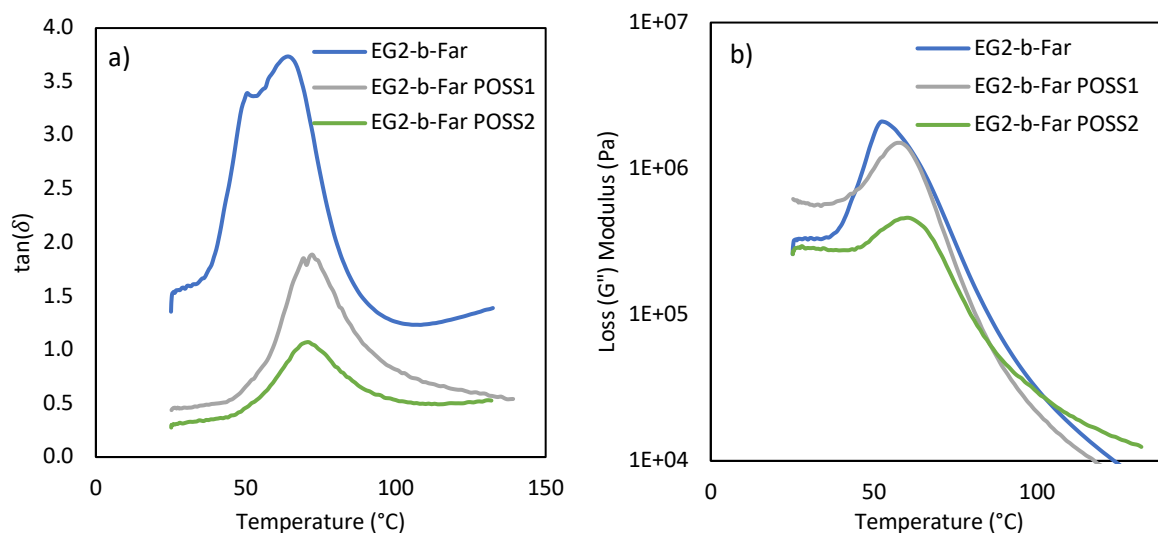


Figure 5-7. DMTA of EG2-Far block copolymers with and without POSS, where a)  $\tan\delta$  and b) loss modulus are plotted as a function of temperature.

Some have argued that the temperature at which  $G''$  is at its maximum is the more accurate  $T_g$  measurement, particularly for polymer mixtures because  $G''$  is the measure of dissipation, which is the transition temperature being considered [69]. In Figure 5-7b, the  $T_g$ s where  $G''$  is at its peak are 51°C, 57°C, and 60°C, which are much closer to the second  $T_g$ s obtained by DSC for EG2-Far block copolymers. Nevertheless, the trend is the same using all methods of  $T_g$  determination, and that is an increase in  $T_g$  with increasing POSS added for all block copolymers. This is consistent with other examples of polymers with added POSS, as POSS decreased chain mobility and increased the rigidity of the polymer chains [39, 66, 70]. However, in the case of polyurethane thermoplastic elastomers, the functionalization with POSS disrupted the crystallinity of the hard segments such that the  $T_g$ s were decreased [67].

The second  $T_g$ s obtained for EGiB1-Far block copolymers were not as straightforward. As shown in Table 5-5, a second  $T_g$  was not observed using DSC. However, from DMTA, there appears to be local maximum  $\tan\delta$  values observed around 110°C in Figure 5-8a, after which  $\tan\delta$  increased very quickly. This may suggest a second  $T_g$  for the EGiB1-Far block copolymers, but it is not definitive. Furthermore, the liquid-like behaviour of the block copolymers is very much influenced by the soft poly(Far) block, especially because EGiB1-Far is largely made of poly(Far) that is below its entanglement molecular weight. It is plausible that the second  $T_g$  could be as high as 110°C, since poly(EGDEMA) and poly(iBOMA) have  $T_g$ s of 28°C and 190°C, respectively, so the  $T_g$  of the statistical EGDEMA/iBOMA copolymer segment is expected to be in between the two values [34, 36]. However, the  $T_g$  of poly(iBOMA) could range from 170°C to 206°C depending on tacticity [71]. Examining  $G''$  in Figure 5-8b, modest maxima were observed as well and  $T_g$ s were estimated as 67°C and 69°C for EGiB1-Far and EGiB1-Far POSS 10, respectively.

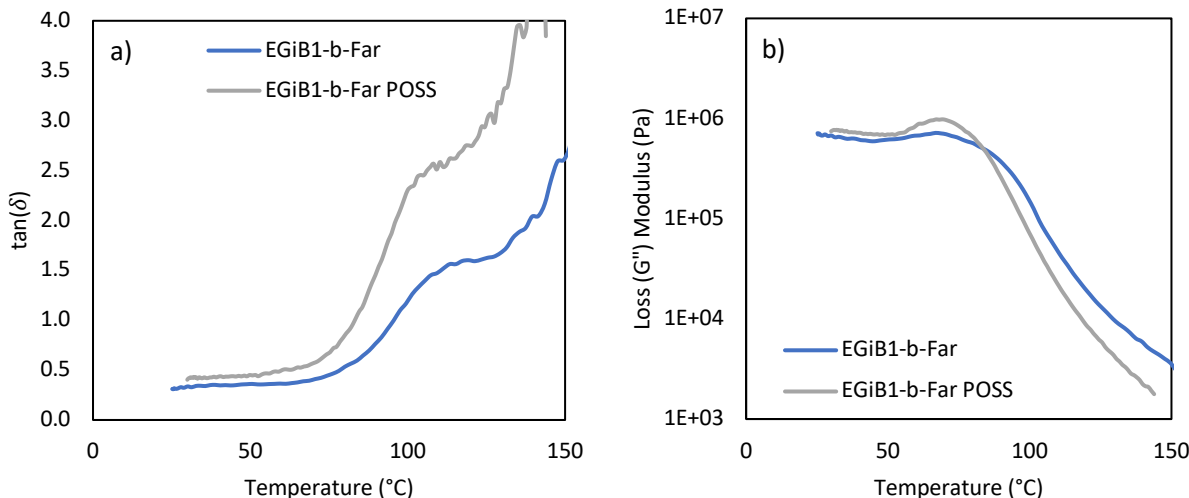


Figure 5-8. DMTA of EGiB1-Far block copolymers with and without POSS, where a)  $\tan\delta$  and b) loss modulus are plotted as a function of temperature.

Similar to EG2-Far block copolymers, more than one  $T_g$  for EGiB2-Far was observed due to the longer poly(methacrylate) blocks. From DSC, there were two  $T_g$ s observed for both EGiB2-Far (-67.8°C and 91.3°C) and EGiB2-Far POSS (-67.5°C and 87.8°C). The first  $T_g$ s observed at around -67°C corresponds with the  $T_g$  of poly(Far) homopolymer and the second  $T_g$ s fall in between the  $T_g$ s of poly(EGDEMA) and poly(iBOMA) homopolymers. According to the Gordon-Taylor equation, random copolymers would exhibit a  $T_g$  between the  $T_g$  of the two homopolymers [72]. Furthermore, compositional drift was not observed with the copolymerization of EGDEMA and iBOMA, since there was an equimolar concentration of each monomer initially and the copolymer composition was also nearly equimolar, which further confirms its random composition, rather than a gradient microstructure. It is important to note that for EGiB2-Far block copolymers, the addition of POSS had negligible effect on  $T_g$ s, likely because out of all the polymer samples, EGiB2-Far block copolymers had the least amount of POSS incorporated at 1.6 mol%.

The DMTA for EGiB2-Far block copolymers revealed much more pronounced  $\tan\delta$  peaks (Figure 5-9a) compared to EGiB1-Far block copolymers. Due to the longer poly(EGDEMA-*co*-iBOMA) blocks, the overall behaviour was less influenced by the flow behaviour of poly(Far) blocks, and therefore obvious  $\tan\delta$  peaks were observed. In Figure 5-9a, the temperature at which  $\tan\delta$  had reached its peak is at 123°C for both EGiB2-Far with and without POSS. Once again, comparing

to  $T_g$ s obtained by DSC,  $T_g$ s observed in the  $\tan\delta$  plots are higher. However, for both DSC and DMTA, the  $T_g$ s that correspond to the poly(methacrylate) blocks did not differ very much with or without POSS. The peaks in  $G''$  as shown in Figure 5-9b indicate  $T_g$ s of 108°C and 103°C for EGiB2-Far and EGiB2-Far POSS, respectively, which also do not show a great difference between samples with and without POSS. Furthermore, the  $T_g$ s observed for the poly(EGDEMA-*co*-iBOMA) blocks using DMTA, regardless of block length (EGiB1-Far versus EGiB2-Far), are very similar.

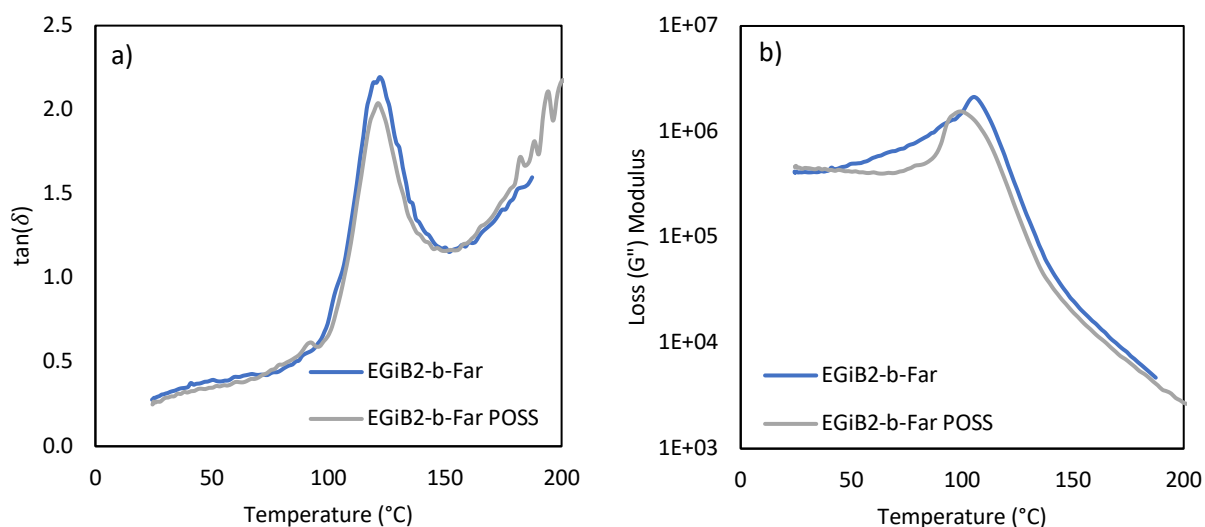


Figure 5-9. DMTA of EGiB2-Far block copolymers with and without POSS, where a)  $\tan\delta$  and b) loss modulus are plotted as a function of temperature.

Two  $T_g$ s were not observed for EG1-Far due to the short poly(EGDEMA) block, therefore a second  $T_g$  was not observed in both DSC and DMTA. Otherwise, the use of DSC and DMTA confirmed distinct  $T_g$ s of the diblock copolymers corresponding to their respective blocks. The addition of POSS resulted in an increase in  $T_g$  for EG1-Far and EG2-Far block copolymers for both the poly(Far) and poly(EGDEMA) blocks. For the block copolymers with added iBOMA in the poly(methacrylate) blocks, the addition of POSS showed negligible difference in  $T_g$ , since the concentration of POSS was fairly low. Additionally, the transition behaviour could have been dominated by the rigid iBOMA units such that the little POSS added made negligible difference.

Nevertheless, distinct  $T_{gs}$  could suggest possible microphase separation for most of these block copolymers, namely EG2-Far, EG1B1-Far, and EG1B2-Far with and without POSS.

To further investigate whether there is microphase separation, polymer films were prepared in the hot press at 120°C for EG2-Far block copolymers and at 160°C for EG1B2-Far block copolymers and cooled slowly overnight to room temperature for small angle X-ray scattering (SAXS) analysis. Higher order peaks were not observed that would be indicative of self-assembled structures. The Flory-Huggins enthalpic interaction parameter,  $\chi$ , was estimated using (1) to provide some insight regarding the miscibility between the two block segments.

$$\chi_{AB} = \frac{\bar{V}}{RT} (\delta_A - \delta_B)^2 \quad (1)$$

The interactions of polymers A and B depend on molar volume of the polymer,  $\bar{V}$ , the solubility parameters,  $\delta_A$  and  $\delta_B$ , of the respective monomers, and temperature,  $T$ . The molar volume of a mixture is determined by  $\bar{V} = \sqrt{V_A V_B}$ . For block copolymers,  $\chi N \approx 10.5$  denotes the order-disorder transition, where  $N$  is overall degree of polymerization [73]. Solubility parameters and molar volumes of some relevant related monomers are summarized in Table 5-7. The solubility parameter of Far and EGDEMA were not found in literature and were calculated based on group component contributions method based on the Hoftyzer-Van Krevelen methodology [74]. Far has a similar solubility parameter compared to other dienes such as butadiene, isoprene, and myrcene. An approximate  $\chi$  was calculated between Far and EGDEMA to be 0.0068 at 120°C (the temperature at which poly(EGDEMA-*b*-Far) polymers were processed for SAXS). Far and EGDEMA in EG1-Far and EG2-Far block copolymers have similar solubility parameters, and therefore have a low  $\chi$  and suggest miscibility. Far and iBOMA have a much higher  $\chi$  of 0.35 at 160°C (the temperature at which poly(EGDEMA-*co*-iBOMA-*b*-Far) polymers were processed for SAXS), however this only suggests that iBOMA and Far have greater immiscibility, but cannot be correlated to the case of EG1B1-Far and EG1B2-Far since the methacrylate blocks are random copolymers of EGDEMA and iBOMA.

Table 5-7. Summary of solubility parameters and molar volumes of relevant monomers.

Monomer	$\delta$ (MPa <sup>1/2</sup> )	$\bar{V}$ (cm <sup>3</sup> mol <sup>-1</sup> )
Butadiene (BD)	16.6 <sup>a</sup>	60.7 <sup>a</sup>
Isoprene (IP)	16.2 <sup>a</sup>	75.7 <sup>a</sup>
Myrcene (Myr)	16.4 <sup>b</sup>	170 <sup>c</sup>
Farnesene (Far)	14.4 <sup>c</sup>	251 <sup>c</sup>
Styrene (St)	17.4 <sup>a</sup>	98 <sup>a</sup>
iBOMA	16.7 <sup>d</sup>	226 <sup>c</sup>
EGDEMA	14.1 <sup>c</sup>	246 <sup>c</sup>

<sup>a)</sup> Values obtained from literature [74]; <sup>b)</sup> Solubility parameter was estimated in literature [75]; <sup>c)</sup> Solubility parameters of farnesene and EGDEMA were calculated based on Hoftyzer-Van Krevelen's Component Group Contributions method; <sup>d)</sup> Solubility parameter of iBOMA obtained from literature [76]; <sup>e)</sup> Molar volumes were calculated based on density and molar mass of monomers.

For reference, typical SBS is made of poly(styrene) blocks with  $M_n \sim 10$ -20,000 g mol<sup>-1</sup> and poly(butadiene) blocks with  $M_n \sim 40$ -80,000 g mol<sup>-1</sup> [77]. The  $\chi$  between poly(styrene) and poly(butadiene) was calculated at 120°C (20°C above  $T_g$  of polystyrene) to be 0.015 [21]. In addition to the higher interaction parameter, the high degrees of polymerization for SBS further enables phase separation. The  $N$  of the block copolymers in this study are fairly short in comparison to SBS and would require much higher degrees of polymerization to enthalpically induce ordered phase separation [73]. However, distinct  $T_g$ s measured in DSC and DMTA still suggest some microphase separation, but the block copolymers are likely weakly segregated and disordered as suggested by SAXS and  $\chi$  approximations.

## 5.5 Conclusions

The polymerization of EGDEMA by nitroxide-mediated polymerization using D7 initiator was done for the first time, where no controlling comonomer was required and chain-ends remained active for chain-extension regardless of high  $\bar{D}$  ( $\sim 1.5$ -1.6). The poly(EGDEMA) macroinitiators were re-initiated for polymerization of Far, a bio-based terpene that is similar in structure to

petroleum-derived butadiene and isoprene. Similarly, the poly(methacrylate) blocks were also synthesized by statistically copolymerizing EGDEMA and iBOMA to form a more rigid methacrylate block. Since EGDEMA has a pendent double bond on the norbornene group, this allowed for thiol-ene clicking with thiol-POSS units onto the block copolymers post-polymerization. Although the conjugation efficiency of the thermal initiated thiol-ene clicking was low,  $^1\text{H}$  NMR showed that thiol-POSS preferentially clicked onto the double bond of EGDEMA and not Far.

Despite the low fraction of POSS incorporation (1.6 – 10 mol% incorporation of POSS), the thermal stability of the poly(Far) blocks was improved and the degradation of isobornyl groups for polymers containing iBOMA units was reduced. These block copolymers containing POSS demonstrated increased mechanical strength as shown by the increase in modulus due to the reinforced physical crosslinks provided by POSS in the poly(methacrylate) blocks. Furthermore, distinct  $T_g$ s were observed using DSC and DMTA for the block copolymers containing longer poly(methacrylate) blocks (around  $-70^\circ\text{C}$  for the rubbery poly(Far) blocks and up to  $110^\circ\text{C}$  for the thermoplastic poly(methacrylate) blocks). This suggests microphase separation, even though microphase morphology was not observed, likely due to the relatively small degrees of polymerization. Nonetheless, incorporation of POSS increased the  $T_g$  of the respective blocks, which confirms the presence of reinforced physical crosslinks and increased stiffness due to the POSS units. Therefore, these novel block copolymers that were easily functionalized with POSS by thiol-ene clicking show good potential eventually for applications as TPEs.

## 5.6 References

- [1] J.G. Drobny, 1. Introduction, Handbook of Thermoplastic Elastomers (2nd Edition), Elsevier 2014.
- [2] R. Bening, D. Handlin, L. Sterna, C. Willis, Novel block copolymers and method for making same, Kraton Polymers US LLC, 2003.
- [3] C.A. Sierra, C. Galán, J.G. Fatou, M.D. Parellada, J.A. Barrio, Thermal and mechanical properties of poly (styrene-*b*-ethylene-*co*-butylene-*b*-styrene) triblock copolymers, *Polymer* 38(17) (1997) 4325-4335.
- [4] A.F. Johnson, D.J. Worsfold, Anionic polymerization of butadiene and styrene, *Journal of Polymer Science Part A: General Papers* 3(2) (1965) 449-455.
- [5] M. Morton, L.J. Fetters, Homogeneous anionic polymerization of unsaturated monomers, *Journal of Polymer Science: Macromolecular Reviews* 2(1) (1967) 71-113.
- [6] M. Morton, L.J. Fetters, E.E. Bostick, Mechanisms of homogeneous anionic polymerization by alkyllithium initiators, *Journal of Polymer Science Part C: Polymer Symposia* 1(1) (1963) 311-323.
- [7] D. Jenkins Aubrey, G. Jones Richard, G. Moad, Terminology for reversible-deactivation radical polymerization previously called "controlled" radical or "living" radical polymerization (IUPAC Recommendations 2010), *Pure and Applied Chemistry*, 2009, p. 483.
- [8] D.A. Shipp, Reversible-Deactivation Radical Polymerizations, *Polymer Reviews* 51(2) (2011) 99-103.

- [9] M.K. Georges, G.K. Hamer, N.A. Listigovers, Block Copolymer Synthesis by a Nitroxide-Mediated Living Free Radical Polymerization Process, *Macromolecules* 31(25) (1998) 9087-9089.
- [10] M.B. Kolichski, L.C. Cocco, D.A. Mitchell, M. Kaminski, Synthesis of myrcene by pyrolysis of  $\beta$ -pinene: Analysis of decomposition reactions, *Journal of Analytical and Applied Pyrolysis* 80(1) (2007) 92-100.
- [11] H. Zheng, J. Chen, C. Li, J. Chen, Y. Wang, S. Zhao, Y. Zeng, Mechanism and kinetics of the pyrolysis of  $\beta$ -pinene to myrcene, *Journal of Analytical and Applied Pyrolysis* 123 (2017) 99-106.
- [12] M. Eisenacher, S. Beschnitt, W. Hölderich, Novel route to a fruitful mixture of terpene fragrances in particular phellandrene starting from natural feedstock geraniol using weak acidic boron based catalyst, *Catalysis Communications* 26 (2012) 214-217.
- [13] G. Brieger, Convenient preparation of trans- $\beta$ -farnesene, *The Journal of Organic Chemistry* 32(11) (1967) 3720-3720.
- [14] G. Brieger, T.J. Nestrick, C. McKenna, Synthesis of trans, trans- $\alpha$ -farnesene, *The Journal of Organic Chemistry* 34(12) (1969) 3789-3791.
- [15] M.I. Hulnik, I.V. Vasilenko, A.V. Radchenko, F. Peruch, F. Ganachaud, S.V. Kostjuk, Aqueous cationic homo- and co-polymerizations of  $\beta$ -myrcene and styrene: a green route toward terpene-based rubbery polymers, *Polymer Chemistry* 9(48) (2018) 5690-5700.
- [16] C. Zhou, Z. Wei, C. Jin, Y. Wang, Y. Yu, X. Leng, Y. Li, Fully biobased thermoplastic elastomers: Synthesis of highly branched linear comb poly( $\beta$ -myrcene)-graft-poly(l-lactide) copolymers with tunable mechanical properties, *Polymer* 138 (2018) 57-64.

- [17] C. Iacob, T. Yoo, J. Runt, Molecular Dynamics of Polyfarnesene, *Macromolecules* 51(13) (2018) 4917-4922.
- [18] T. Yoo, S.K. Henning, Synthesis and characterization of farnesene-based polymers, *Rubber Chemistry and Technology* 90(2) (2017) 308-324.
- [19] S.B. Luk, L.A. Azevedo, M. Maric, Reversible deactivation radical polymerization of bio-based dienes, *Reactive and Functional Polymers* 162 (2021) 104871.
- [20] P. Sarkar, A.K. Bhowmick, Synthesis, characterization and properties of a bio-based elastomer: polymyrcene, *RSC Advances* 4(106) (2014) 61343-61354.
- [21] J. Brandrup, E.H. Immergut, E.A. Grulke, *Polymer handbook*, 4th ed. ed., Wiley, New York, 1999.
- [22] S.B. Luk, M. Marić, Nitroxide-Mediated Polymerization of Bio-Based Farnesene with a Functionalized Methacrylate, *Macromolecular Reaction Engineering* 13(3) (2019) 1800080.
- [23] S.B. Luk, M. Marić, Polymerization of Biobased Farnesene in Miniemulsions by Nitroxide-Mediated Polymerization, *ACS Omega* 6(7) (2021) 4939-4949.
- [24] A. Métafiot, J.F. Gérard, B. Defoort, M. Marić, Synthesis of  $\beta$ -myrcene/glycidyl methacrylate statistical and amphiphilic diblock copolymers by SG1 nitroxide-mediated controlled radical polymerization, *Journal of Polymer Science Part A: Polymer Chemistry* 56(8) (2018) 860-878.
- [25] A.L. Hook, C.Y. Chang, J. Yang, J. Lockett, A. Cockayne, S. Atkinson, Y. Mei, R. Bayston, D.J. Irvine, R. Langer, D.G. Anderson, P. Williams, M.C. Davies, M.R. Alexander, Combinatorial discovery of polymers resistant to bacterial attachment, *Nature Biotechnology* 30(9) (2012) 868-875.

- [26] B.J. Tyler, A. Hook, A. Pelster, P. Williams, M. Alexander, H.F. Arlinghaus, Development and characterization of a stable adhesive bond between a poly(dimethylsiloxane) catheter material and a bacterial biofilm resistant acrylate polymer coating, *Biointerphases* 12(2) (2017) 02C412.
- [27] F. Koschitzki, R. Wanka, L. Sobota, J. Koc, H. Gardner, K.Z. Hunsucker, G.W. Swain, A. Rosenhahn, Amphiphilic Dicyclopentenyl/Carboxybetaine-Containing Copolymers for Marine Fouling-Release Applications, *ACS Applied Materials & Interfaces* 12(30) (2020) 34148-34160.
- [28] A. Maupu, Y. Kanawati, A. Métafiot, M. Maric, Ethylene Glycol Dicyclopentenyl (Meth)Acrylate Homo and Block Copolymers via Nitroxide Mediated Polymerization, *Materials* 12(9) (2019).
- [29] Y. Guillaneuf, D. Gigmes, S.R.A. Marque, P. Tordo, D. Bertin, Nitroxide-Mediated Polymerization of Methyl Methacrylate Using an SG1-Based Alkoxyamine: How the Penultimate Effect Could Lead to Uncontrolled and Unliving Polymerization, *Macromolecular Chemistry and Physics* 207(14) (2006) 1278-1288.
- [30] B. Charleux, J. Nicolas, O. Guerret, Theoretical Expression of the Average Activation–Deactivation Equilibrium Constant in Controlled/Living Free-Radical Copolymerization Operating via Reversible Termination. Application to a Strongly Improved Control in Nitroxide-Mediated Polymerization of Methyl Methacrylate, *Macromolecules* 38(13) (2005) 5485-5492.
- [31] J. Nicolas, C. Dire, L. Mueller, J. Belleney, B. Charleux, S.R.A. Marque, D. Bertin, S. Magnet, L. Couvreur, Living Character of Polymer Chains Prepared via Nitroxide-Mediated Controlled Free-Radical Polymerization of Methyl Methacrylate in the Presence of a Small Amount of Styrene at Low Temperature, *Macromolecules* 39(24) (2006) 8274-8282.

- [32] N. Ballard, M. Aguirre, A. Simula, A. Agirre, J.R. Leiza, J.M. Asua, S. van Es, New Class of Alkoxyamines for Efficient Controlled Homopolymerization of Methacrylates, *ACS Macro Letters* 5(9) (2016) 1019-1022.
- [33] N. Ballard, A. Simula, M. Aguirre, J.R. Leiza, S. van Es, J.M. Asua, Synthesis of poly(methyl methacrylate) and block copolymers by semi-batch nitroxide mediated polymerization, *Polymer Chemistry* 7(45) (2016) 6964-6972.
- [34] P. Mandal, N.K. Singha, Tailor-made polymethacrylate bearing bicyclo-alkenyl functionality via selective ATRP at ambient temperature and its post-polymerization modification by 'thiol-ene' reaction, *RSC Advances* 4(11) (2014) 5293-5299.
- [35] P. Mandal, S. Choudhury, N.K. Singha, Acrylic ABA triblock copolymer bearing pendant reactive bicycloalkenyl functionality via ATRP and tuning its properties using thiol-ene chemistry, *Polymer* 55(22) (2014) 5576-5583.
- [36] A. Matsumoto, K. Mizuta, T. Otsu, Synthesis and thermal properties of poly(cycloalkyl methacrylate)s bearing bridged- and fused-ring structures, *Journal of Polymer Science Part A: Polymer Chemistry* 31(10) (1993) 2531-2539.
- [37] E. Ayandele, B. Sarkar, P. Alexandridis, Polyhedral Oligomeric Silsesquioxane (POSS)-Containing Polymer Nanocomposites, *Nanomaterials* 2(4) (2012).
- [38] W. Zhang, G. Camino, R. Yang, Polymer/polyhedral oligomeric silsesquioxane (POSS) nanocomposites: An overview of fire retardance, *Progress in Polymer Science* 67 (2017) 77-125.
- [39] P.T. Mather, H.G. Jeon, A. Romo-Uribe, T.S. Haddad, J.D. Lichtenhan, Mechanical Relaxation and Microstructure of Poly(norbornyl-POSS) Copolymers, *Macromolecules* 32(4) (1999) 1194-1203.

- [40] P. Groch, K. Dziubek, K. Czaja, M. Grzymek, Investigation of thermal stability of ethylene copolymers with POSS - Study under static and dynamic conditions, *Polymer Degradation and Stability* 156 (2018) 218-227.
- [41] M. Niu, R. Xu, P. Dai, Y. Wu, Novel hybrid copolymer by incorporating POSS into hard segments of thermoplastic elastomer SEBS via click coupling reaction, *Polymer* 54(11) (2013) 2658-2667.
- [42] N. Ballard, M. Aguirre, A. Simula, J.R. Leiza, S. van Es, J.M. Asua, High solids content nitroxide mediated miniemulsion polymerization of n-butyl methacrylate, *Polymer Chemistry* 8(10) (2017) 1628-1635.
- [43] S. Noppalit, A. Simula, L. Billon, J.M. Asua, On the nitroxide mediated polymerization of methacrylates derived from bio-sourced terpenes in miniemulsion, a step towards sustainable products, *Polymer Chemistry* 11(6) (2020) 1151-1160.
- [44] K. Philipps, T. Junkers, J.J. Michels, The block copolymer shuffle in size exclusion chromatography: the intrinsic problem with using elugrams to determine chain extension success, *Polymer Chemistry* (2021).
- [45] L.J. Fetters, D.J. Lohse, R.H. Colby, Chain Dimensions and Entanglement Spacings, in: J.E. Mark (Ed.), *Physical Properties of Polymers Handbook*, Springer New York, New York, NY, 2007, pp. 447-454.
- [46] J. Justynska, Z. Hordyjewicz, H. Schlaad, Toward a toolbox of functional block copolymers via free-radical addition of mercaptans, *Polymer* 46(26) (2005) 12057-12064.
- [47] J. Justynska, Z. Hordyjewicz, H. Schlaad, New Functional Diblock Copolymers Through Radical Addition of Mercaptans, *Macromolecular Symposia* 240(1) (2006) 41-46.

- [48] M. Uygun, M.A. Tasdelen, Y. Yagci, Influence of Type of Initiation on Thiol–Ene “Click” Chemistry, *Macromolecular Chemistry and Physics* 211(1) (2010) 103-110.
- [49] B.D. Fairbanks, D.M. Love, C.N. Bowman, Efficient Polymer-Polymer Conjugation via Thiol-ene Click Reaction, *Macromolecular Chemistry and Physics* 218(18) (2017) 1700073.
- [50] L.M. Campos, K.L. Killops, R. Sakai, J.M.J. Paulusse, D. Damiron, E. Drockenmuller, B.W. Messmore, C.J. Hawker, Development of Thermal and Photochemical Strategies for Thiol–Ene Click Polymer Functionalization, *Macromolecules* 41(19) (2008) 7063-7070.
- [51] S.P.S. Koo, M.M. Stamenović, R.A. Prasath, A.J. Inglis, F.E. Du Prez, C. Barner-Kowollik, W. Van Camp, T. Junker, Limitations of radical thiol-ene reactions for polymer–polymer conjugation, *Journal of Polymer Science Part A: Polymer Chemistry* 48(8) (2010) 1699-1713.
- [52] J. Justynska, H. Schlaad, Modular Synthesis of Functional Block Copolymers, *Macromolecular Rapid Communications* 25(16) (2004) 1478-1481.
- [53] T.M. Roper, C.A. Guymon, E.S. Jönsson, C.E. Hoyle, Influence of the alkene structure on the mechanism and kinetics of thiol–alkene photopolymerizations with real-time infrared spectroscopy, *Journal of Polymer Science Part A: Polymer Chemistry* 42(24) (2004) 6283-6298.
- [54] J. Yan, R.J. Spontak, Toughening Poly(lactic acid) with Thermoplastic Elastomers Modified by Thiol–ene Click Chemistry, *ACS Sustainable Chemistry & Engineering* 7(12) (2019) 10830-10839.
- [55] F. Shao, X.F. Ni, Z.Q. Shen, Preparation of amphiphilic graft copolymer with polyisoprene backbone by combination of anionic polymerization and “click” reaction, *Chinese Chemical Letters* 23(3) (2012) 347-350.

- [56] N.B. Cramer, S.K. Reddy, A.K. O'Brien, C.N. Bowman, Thiol–Ene Photopolymerization Mechanism and Rate Limiting Step Changes for Various Vinyl Functional Group Chemistries, *Macromolecules* 36(21) (2003) 7964-7969.
- [57] C.E. Hoyle, T.Y. Lee, T. Roper, Thiol–enes: Chemistry of the past with promise for the future, *Journal of Polymer Science Part A: Polymer Chemistry* 42(21) (2004) 5301-5338.
- [58] D.E. Fagnani, J.L. Tami, G. Copley, M.N. Clemons, Y.D.Y.L. Getzler, A.J. McNeil, 100th Anniversary of Macromolecular Science Viewpoint: Redefining Sustainable Polymers, *ACS Macro Letters* 10(1) (2021) 41-53.
- [59] U. Kalita, S. Samanta, S.L. Banerjee, N.C. Das, N.K. Singha, Biobased Thermoplastic Elastomer Based on an SMS Triblock Copolymer Prepared via RAFT Polymerization in Aqueous Medium, *Macromolecules* (2021).
- [60] M.P. Luda, M. Guaita, O. Chiantore, Thermal degradation of polybutadiene, 2. Overall thermal behaviour of polymers with different microstructures, *Die Makromolekulare Chemie* 193(1) (1992) 113-121.
- [61] K. McCreedy, H. Keskkula, Application of thermogravimetric analysis to the thermal decomposition of polybutadiene, *Journal of Applied Polymer Science* 22(4) (1978) 999-1005.
- [62] R.A. Mantz, P.F. Jones, K.P. Chaffee, J.D. Lichtenhan, J.W. Gilman, I.M.K. Ismail, M.J. Burmeister, Thermolysis of Polyhedral Oligomeric Silsesquioxane (POSS) Macromers and POSS–Siloxane Copolymers, *Chemistry of Materials* 8(6) (1996) 1250-1259.
- [63] I.C. McNeill, W.T.K. Stevenson, Thermal degradation of styrene-butadiene diblock copolymer: Part 2—Characteristics and mechanism of degradation of the copolymer, *Polymer Degradation and Stability* 10(4) (1985) 319-334.

- [64] L. Zheng, R.M. Kasi, R.J. Farris, E.B. Coughlin, Synthesis and thermal properties of hybrid copolymers of syndiotactic polystyrene and polyhedral oligomeric silsesquioxane, *Journal of Polymer Science Part A: Polymer Chemistry* 40(7) (2002) 885-891.
- [65] T.S. Haddad, J.D. Lichtenhan, Hybrid Organic–Inorganic Thermoplastics: Styryl-Based Polyhedral Oligomeric Silsesquioxane Polymers, *Macromolecules* 29(22) (1996) 7302-7304.
- [66] S. Spoljaric, A. Genovese, R.A. Shanks, Novel elastomer-dumbbell functionalized POSS composites: Thermomechanical and Morphological Properties, *Journal of Applied Polymer Science* 123(1) (2012) 585-600.
- [67] E. McMullin, H.T. Rebar, P.T. Mather, Biodegradable Thermoplastic Elastomers Incorporating POSS: Synthesis, Microstructure, and Mechanical Properties, *Macromolecules* 49(10) (2016) 3769-3779.
- [68] J.M. Hutchinson, Determination of the glass transition temperature, *Journal of Thermal Analysis and Calorimetry* 98(3) (2009) 579.
- [69] J. Rieger, The glass transition temperature  $T_g$  of polymers—Comparison of the values from differential thermal analysis (DTA, DSC) and dynamic mechanical measurements (torsion pendulum), *Polymer Testing* 20(2) (2001) 199-204.
- [70] K.S. Lee, Y.-W. Chang, Thermal and mechanical properties of poly( $\epsilon$ -caprolactone)/polyhedral oligomeric silsesquioxane nanocomposites, *Polymer International* 62(1) (2013) 64-70.
- [71] J.M. Yu, P. Dubois, R. Jérôme, Synthesis and Properties of Poly[isobornyl methacrylate (IBMA)-*b*-butadiene (BD)-*b*-IBMA] Copolymers: New Thermoplastic Elastomers of a Large Service Temperature Range, *Macromolecules* 29(23) (1996) 7316-7322.

- [72] E. Penzel, J. Rieger, H.A. Schneider, The glass transition temperature of random copolymers: 1. Experimental data and the Gordon-Taylor equation, *Polymer* 38(2) (1997) 325-337.
- [73] F.S. Bates, G.H. Fredrickson, Block copolymer thermodynamics: theory and experiment, *Annual review of physical chemistry* 41(1) (1990) 525-557.
- [74] D.W.V. Krevelen, K.T. Nijenhuis, *Properties of Polymers - Their Correlation with Chemical Structure; Their Numerical Estimation and Prediction from Additive Group Contributions* (4th, Completely Revised Edition), Elsevier, 1976, pp. 213-216.
- [75] B. Brüster, Y.-O. Adjoua, R. Dieden, P. Grysan, C.E. Federico, V. Berthé, F. Addiego, Plasticization of Polylactide with Myrcene and Limonene as Bio-Based Plasticizers: Conventional vs. Reactive Extrusion, *Polymers* 11(8) (2019).
- [76] İ. Kaya, E. Özdemir, Thermodynamic interactions and characterisation of poly(isobornyl methacrylate) by inverse gas chromatography at various temperatures, *Polymer* 40(9) (1999) 2405-2410.
- [77] M. Morton, J.E. McGrath, P.C. Juliano, Structure-property relationships for styrene-diene thermoplastic elastomers, *Journal of Polymer Science Part C: Polymer Symposia* 26(1) (1969) 99-115.

## 6 Hydrogenation of poly(myrcene) and poly(farnesene) using diimide reduction at ambient pressure

This chapter explores another post-polymerization modification method and it is in collaboration with Dr. Adrien Metafiot and two summer students, Judith Morize and Emmanuel Edeh, who completed the study on hydrogenation of poly(Myrcene). The chemical hydrogenation of poly(Myrcene) was based on Hahn's modified method using *p*-toluene sulfonyl hydrazide (TSH), which forms diimides under thermal degradation, to reduce the double bonds of poly(dienes). The chemical hydrogenation was optimized by performing a semi-batch addition of TSH into a solution of poly(Myrcene) in xylene and tributylamine (TBA) at 125 °C to avoid unwanted autohydrogenation of diimides. Almost complete hydrogenation of both the backbone and pendant double bonds (97.2% and 94.0%, respectively) of poly(Myrcene) was achieved. Therefore, this semi-batch approach was also applied to the hydrogenation of poly(Farnesene) and almost complete hydrogenation was achieved as well (96.8% and 99.6% for the backbone and pendant double bonds, respectively). Thermal stability of poly(Myrcene) and poly(Farnesene) improved after hydrogenation and their viscosities also increased. Poly(Myrcene) displayed a large increase in viscosity by two orders of magnitude ( $10^2$  Pa s to  $10^4$  Pa s) after hydrogenation because its  $M_n$  of  $56 \text{ kg mol}^{-1}$  was much higher than its entanglement molecular weight of  $12 \text{ kg mol}^{-1}$  (for saturated poly(Myrcene)) [47]. The viscosity for poly(Farnesene) only increased by 1.5 times ( $\sim 10^4$  Pa s) after hydrogenation since its  $M_n$  of  $62 \text{ kg mol}^{-1}$  was only slightly higher than its entanglement molecular weight of  $50 \text{ kg mol}^{-1}$ . However, unsaturated poly(Farnesene) displayed better entanglement compared to unsaturated poly(Myrcene) due to its longer side chains. This chapter was published in *Journal of Polymer Science* in an advance online publication (S.B. Luk, A. Métafiot, J. Morize, E. Edeh, M. Maric, Hydrogenation of poly(myrcene) and poly(farnesene) using diimide reduction at ambient pressure, *Journal of Polymer Science* advance online publication) [52]. The supporting information of this publication is in Appendix D, and the supporting figures and tables are referred to as Figure D-X and Table D-X in this chapter.

## 6.1 Abstract

Ambient pressure chemical hydrogenation using *p*-toluene sulfonyl hydrazide (TSH) via thermal diimide formation ( $N_2H_2$ ) permitted reduction of double bonds of poly(myrcene) (poly[Myr]) and poly(farnesene) (poly[Far]). Both pendent and backbone double bonds in poly(Myr) ( $M_n = 56$  kg/mol) and poly(Far) ( $M_n = 62$  kg/mol) synthesized by conventional free radical polymerization were hydrogenated to almost completion. Furthermore, TSH semi-batch addition efficiently hydrogenated double bonds, while avoiding undesired autohydrogenation of diimides that occurred in batch mode. Thermal stability improved for hydrogenated poly(Myr) and poly(Far), where temperature at 10% weight loss ( $T_{10\%}$ ) increased from 188 to 404°C for poly(Myr) and from 310 to 379°C for poly(Far).  $T_g$ s of poly(Myr) and poly(Far) also increased by about 10–25°C, indicating increased stiffness after hydrogenation. Finally, viscosities of poly(Myr) and poly(Far) were also increased after hydrogenation, and a greater increase was observed for poly(Myr) (by two orders of magnitude from  $10^2$  to  $10^4$  Pa s) due to its  $M_n$  being much higher than its entanglement molecular weight. Poly(Far) viscosity only increased by 1.5 times after hydrogenation ( $\sim 10^4$  Pa s), comparable to the poly(Myr) after hydrogenation, suggesting unsaturated poly(Far) was more entangled than unsaturated poly(Myr) because of its longer side chains.

## 6.2 Introduction

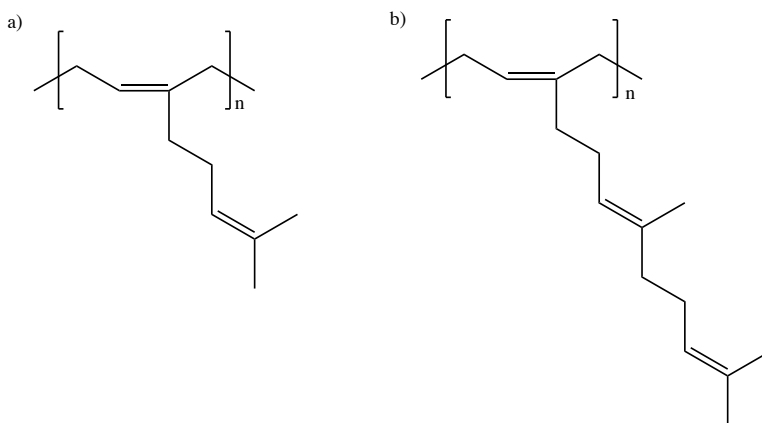
1,3-Dienes are conjugated hydrocarbons that contain two double bonds separated by one single bond and can be easily polymerized. Common 1,3-dienes are butadiene (BD) and isoprene (IP), which are byproducts of crude oil cracking, and their polymers are used in many applications such as automotive parts, tires, and seals for O-rings, gaskets, and hoses [1]. Poly(BD) and poly(IP) are considered synthetic rubbers or elastomers because of their low glass transition temperatures ( $T_g$ ) and viscoelastic properties. Poly(IP) is also known as natural rubber (mostly *cis*-1,4-poly(isoprene)) as it can be found naturally in tree sap [2]. Furthermore, the remaining double bond after polymerization allows for crosslinking, thereby forming thermosets that are resistant to chemical and thermal degradation [3]. Alternatively for poly(1,3-dienes) that are not chemically crosslinked, they can be blended with thermoplastics to obtain a final material with synergistic

effects in mechanical and physical properties. 1,3-Dienes can also be copolymerized with mainly styrene (St), methyl methacrylate (MMA) and their derivatives to make thermoplastic elastomers (TPEs) [4]. The glassy thermoplastic portion ( $T_g > T_{\text{room}}$ ) acts as physical crosslinks, while maintaining viscoelastic properties of the rubbery portion ( $T_g < T_{\text{room}}$ ), and TPEs can be processed at higher temperatures, like thermoplastics.

The remaining double bonds in poly(dienes) present several disadvantages, as they are susceptible to solvent and thermal degradation. The unsaturated compounds exhibit different mechanical and rheological properties, as well as polymer-polymer miscibility as their saturated analogs. Poly(styrene-*b*-butadiene-*b*-styrene) SBS triblock copolymers are TPEs and are often blended with crystalline poly(propylene) (PP) as a toughener to improve impact and tensile strength [5]. SBS can be partially hydrogenated and form poly(styrene-*b*-ethylene-*co*-butadiene-*b*-styrene) (SEBS), which can also be blended with PP [6,7]. Similarly, poly(styrene-*b*-isoprene-*b*-styrene) (SIS) can be hydrogenated to form poly(styrene-*b*-ethylene-*co*-propylene-*b*-styrene) (SEPS) [8]. SEBS/PP blends showed improved impact strength compared to SBS/PP blends, as well as increased elongation at break due to the smaller droplets of TPE that are better dispersed in the matrix [9]. SEBS also has a higher  $T_g$  for the rubbery block at  $-50^\circ\text{C}$  compared to a  $T_g$  of  $-86^\circ\text{C}$  for SBS [10]. Moreover, hydrogenated poly(dienes) have lower hydrodynamic volumes compared to their unsaturated poly(dienes), and therefore require lower molecular weights in order to entangle and exhibit viscoelastic properties [11,12].

Recently, there has been growing interest in replacing traditional petroleum-derived monomers with bio-derived monomers. Myrcene (Myr) and farnesene (Far) are terpenes that are found in nature and are also 1,3-dienes with longer sidechains and lower volatility compared to BD and IP. Myr can be produced by pyrolysis of  $\beta$ -pinene and Far can be produced from dehydration of terpenoids or fermentation using microorganisms [13–16]. Due to their lower volatility, these bio-based dienes are more easily polymerized at ambient pressures in numerous ways including ionic polymerization, redox emulsion, catalytic/coordination polymerization, reversible addition-fragmentation transfer polymerization (RAFT), and nitroxide-mediated polymerization (NMP) [17–31]. The longer sidechains of poly(Myr) and poly(Far) provide great potential as promising elastomers due their bottlebrush-like structure. However their degree of unsaturation is higher

compared to poly(BD) and poly(IP) [32]. Indeed, a poly(Myr) repeating unit contains two double bonds and a poly(Far) repeating unit has three double bonds as shown in Scheme 6-1. As a result, the entanglement molecular weights ( $M_e$ ) of poly(Myr) and poly(Far) are much greater than poly(BD) and poly(IP) (i.e.  $M_{e,Myr} = 18,000\text{--}25,000 \text{ g mol}^{-1}$  and  $M_{e,Far} = 50,000 \text{ g mol}^{-1}$  versus  $M_{e,BD} = 1,500\text{--}1,900 \text{ g mol}^{-1}$  and  $M_{e,IP} = 3,000\text{--}5,000 \text{ g mol}^{-1}$ , where  $M_e$  depends on composition of *cis* and *trans* or 1,2- and 1,4-addition repeating units) [33,34]. Therefore, the hydrogenation of poly(Myr) and poly(Far) is beneficial in order to lower their  $M_e$ s and have comparable viscoelastic properties without achieving high molecular weights. In fact, the hydrogenation of poly(1,4-Myr) lowered the  $M_e$  from  $18,000 \text{ g mol}^{-1}$  to  $12,000 \text{ g mol}^{-1}$  [33].



Scheme 6-1. Chemical structures of a) poly(Myr) and b) poly(Far) shown by 1,4-addition.

Hydrogenation of poly(dienes) is straightforward and is commonly done industrially using metal catalysts (homogeneous or heterogeneous) [12, 35–37]. However, catalytic addition of hydrogen gas requires specialized high pressure reactors. Another method developed by Hahn employs thermal degradation of *p*-toluene sulfonyl hydrazide (TSH) to generate diimides in order to chemically hydrogenate poly(dienes) without the use of pressurized reactors, but requires at least stoichiometric amounts of TSH for complete hydrogenation [38]. Early hydrogenation studies of poly(BD) and poly(IP) using TSH showed incomplete hydrogenation due to side reactions like degradation and cyclization. Eventually, modification of the Hahn method was done by adding a base like tripropylamine (TPA) with TSH, which helped minimize side reactions and chain cleavage of polymers [38–41]. Chemical hydrogenation using TSH/TPA has successfully hydrogenated poly(BD) and poly(IP) block copolymers and homopolymers, while showing good

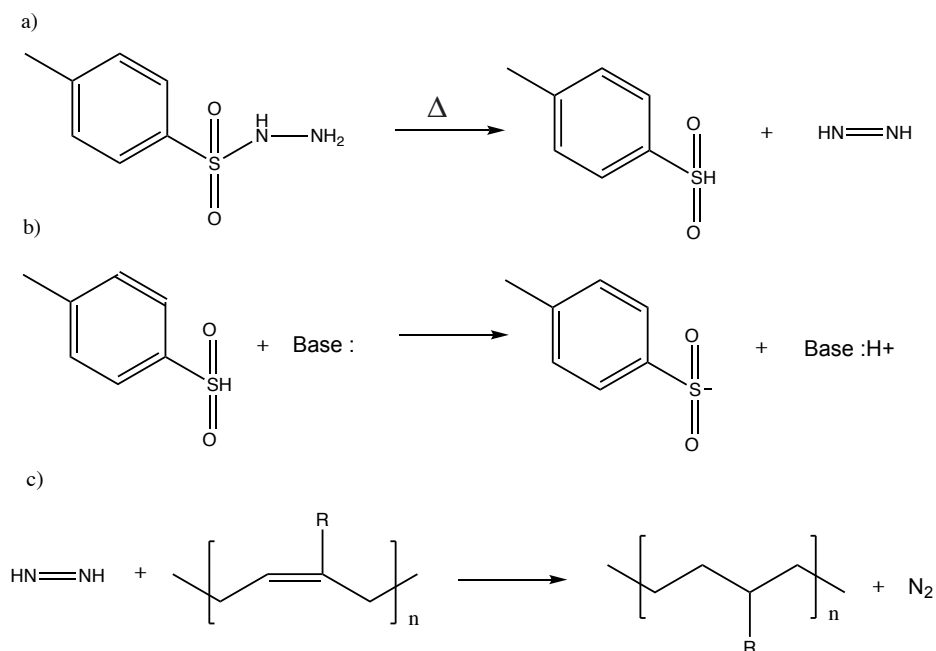
tolerance for functional groups [42–46]. Diimides have also been used to hydrogenate polymers synthesized via ring opening metathesis polymerization of various substituted cyclooctenes [47–50].

There are several examples of catalytic hydrogenation of Myr monomer and one example of hydrogenation of poly( $\beta$ -pinene) using diimides[51–55]. However, the chemical hydrogenation of bio-based poly(dienes) has not yet been explored. The goal of this study is to optimize the hydrogenation of poly(Myr) and poly(Far) to almost completion using diimides at ambient pressure. Poly(Myr) and poly(Far) were synthesized via free radical polymerization in bulk such that their average molecular weights are above their  $M_e$ . Several modes of operation for hydrogenation were investigated (i.e. batch reaction, semi-batch addition of TSH, and with and without solvent) and suggested conditions for high hydrogenation degree of bio-based poly(dienes) was provided for the first time. Additionally, their thermal and rheological properties were compared before and after hydrogenation to assess the change due to the additional processing steps.

### 6.3 Results and discussion

#### 6.3.1 Hydrogenation of poly(Myr) in batch mode

Preliminary hydrogenation experiments done with poly(Myr) were based on similar studies of hydrogenation of poly(dienes) using diimides found in literature [38,41–45]. In these studies, TSH would undergo thermal degradation to form a *p*-tolylsulfonic acid and a diimide, the latter which would chemically hydrogenate an alkene (Scheme 6-2). However, early studies of hydrogenation using TSH resulted in side reactions such as cyclization and chain cleavage due to nucleophilic attack of *p*-tolylsulfonic acid on the polymer backbone [39–41]. Hahn modified this method by adding a base like tripropylamine (TPA) that would deprotonate *p*-tolylsulfonic acid, and therefore avoid chain cleavage by protonation of the polymer backbone [38]. SBS and SIS triblock copolymers were hydrogenated with TSH/TPA, and SBS reached almost 100% hydrogenation whereas SIS reached at maximum of 69% hydrogenation using 6 molar equivalent of TSH/TPA per double bond.



Scheme 6-2. Hahn's modified chemical hydrogenation of poly(dienes) using diimide ( $N_2H_2$ ) [38]. a) Thermal degradation of TSH to form diimide in the presence of b) a base to deprotonate the acidic *p*-tolylsulfonic acid, and c) diimide hydrogenation of poly(diene). The *R* group can represent an H for butadiene,  $CH_3$  for isoprene, or other alkyl groups.

In this study, poly(Myrr) was hydrogenated using TSH with tributylamine (TBA) in slight excess (1:1.2 TSH:TBA molar ratio) as a base to deprotonate the acidic TSH byproduct. Like the studies in literature, hydrogenation reactions were done in batch, where all reagents were added initially into the reactor. Furthermore, BHT was added to prevent oxidative degradation of the polymer chains. Two hydrogenation reactions were done in batch using 2.0 and 4.0 molar equivalents of TSH per double bond of poly(Myrr) and their hydrogenation degrees over 4 hours of reaction are shown in Figure 6-1. Because poly(Myrr) has a double bond in the backbone due to mostly 1,4-addition and a pendent double bond in its side chain, the hydrogenation of both the backbone and pendent double bonds were quantified using  $^1H$  NMR.

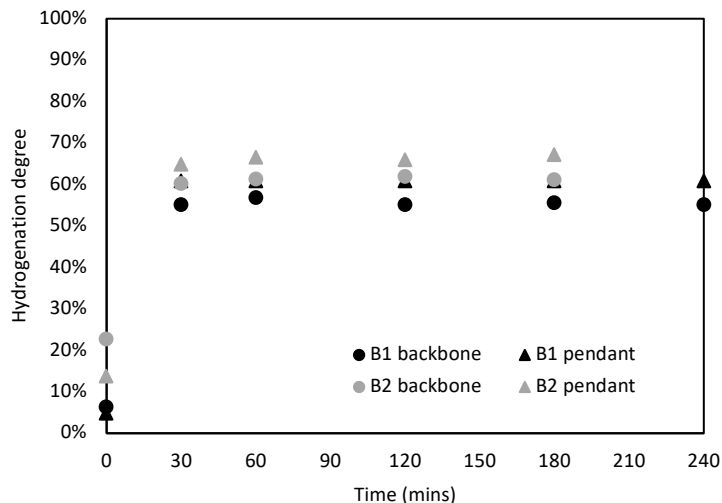
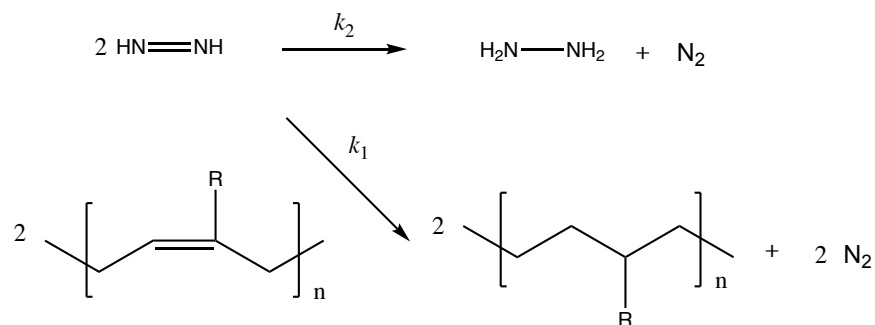


Figure 6-1. Hydrogenation of poly(Myrr) in batch using 2.0 (B1) and 4.0 (B2) mol eq. of TSH per double bond.

The final hydrogenation degrees when using initially 2.0 molar eq. of TSH per double bond (hydrogenation reaction abbreviated B1) were 55% and 61% for the backbone and pendant double bonds, respectively. With 4.0 molar eq. of TSH per double bond used in the feed (hydrogenation reaction abbreviated B2), the hydrogenation degrees were 63% and 65% for the backbone and pendant double bonds, respectively. By increasing from 2.0 to 4.0 mol eq. of TSH per double bond, it only increased the hydrogenation degree of poly(Myrr) slightly. Furthermore, the hydrogenation of the backbone is slightly higher than that of the pendant double bond, but also not very significant, which suggests that the pendant double bond is almost as accessible as the backbone for hydrogenation and the steric hindrance are comparable for both double bonds.

In Hahn's study of the hydrogenation of SBS and SIS triblock copolymers, the double bonds of isoprene units could not be completely hydrogenated in comparison to butadiene double bonds, which reached complete hydrogenation [38]. This was attributed to steric hindrance from the methyl group of IP, which then favoured the undesired autohydrogenation of diimide (Scheme 6-3). It can be seen in Figure 6-1 that the hydrogenation degree increased significantly in the first 30 mins of the reaction, and then essentially remained constant. In the beginning of the batch reaction, a high concentration of diimide led to fast hydrogenation of the double bonds of poly(Myrr). However, as the reaction progressed and the double bonds became less available for hydrogenation,  $k_2$  became more favourable than  $k_1$ . Due to the lowered concentration of double

bonds, any excess TSH remaining in the batch reaction would inevitably lead to autohydrogenation, such that increasing TSH from 2.0 to 4.0 mol eq. had negligible improvement on the hydrogenation degree of poly(Myr).



Scheme 6-3. Desired hydrogenation of poly(diene) using diimide ( $k_1$ ) versus the competing autohydrogenation reaction of diimide ( $k_2$ ).

Although hydrogenation of SIS triblock copolymers using Hahn's modified method did not reach complete hydrogenation, later studies showed that high degrees of hydrogenation (> 95%) can be obtained by batch hydrogenation of poly(isoprene-*b*-styrene) diblock copolymer and liquid natural rubber [38,42,45]. Another study used the semi-batch approach and added TSH in three separate batches throughout the reaction, and achieved complete hydrogenation of poly(IP) and poly(1,3-pentadiene) [46]. Therefore, semi-batch hydrogenation of poly(Myr) would be advantageous since the concentration of diimide is kept low in the reaction medium, which would minimize the unwanted autohydrogenation reaction. Furthermore, a constant supply of diimide would ensure that the limited amount of diimide available would favour towards the hydrogenation of the double bonds.

### 6.3.2 Hydrogenation of poly(Myr) in semi-batch mode

Hydrogenation of poly(Myr) was studied in a semi-batch operation, and the first two semi-batch reactions were done by adding a TSH solution continuously into the reaction using a dropping funnel. TSH was dissolved in two different solvents, 1,4-dioxane and pyridine (i.e. SB1 and SB2), although TSH was not completely soluble in either solvent. A peristaltic pump was originally used to add the TSH solution to the reaction, but the partially insoluble TSH powder in 1,4-dioxane and

pyridine caused blockages in the tubing. Additionally, poly(Myrr) was not dissolved in xylene in the first two semi-batch reactions to minimize the use of organic solvents and because a solvent would be added with the TSH solution. Therefore, excess TBA was added initially to dissolve the poly(Myrr) in the reactor. The hydrogenation degrees of poly(Myrr) in SB1 and SB2 are shown in Figure 6-2, where 2.0 mol eq. of TSH was added per double bond.

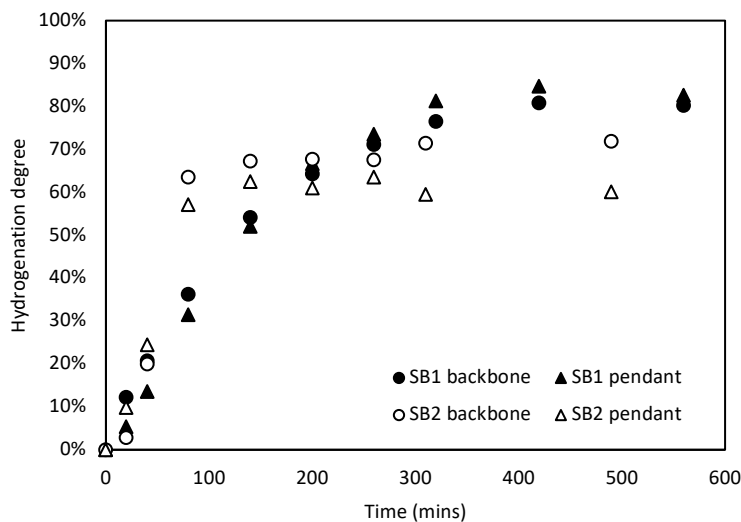


Figure 6-2. Hydrogenation of poly(Myrr) in semi-batch using 2.0 mol eq. of TSH per double bond, where TSH was dissolved in 1,4-dioxane (SB1) and pyridine (SB2) and added continuously throughout the reaction.

Semi-batch hydrogenation was more successful than the batch case, as higher hydrogenation degrees were achieved as seen in Figure 6-2. SB1 achieved hydrogenation degrees of 80% and 83% for the backbone and pendant double bonds, respectively, and the hydrogenation showed a gradual increase using 1,4-dioxane, unlike hydrogenation in batch. Even though higher degrees of hydrogenation were achieved, poly(Myrr) was still not completely hydrogenated. One issue was due to the low boiling point of 1,4-dioxane ( $T_b = 101^\circ\text{C}$ ), which effectively lowered the reaction temperature to  $101^\circ\text{C} - 104^\circ\text{C}$  even though the reaction temperature was set at  $125^\circ\text{C}$ .

Therefore, pyridine was used as a solvent to dissolve TSH because it has a higher boiling point ( $T_b = 115^\circ\text{C}$ ). Final hydrogenation degrees by adding TSH in pyridine reached 72% and 60% for backbone and pendent double bonds, respectively, which was lower than what was achieved using TSH in 1,4-dioxane. Furthermore, hydrogenation seemed to increase steadily up until 100 min, then plateaued as seen in Figure 6-2. The reaction mixture also turned orange at the end of reaction and side degradation reactions were suspected. An earlier study for hydrogenation of poly(isoprene) used TSH and pyridine as a base suppressant for chain cleavage, however it resulted in severe chain degradation. Furthermore, higher concentrations of pyridine led to slower rates of hydrogenation [40]. Evidently, pyridine does not act as a base like TBA to deprotonate the TSH acid by-product, but rather accelerated chain cleavage.

Since a suitable solvent could not be found to fully dissolve TSH into solution for semi-batch addition, dry TSH powder was added in small batches (1 g for every 15 min) throughout the reaction instead. Similar to SB1 and SB2, SB3 did not include any xylene to dissolve poly(My) initially, but the dry TSH powder was not fully soluble in the poly(My)/TBA mixture, and therefore hydrogenation did not occur. The reaction mixture turned yellow, then brown, and eventually purple towards the conclusion of the experiment. Consequently, the remaining semi-batch reactions included xylene as a solvent, which was required to dissolve both poly(My) and TSH into a homogenous mixture.

In SB4, poly(My) was dissolved in xylene and TBA, and 2.0 mol eq. of dry TSH powder per double bond was added throughout the reaction. The hydrogenation degrees of SB4 are shown in Figure 6-3, and high degrees of hydrogenation were achieved (89% and 88% for the backbone and pendent double bonds, respectively). The ratio of TSH to double bond was increased to 2.5 and 3.0 mol eq. and the highest degrees of hydrogenation were achieved using 3.0 mol eq. of TSH, reaching 97% and 94% for the backbone and pendent double bonds, respectively. The semi-batch reactions with continuous addition of dry TSH powder also maintained the reaction temperature at  $125^\circ\text{C}$  unlike SB1 and SB2 where the temperatures were lowered due to the low boiling points of the solvents. Therefore, adding dry TSH powder had the most success in achieving almost complete hydrogenation of poly(My) for both the backbone and pendent double bonds.

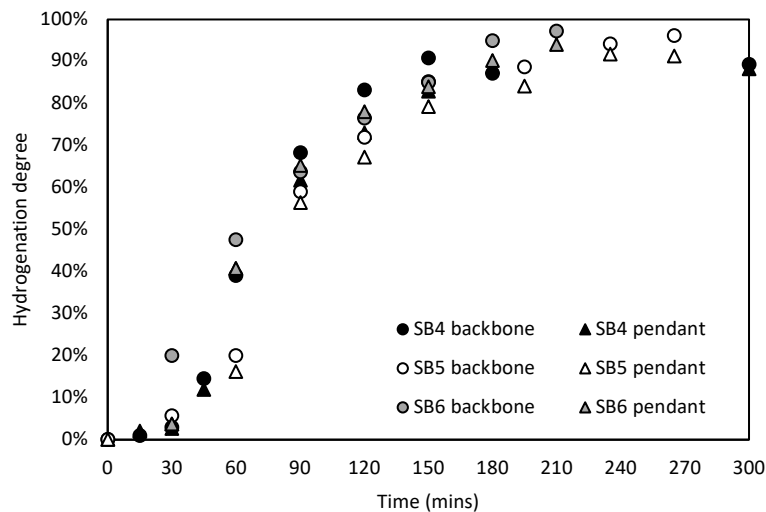


Figure 6-3. Hydrogenation of poly(Myr) in semi-batch by adding dry TSH powder (1 g for every 15 min) at 2.0 (SB4), 2.5 (SB5), and 3.0 (SB6) mol eq. of TSH per double bond.

The progression of the hydrogenation reactions of poly(Myristic acid) were quantified by  $^1\text{H}$  NMR. As an example, the series of  $^1\text{H}$  NMR spectra for SB6 is shown in Figure 6-4. The doublet at 1.6 ppm (A) represents the two unsaturated methyl groups of the Myr repeating unit, which disappear as the hydrogenation reaction occurs. The appearance of the doublet at 0.8 ppm (B) represents the saturated methyl group protons of backbone double bonds as they become hydrogenated. Lastly, the disappearance of the peak at 5.1 ppm (C) represents the hydrogenation of the pendent double bonds of the poly(Myristic acid). At the end of the reaction, it is evident that there is a minimal fraction of pendent and backbone double bonds remaining.

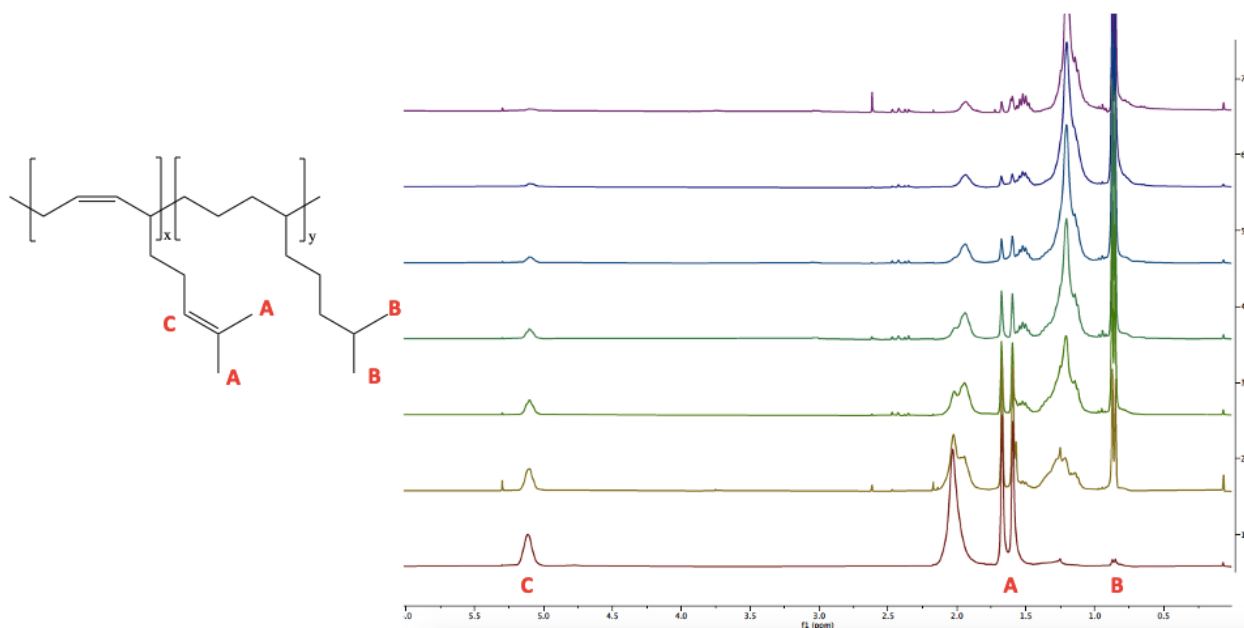


Figure 6-4.  $^1\text{H}$  NMR ( $\text{CDCl}_3$ ) spectra of SB6 hydrogenation reaction of poly(Myristic acid) from time = 0 min (bottom, red) to time = 210 min (top, purple).

The molecular weight distribution (MWD) of poly(Myristic acid) synthesized by free radical polymerization is compared with the MWDs of the hydrogenated poly(Myristic acid) made by the semi-batch method. As seen in Figure 6-5, the molecular weights of poly(Myristic acid) measured from GPC did not change significantly after hydrogenation, indicating there was no chain cleavage from TSH acidic by-products, or from any thermal or oxidative degradation.

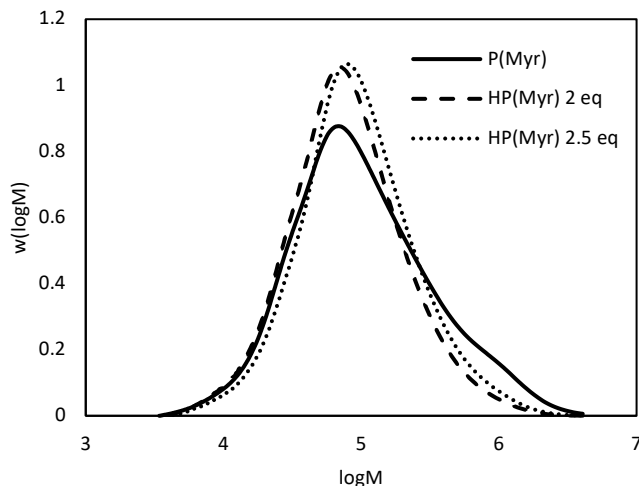


Figure 6-5. Molecular weight distributions of poly(Myrrhen) before and after hydrogenation in semi-batch using 2.0 and 2.5 mol eq. of TSH per double bond.

### 6.3.3 Hydrogenation of poly(Far) in semi-batch mode

Since the hydrogenation of poly(Myrrhen) was optimized by adding dry TSH powder in semi-batch operation, the hydrogenation of poly(Far) was done using the same method. In SB7, SB8, and SB9, poly(Far) was hydrogenated with 2.0, 2.5, and 3.0 mol eq of TSH per double bond of poly(Far), except now there are three double bonds per repeating unit instead of two. The hydrogenation degrees with reaction time are shown in Figure 6-6. Similar to the hydrogenation of poly(Myrrhen) in semi-batch mode, the highest degrees of hydrogenation for poly(Far) was achieved using 3.0 mol eq of TSH. Almost complete hydrogenation was reached for poly(Far) at 97% and >99% of hydrogenation for the backbone and pendent double bonds, respectively.

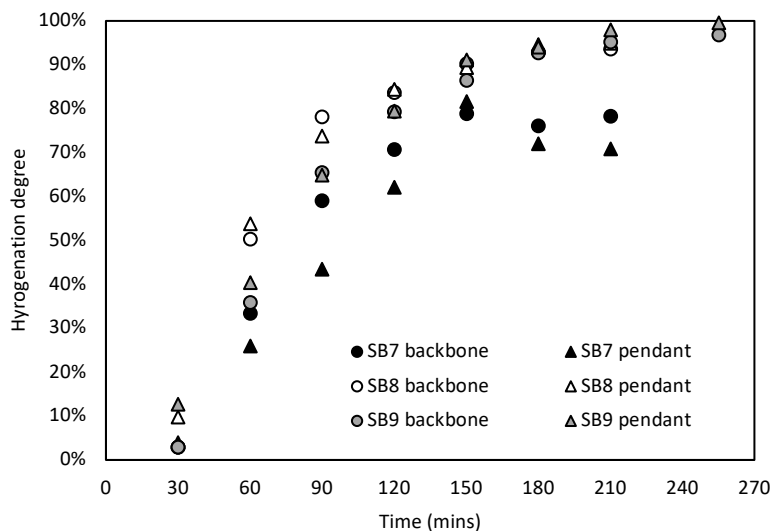


Figure 6-6. Hydrogenation of poly(Far) in semi-batch by adding dry TSH powder (1 g for every 15 min) at 2.0 (SB7), 2.5 (SB8), and 3.0 (SB9) mol eq. of TSH per double bond.

A series of  $^1\text{H}$  NMR spectra for the hydrogenation of poly(Far) in semi-batch is shown in Figure 6-7. Similar to the hydrogenation of poly(Myrr), there is the disappearance of the doublet peak representing the three unsaturated methyl group protons at 1.6 ppm (A), and appearance of the saturated methyl groups at 0.8 ppm (B) from the hydrogenation of the backbone double bond. There is also the disappearance of the unsaturated proton peak at 5.1 ppm (C), which represents the hydrogenation of the pendent double bonds in the side chains of poly(Far).

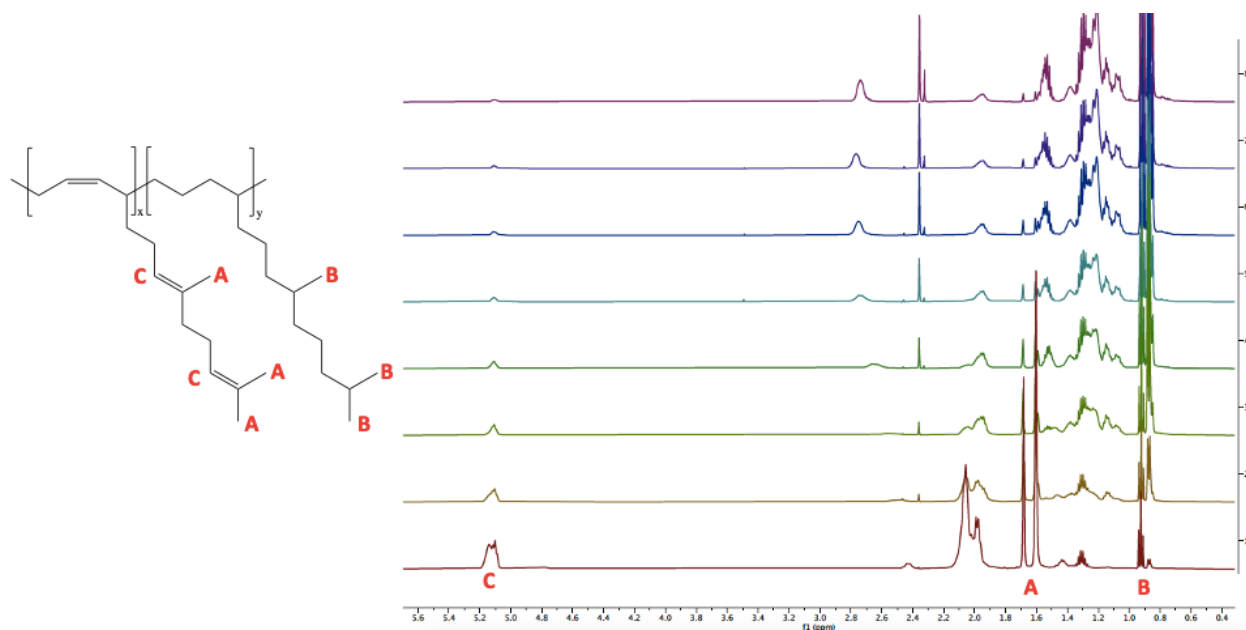


Figure 6-7.  $^1\text{H}$  NMR ( $\text{CDCl}_3$ ) spectra of SB9 hydrogenation reaction of poly(Far) from time = 0 min (bottom, red) to time = 255 min (top, purple).

Furthermore, the MWDs of poly(Far) before and after hydrogenation are shown in Figure 6-8. There is a prominent molecular weight shoulder for poly(Far) as a result of the free radical polymerization at low initiator loading, hence the high  $\bar{D}$  of 6.6. Similarly, there is a negligible difference in the MWD after almost complete hydrogenation using 2.5 and 3.0 eq TSH per double bond, indicating there was no polymer chain degradation.

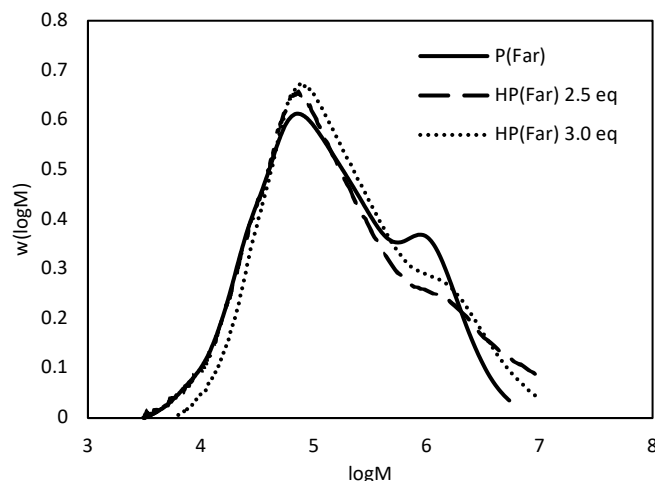


Figure 6-8. Molecular weight distributions of poly(Far) before and after hydrogenation in semi-batch using 2.5, and 3.0 mol eq. of TSH per double bond.

It is apparent that the semi-batch addition of dry TSH powder was very effective in almost completely hydrogenating the double bonds of both poly(Myrcene) and poly(Far). The most efficient hydrogenation was achieved by adding 3.0 mol eq. of TSH per double bond. The final hydrogenation degrees for all experiments for poly(Myrcene) and poly(Far) are summarized in Table 6-1. Furthermore, the hydrogenated poly(dienes) were not expected to have any stereochemistry, as they become saturated alkyl chains comprised of  $\sigma$ -bonds. Although the manual addition of TSH required opening the reactor every time,  $N_2$  gas generated by the reaction itself was able to maintain a nitrogen atmosphere for the reaction. Although the addition of dry TSH powder could have been automated by using a powder dispenser, manual addition of the powder was still sufficient as shown by the semi-batch experiments in this study.

Table 6-1. Summary of final hydrogenation degrees of poly(Myrcene) and poly(Far) for both pendent and backbone double bonds.

Experiment ID	Poly(diene)	Molar eq. of TSH <sup>a</sup>	Hydrogenation degree of pendent double bonds <sup>b</sup>	Hydrogenation degree of backbone double bonds <sup>c</sup>
B1	Poly(Myrcene)	2.0	61%	55%
B2	Poly(Myrcene)	4.0	65%	63%

SB1	Poly(Myrr)	2.0	83%	80%
SB2	Poly(Myrr)	2.0	60%	72%
SB4	Poly(Myrr)	2.0	88%	89%
SB5	Poly(Myrr)	2.5	91%	96%
SB6	Poly(Myrr)	3.0	94%	97%
SB7	Poly(Far)	2.0	81%	79%
SB8	Poly(Far)	2.5	95%	94%
SB9	Poly(Far)	3.0	99%	97%

a) Molar equivalent of TSH was added per double bond per repeating unit of poly(Myrr) or poly(Far); b) Hydrogenation degrees were determined using  $^1\text{H}$  NMR.

#### 6.3.4 Thermal behaviour of hydrogenated poly(Myrr) and poly(Far)

The thermal stability of the bio-based polymers was analyzed before and after hydrogenation. The thermal degradations of poly(Myrr) and the hydrogenated poly(Myrr) in semi-batch mode with 2.5 and 3.0 mol eq. of TSH per double bond were measured using TGA as shown in Figure 6-9. The degradation of poly(Myrr) shows an initial degradation at 170°C and its weight decreased by 25 wt% until a second degradation occurred at 360°C. This two-step degradation is consistent with the thermal degradation of poly(Myrr) in literature, as well as for poly(BD) [21,56]. Poly(BD) homopolymer showed a two-step degradation for polymers containing the 1,4-addition (*cis* or *trans*) conformation, however there was only one degradation step for poly(BD) polymerized by 1,2-addition [57]. Poly(Myrr) polymerized by redox emulsion mostly consisting of 1,4-addition units also showed a distinct two-step degradation [21]. The initial degradation of poly(BD) is attributed to its depolymerization into butadiene and vinylcyclohexene by-products, and the second step is the degradation of cyclized and crosslinked polymer units [56]. Since poly(Myrr) in this study was also mostly comprised of 1,4-addition units, it is not surprising that it exhibited a two-step degradation as well.

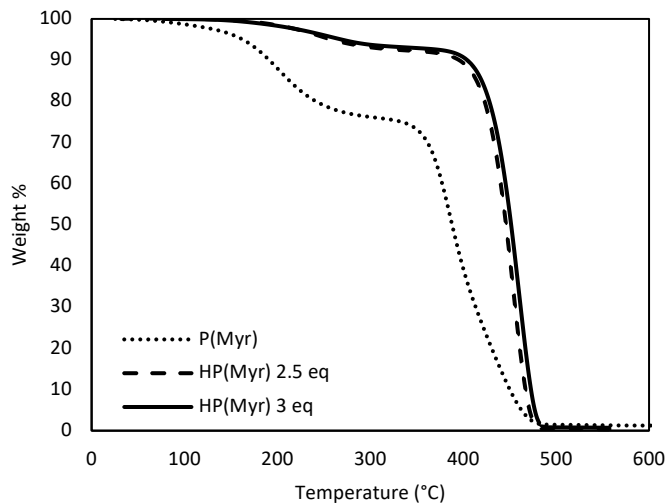


Figure 6-9. Thermal degradation of poly(My) showing weight loss with temperature before (dotted line) and after semi-batch hydrogenation using 2.5 (dashed line) and 3 mol eq (solid line) of TSH per double bond.

The thermal degradation of poly(My) showed great improvement after almost complete hydrogenation as seen in Figure 6-9 (HP(My) 2.5 eq and HP(My) 3 eq). The initial degradation lessened to 7 wt% loss, and the degradation temperature at 10 wt% loss ( $T_{10\%}$ ) is at 404°C. This suggests that after saturation of the backbone double bonds, the depolymerization of the polymer units by 1,4-addition was minimized. Furthermore, the saturation of the pendent double bonds likely decreased the cyclization between monomer units. Therefore, the thermal stability of the hydrogenated poly(My) is significantly improved. This is consistent with other poly(dienes), where an increase in thermal stability was shown after hydrogenation of the double bonds [42,43,45].

Poly(Far) also shows an initial degradation at 125°C but only 4 wt% of its initial mass had degraded, therefore it is not as severe as poly(My) where 20 wt% of its initial mass degraded. Furthermore, poly(Far) exhibited a  $T_{10\%}$  at 310°C (Figure 6-10). The low initial thermal degradation of poly(Far) is similar to the work recently done by our group showing the degradation of poly(farnesene-*b*-ethylene glycol dicyclopentenyl methacrylate) (poly(Far-*b*-EGDEMA) [58]. The diblock copolymer had a very short block of poly(EGDEMA) and was mostly comprised of poly(Far), and it also had a 4 wt% decrease at 125°C. Even though both poly(Far) and poly(My) were polymerized by 1,4-addition, the lower initial degradation of poly(Far) suggests the longer

side chains may have helped to prevent the depolymerization degradation, and therefore has better thermal stability compared to poly(Myrr). Nonetheless, much improvement in thermal stability was shown after almost complete hydrogenation using 2.5 and 3.0 mol eq. of TSH per double bond, where  $T_{10\%}$  increased to 379°C.

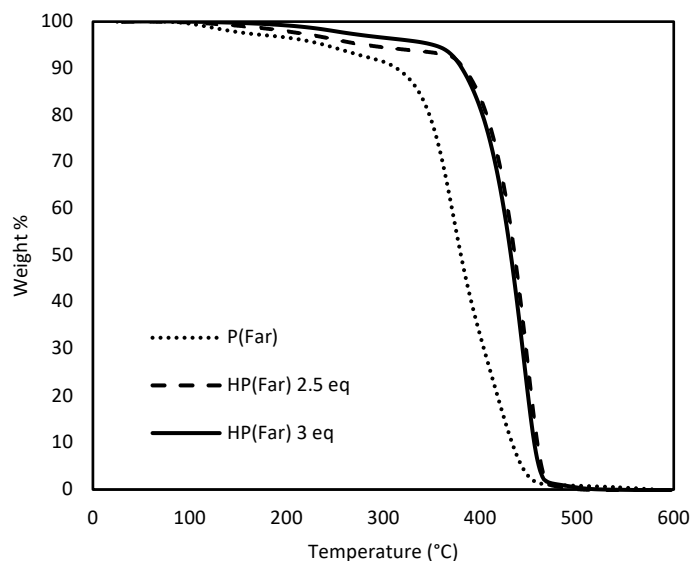


Figure 6-10. Thermal degradation of poly(Far) with temperature before (dotted line) and after semi-batch hydrogenation using 2.5 (dashed line), and 3.0 mol eq (solid line) of TSH per double bond.

Glass transition temperatures of the hydrogenated poly(Myrr) and poly(Far) were measured using DSC and are summarized in Table 6-2. With increased degrees of hydrogenation (by increasing TSH per double bond), the  $T_g$  also increased compared to their respective unsaturated poly(dienes).  $T_g$ s of the unsaturated poly(Myrr) and poly(Far) were not detected using the DSC in this study. This could be due to the high dispersity of the polymers made by free radical polymerization such that the presence of shorter chains could have plasticized the polymer and lowered the  $T_g$  to below or very close to the lowest possible temperature of -90°C for the DSC that was used. There are several reported  $T_g$ s of poly(Myrr), where homopolymerization of Myrr via nitroxide-mediated polymerization exhibited a  $T_g$  of -77°C and homopolymerization of Myrr by persulfate-initiated emulsion exhibited a  $T_g$  of -73°C [21,29]. However, poly(Myrr) synthesized by redox emulsion and RAFT polymerization both had a  $T_g$  of -60°C [21–24]. Evidently, poly(Myrr) with highly ordered microstructures (>90 mol% 1,4-*cis*) and/or higher molecular weight exhibit higher  $T_g$ s [59].

Although  $T_g$  of poly(Myrr) before hydrogenation was not detected using DSC, the  $T_g$ s of the hydrogenated poly(Myrr) are all higher than the reported values of unsaturated poly(Myrr). Furthermore, it has been shown that poly(Myrr) polymerized with predominantly 1,4-addition had a  $T_g$  of  $-68^\circ\text{C}$  compared to a  $T_g$  of  $-54^\circ\text{C}$  after hydrogenation [60].  $T_g$  of poly(Far) in this study was also not observed in DSC but it is reported to be  $-73^\circ\text{C}$  [34]. Similarly,  $T_g$ s of the hydrogenated poly(Far) also increased compared to the unsaturated analog. An increase in  $T_g$  suggests an increase in stiffness of polymer chains as a result of the saturation of double bonds, and this is consistent with other hydrogenated poly(diene) homopolymers and copolymers in literature [10,42,43,46,61].

Table 6-2. Glass transition temperatures of poly(Myrr) and poly(Far) before and after hydrogenation.

	$T_g$ of unsaturated poly(diene) [ $^\circ\text{C}$ ]	$T_g$ of hydrogenated poly(dienes) [ $^\circ\text{C}$ ]	
		2.5 mol eq. TSH	3.0 mol eq. TSH
Poly(Myrr)	-77 <sup>a</sup>	-54	-52
Poly(Far)	-73 <sup>b</sup>	-66	-63

<sup>a)</sup> Obtained from references 20 for poly(Myrr) mostly made of 1,4-addition units; <sup>b)</sup> Obtained from reference 32

The thermal behaviour of these bio-based poly(dienes) was certainly affected after hydrogenation of the double bonds. A significant improvement in thermal stability was shown after the hydrogenation of poly(Myrr), where the initial depolymerization degradation was greatly decreased. Furthermore, an increase in  $T_{10\%}$  for both hydrogenated poly(Myrr) and poly(Far) compared to the unsaturated poly(dienes) was also observed. Their  $T_g$ s also increased after hydrogenation, which indicate stiffer polymer chains.

### 6.3.5 Rheology of hydrogenated poly(Myrr) and poly(Far)

To further investigate the change in the properties of the bio-based poly(dienes) after hydrogenation, their steady shear viscosities were measured as a function of shear rate using the rheometer. In Figure 6-11a, the viscosity of the unsaturated poly(Myrr) decreased slightly from  $1.41 \times 10^2 \text{ Pa s}$  to  $1.15 \times 10^2 \text{ Pa s}$  by increasing the shear rate from  $0.1$  to  $10 \text{ s}^{-1}$ . After hydrogenation,

the viscosity of the hydrogenated poly(Myrr) increased significantly by two orders of magnitude to  $2.53 \times 10^4$  Pa s (HP(Myrr) 3 eq in Figure 11a), which confirms that hydrogenated poly(Myrr) did increase in stiffness. By increasing shear rate from  $0.1 \text{ s}^{-1}$  to  $10 \text{ s}^{-1}$ , the viscosity of hydrogenated poly(Myrr) decreased by an order of magnitude to  $2.70 \times 10^3$  Pa s, which demonstrates more shear-thinning behaviour. Conversely, the viscosity of poly(Far) only increased slightly after hydrogenation as seen in Figure 6-11b (HP(Far) 2.5 eq and HP(Far) 3 eq). The viscosity of poly(Far) at low shear rates  $< 1 \text{ s}^{-1}$  is about  $1 \times 10^4$  Pa s and decreased an order of magnitude at a shear rate of  $10 \text{ s}^{-1}$  indicative of shear-thinning behaviour.

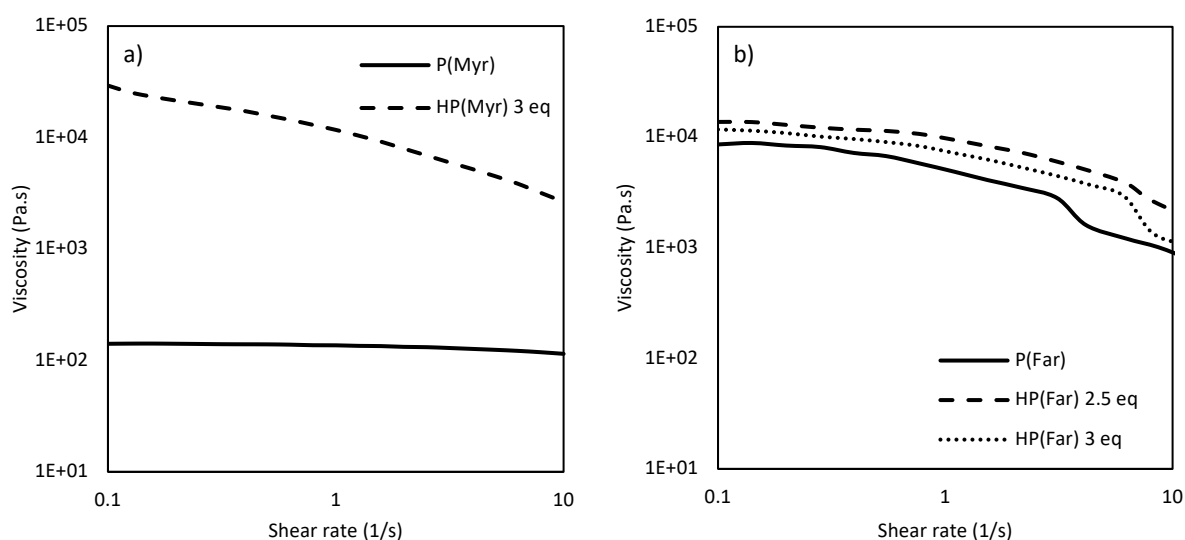


Figure 6-11. Viscosity as a function of steady shear rate for a) poly(Myrr) and b) poly(Far) before and after hydrogenation.

The difference in viscosities before and after hydrogenation is much greater for poly(Myrr) than for poly(Far). Rheological studies of bottlebrush polymers have shown that the length of side chains have a great effect on the conformation of the polymer chains, as well as the ratio between the length of the backbone and the length of the side chains [62,63]. For bottlebrush polymers with compact side chains, viscosity has a weak dependence on molecular weight even after the molecular weight has surpassed the critical or entanglement molecular weight. This is due to the one-dimensional growth of the polymer chain as  $DP_n$  of the backbone increases, while the length of the side chains remains fixed, meaning that the polymer chains change from a spherical to a cylindrical shape. Furthermore, the high density of side chains reduces the frictional effects of the

side chains on the backbone. Therefore, increased molecular weight has little effect on viscosity such that higher molecular weight bottlebrush polymers can behave similarly to linear unentangled polymers.

Although both poly(Myrr) and poly(Far) in this study were synthesized above their entanglement molecular weights, poly(Myrr) has an  $M_n$  of 56 kg mol<sup>-1</sup>, which is more than three times its literature  $M_e$  of 18 kg mol<sup>-1</sup>. After hydrogenation, the entanglement spacing in between branches becomes more compact, and effectively lowers the  $M_e$  to 12 kg mol<sup>-1</sup> [33]. Therefore, entanglement of poly(Myrr) is significantly increased and it is reflected in the significant increase in viscosity. On the other hand, poly(Far) has an  $M_n$  of 62 kg mol<sup>-1</sup>, which is only slightly above its  $M_e$  of 50 kg mol<sup>-1</sup>. However, poly(Far) has longer sidechains which would exhibit a higher degree of entanglement, and thus the unsaturated poly(Far) has a higher viscosity compared to unsaturated poly(Myrr). Nonetheless, its entanglement was only slightly improved even after hydrogenation as seen by the slight increase in viscosity. Therefore, the  $DP_n$  of poly(Far) would likely have to be much higher in order to see a significant increase in entanglements and subsequently viscosity, after hydrogenation.

#### 6.4 Conclusion

Hydrogenation of poly(dienes) has been well-studied for homopolymers and copolymers containing butadiene or isoprene. However, hydrogenation of bio-based poly(Myrr) and poly(Far) has not been reported. Furthermore, the hydrogenation was done at ambient pressure using diimide generated by thermal degradation of TSH and was optimized in a semi-batch process to efficiently hydrogenate the backbone and pendent double bonds of poly(Myrr) and poly(Far). By adding 3.0 mol eq. of TSH per double bond in a semi-batch fashion, almost complete hydrogenation was achieved for poly(Myrr) (97% and 94% for the backbone and pendent double bonds, respectively) and poly(Far) (97% and >99% for the backbone and pendent double bonds, respectively). The thermal stability of poly(Myrr) and poly(Far) also improved after hydrogenation as the depolymerization and cyclization degradations were reduced and  $T_{10\%}$  degradation temperatures were increased. Glass transition temperatures also increased after hydrogenation, suggesting stiffer polymer chains after saturation of the double bonds, which was also shown by the increase in

viscosities of the hydrogenated polymers. Although a greater increase in viscosity for poly(Myrcene) was observed compared to poly(Farnesene) due to the molecular weight of poly(Myrcene) being much higher than its  $M_e$ , the hydrogenated poly(Myrcene) and poly(Farnesene) possessed greater thermal stability and higher glass transition temperatures, which is consistent with the hydrogenation of poly(BD) and poly(IP) found in literature. Furthermore, these hydrogenated bio-based poly(dienes) can substitute midblocks of TPES such as SEBS and SEPS, or copolymerized with bio-based outer thermoplastic blocks made of different methacrylates or acrylates, for example.

### 6.5 Experimental Section/Methods

*Materials.*  $\beta$ -Myrcene monomer (Myr,  $\geq 95\%$ ) was purchased from Millipore Sigma. Trans- $\beta$ -farnesene monomer (Far,  $\geq 95\%$ ) was obtained from Amyris Inc. Monomers were purified using 1.0 g of aluminum oxide (basic  $\text{Al}_2\text{O}_3$ , activated, Brockmann I) and 0.05 g calcium hydride ( $\text{CaH}_2$ ,  $\geq 90\%$ ) per 50 mL of monomer, which were used as received from Millipore Sigma. Dicumyl peroxide (DCP, 98%) initiator, *p*-toluene sulfonyl hydrazide (TSH, 97%), tributylamine (TBA,  $\geq 98.5\%$ ), 3,5-di-*tert*-butylhydroxytoluene (BHT,  $\geq 99\%$ ) were purchased from Millipore Sigma and used as received. Xylene ( $\geq 98.5\%$ ), methanol (MeOH,  $\geq 99.8\%$ ), tetrahydrofuran (THF, 99.9% HPLC grade), 1,4-dioxane ( $\geq 99\%$ ), and pyridine ( $\geq 99\%$ ) were purchased from Fisher Chemicals and used as received. Deuterated chloroform ( $\text{CDCl}_3$ , 99.9% D) was purchased from Cambridge Isotope Laboratories, USA and used as received.

*Free radical polymerization of Myrcene and Farnesene in bulk.* The synthesis of poly(Myrcene) was done by free radical polymerization in bulk. DCP thermal initiator (0.18 g) and Myrcene monomer (117 g) were added into a 250 mL three-neck round bottom flask, with a condenser attachment to prevent evaporation of monomer during polymerization. The reaction mixture was purged with nitrogen for 30 mins, and polymerization proceeded at  $120^\circ\text{C}$  with stirring for 6 h and reached a conversion of  $X_{\text{myr}} = 76\%$  (see Appendix D Figure D-1), final number-average molecular weight ( $M_n$ ) of  $57 \text{ kg mol}^{-1}$  and dispersity ( $\mathcal{D}$ ) of 3.6. Poly(Myrcene) was confirmed by  $^1\text{H}$  NMR to be mostly polymerized by 1,4-addition (86 mol%) with some units of 1,2- and 3,4-addition (7 mol% each) (Figure D-2). However, *cis*- or *trans*- stereochemistry was not confirmed via  $^{13}\text{C}$  NMR. Poly(Farnesene) was synthesized in a similar manner using DCP initiator (0.05 g) and Farnesene monomer (10 g) in bulk at

120°C for 2 h. The reaction mixture was purged with nitrogen for 30 mins, and the polymerization proceeded at 115°C with stirring for 2 h, reaching a conversion of  $X_{\text{Far}} = 64\%$  (Figure D-3) and final  $M_n$  of  $62 \text{ kg mol}^{-1}$ ,  $\bar{D} = 6.6$ . The Poly(Far) was more predominantly polymerized by 1,4-addition (96.8 mol% 1,4-addition, 1.9 mol% 1,2-addition, and 1.3 mol% 3,4-addition) compared to Myr as seen in Figure D-4. The final polymers were precipitated using methanol, then dried under air overnight and in the vacuum oven at room temperature for a day.

*Hydrogenation of poly(Myrr) in batch mode.* Hydrogenation experiments of poly(Myrr) (obtained from free radical polymerization in bulk) were done in batch, where all reagents were added initially into the reactor. In a 250 mL three-neck round bottom flask equipped with a condenser, magnetic stir bar, and nitrogen influx, poly(Myrr) was dissolved in xylene at approximately 3.3 – 4.0% w/v. The amount of TSH added was based on 2.5 or 4.0 molar equivalent of TSH per double bond of poly(Myrr), which was estimated based on the number average degree of polymerization ( $DP_n$ ) of poly(Myrr) measured from gel permeation chromatography (GPC). Every repeating unit of poly(Myrr) has 2 double bonds (Scheme 6-1), therefore the number of double bonds is two times the  $DP_n$ . TBA was also added in slight excess relative to TSH to neutralize the acidic by-product of TSH thermal degradation. Finally, a very low concentration of BHT was also added to prevent oxidative degradation of the poly(Myrr) chains. A summary of hydrogenation experiments in batch are shown in Table 6-3. Hydrogenation reactions took place at 125°C for up to 4 h, and samples were taken periodically to be analyzed by  $^1\text{H}$  NMR to quantify hydrogenation degree. The final polymer after hydrogenation was also analyzed by GPC to check for polymer chain degradation.

Table 6-3. Summary of experiments for hydrogenation of poly(Myrr) in batch.

Experiment ID	$m_{\text{poly(Myrr)}} \text{ (g)}$ a	$V_{\text{xylene}} \text{ (mL)}$	Mol eq. of TSH <sup>b</sup>	$m_{\text{TSH}} \text{ (g)}$ <sup>c</sup>	$m_{\text{TBA}} \text{ (g)}$ <sup>c</sup>	$m_{\text{BHT}} \text{ (g)}$
B1	2.0	50	2.5	6.80	6.85	0.01
B2	2.0	60	4.0	10.9	11.0	0.01

a) Concentration of poly(Myrr) in xylene solution is 3.3 to 4.0% w/v; b) Molar equivalent amount of TSH added for hydrogenation is per double bond per repeating unit of poly(Myrr), calculated based on molecular weight measured from GPC; c) Mass of TSH is determined based on molar equivalent amount of TSH required, and mass of TBA is added in slight excess.

*Hydrogenation of poly(Myrr) in semi-batch mode.* Hydrogenation experiments of poly(Myrr) were done in semi-batch, where TSH was slowly added throughout the reaction. Similarly, the hydrogenation reactions were done in a 250 mL three-neck round bottom flask equipped with condenser, magnetic stir bar, nitrogen influx. Several experimental setups were investigated including only dissolving poly(Myrr) in TBA and no xylene, dissolving TSH in a solvent and adding the TSH solution to reaction mixture by a dropping funnel, and adding dry TSH powder manually to the reaction mixture. The flow rate of TSH addition by dropping funnel was calculated based on total volume of solution added over the total time of TSH addition. The addition of dry TSH powder was 1 g for every 15 mins until the total amount has been added to the reaction mixture. A summary of the semi-batch experimental formulations is shown in Table 6-4. In the experiments where poly(Myrr) was not dissolved in xylene, excess TBA was added to solubilize the polymer. In all cases, reaction mixtures were purged with nitrogen for 30 mins and hydrogenation of poly(Myrr) was done at 125°C for up to 9 h depending on the rate of TSH addition.

Table 6-4. Summary of experiments for hydrogenation of poly(Myrr) in semi-batch conditions.

Experiment ID	$m_{\text{poly(Myrr)}}$ (g)	$V_{\text{xylene}}$ (mL)	Mol eq. of TSH <sup>b</sup>	$m_{\text{TSH}}$ (g)	TSH solvent	$V_{\text{TSH}}$ solvent (mL)	TSH addition rate	$m_{\text{TBA}}$ (g)	$m_{\text{BHT}}$ (g)
SB1	2.0	0.0	2.0	10.9	1,4-Dioxane	63.6 <sup>c</sup>	0.30 mL/min <sup>d</sup>	30.9 <sup>f</sup>	0.01
SB2	2.0	0.0	2.0	10.9	Pyridine	48.7 <sup>c</sup>	0.43 mL/min <sup>d</sup>	22.5 <sup>f</sup>	0.01
SB3	2.0	0.0	2.0	10.9	--	--	1g/15min <sup>e</sup>	34.3 <sup>f</sup>	0.01
SB4	2.0 <sup>a</sup>	56	2.0	11.0	--	--	1g/15min <sup>e</sup>	14.2 <sup>g</sup>	0.01
SB5	2.0 <sup>a</sup>	72	2.5	14.0	--	--	1g/15min <sup>e</sup>	21.0 <sup>g</sup>	0.01
SB6	2.0 <sup>a</sup>	60	3.0	16.4	--	--	1g/15min <sup>e</sup>	23.4 <sup>g</sup>	0.01

<sup>a)</sup> Concentration of poly(Myrr) in xylene solution is 2.8 to 3.3% w/v; <sup>b)</sup> Molar equivalent amount of TSH added for hydrogenation is per double bond per repeating unit of poly(Myrr), calculated based on molecular weight measured from GPC; <sup>c)</sup> Volume of solvent for TSH solutions is based on approximately 20% w/w of TSH in 1,4-dioxane or pyridine; <sup>d)</sup> Flow rate of TSH solution was

calculated based on total volume of solution added over total time of addition; <sup>e)</sup> Dry TSH powder was added in small batches throughout the reaction at 1 g for every 15 min until all of the required TSH is added; <sup>f)</sup> Excess TBA was added to solubilize poly(Myrr) in absence of xylene as solvent; <sup>g)</sup> TBA was added in slight excess (1:1.2 TSH:TBA molar ratio)

*Hydrogenation of poly(Far) in semi-batch mode.* After optimization of the semi-batch hydrogenation of poly(Myrr), hydrogenation of poly(Far) was also done in semi-batch. Similar to the hydrogenation experiments of poly(Myrr), poly(Far) (obtained from free radical polymerization in bulk) was dissolved in xylene (about 3.3% w/v) in a 250 mL three-neck round bottom flask equipped with a condenser, magnetic stirring, and nitrogen influx. The amount of TSH added was calculated based on three double bonds per repeating unit of poly(Far) (Scheme 6-1), which was estimated based on the DP<sub>n</sub> from GPC. In these semi-batch hydrogenation experiments, 2.0 – 3.0 molar equivalent of TSH was added per double bond in poly(Far). TBA in slight excess relative to TSH (1:1.2 TSH:TBA) was also added to the polymer solution, as well as small amounts of BHT. The polymer solution was then purged with nitrogen for 30 mins. TSH dry powder was added manually (1 g for every 15 min) to the reaction mixture, and the hydrogenation reaction was done at 125°C for up to 4.5 h. A summary of the semi-batch experimental recipes for hydrogenation of poly(Far) is shown in Table 6-5.

Table 6-5. Summary of experiments for hydrogenation of poly(Far) in semi-batch.

Experiment ID	$m_{\text{poly(Far)}} \text{ (g)}^a$	$V_{\text{xylene}}$ (mL)	Mol eq. of TSH <sup>b</sup>	$m_{\text{TSH}}$ (g)	TSH addition rate <sup>c</sup>	$m_{\text{TBA}}$ (g) <sup>d</sup>	$m_{\text{BHT}}$ (g) <sup>d</sup>
SB7	2.4	60.0	2.0	13.0	1g/15min	15.5	0.01
SB8	1.9	60.0	2.5	12.6	1g/15min	15.1	0.01
SB9	1.9	60.0	3.0	15.4	1g/15min	18.4	0.01

<sup>a)</sup> Concentration of poly(Far) in xylene solution is approximately 4.0% w/v; <sup>b)</sup> Molar equivalent amount of TSH added for hydrogenation is per double bond per repeating unit of poly(Far), calculated based on molecular weight measured from GPC; <sup>c)</sup> Dry TSH powder was added in small batches throughout the reaction at 1 g for every 15 min until all of the required TSH is added; <sup>d)</sup> Mass of TSH is determined based on molar equivalent amount of TSH required, and mass of TBA is added in slight excess (1:1.2 of TSH:TBA molar ratio).

*Polymer characterization.* Conversions and hydrogenation degrees of the poly(My) and poly(Far) samples were determined using  $^1\text{H}$  NMR (Bruker AVIIIHD 500 MHz spectrometer, 16 scans). For the hydrogenation experiments, 1 mL samples were taken periodically, and the polymers were precipitated from solution using excess methanol. The dried polymer samples were redissolved in  $\text{CDCl}_3$  for  $^1\text{H}$  NMR analysis. Hydrogenation degree calculations can be found in Appendix D (Figure D-5 and D-6). Number average molecular weight ( $M_n$ ) and dispersity ( $\mathcal{D} = M_w/M_n$ ) of polymer samples were characterized using gel permeation chromatography (GPC, Water Breeze) with HPLC grade THF as an eluent at a flow rate of  $0.3 \text{ mL min}^{-1}$ . The GPC has three Waters Styragel HR columns (HR1 with a molecular weight measurement range of  $10^2$  to  $5 \times 10^3 \text{ g mol}^{-1}$ , HR2 with a molecular weight measurement range of  $5 \times 10^2$  to  $2 \times 10^4 \text{ g mol}^{-1}$ , and HR4 with a molecular weight measurement range of  $5 \times 10^3$  to  $6 \times 10^5 \text{ g mol}^{-1}$ ), a guard column, and a refractive index (RI 2414) detector. The columns were heated to  $40^\circ\text{C}$  during analysis. The molecular weights were determined relative to poly(styrene) calibration standards from Scientific Polymer Products Inc. (ranging from 570 to  $2,754,000 \text{ g mol}^{-1}$ ).

*Thermal stability and glass transition temperature analysis.* Polymer samples were analyzed by thermogravimetric analysis (TGA) to evaluate their thermal degradation before and after hydrogenation using Discovery 5500 TGA (TA Instruments). Polymer samples weighing between 5 – 10 mg were placed in platinum pans and they were analyzed from room temperature to  $600^\circ\text{C}$  under nitrogen flow at a heating rate of  $10^\circ\text{C min}^{-1}$ . Differential scanning calorimetry (DSC) was also done using Discovery 2500 from TA instruments. Polymer samples were heated up from room temperature to  $50^\circ\text{C}$  to remove any thermal history, then cooled to  $-95^\circ\text{C}$ , then heated up to  $20^\circ\text{C}$  again to determine  $T_g$ . The heating rate used for all three cycles was  $10^\circ\text{C min}^{-1}$ .

*Rheology.* Dynamic viscosity of polymer samples before and after hydrogenation was measured using the MCR302 rheometer from Anton Paar Instruments. Polymer samples were placed between parallel plates with a 1 mm gap, and the viscosity was measured at steady shear from 0.1

## 6.6 References

- [1] J. G. Drobny, In Handbook of Thermoplastic Elastomers; Drobny, J. G., Ed.; William Andrew Publishing: Norwich, NY, **2007**, pp 281-315.
- [2] H. Mooibroek, K. Cornish. *Appl. Microbiol. Biotechnol.* **2000**, *53*, 355-365.
- [3] S. H. Chough, D. H. Chang. *J. Appl. Polym. Sci.* **1996**, *61*, 449-454.
- [4] J. G. Drobny, In Handbook of Thermoplastic Elastomers (2nd Edition); Elsevier, **2014**.
- [5] E. N. Kresge. *Rubber Chem. Technol.* **1991**, *64*, 469-480.
- [6] A. K. Gupta, S. N. Purwar. *J. Appl. Polym. Sci.* **1984**, *29*, 1595-1609.
- [7] B. Ohlsson, B. Törnell. *Polym. Eng. Sci.* **1996**, *36*, 1547-1556.
- [8] S. Bhattacharjee, P. Rajagopalan, A. K. Bhowmick, B. N. Avasthi. *J. Appl. Polym. Sci.* **1993**, *49*, 1971-1977.
- [9] F. O. M. S. Abreu, M. M. C. Forte, S. A. Liberman. *J. Appl. Polym. Sci.* **2005**, *95*, 254-263.
- [10] F. Lin, C. Wu, D. Cui. *J. Polym. Sci., Part A: Polym. Chem.* **2017**, *55*, 1243-1249.
- [11] L. J. Fetters, D. J. Lohse, R. H. Colby, In Physical Properties of Polymers Handbook; Mark, J. E., Ed.; Springer New York: New York, NY, **2007**, pp 447-454.
- [12] J. M. Carella, W. W. Graessley, L. J. Fetters. *Macromolecules* **1984**, *17*, 2775-2786.

- [13] M. B. Kolicheski, L. C. Cocco, D. A. Mitchell, M. Kaminski. *J. Anal. Appl. Pyrolysis* **2007**, *80*, 92-100.
- [14] G. Brieger. *J. Org. Chem.* **1967**, *32*, 3720-3720.
- [15] G. Brieger, T. J. Nestrick, C. McKenna. *J. Org. Chem.* **1969**, *34*, 3789-3791.
- [16] J. Crock, M. Wildung, R. Croteau. *Proc. Natl. Acad. Sci. U. S. A.* **1997**, *94*, 12833.
- [17] M. I. Hulnik, I. V. Vasilenko, A. V. Radchenko, F. Peruch, F. Ganachaud, S. V. Kostjuk. *Polym. Chem.* **2018**, *9*, 5690-5700.
- [18] C. Zhou, Z. Wei, C. Jin, Y. Wang, Y. Yu, X. Leng, Y. Li. *Polymer* **2018**, *138*, 57-64.
- [19] C. Zhou, Z. Wei, X. Lei, Y. Li. *RSC Adv.* **2016**, *6*, 63508-63514.
- [20] P. Sahu, A. K. Bhowmick. *Ind. Eng. Chem. Res.* **2019**, *58*, 20946-20960.
- [21] P. Sarkar, A. K. Bhowmick. *RSC Adv.* **2014**, *4*, 61343-61354.
- [22] B. Liu, D. T. Liu, S. H. Li, G. P. Sun, D. M. Cui. *Chin. J. Polym. Sci.* **2016**, *34*, 104-110.
- [23] S. Loughmari, A. Hafid, A. Bouazza, A. El Bouadili, P. Zinck, M. Visseaux. *J. Polym. Sci., Part A: Polym. Chem.* **2012**, *50*, 2898-2905.
- [24] J. Hilschmann, G. Kali. *Eur. Polym. J.* **2015**, *73*, 363-373.
- [25] N. Bauer, J. Brunke, G. Kali. *ACS Sustainable Chem. Eng.* **2017**, *5*, 10084-10092.

- [26] U. Kalita, S. Samanta, S. L. Banerjee, N. C. Das, N. K. Singha. *Macromolecules* **2021**.
- [27] A. Métafiot, L. Gagnon, S. Pruvost, P. Hubert, J. F. Gérard, B. Defoort, M. Marić. *RSC Adv.* **2019**, *9*, 3377-3395.
- [28] A. Métafiot, J. F. Gérard, B. Defoort, M. Marić. *J. Polym. Sci., Part A: Polym. Chem.* **2018**, *56*, 860-878.
- [29] A. Métafiot, Y. Kanawati, J. F. Gérard, B. Defoort, M. Marić. *Macromolecules* **2017**, *50*, 3101-3120.
- [30] S. B. Luk, M. Marić. *Macromol. React. Eng.* **2019**, *13*, 1800080.
- [31] S. B. Luk, M. Marić. *ACS Omega* **2021**, *6*, 4939-4949.
- [32] M. Abbasi, L. Faust, M. Wilhelm. *Adv. Mater.* **2019**, *31*, 1806484.
- [33] L. J. Fetters, D. J. Lohse, D. Richter, T. A. Witten, A. Zirkel. *Macromolecules* **1994**, *27*, 4639-4647.
- [34] C. Iacob, T. Yoo, J. Runt. *Macromolecules* **2018**, *51*, 4917-4922.
- [35] J. C. Falk, R. J. Schlott. *Macromolecules* **1971**, *4*, 152-154.
- [36] V. A. Escobar Barrios, R. Herrera Nájera, A. Petit, F. Pla. *Eur. Polym. J.* **2000**, *36*, 1817-1834.
- [37] J. T. Gotro, W. W. Graessley. *Macromolecules* **1984**, *17*, 2767-2775.

- [38] S. F. Hahn. *J. Polym. Sci., Part A: Polym. Chem.* **1992**, *30*, 397-408.
- [39] H. J. Harwood, D. B. Russell, J. J. A. Verthe, J. Zymonas. *Die Makromolekulare Chemie* **1973**, *163*, 1-12.
- [40] T. D. Nang, Y. Katabe, Y. Minoura. *Polymer* **1976**, *17*, 117-120.
- [41] H. G. M. Edwards, D. W. Farwell, A. F. Johnson, I. R. Lewis, N. Webb, N. J. Ward. *Macromolecules* **1992**, *25*, 525-529.
- [42] P. Phinyocheep, S. Pasiri, O. Tavichai. *J. Appl. Polym. Sci.* **2003**, *87*, 76-82.
- [43] C. K. Santin, M. M. Jacobi, R. H. Schuster, M. Santoso. *J. Therm. Anal. Calorim.* **2010**, *101*, 273-279.
- [44] N. Petzetakis, G. M. Stone, N. P. Balsara. *Macromolecules* **2014**, *47*, 4151-4159.
- [45] N. H. A. Azhar, N. Jamaluddin, H. Md Rasid, M. J. Mohd Yusof, S. F. M. Yusoff. *Int. J. Polym. Sci.* **2015**, *2015*, 243038.
- [46] G. Ricci, A. C. Boccia, G. Leone, I. Pierro, G. Zanchin, M. Scoti, F. Auriemma, C. De Rosa. *Molecules* **2017**, *22*, 755.
- [47] M. A. Hillmyer, W. R. Laredo, R. H. Grubbs. *Macromolecules* **1995**, *28*, 6311-6316.
- [48] H. Yang, M. Islam, C. Budde, S. J. Rowan. *J. Polym. Sci., Part A: Polym. Chem.* **2003**, *41*, 2107-2116.

- [49] C. P. Radano, O. A. Scherman, N. Stingelin-Stutzmann, C. Müller, D. W. Breiby, P. Smith, R. A. J. Janssen, E. W. Meijer. *J. Am. Chem. Soc.* **2005**, *127*, 12502-12503.
- [50] Y. Wang, M. A. Hillmyer. *ACS Macro Lett.* **2017**, *6*, 613-618.
- [51] P. A. Robles-Dutenhefner, M. G. Speziali, E. M. B. Sousa, E. N. dos Santos, E. V. Gusevskaya. *Appl, Catal., A* **2005**, *295*, 52-58.
- [52] N. I. Tracy, D. Chen, D. W. Crunkleton, G. L. Price. *Fuel* **2009**, *88*, 2238-2240.
- [53] E. Bogel-Łukasik, M. Gomes da Silva, I. D. Nogueira, R. Bogel-Łukasik, M. Nunes da Ponte. *Green Chem.* **2009**, *11*, 1847-1856.
- [54] M. Guerrero, N. J. S. Costa, L. L. R. Vono, L. M. Rossi, E. V. Gusevskaya, K. Philippot. *J. Mater. Chem. A* **2013**, *1*, 1441-1449.
- [55] K. Satoh, H. Sugiyama, M. Kamigaito. *Green Chem.* **2006**, *8*, 878-882.
- [56] D. W. Brazier, N. V. Schwartz. *J. Appl. Polym. Sci.* **1978**, *22*, 113-124.
- [57] M. P. Luda, M. Guaita, O. Chiantore. *Die Makromolekulare Chemie* **1992**, *193*, 113-121.
- [58] S. B. Luk, M. Marić. POLYMER-21-1277, submitted: June **2021**.
- [59] R. E. Díaz de León Gómez, F. J. Enríquez-Medrano, H. Maldonado Textle, R. Mendoza Carrizales, K. Reyes Acosta, H. R. López González, J. L. Olivares Romero, L. E. Lugo Uribe. *Can. J. Chem. Eng.* **2016**, *94*, 823-832.

- [60] P. Hattam, S. Gauntlett, J. W. Mays, N. Hadjichristidis, R. N. Young, L. J. Fetters. *Macromolecules* **1991**, *24*, 6199-6209.
- [61] M. De Sarkar, P. P. De, A. K. Bhowmick. *J. Appl. Polym. Sci.* **1997**, *66*, 1151-1162.
- [62] S. J. Dalsin, M. A. Hillmyer, F. S. Bates. *ACS Macro Lett.* **2014**, *3*, 423-427.
- [63] S. J. Dalsin, M. A. Hillmyer, F. S. Bates. *Macromolecules* **2015**, *48*, 4680-4691.

## 7 Conclusions and future work

This body of work offers significant insight on the polymerization of Far using NMP, as well as its copolymerization with various functionalized methacrylates (i.e. GMA, iBOMA, and EGDEMA) using different modes of operation. A wide array of materials were synthesized exhibiting properties that could be used as modifiers, thermoplastic elastomers, and compatibilizers. Although both NHS-BB and D7 showed good control over the polymerization of Far, its copolymerization with methacrylates is more effective using D7 due its ability to demonstrate linear polymer chain growth and maintain active chain-ends for re-initiation. The polymerization of Far in miniemulsion via NMP revealed many challenges, but livingness of polymer chains was achieved followed by successful chain-extension. However, the phenomena regarding increased chain-end fidelity at higher surfactant concentration remains unknown and would require further investigation. The block copolymer synthesis of poly(EGDEMA-*b*-Far) and poly(EGDEMA-*co*-iBOMA-*b*-Far) functionalized with POSS presented promising properties as alternative TPEs, as their mechanical properties were reinforced by the addition of POSS and iBOMA and thermal stability was enhanced. An optimization of block lengths is still needed in order to achieve good entanglement of the poly(Far) blocks. Furthermore, the hydrogenation of poly(Myrr) and poly(Far) using diimides was straightforward and showed great efficiency in saturating their double bonds, and improved thermal and rheological behaviours were demonstrated.

Currently, there are several upcoming collaborative projects that are based on the work that was highlighted in this thesis. The ease of thiol-ene click chemistry as shown by the addition of POSS onto the norbornenyl group of EGDEMA units motivated the thiol-ene clicking of thiol-boronic esters to impart self-healing properties. UV-initiated thiol-ene clicking will be used instead since it is shown to be much more efficient than thermally-initiated systems. Additionally, a terpene-based methacrylate has been synthesized by transesterification between geraniol and methacrylic acid to form a methacrylate with a myrcene side chain. A similar terpene-based methacrylate demonstrated effective polymerization using D7 and in miniemulsion [48], therefore it will be used to make block copolymers also with self-healing properties. Another collaborative project involves

blending high molecular weight poly(Far) or poly(Far-*co*-GMA) with poly(lactic acid) (PLA) in order to toughen the biodegradable, but brittle PLA. The epoxy functional groups from GMA would aid in compatibilizing the two polymers in the blend. The chemical hydrogenation of poly(Far-*co*-GMA) can also be explored, to see if the epoxy functionalities can be preserved after hydrogenation. Furthermore, the increased viscoelastic properties of hydrogenated poly(Far) could provide enhanced toughening properties and thermal stability when blended with PLA.

Moreover, the study of miniemulsion polymerization of Far can continue using RAFT polymerization instead of NMP. A great deal of success was shown in studies using seeded miniemulsion of BD via RAFT polymerization to make poly(St-*b*-BD) [53]. Particles containing poly(St)-RAFT chain transfer agents were dispersed in water with surfactant, then swollen with BD monomer, therefore polymerization loci were ensured to be inside every particle. SBS triblock copolymers were also made by seeded miniemulsion by RAFT [54]. Furthermore, compartmentalization was observed, and polymerization rates increased as a result. Poly(St-*b*-Myr-*b*-St) (SMS) triblock copolymer was also synthesized by bifunctional RAFT agent in seeded emulsion, and block copolymers with 20–30 wt% poly(St) content showed comparable tensile strength and elongation at break as commercial SIS and SBS block copolymers [41]. Therefore, seeded emulsion via RAFT can indeed be applied to polymerization of Far to synthesize alternative TPE materials.

In conclusion, the work done on polymerization of Far thus far is only the beginning, and there is much more that can be done to optimize its polymerization kinetics by RDRP such that more innovative materials can be made. The advantages of Far do not only encompass its sustainability factor, but also its superior viscoelastic properties due to the entanglement of the long side chains. However, much higher molecular weights must be achieved in order to reach sufficient entanglement. Furthermore, post-polymerization techniques have been already been shown to enhance the mechanical strength and thermal behaviour of poly(Far) homo- and copolymers, and the possibility of adding self-healing properties will certainly be interesting as well.

## 8 References

- [1] T. Yoo, S.K. Henning, Synthesis and characterization of farnesene-based polymers, *Rubber Chemistry and Technology* 90(2) (2017) 308-324.
- [2] C. Wahlen, J. Blankenburg, P. von Tiedemann, J. Ewald, P. Sajkiewicz, A.H.E. Müller, G. Floudas, H. Frey, Tapered Multiblock Copolymers Based on Farnesene and Styrene: Impact of Biobased Polydiene Architectures on Material Properties, *Macromolecules* 53(23) (2020) 10397-10408.
- [3] A. Bahena, I. Magaña, H.R. López González, R. Handa, F.J. Enríquez-Medrano, S. Kumar, R.M. Carrizales, S. Fernandez, L. Valencia, R.E. Díaz de León Gómez, Bio-elastomer nanocomposites reinforced with surface-modified graphene oxide prepared via in situ coordination polymerization, *RSC Advances* 10(60) (2020) 36531-36538.
- [4] J.L. González-Zapata, F.J. Enríquez-Medrano, H.R. López González, J. Revilla-Vázquez, R.M. Carrizales, D. Georgouvelas, L. Valencia, R.E. Díaz de León Gómez, Introducing random bio-terpene segments to high cis-polybutadiene: making elastomeric materials more sustainable, *RSC Advances* 10(72) (2020) 44096-44102.
- [5] C. Iacob, T. Yoo, J. Runt, Molecular Dynamics of Polyfarnesene, *Macromolecules* 51(13) (2018) 4917-4922.
- [6] D.J. McPhee, M.J. Graham, Adhesives compositions comprising a polyfarnesene, Amyris Inc., United States, 2010.
- [7] K.A. Nelson, A. Pierre-Justin, N.P. Hansen, Farnesene-based tackifying resins and adhesive compositions containing the same, Fina Technology Inc., United States, 2018.

- [8] N. Tian, H. Chao, Polyols derived from farnesene for polyurethanes, Fina Technology Inc, United States, 2018.
- [9] T. Yoo, H. Chao, S.K. Henning, Farnesene-based polymers and liquid optically clear adhesive compositions incorporating the same, Fina Technology, United States, 2018.
- [10] J. Zhang, J. Chen, M. Yao, Z. Jiang, Y. Ma, Hydrolysis-resistant polyurethane elastomers synthesized from hydrophobic bio-based polyfarnesene diol, *Journal of Applied Polymer Science* 136(25) (2019) 47673.
- [11] S.B. Luk, L.A. Azevedo, M. Maric, Reversible deactivation radical polymerization of bio-based dienes, *Reactive and Functional Polymers* 162 (2021) 104871.
- [12] A. Chauvel, G. Lefebvre, L. Castex, Steam cracking, Petrochemicals processes, Editions Technip, Paris, 1989.
- [13] J. Brandrup, E.H. Immergut, E.A. Grulke, Polymer handbook, 4th ed. ed., Wiley, New York, 1999.
- [14] I. Kopal, P. Košťal, Z. Jančíková, J. Valíček, M. Harničárová, P. Hybler, M. Kušnerová, Modifications of Viscoelastic Properties of Natural Rubber/Styrene-Butadiene Rubber Blend by Electron Beam Irradiation, in: A. Öchsner, H. Altenbach (Eds.), *Improved Performance of Materials: Design and Experimental Approaches*, Springer International Publishing, Cham, 2018, pp. 219-229.
- [15] M.P. Bertin, G. Marin, J.P. Montfort, Viscoelastic properties of acrylonitrile-butadiene-styrene (ABS) polymers in the molten state, *Polymer Engineering & Science* 35(17) (1995) 1394-1406.

- [16] S. H. Chough, D. H. Chang, Kinetics of sulfur vulcanization of NR, BR, SBR, and their blends using a rheometer and DSC, *Journal of Applied Polymer Science* 61(3) (1996) 449-454.
- [17] J.G. Drobny, 1. Introduction, *Handbook of Thermoplastic Elastomers* (2nd Edition), Elsevier 2014.
- [18] J.G. Drobny, 15. Applications of Thermoplastic Elastomers, in: J.G. Drobny (Ed.), *Handbook of Thermoplastic Elastomers*, William Andrew Publishing, Norwich, NY, 2007, pp. 281-315.
- [19] R.E. Díaz de León Gómez, F.J. Enríquez-Medrano, H. Maldonado Textle, R. Mendoza Carrizales, K. Reyes Acosta, H.R. López González, J.L. Olivares Romero, L.E. Lugo Uribe, Synthesis and characterization of high cis-polymyrcene using neodymium-based catalysts, *The Canadian Journal of Chemical Engineering* 94(5) (2016) 823-832.
- [20] E. Grune, J. Bareuther, J. Blankenburg, M. Appold, L. Shaw, A.H.E. Müller, G. Floudas, L.R. Hutchings, M. Gallei, H. Frey, Towards bio-based tapered block copolymers: the behaviour of myrcene in the statistical anionic copolymerisation, *Polymer Chemistry* 10(10) (2019) 1213-1220.
- [21] X. Guo, X. Liu, S. Shan, W. Zhao, H. Su, Q. Jia, Green approach toward sustainable adhesive: Synthesis and characterization of poly(myrcene sulfone), *Journal of the Taiwan Institute of Chemical Engineers* 95 (2019) 208-216.
- [22] M.I. Hulnik, I.V. Vasilenko, A.V. Radchenko, F. Peruch, F. Ganachaud, S.V. Kostjuk, Aqueous cationic homo- and co-polymerizations of  $\beta$ -myrcene and styrene: a green route toward terpene-based rubbery polymers, *Polymer Chemistry* 9(48) (2018) 5690-5700.

- [23] B. Liu, D. T. Liu, S. H. Li, G. P. Sun, D. M. Cui, High trans-1,4 (co)polymerization of  $\beta$ -myrcene and isoprene with an iminophosphonamide lanthanum catalyst, *Chinese Journal of Polymer Science* 34(1) (2016) 104-110.
- [24] A. Métafiot, Y. Kanawati, J. F. Gérard, B. Defoort, M. Marić, Synthesis of  $\beta$ -Myrcene-Based Polymers and Styrene Block and Statistical Copolymers by SG1 Nitroxide-Mediated Controlled Radical Polymerization, *Macromolecules* 50(8) (2017) 3101-3120.
- [25] J. Crock, M. Wildung, R. Croteau, Isolation and bacterial expression of a sesquiterpene synthase cDNA clone from peppermint (*Mentha X Piperita* L.) that produces the aphid alarm pheromone (E)- $\beta$ -farnesene, *Proceedings of the National Academy of Sciences* 94(24) (1997) 12833.
- [26] H. Zheng, J. Chen, C. Li, J. Chen, Y. Wang, S. Zhao, Y. Zeng, Mechanism and kinetics of the pyrolysis of  $\beta$ -pinene to myrcene, *Journal of Analytical and Applied Pyrolysis* 123 (2017) 99-106.
- [27] M. Abbasi, L. Faust, M. Wilhelm, Comb and Bottlebrush Polymers with Superior Rheological and Mechanical Properties, *Advanced Materials* 31(26) (2019) 1806484.
- [28] D. Jenkins Aubrey, G. Jones Richard, G. Moad, Terminology for reversible-deactivation radical polymerization previously called "controlled" radical or "living" radical polymerization (IUPAC Recommendations 2010), *Pure and Applied Chemistry* 82(2) (2009) 483.
- [29] D.A. Shipp, Reversible-Deactivation Radical Polymerizations, *Polymer Reviews* 51(2) (2011) 99-103.
- [30] B. Klumperman, 6.12 - Controlled Composition: Statistical, Gradient, and Alternating Copolymers, in: K. Matyjaszewski, M. Möller (Eds.), *Polymer Science: A Comprehensive Reference*, Elsevier, Amsterdam, 2012, pp. 433-453.

- [30] M.K. Georges, G.K. Hamer, N.A. Listigovers, Block Copolymer Synthesis by a Nitroxide-Mediated Living Free Radical Polymerization Process, *Macromolecules* 31(25) (1998) 9087-9089.
- [31] E. Guégain, Y. Guillaneuf, J. Nicolas, Nitroxide-Mediated Polymerization of Methacrylic Esters: Insights and Solutions to a Long-Standing Problem, *Macromolecular Rapid Communications* 36(13) (2015) 1227-1247.
- [32] N. Ballard, M. Aguirre, A. Simula, A. Agirre, J.R. Leiza, J.M. Asua, S. van Es, New Class of Alkoxyamines for Efficient Controlled Homopolymerization of Methacrylates, *ACS Macro Letters* 5(9) (2016) 1019-1022.
- [33] H.S. Yu, J.S. Kim, V. Vasu, C.P. Simpson, A.D. Asandei, Cu-Mediated Butadiene ATRP, *ACS Catalysis* 10(12) (2020) 6645-6663.
- [34] Y.F. Zhu, F.J. Jiang, P.P. Zhang, J. Luo, H.D. Tang, Atom transfer radical polymerization and copolymerization of isoprene catalyzed by copper bromide/2,2'-bipyridine, *Chinese Chemical Letters* 27(6) (2016) 910-914.
- [35] J. Hilschmann, G. Kali, Bio-based polymyrcene with highly ordered structure via solvent free controlled radical polymerization, *European Polymer Journal* 73 (2015) 363-373.
- [36] N. Bauer, J. Brunke, G. Kali, Controlled Radical Polymerization of Myrcene in Bulk: Mapping the Effect of Conditions on the System, *ACS Sustainable Chemistry & Engineering* 5(11) (2017) 10084-10092.
- [37] Luk, S. B., Marić, M., Nitroxide-Mediated Polymerization of Bio-Based Farnesene with a Functionalized Methacrylate. *Macromol. React. Eng.* 13(3) (2019) 1800080.

- [38] P. Sahu, A.K. Bhowmick, Redox Emulsion Polymerization of Terpenes: Mapping the Effect of the System, Structure, and Reactivity, *Industrial & Engineering Chemistry Research* 58(46) (2019) 20946-20960.
- [39] P. Sarkar, A.K. Bhowmick, Synthesis, characterization and properties of a bio-based elastomer: polymyrcene, *RSC Advances* 4(106) (2014) 61343-61354.
- [40] U. Kalita, S. Samanta, S.L. Banerjee, N.C. Das, N.K. Singha, Biobased Thermoplastic Elastomer Based on an SMS Triblock Copolymer Prepared via RAFT Polymerization in Aqueous Medium, *Macromolecules* (2021).
- [41] S. B. Luk, M. Maric, Polymerization of Biobased Farnesene in Miniemulsions by Nitroxide-Mediated Polymerization, *ACS Omega* 6(7) (2021) 4939-4949.
- [42] H. Maehata, C. Buragina, M. Cunningham, B. Keoshkerian, Compartmentalization in TEMPO-Mediated Styrene Miniemulsion Polymerization, *Macromolecules* 40(20) (2007) 7126-7131.
- [43] P.B. Zetterlund, M. Okubo, Compartmentalization in Nitroxide-Mediated Radical Polymerization in Dispersed Systems, *Macromolecules* 39(26) (2006) 8959-8967.
- [44] P. Mandal, N.K. Singha, Tailor-made polymethacrylate bearing bicyclo-alkenyl functionality via selective ATRP at ambient temperature and its post-polymerization modification by 'thiol-ene' reaction, *RSC Advances* 4(11) (2014) 5293-5299.
- [45] A.L. Hook, C.Y. Chang, J. Yang, J. Lockett, A. Cockayne, S. Atkinson, Y. Mei, R. Bayston, D.J. Irvine, R. Langer, D.G. Anderson, P. Williams, M.C. Davies, M.R. Alexander, Combinatorial discovery of polymers resistant to bacterial attachment, *Nature Biotechnology* 30(9) (2012) 868-875.

- [46] B.J. Tyler, A. Hook, A. Pelster, P. Williams, M. Alexander, H.F. Arlinghaus, Development and characterization of a stable adhesive bond between a poly(dimethylsiloxane) catheter material and a bacterial biofilm resistant acrylate polymer coating, *Biointerphases* 12(2) (2017) 02C412.
- [47] F. Koschitzki, R. Wanka, L. Sobota, J. Koc, H. Gardner, K.Z. Hunsucker, G.W. Swain, A. Rosenhahn, Amphiphilic Dicyclopentenyl/Carboxybetaine-Containing Copolymers for Marine Fouling-Release Applications, *ACS Applied Materials & Interfaces* 12(30) (2020) 34148-34160.
- [48] A. Maupu, Y. Kanawati, A. Métafiot, M. Maric, Ethylene Glycol Dicyclopentenyl (Meth)Acrylate Homo and Block Copolymers via Nitroxide Mediated Polymerization, *Materials* 12(9) (2019).
- [49] L.J. Fetters, D.J. Lohse, D. Richter, T.A. Witten, A. Zirkel, Connection between Polymer Molecular Weight, Density, Chain Dimensions, and Melt Viscoelastic Properties, *Macromolecules* 27(17) (1994) 4639-4647.
- [50] S. Noppalit, A. Simula, L. Billon, J.M. Asua, On the nitroxide mediated polymerization of methacrylates derived from bio-sourced terpenes in miniemulsion, a step towards sustainable products, *Polymer Chemistry* 11(6) (2020) 1151-1160.
- [51] S. B. Luk, A. Métafiot, J. Morize, E. Edeh, M. Maric, Hydrogenation of poly(myrcene) and poly(farnesene) using diimide hydrogenation at ambient pressure, *Journal of Polymer Science* (2021) Advance online publication.
- [52] R. Wei, Y. Luo, Z. Li, Synthesis of structured nanoparticles of styrene/butadiene block copolymers via RAFT seeded emulsion polymerization, *Polymer* 51(17) (2010) 3879-3886.
- [53] R. Wei, Y. Luo, W. Zeng, F. Wang, S. Xu, Styrene–Butadiene–Styrene Triblock Copolymer Latex via Reversible Addition–Fragmentation Chain Transfer Miniemulsion Polymerization, *Industrial & Engineering Chemistry Research* 51(47) (2012) 15530-15535.



## 9 Appendices

The appendices contains the supporting information for all the published articles and submitted manuscripts.

9.1 Appendix A: Supporting Information for “Nitroxide-mediated polymerization of bio-based farnesene with incorporation of functional glycidyl methacrylate”

The homopolymerization of farnesene is mostly by 1,4-addition, as opposed to 1,2-addition, as shown in Figure A1. The broad peak at  $\delta=5.2$  ppm after 240 minutes of polymerization is the shift of proton C due to the formation of a double bond after 1,4-addition. The small peak at  $\delta=4.8$  ppm is the shift of the vinyl protons D and D' as a result of 1,2-addition.

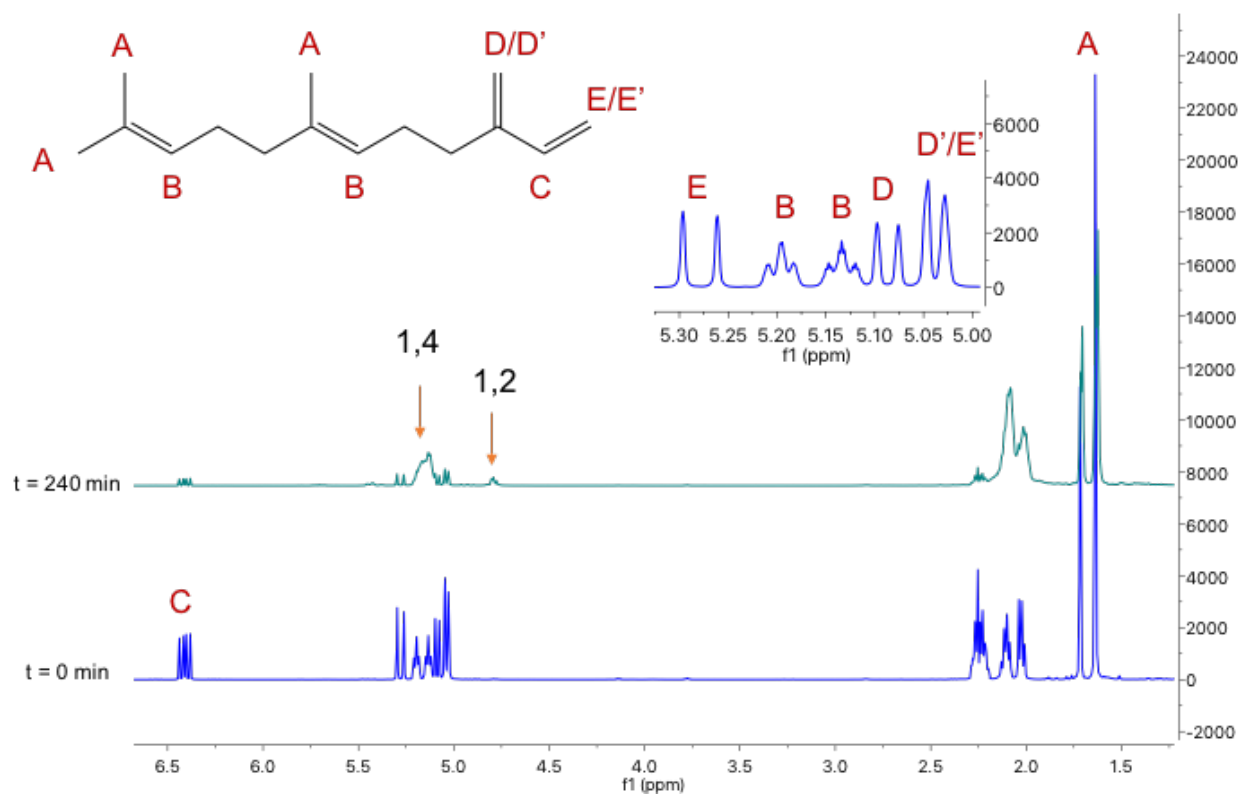


Figure A-1. <sup>1</sup>H NMR spectra (500 MHz) for polymerization of farnesene at t = 0 and 240 mins in CDCl<sub>3</sub>.

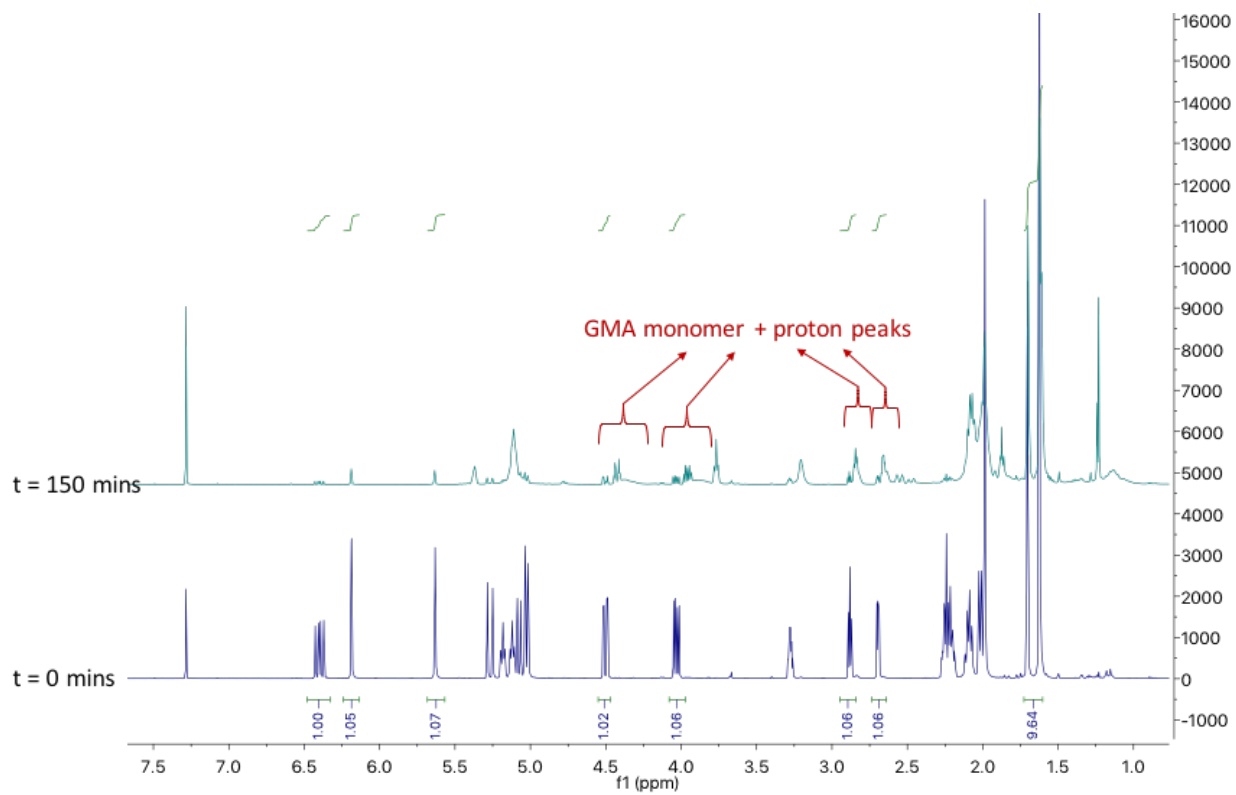


Figure A-2. <sup>1</sup>H NMR spectra (500 MHz) of 50/50 molar ratio of Far/GMA copolymerization at t = 0 and 150 mins in CDCl<sub>3</sub>.

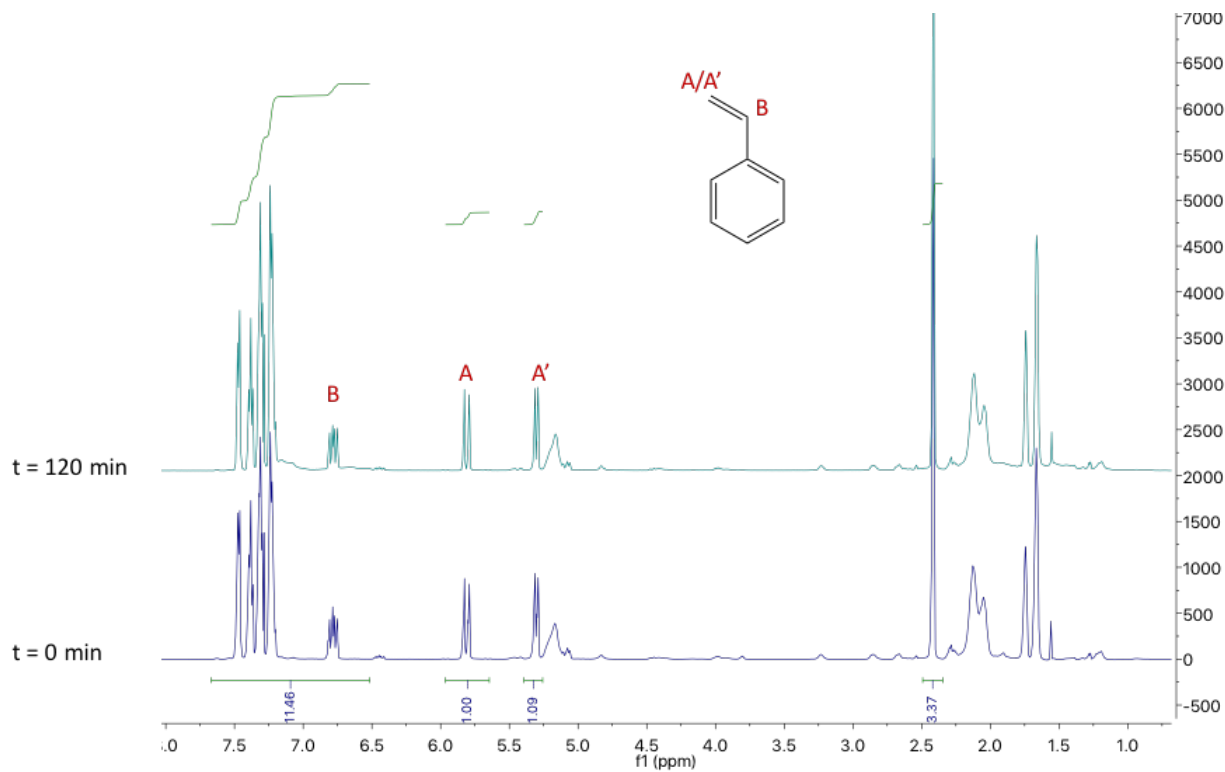


Figure A-3.  $^1\text{H}$  NMR spectra (500 MHz) of chain-extension of 80/20 molar ratio Far/GMA macroinitiator with styrene in toluene at  $t = 0$  and 120 mins in  $\text{CDCl}_3$ .

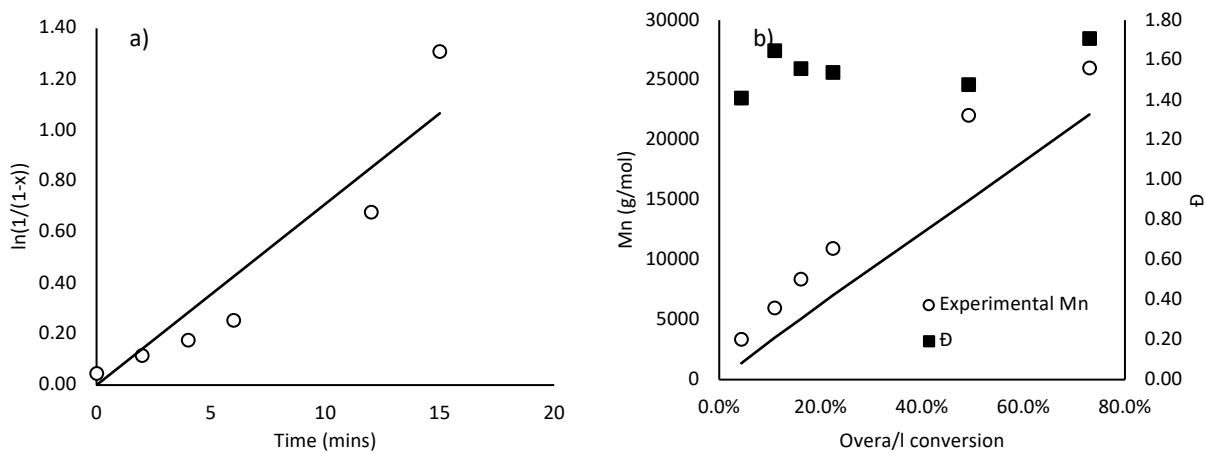


Figure A-4. a) Linearized conversion as a function of time and b)  $M_n$  and  $\bar{D}$  vs. Conversion plots for random copolymerization of 10/90 molar ratio of Far/GMA at  $120^\circ\text{C}$  with NHS.BB in bulk.

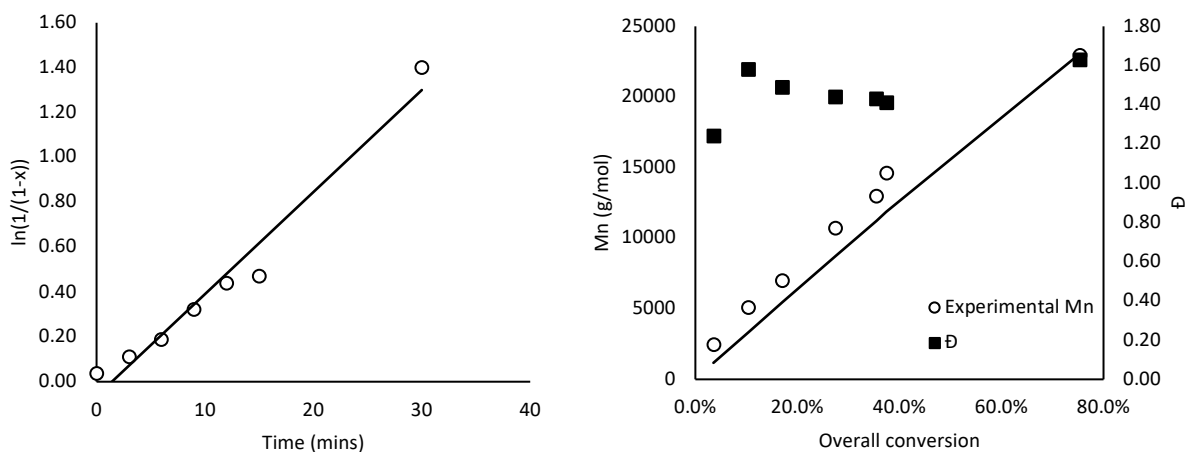


Figure A-5. a) Linearized conversion as a function of time and b)  $M_n$  and  $\bar{D}$  vs. Conversion plots for random copolymerization of 20/80 molar ratio of Far/GMA at 120°C with NHS.BB in bulk.

Table A-1. Summary of experimental conditions for Far/GMA statistical copolymerizations using NHS-BB in bulk at 120°C. Final conversion ( $X$ ), number average molecular weight ( $M_n$ ), dispersity ( $\bar{D}$ ), and final polymer compositions ( $F_{\text{Far}}$  and  $F_{\text{GMA}}$ ) are reported.

$f_{\text{Far},0}$	$m_{\text{NHS-BB}}$ (g)	$m_{\text{Far}}$ (g)	$m_{\text{GMA}}$ (g)	$X$	$M_n$ (g/mol)	$\bar{D}$	$F_{\text{Far}}$	$F_{\text{GMA}}$
<b>0.1</b>	0.1	1.08	6.79	73%	26000	1.71	0.12	0.88
<b>0.2</b>	0.1	2.08	5.79	75%	22900	1.63	0.25	0.75
<b>0.3</b>	0.1	3.00	4.87	88%	29200	1.50	0.34	0.66
<b>0.4</b>	0.1	3.21	3.35	92%	21900	1.67	0.42	0.58
<b>0.5</b>	0.12	4.64	3.23	86%	24300	1.54	0.51	0.49
<b>0.7</b>	0.08	4.85	1.45	65%	20300	1.29	0.65	0.35
<b>0.9</b>	0.1	7.31	0.56	60%	17900	1.23	0.85	0.15

Table A-2. Summary of Far monomer and polymer compositions, and their conversions for Far/GMA statistical polymerization with NHS-BB in bulk for Mayo-Lewis plot at 120 and 90°C.

$f_{\text{Far},0}$	$X_{120\text{C}}$	$F_{\text{Far}, 120\text{C}}$	$X_{90\text{C}}$	$F_{\text{Far}, 90\text{C}}$
<b>0.05</b>	--	--	6.3%	0.12
<b>0.1</b>	10.8%	0.25	6.8%	0.22
<b>0.2</b>	10.4%	0.37	8.4%	0.4
<b>0.3</b>	21.1%	0.44	--	--
<b>0.4</b>	27.3%	0.5	--	--
<b>0.5</b>	22.4%	0.56	--	--

<b>0.7</b>	13.7%	0.66	--	--
<b>0.9</b>	13.6%	0.86	--	--

Table A-3. Chain-extension of GMA-rich macroinitiator with St in 50 wt% toluene at 110°C.

<b>Time (mins)</b>	<b>X</b>	<b><math>M_n</math> (kg/mol)</b>	<b><math>\bar{D}</math></b>
<b>0</b>	7%	22.9	1.44
<b>30</b>	18%	28.6	1.54
<b>60</b>	21%	29.1	1.62
<b>120</b>	22%	29.3	1.77

Table A-4. Chain-extension of Far-rich macroinitiator with St in 50 wt% toluene at 110°C.

<b>Time (mins)</b>	<b>X</b>	<b><math>M_n</math> (kg/mol)</b>	<b><math>\bar{D}</math></b>
<b>0</b>	3%	22.0	1.22
<b>30</b>	13%	22.7	1.30
<b>60</b>	14%	25.6	1.29
<b>120</b>	22%	27.7	1.34

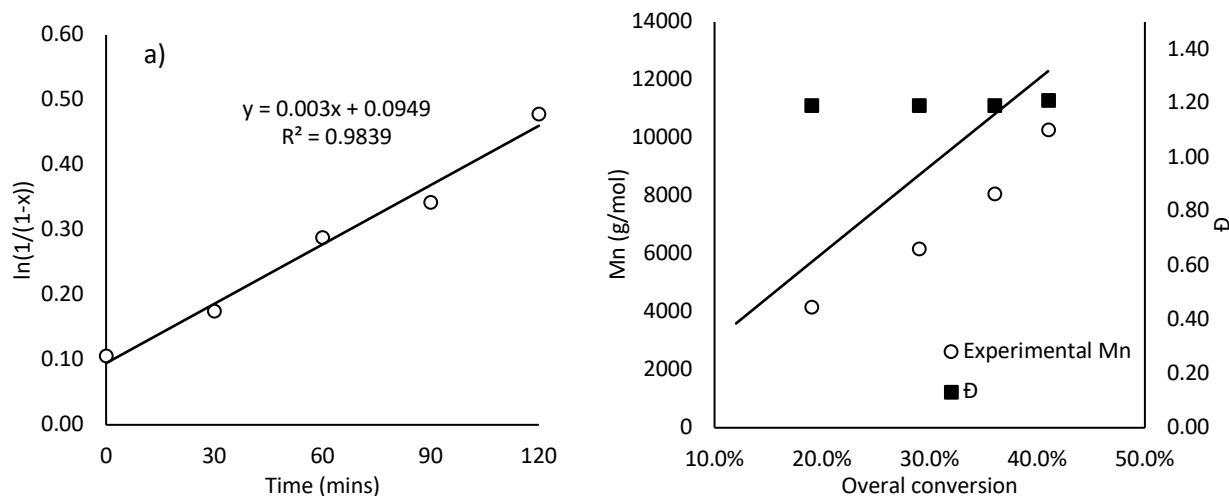


Figure A-6. Synthesis of Far homopolymer macroinitiator using NHS-BB in bulk at 120°C. a) Linearized conversion vs. time plot, b) molecular weight ( $M_n$ ) vs. conversion and dispersity ( $\bar{D}$ ) vs. conversion plots.

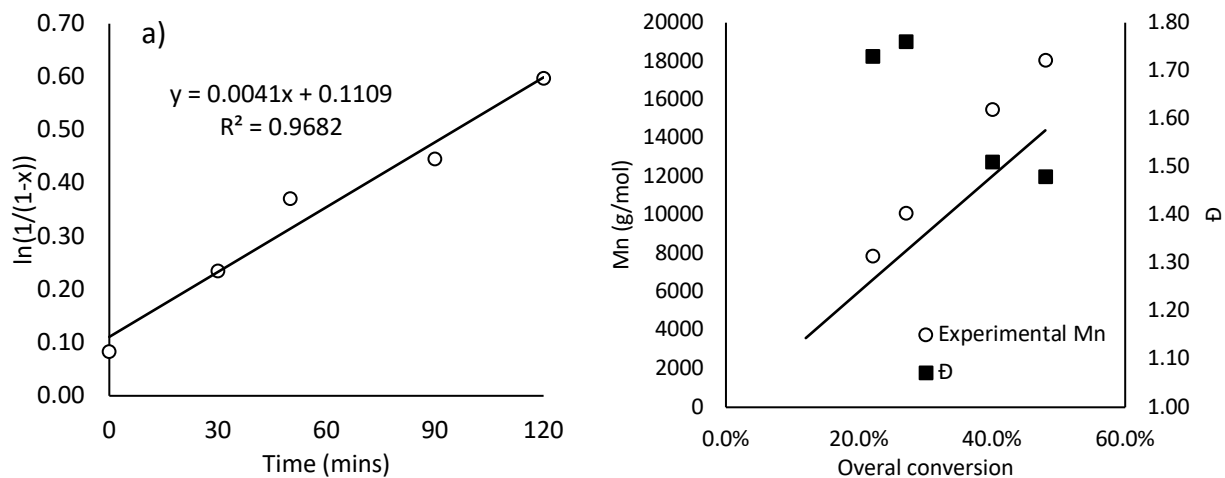


Figure A-7. Synthesis of Far homopolymer macroinitiator using CCDP in bulk at 120°C. a) Linearized conversion vs. time plot, b) molecular weight ( $M_n$ ) vs. conversion and dispersity ( $\bar{D}$ ) vs. conversion plots

9.2 Appendix B: Supporting information for “Polymerization of bio-based farnesene in miniemulsions by nitroxide-mediated polymerization”

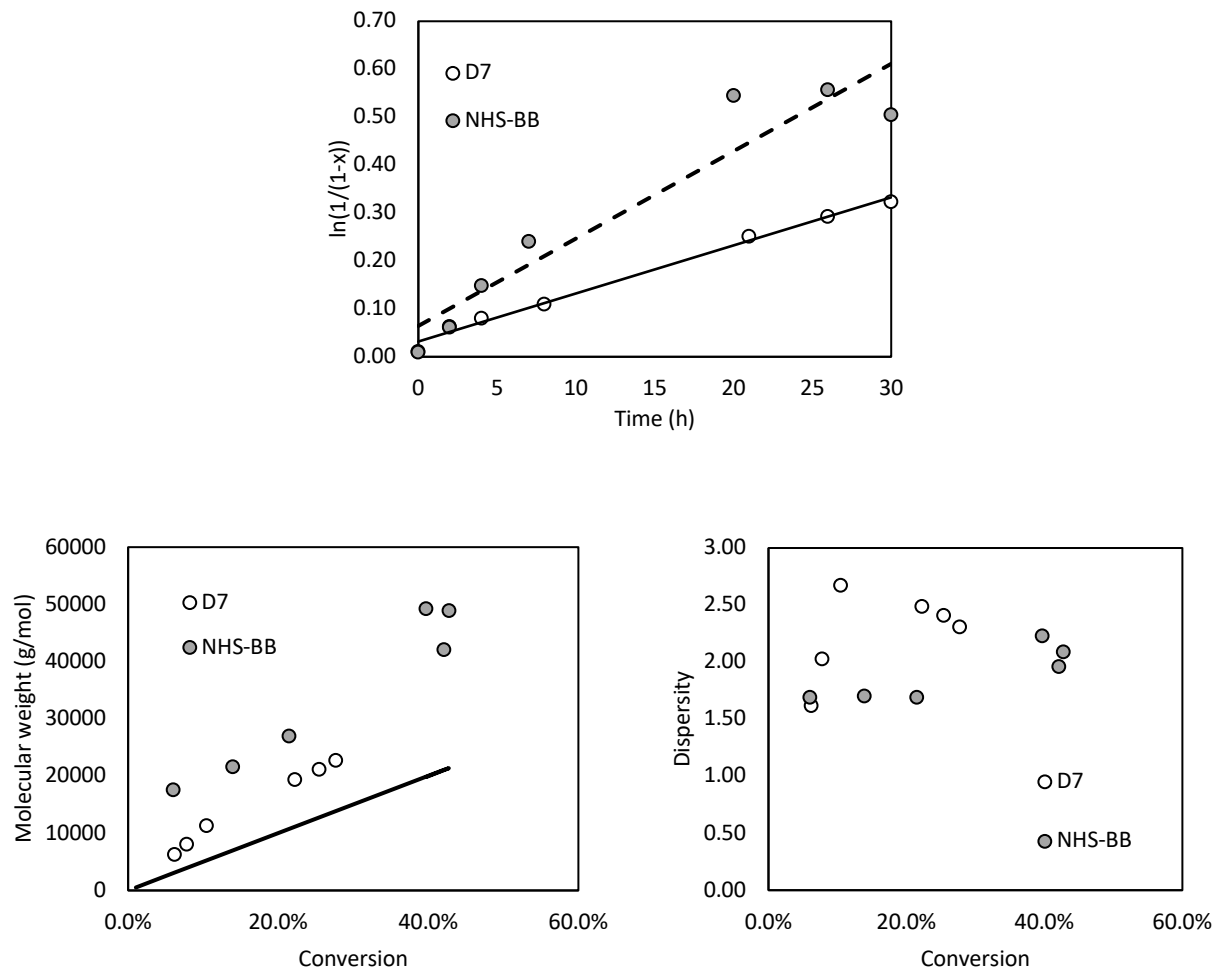


Figure B-1.  $\ln(1/(1-X))$  vs. time,  $M_n$  and Dispersity vs. time plots for farnesene homopolymerization miniemulsions done with D7 and NHS-BB initiators at 20 wt% monomer and 5 wt% surfactant for 30 h.

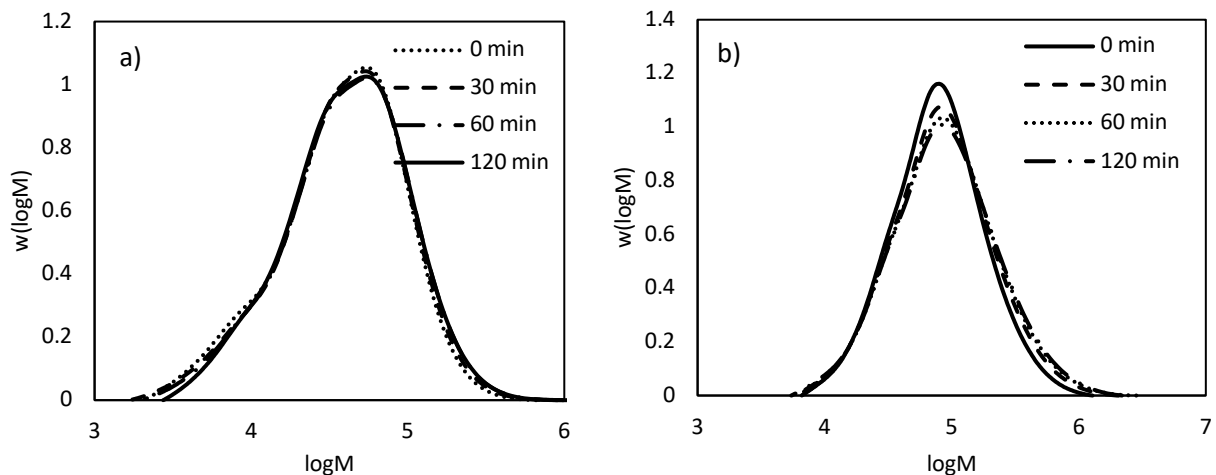


Figure B-2. MWDs of chain-extension reactions with St for poly(Far) made in miniemulsion using a) D7 and b) NHS-BB in 20 wt% monomer and 5 wt% surfactant.

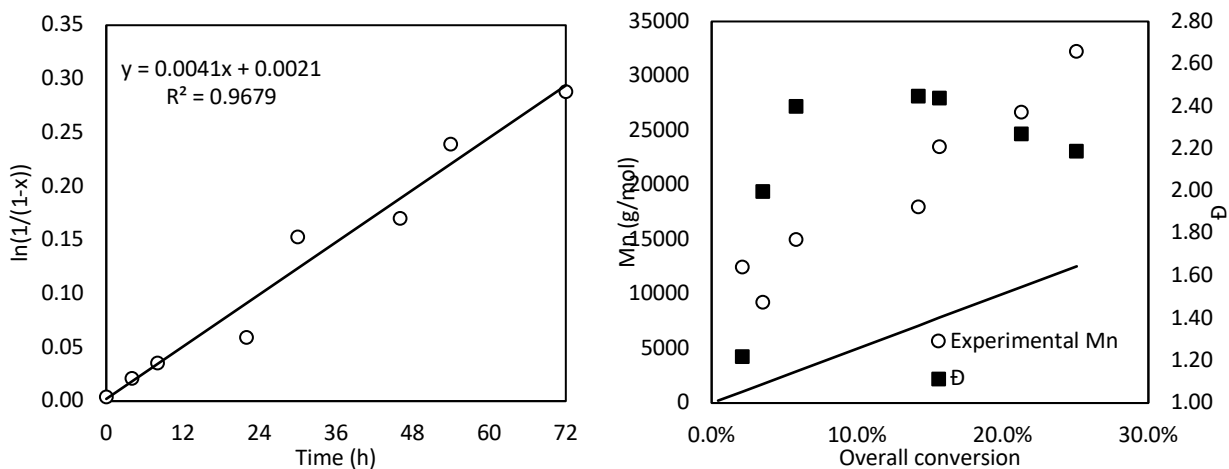


Figure B-3.  $\ln(1/(1-X))$  vs. time,  $M_n$  and Dispersity vs. time plots for farnesene homopolymerization miniemulsions done with D7 at 20 wt% monomer and 5 wt% surfactant for 72 h.

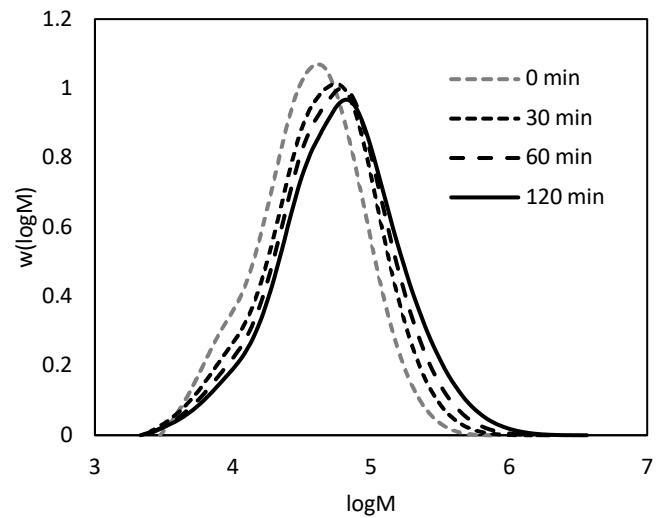


Figure B-4. MWD of chain-extension reactions with St for poly(Far) made in miniemulsion using D7 in 20 wt% monomer and 15 wt% surfactant after 72 h.

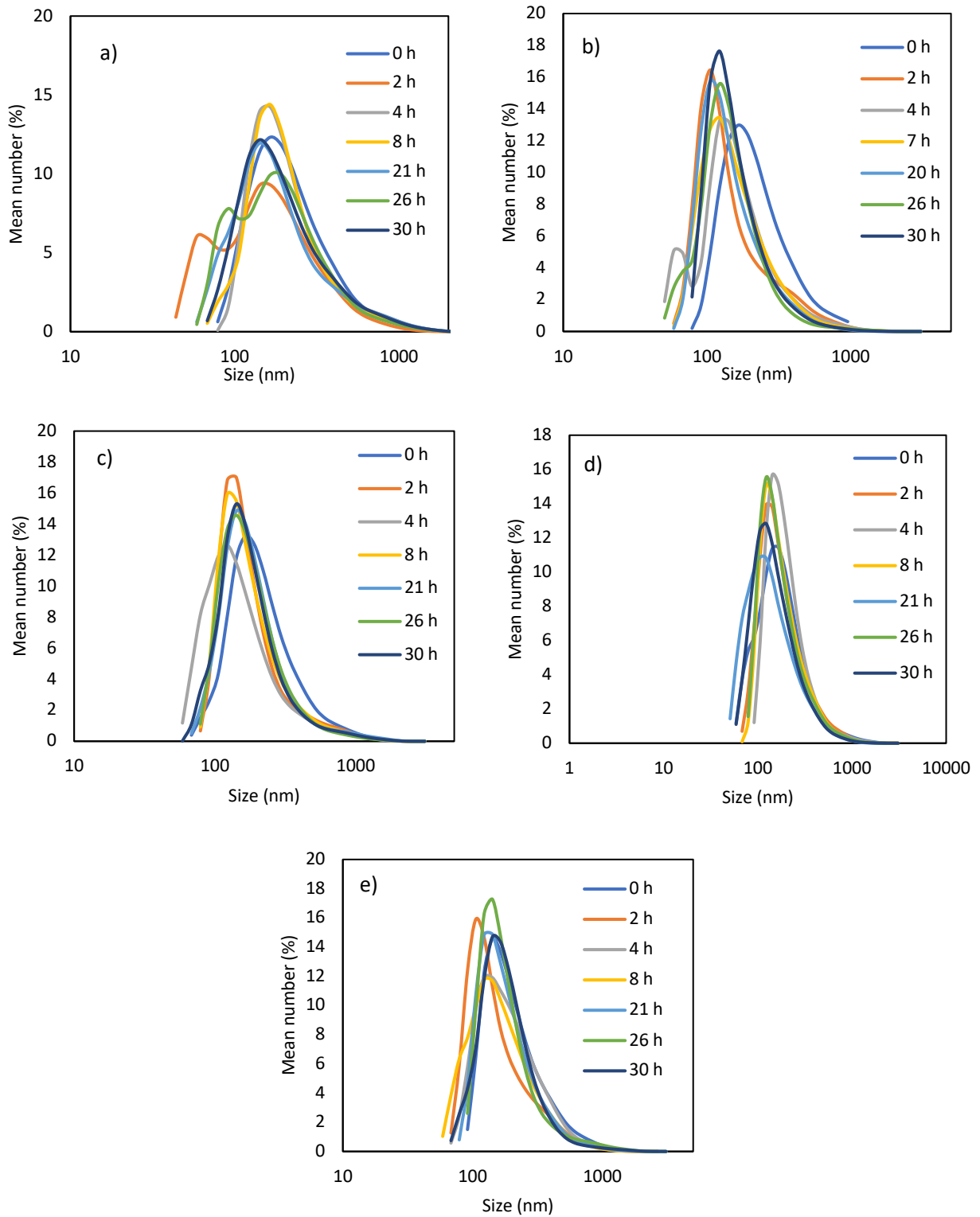


Figure B-5. Number-averaged particle size distribution from DLS for a) Exp 1, b) Exp 2, c) Exp 3, d) Exp 4, and e) Exp 5.

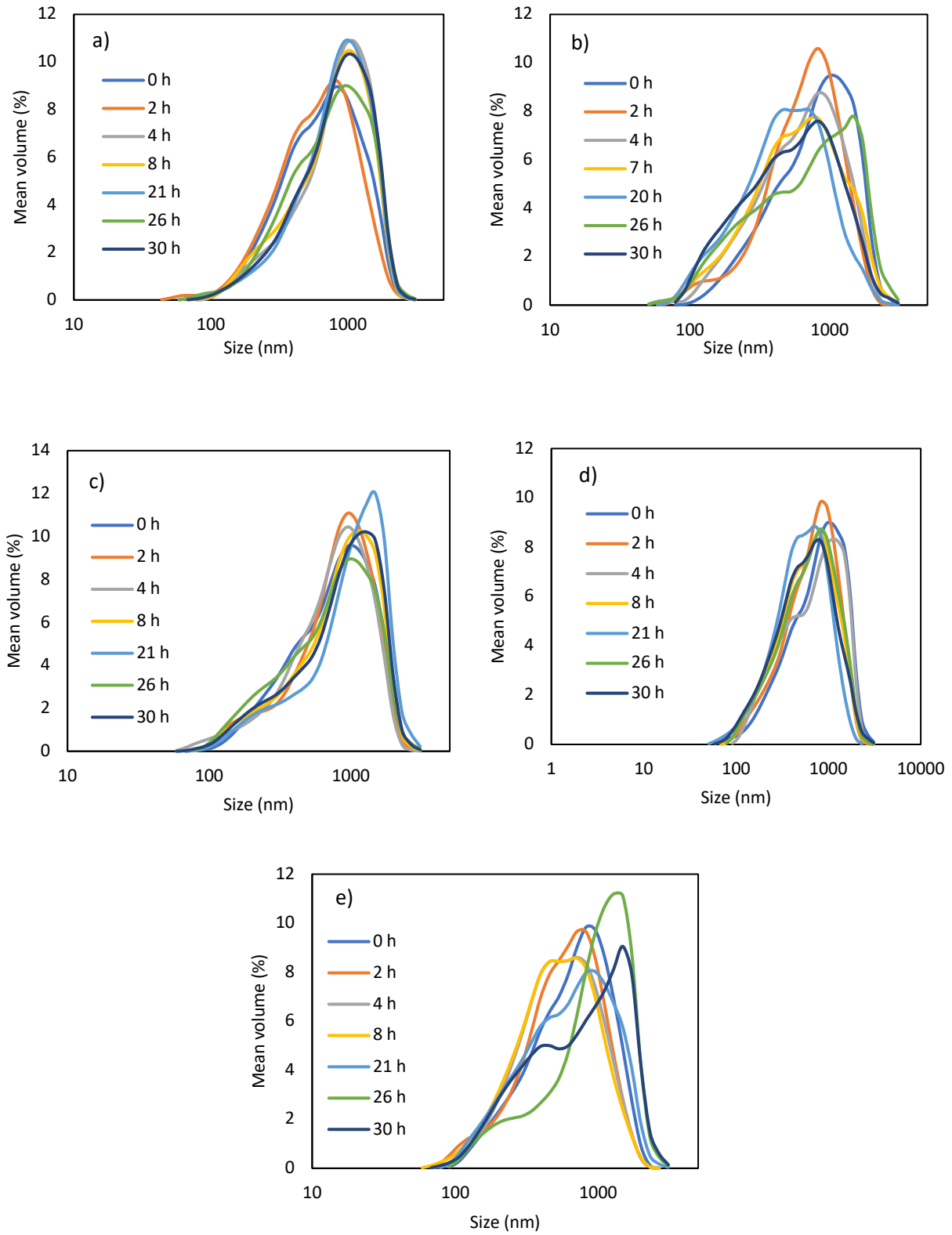


Figure B-6. Volume-averaged particle size distribution from DLS for a) Exp 1, b) Exp 2, c) Exp 3, d) Exp 4, and e) Exp 5.

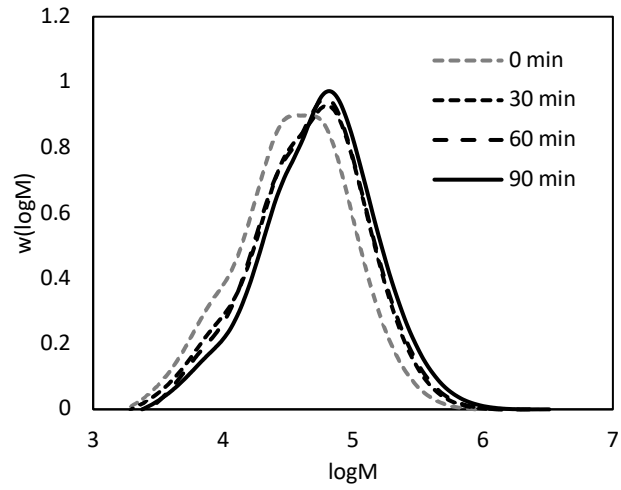


Figure B-7. MWD of chain-extension reactions with iBOMA for poly(Far) made in miniemulsion using D7 in 20 wt% monomer and 15 wt% surfactant after 72 h.

9.3 Appendix C: Supporting information for “Farnesene and norbornenyl methacrylate block copolymers: application of thiol-ene clicking to improve thermal and mechanical properties”

The  $^1\text{H}$  NMR spectra of EGDEMA monomer is shown in Figure C-1. Conversion of polymerization of EGDEMA via nitroxide-mediated polymerization was calculated according to the NMR spectra as shown in Figure C-2.

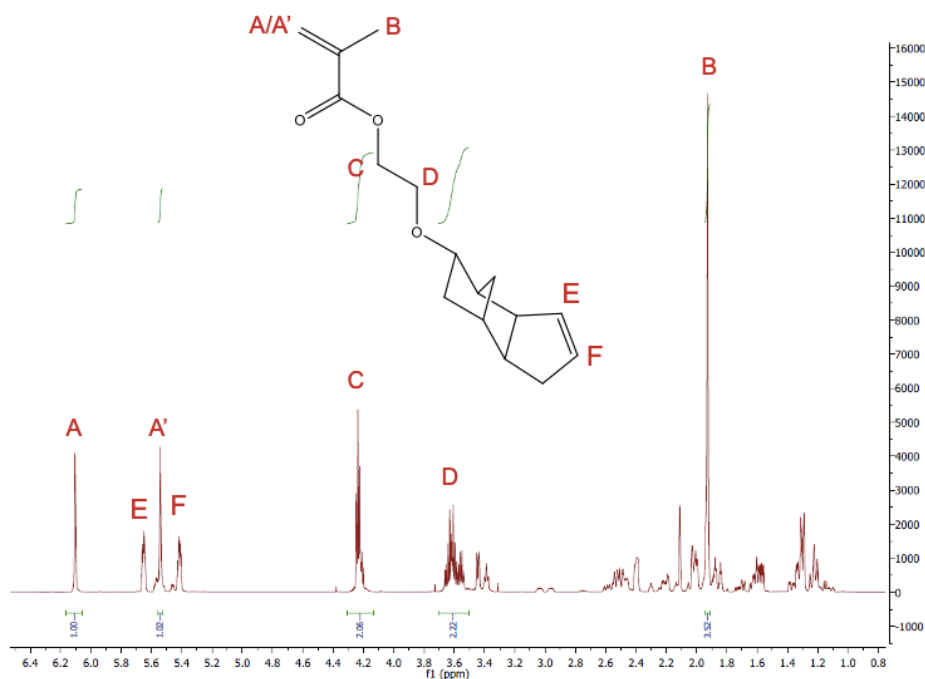


Figure C-1.  $^1\text{H}$  NMR (500 MHz) spectra of ethylene glycol dicyclopentenyl ether methacrylate (EGDEMA) monomer in  $\text{CDCl}_3$ .

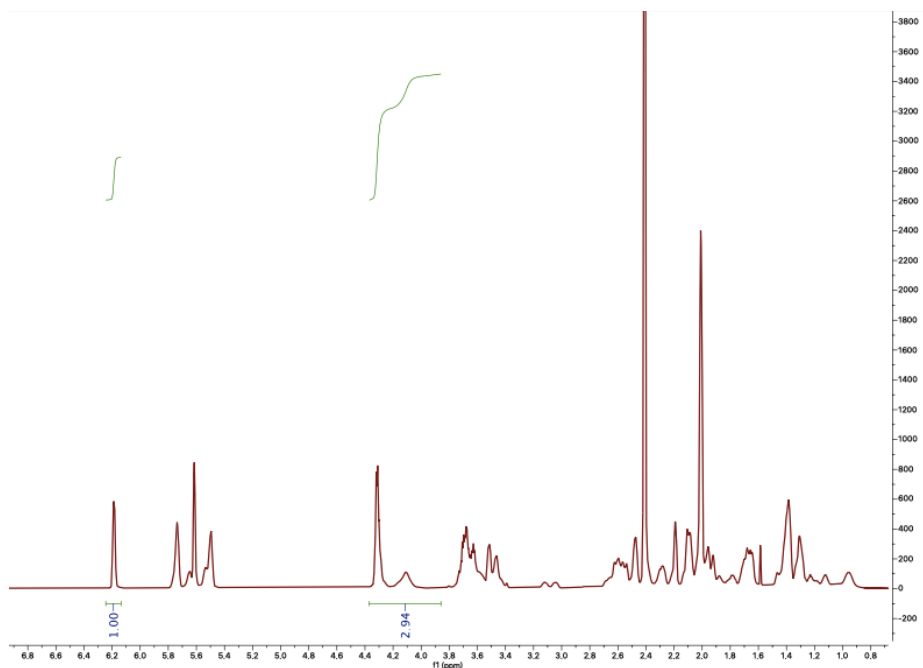


Figure C-2. <sup>1</sup>H NMR (500 MHz) spectra of polymerization of EGDEMA after 60 mins in CDCl<sub>3</sub>.

The conversion of EGDEMA polymerization was calculated using the vinyl proton that is polymerized by NMP at 6.2 ppm, and the monomer plus proton peaks are at 3.8 – 4.4 ppm. The conversion is therefore calculated using the following equation.

$$X_{EGDEMA} = \left(1 - \frac{m}{m + p}\right) \times 100\% = \left(1 - \frac{A_{6.2}}{A_{3.8-4.4}}\right) \times 100\%$$

Similarly, the copolymerization of equimolar EGDEMA and iBOMA monomers are characterized using <sup>1</sup>H NMR as shown in Figure C-3. The conversion of EGDEMA and iBOMA copolymerization is calculated based on the spectra shown in Figure C-4.

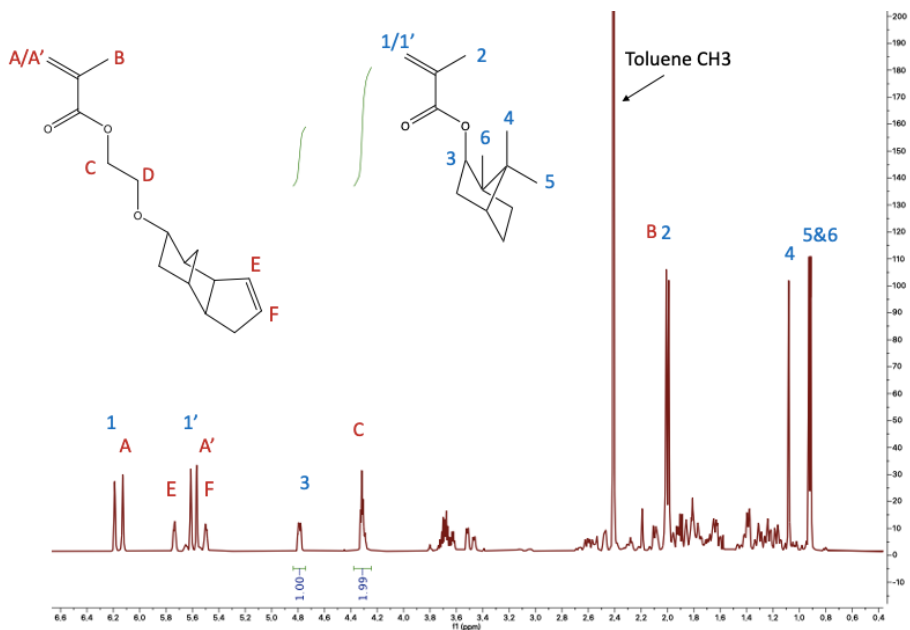


Figure C-3.  $^1\text{H}$  NMR (500 MHz) spectra of equimolar EGDEMA and iBOMA monomers in  $\text{CDCl}_3$ .

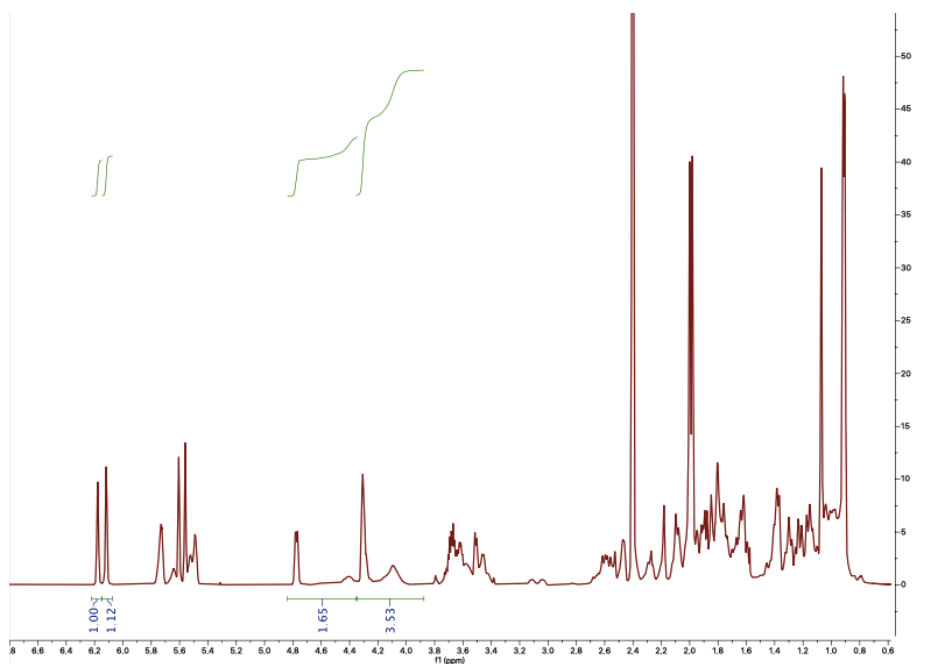


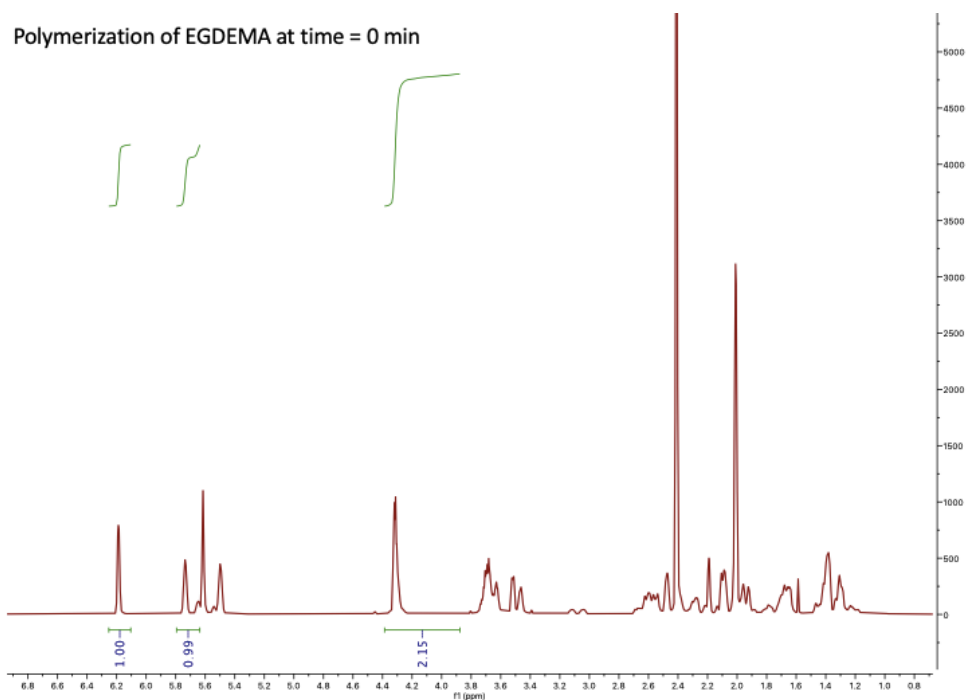
Figure C-4.  $^1\text{H}$  NMR (500 MHz) spectra of copolymerization of EGDEMA and iBOMA after 120 mins in  $\text{CDCl}_3$ .

The conversion for equimolar copolymerization of EGDEMA and iBOMA is calculated using the same protons as EGDEMA homopolymerization ( $A_{6.2}$  and  $A_{3.8-4.2}$  are the integrated areas peak

areas), the vinyl proton of iBOMA at 6.1 ppm and the monomer and proton peaks at 4.4 – 4.8 ppm. The following equation was used to calculating the conversion of the copolymerization.

$$X_{EGDEMA\&iBOMA} = \left[ \frac{A_{6.2}}{A_{6.2} + A_{6.1}} \left( 1 - \frac{A_{6.2}}{A_{3.8-4.2}} \right) + \frac{A_{6.1}}{A_{6.2} + A_{6.1}} \left( 1 - \frac{A_{6.1}}{A_{4.4-4.8}} \right) \right] \times 100\%$$

Alternatively, conversion of EGDEMA polymerization can be calculated relative to the pendent double bond protons assuming they are also inert and do not participate in polymerization. These conversions are compared with previous calculations which were relative to the inert CH<sub>2</sub> protons to verify that the pendent double bonds are not polymerized via NMP. The integration of one of the pendent double bond proton at 5.7 ppm is shown in Figure C-5. At time = 0 min, the integration of the pendent double bond proton is equal to the vinyl proton of EGDEMA and after 60 mins of polymerization, the integration of pendent double bond proton is higher than the vinyl proton.



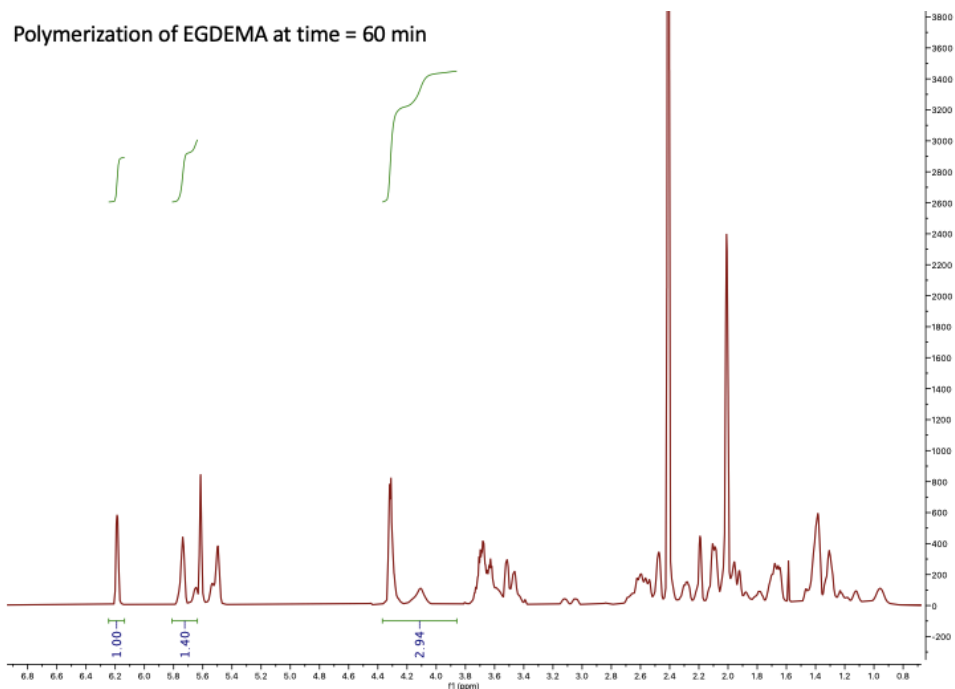


Figure C-5.  $^1\text{H}$  NMR of EGDEMA homopolymerization at time = 0 min and 60 min.

The conversion calculated relative to the pendent double bond is calculated using the integration of the pendent proton peak at 5.7 ppm ( $A_{5.7}$ ) relative to the vinyl proton peak at 6.2 ppm ( $A_{6.2}$ ) using the below equation.

$$X_{EGDEMA}^{pendent} = \left(1 - \frac{m}{m + p}\right) \times 100\% = \left(1 - \frac{A_{6.2}}{A_{5.7}}\right) \times 100\%$$

The conversions of EGDEMA polymerization calculated relative to inert  $\text{CH}_2$  protons compared to inert pendent double bond protons are shown in Table C-1. The two methods give comparable conversions given the inherent error of  $^1\text{H}$  NMR spectra, therefore the pendent double bonds of EGDEMA can be considered inert in the polymerization reactions.

Table C-1: Summary of conversions of EGDEMA polymerization and EGDEMA and iBOMA copolymerization using the pendent proton peaks compared to the CH2 proton peaks.

Macroinitiator ID	Conversion of EGDEMA calculated using CH2 protons (A <sub>3.8-4.4</sub> )	Conversion of EGDEMA calculated using pendent proton (A <sub>5.7</sub> )
EG1	32.0%	28.6%
EG2	46.7%	47.1%
EGiB1 <sup>a</sup>	36.7%	35.5%
EGiB2 <sup>a</sup>	48.2%	41.9%

a) For the equimolar copolymerizations of EGDEMA and iBOMA, the conversions calculated in this table are for EGDEMA monomer only and does not include conversion of iBOMA.

The chain-extension of poly(EGDEMA) macroinitiators with Far is shown in Figure C-6.

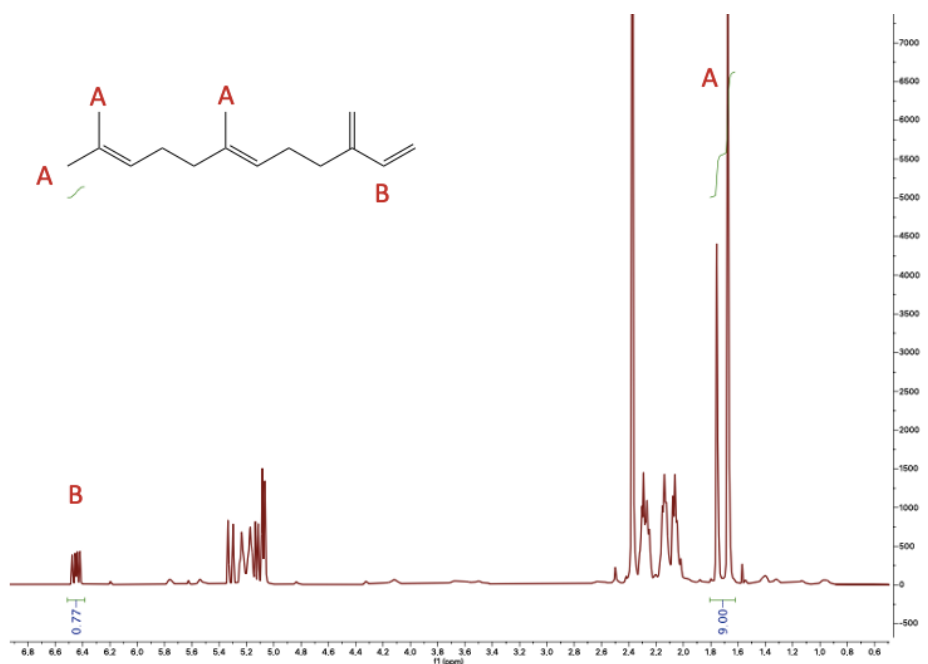


Figure C-6. <sup>1</sup>H NMR (500 MHz) spectra of chain-extension of poly(EGDEMA) macroinitiators with Far after 120 mins in CDCl<sub>3</sub>.

The chain-extension reaction is monitored by tracking the disappearance of the proton (B) adjacent to the vinyl protons of Far at 6.45 ppm, and the 9 CH<sub>3</sub> protons (A) of Far at 1.7 ppm, which are

present in both Far monomer and polymer. Therefore, the conversion of chain-extension is calculated using the equation,

$$X_{chain-extension} = \left(1 - \frac{A_{6.45}}{A_{1.7}}\right) \times 100\%$$

The  $^1\text{H}$  NMR of thiol-POSS is shown in Figure C-7. The thiol proton at 1.3 ppm would disappear after thiol-ene clicking.

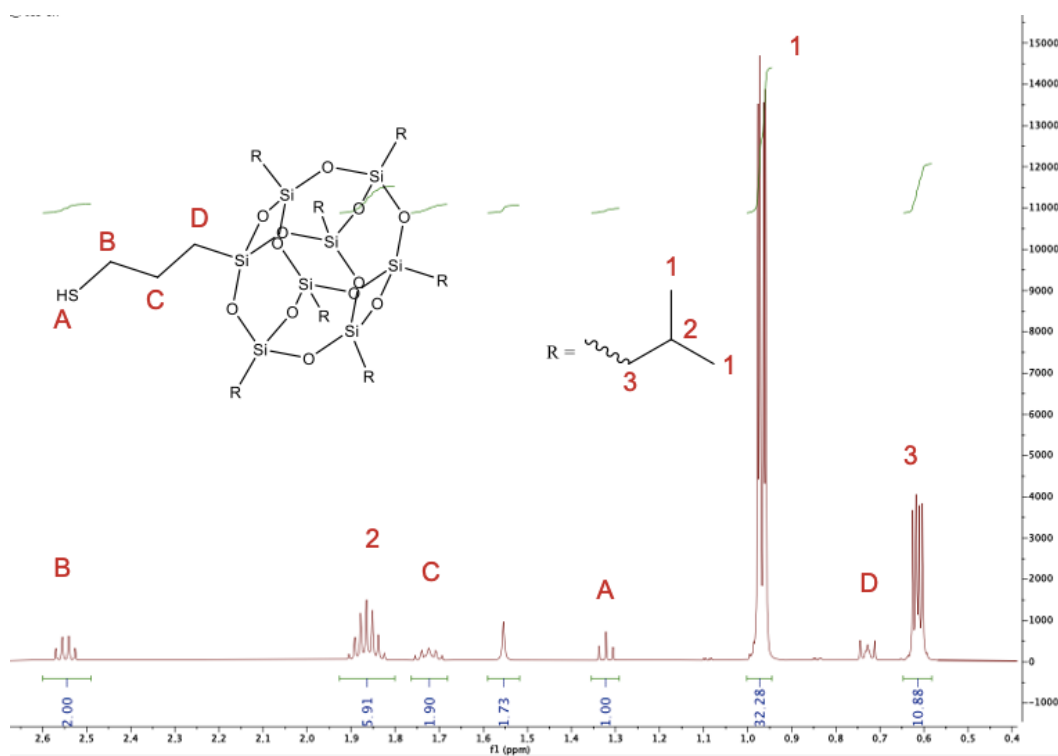


Figure C-7.  $^1\text{H}$  NMR (500 MHz) spectra of thiol-POSS in  $\text{CDCl}_3$ .

To quantify the thiol-ene clicking reaction with the poly(EGDEMA-*b*-Far) block copolymers,  $^1\text{H}$  NMR of the final polymers were done and an example spectra is shown in Figure C-8.

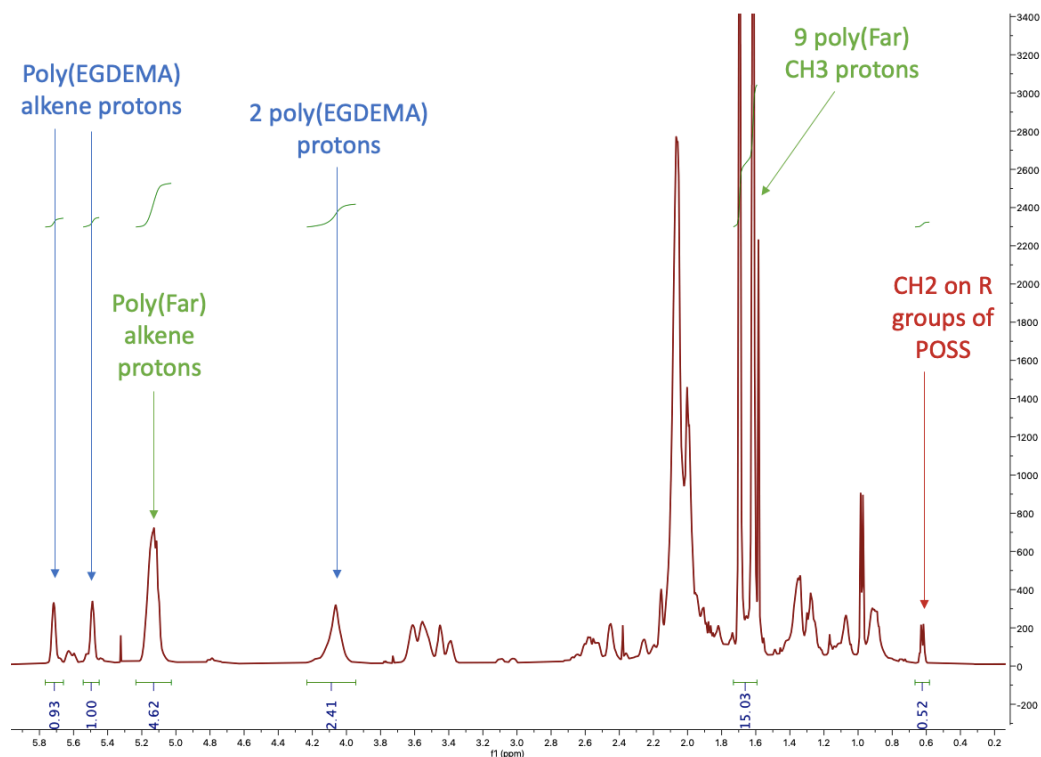


Figure C-8.  $^1\text{H}$  NMR (500 MHz) spectra of poly(EGDEMA-*b*-Far) block copolymer clicked with thiol-POSS in  $\text{CDCl}_3$ .

To find the concentration of double bonds of EGDEMA that remained after thiol-ene clicking, the alkene protons of EGDEMA at 5.4 and 5.7 ppm are compared to the 2 poly(EGDEMA) protons at 4.0 ppm.

$$\text{EGDEMA}(C = C) = \frac{A_{5.4}}{A_{4.0}/2}$$

To find the concentration of double bonds of Far that remained after thiol-ene clicking, the 3 poly(Far) alkene protons at 5.1 ppm are compared to the 9  $\text{CH}_3$  protons of poly(Far) at 1.6 ppm.

$$\text{Far}(C = C) = \frac{A_{5.1}/3}{A_{1.6}/9}$$

The copolymer composition of the block copolymers ( $F_{EGDEMA}$ ,  $F_{Far}$ ,  $F_{POSS}$ ) is calculated by finding the mole fractions of each component by integrating the poly(Far) peak at 5.1 ppm (3 equivalent protons), poly(EGDEMA) peak at 4.0 ppm (2 equivalent protons), and the CH<sub>2</sub> protons of the R group of POSS at 0.6 ppm (14 equivalent protons, 7 R groups per POSS). However, even though there are 7 R groups per POSS, as seen in the <sup>1</sup>H NMR spectra for thiol-POSS in Figure C-7, only 11 protons are quantified per 2 CH<sub>2</sub> protons on the mercaptopropyl group. Therefore, the copolymer compositions were calculated assuming 11 POSS CH<sub>2</sub> protons at 0.6 ppm per mole.

$$F_{EGDEMA} = \frac{A_{4.0}/2}{A_{4.0}/2 + A_{5.1}/3 + A_{0.6}/11}$$

$$F_{Far} = \frac{A_{5.1}/3}{A_{4.0}/2 + A_{5.1}/3 + A_{0.6}/11}$$

$$F_{POSS} = \frac{A_{0.6}/11}{A_{4.0}/2 + A_{5.1}/3 + A_{0.6}/11}$$

Similarly, poly(EGDEMA-*co*-iBOMA-*b*-Far) block copolymers are characterized using <sup>1</sup>H NMR spectra shown in Figure C-9. The calculations to find remaining double bonds remain the same.

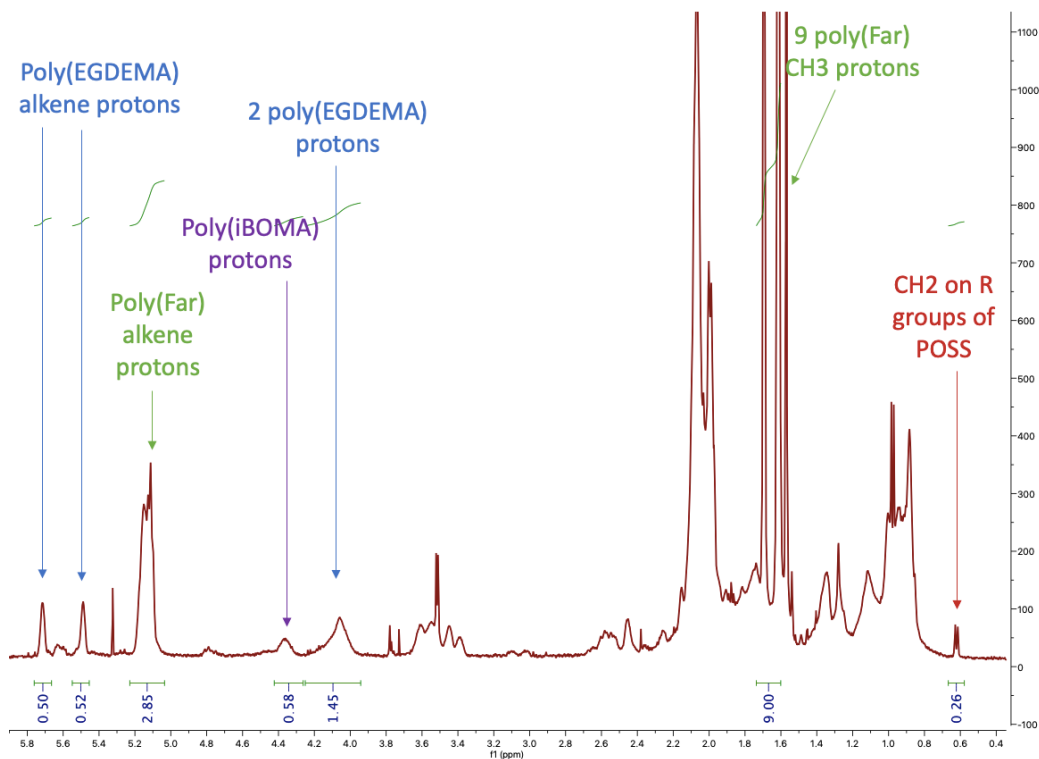


Figure C-9. <sup>1</sup>H NMR (500 MHz) spectra of poly(EGDEMA-*co*-iBOMA-*b*-Far) block copolymer clicked with thiol-POSS in CDCl<sub>3</sub>.

The copolymer composition of the poly(EGDEMA-*co*-iBOMA-*b*-Far) block copolymers ( $F_{EGDEMA}$ ,  $F_{iBOMA}$ ,  $F_{Far}$ ,  $F_{POSS}$ ) is calculated with the addition of including poly(iBOMA) protons at 4.4 ppm as well. Therefore,

$$F_{EGDEMA} = \frac{A_{4.0}/2}{A_{4.0}/2 + A_{4.4} + A_{5.1}/3 + A_{0.6}/11}$$

$$F_{iBOMA} = \frac{A_{4.4}}{A_{4.0}/2 + A_{4.4} + A_{5.1}/3 + A_{0.6}/11}$$

$$F_{Far} = \frac{A_{5.1}/3}{A_{4.0}/2 + A_{4.4} + A_{5.1}/3 + A_{0.6}/11}$$

$$F_{POSS} = \frac{A_{0.6}/14}{A_{4.0}/2 + A_{4.4} + A_{5.1}/3 + A_{0.6}/11}$$

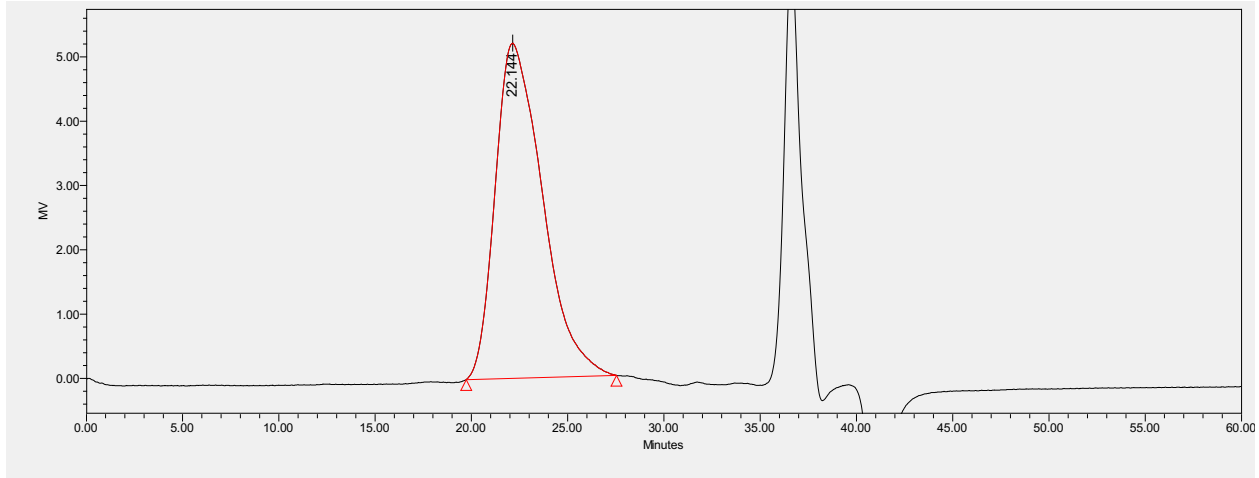
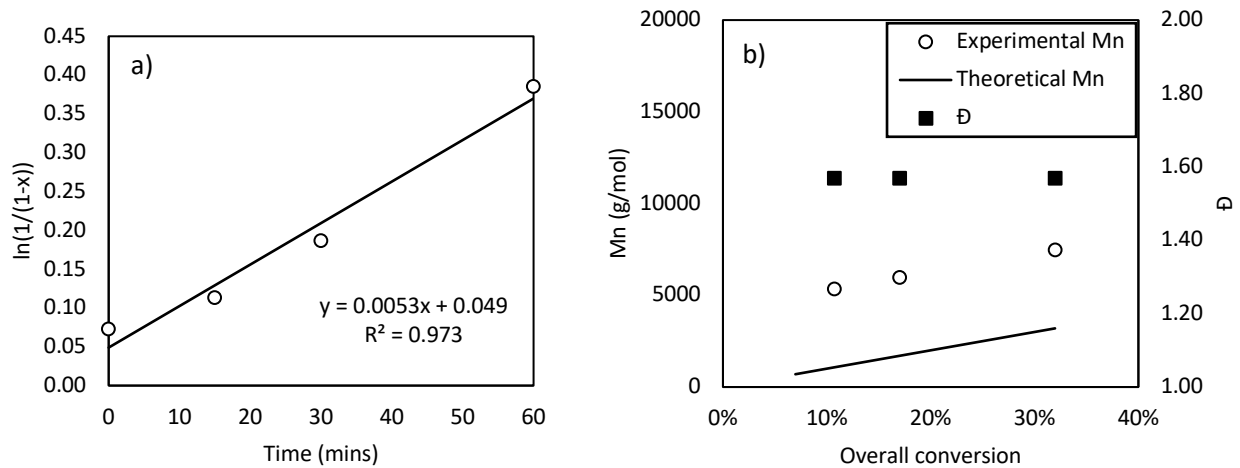


Figure C-1: GPC chromatograph of EGiB2-Far-POSS10 after purification following thiol-ene clicking showing absence of unreacted POSS that would appear at 28-31 min elution time.

The kinetic plots,  $M_n$  and  $\bar{D}$  versus conversion plots for homopolymerization of EGDEMA using D7 initiator at 90°C are shown in Figure C-11.



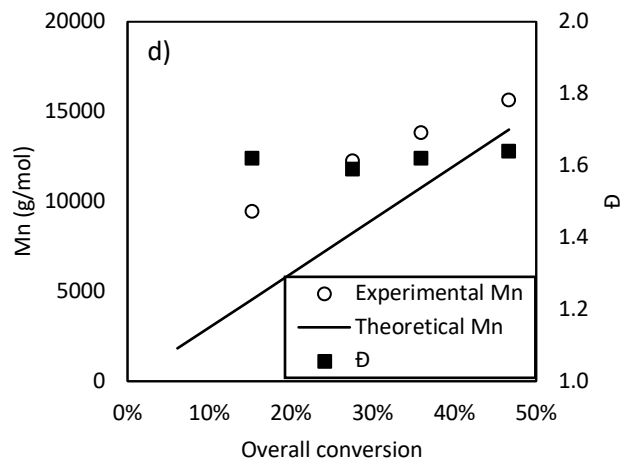
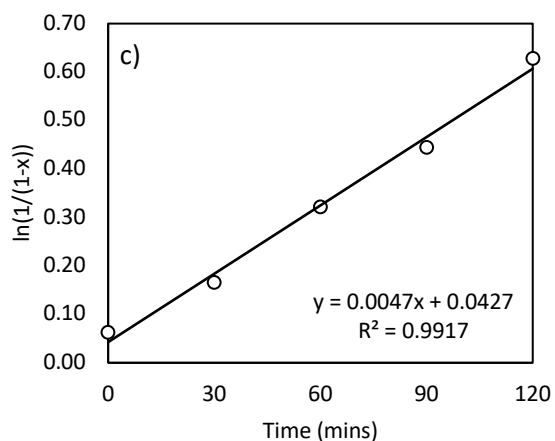
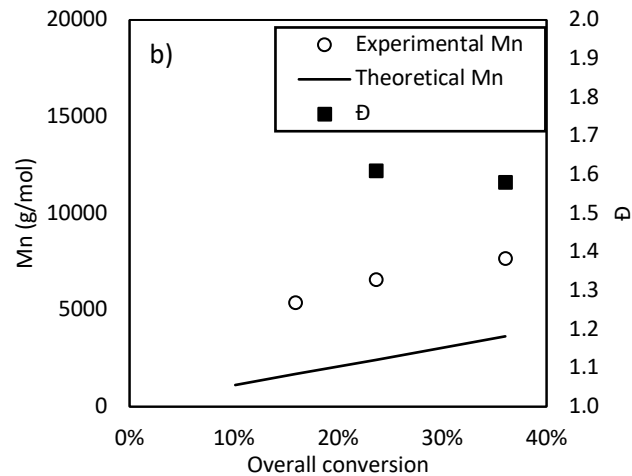
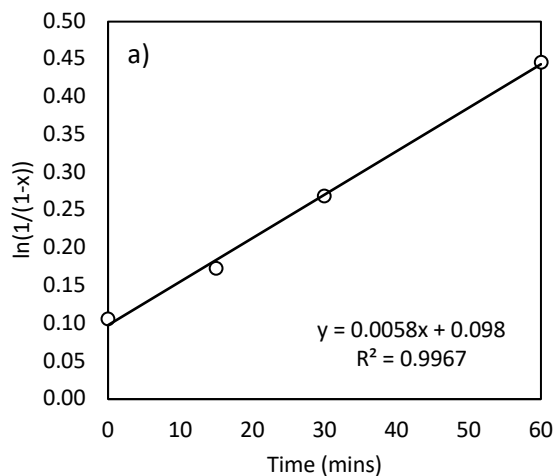


Figure C-11. Kinetic plots for homopolymerization of a) EG1 and b)  $M_n$  and  $\bar{D}$  versus conversion for EG1, as well as kinetic plots for c) EG2 and d)  $M_n$  and  $\bar{D}$  versus conversion for EG2.

The semi-logarithmic kinetic plots,  $M_n$  and  $\bar{D}$  versus conversion plots for copolymerization of EGDEMA and iBOMA using D7 initiator at 90°C are shown in Figure C-12.



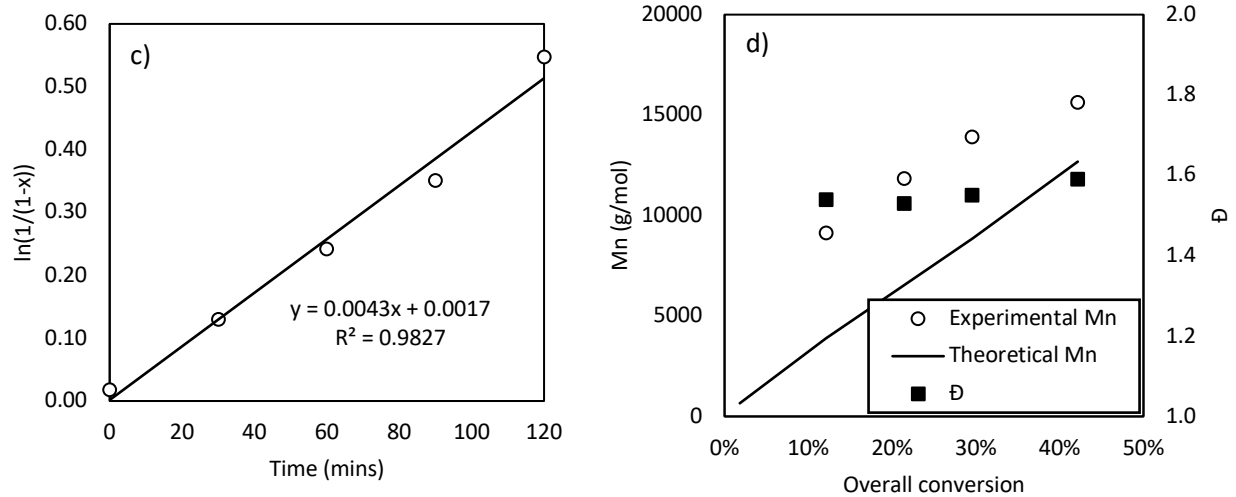


Figure C-12. Kinetic plots for equimolar copolymerization of a) EGiB1 and b)  $M_n$  and  $\bar{D}$  versus conversion for EGiB1, as well as kinetic plots for c) EGiB2 and d)  $M_n$  and  $\bar{D}$  versus conversion for EGiB2.

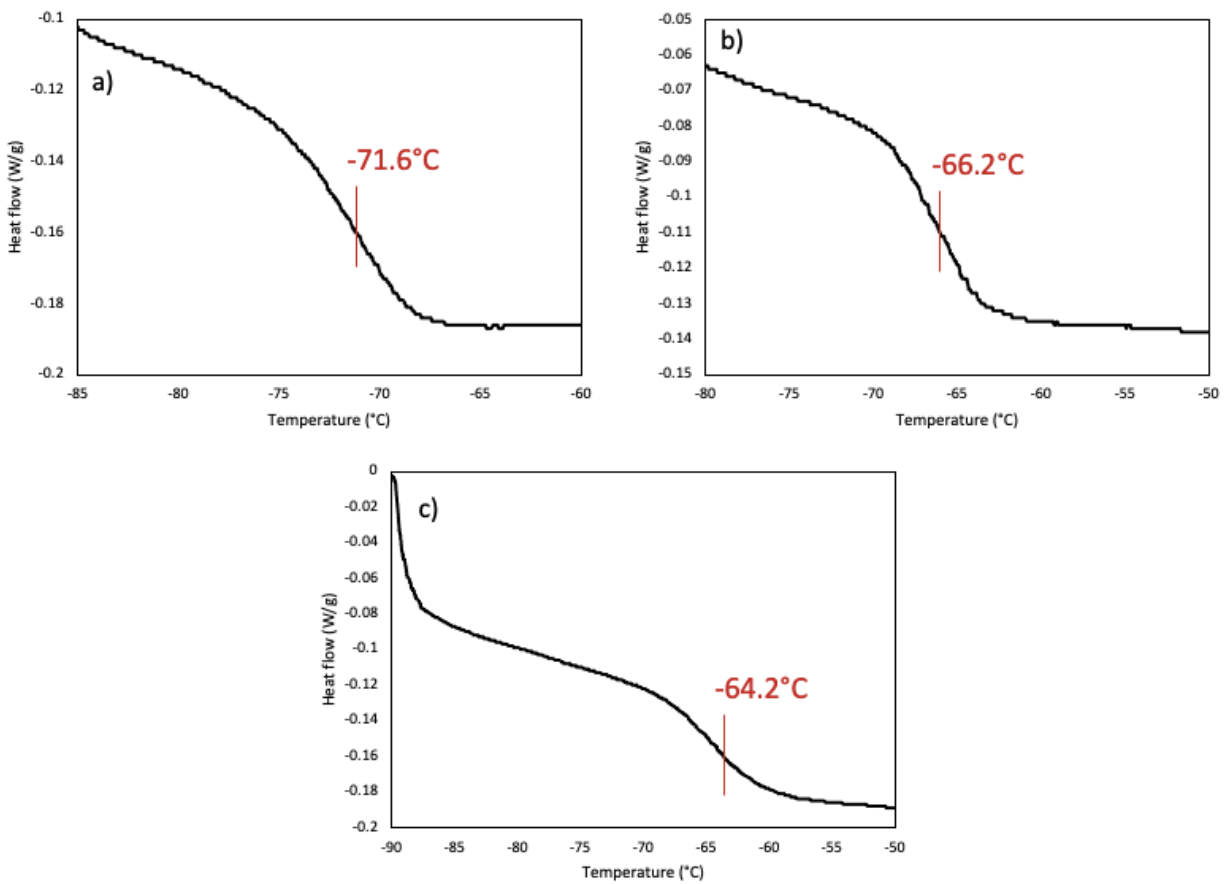


Figure C-13. DSC heat flow vs. temperature plots for a) EG1-Far, b) EG1-Far POSS10, and c) EG1-Far POSS20 block copolymers to determine  $T_g$ .

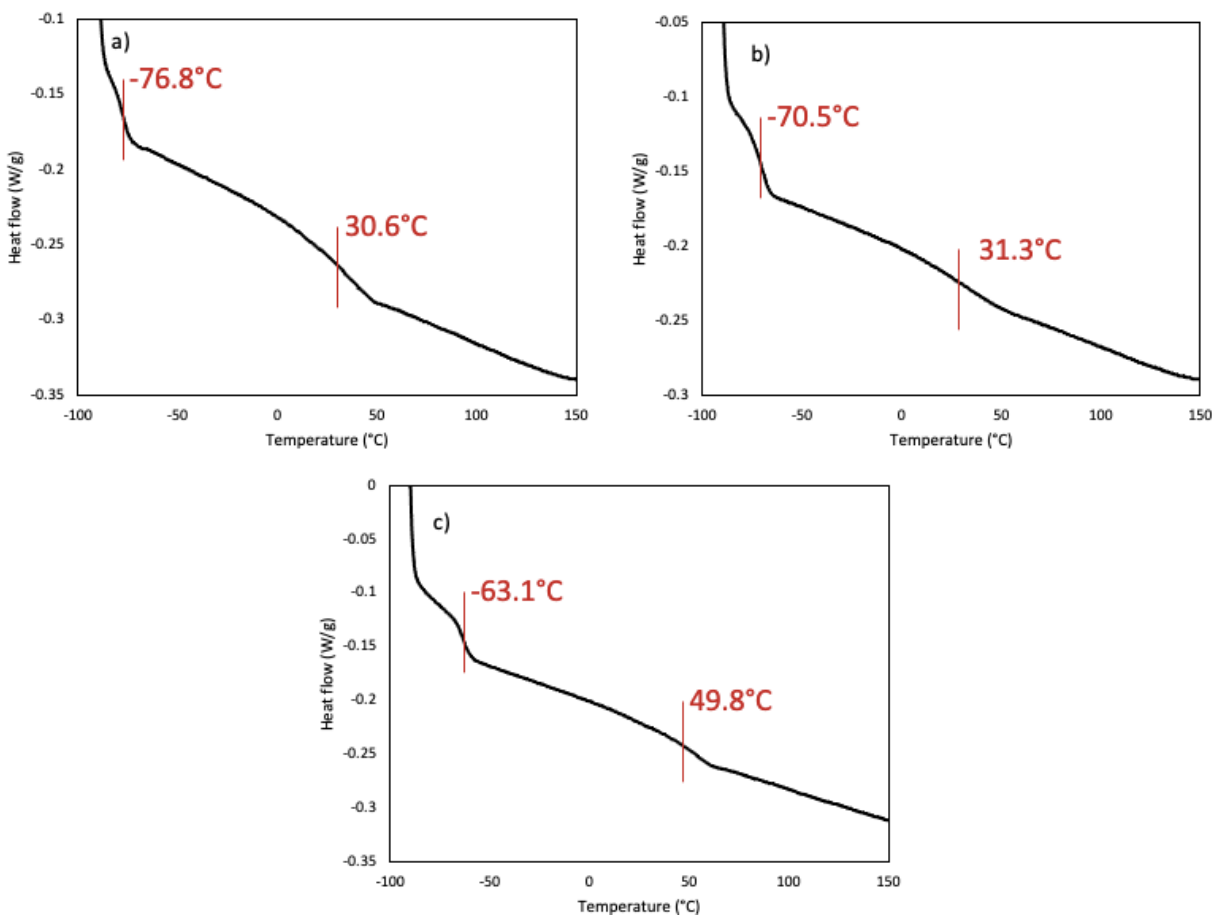


Figure C-14. DSC heat flow vs. temperature plots for a) EG2-Far, b) EG2-Far POSS10, and c) EG2-Far POSS20 block copolymers to determine  $T_g$ .

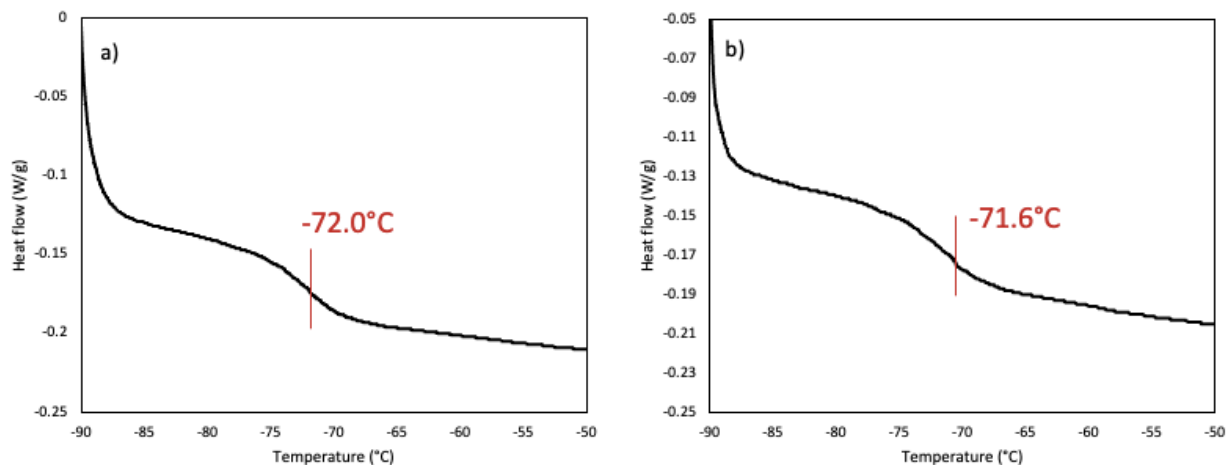


Figure C-15. DSC heat flow vs. temperature plots for a) EGiB1-Far and b) EGiB1-Far POSS10 block copolymers to determine  $T_g$ .

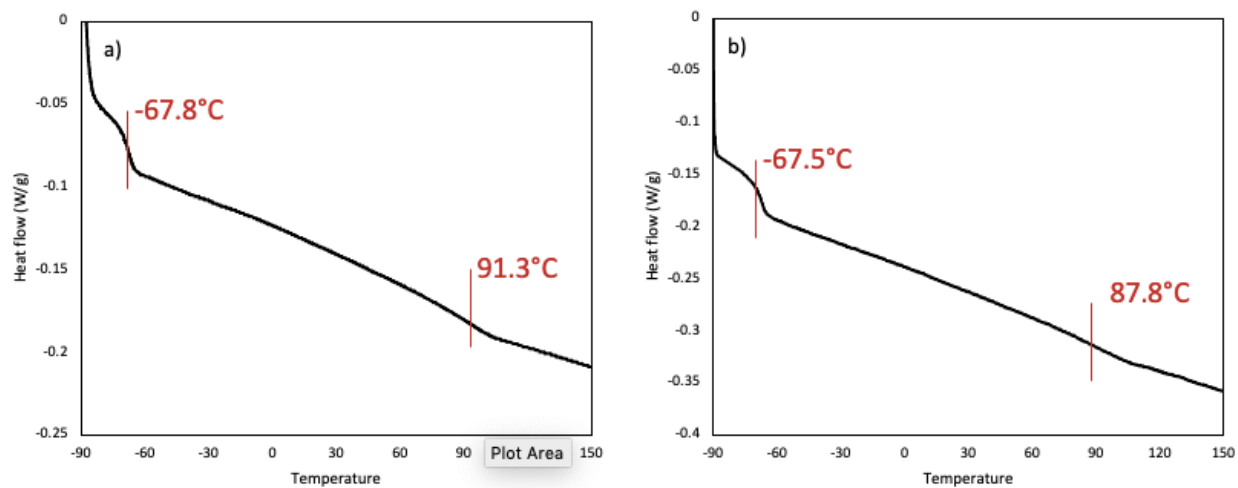


Figure C-16. DSC heat flow vs. temperature plots for a) EGiB2-Far and b) EGiB2-Far POSS10 block copolymers to determine  $T_g$ .

9.4 Appendix D: Supporting information for “Hydrogenation of poly(myrcene) and poly(farnesene) using diimide reduction at ambient pressure”

The conversion of poly(Myrcene) via free radical polymerization after 6 h in bulk is calculated based on the  $^1\text{H}$  NMR spectra shown in Figure D-1. There are 6  $\text{CH}_3$  protons at 1.6 ppm, which represent the methyl groups of Myrcene monomer and poly(Myrcene), and 1  $=\text{CH}-$  proton adjacent to the vinyl carbon at 6.4 ppm, which disappears during polymerization. Therefore, conversion can be calculated as such,

$$X_{\text{Myrcene}} = \left( 1 - \frac{A_{6.4}}{\frac{A_{1.6}}{6}} \right) \times 100\%$$

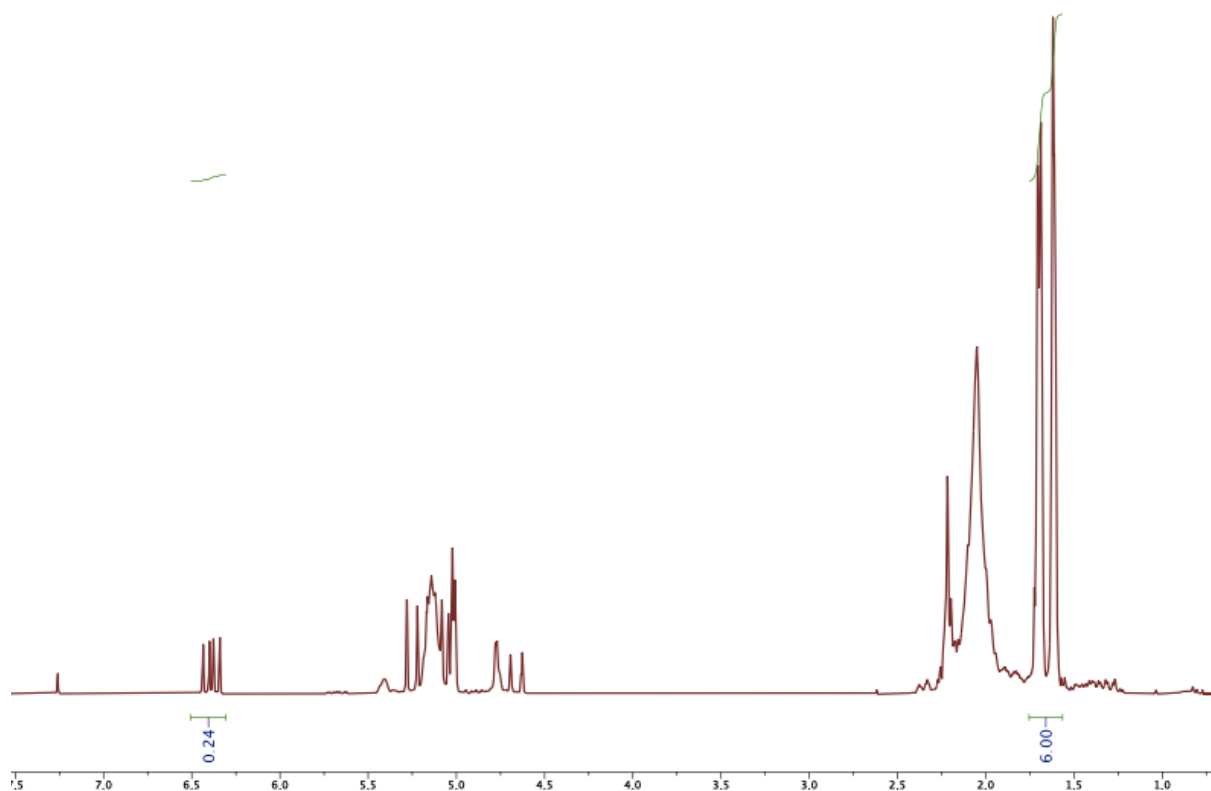


Figure D-1.  $^1\text{H}$  NMR (500 MHz) of poly(Myrcene) in  $\text{CDCl}_3$  by free radical polymerization in bulk after 6 h.

Myr was mostly polymerized by 1,4-addition as characterized by  $^1\text{H}$  NMR shown in Figure D-2. The peak for =CH- proton by 1,4-addition is at 5.2 ppm, for 1,2-addition the peak is at 4.7 ppm and for 3,4-addition the peak is at 5.4 ppm.

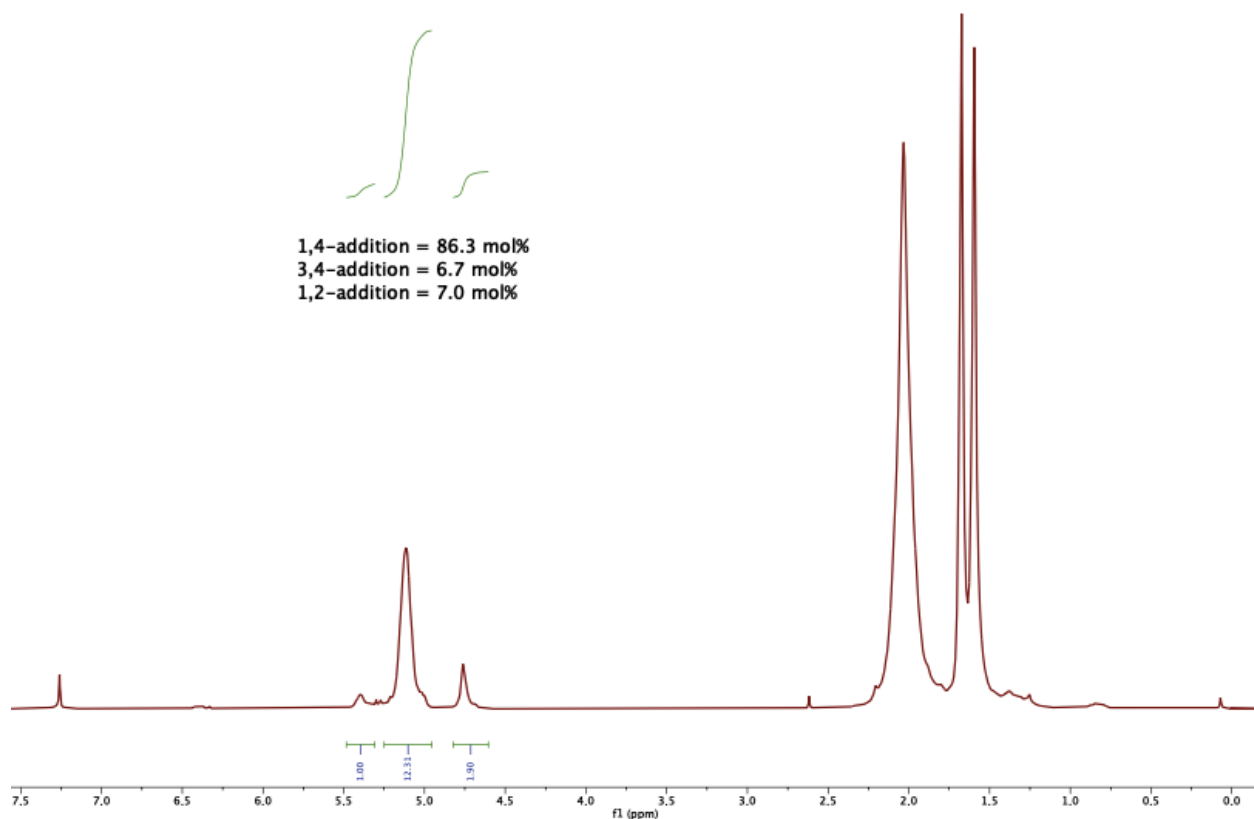


Figure D-2.  $^1\text{H}$  NMR (500 MHz) of poly(Myristic acid) in  $\text{CDCl}_3$  after purification for characterization.

The conversion of Far free radical polymerization in bulk was determined by  $^1\text{H}$  NMR as shown in Figure D-3. There are 9  $\text{CH}_3$  protons at 1.7 ppm that represent the 3 methyl groups of Far and poly(Far), and the =CH- proton adjacent to the vinyl carbon at 6.4 ppm that disappears with polymerization. Therefore, conversion of Far is calculated as such

$$X_{Far} = \left(1 - \frac{A_{0.4}}{A_{1.7}/9}\right) \times 100\%$$

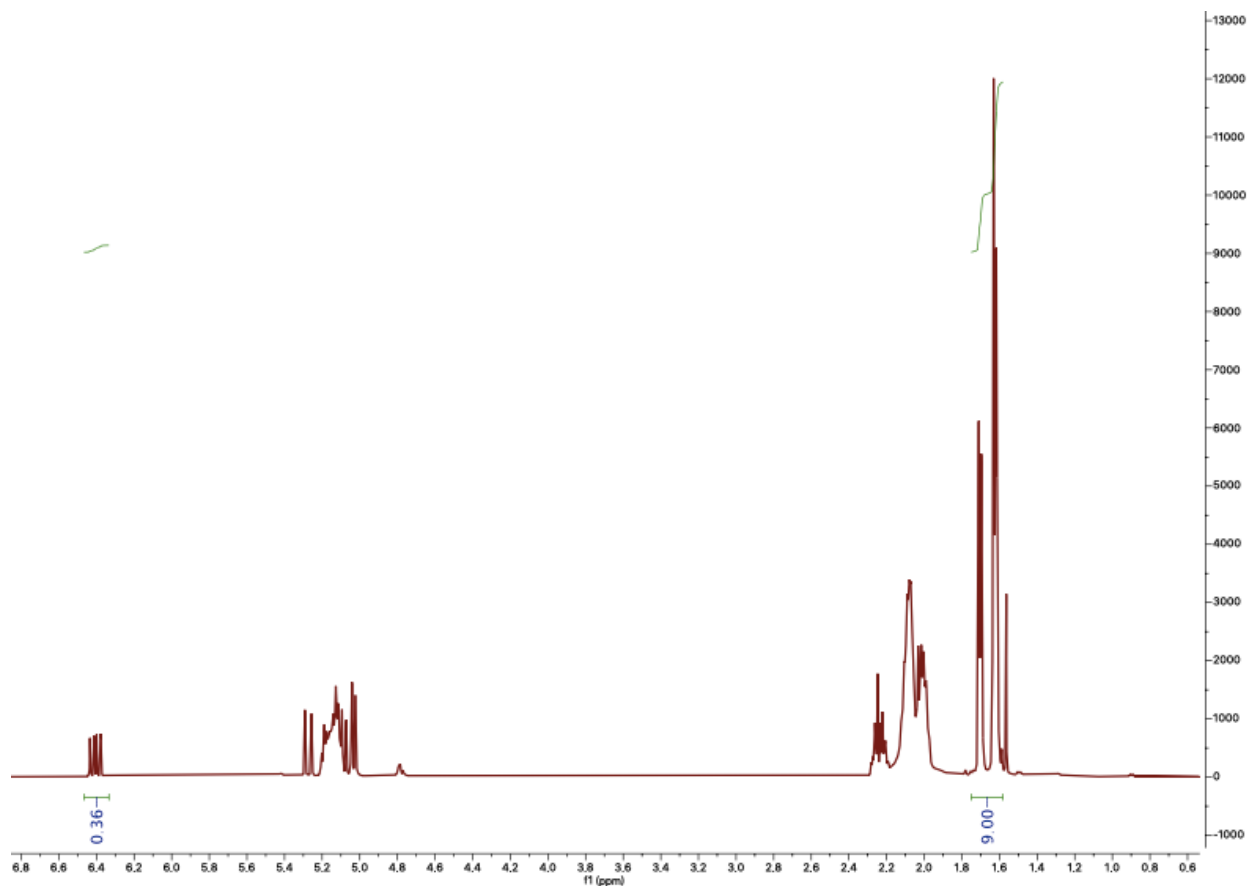


Figure D-3. <sup>1</sup>H NMR (500 MHz) of poly(Far) in CDCl<sub>3</sub> by free radical polymerization in bulk after 2 h.

Far was mostly polymerized by 1,4-addition as characterized by <sup>1</sup>H NMR shown in Figure D-4. The peak for =CH- proton by 1,4-addition is at 5.2 ppm, for 1,2-addition the peak is at 4.8 ppm and for 3,4-addition the peak is at 5.4 ppm. There was some residual monomer (6 mol%) leftover after purification of poly(Far).

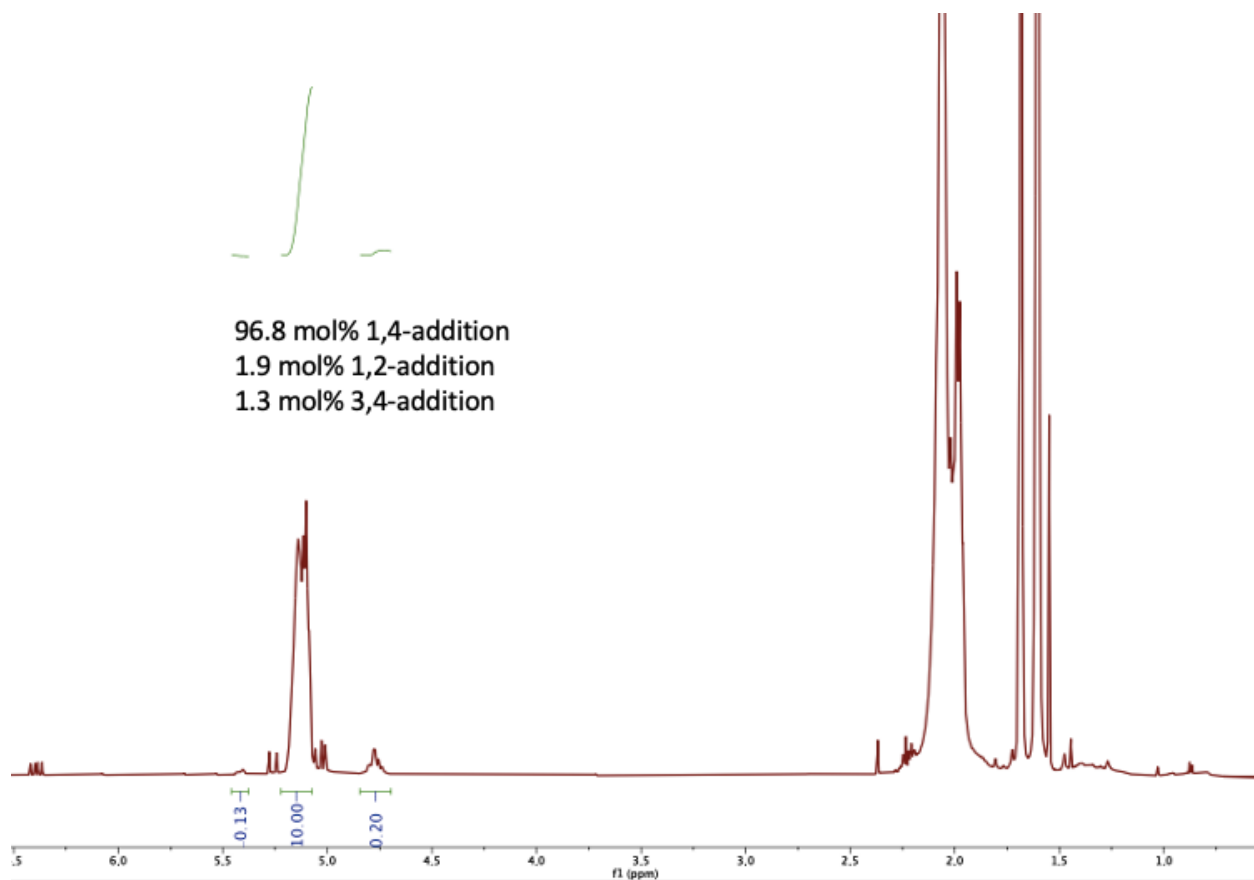


Figure D-4.  $^1\text{H}$  NMR (500 MHz) of poly(Far) in  $\text{CDCl}_3$  after purification for characterization.

The degree of hydrogenation of poly(My) is calculated using  $^1\text{H}$  NMR as well as shown in Figure D-5. The protons (6  $\text{CH}_3$  and  $\text{CH}_2\text{s}$ ) at 0.7 ppm and 1 – 1.6 ppm represent saturated poly(My), where 1,4-addition backbone double bond has been hydrogenated. The doublet at 1.6 ppm represents the 6  $\text{CH}_3$  protons of the unsaturated 1,4-addition backbone double bond, and the peak at 5.1 ppm represents the  $=\text{CH}-$  proton of the pendant branches of poly(My). The hydrogenation of the backbone and pendant double bonds is calculated as such

$$HD_{backbone} = \left( 1 - \frac{A_{1.6}}{A_{1.6} + A_{0.7}} \right) \times 100\%$$

$$HD_{pendant} = \left( 1 - \frac{\frac{A_{5.1}}{2}}{\frac{A_{1.6}}{6} + \frac{A_{0.7}}{6}} \right) \times 100\%$$

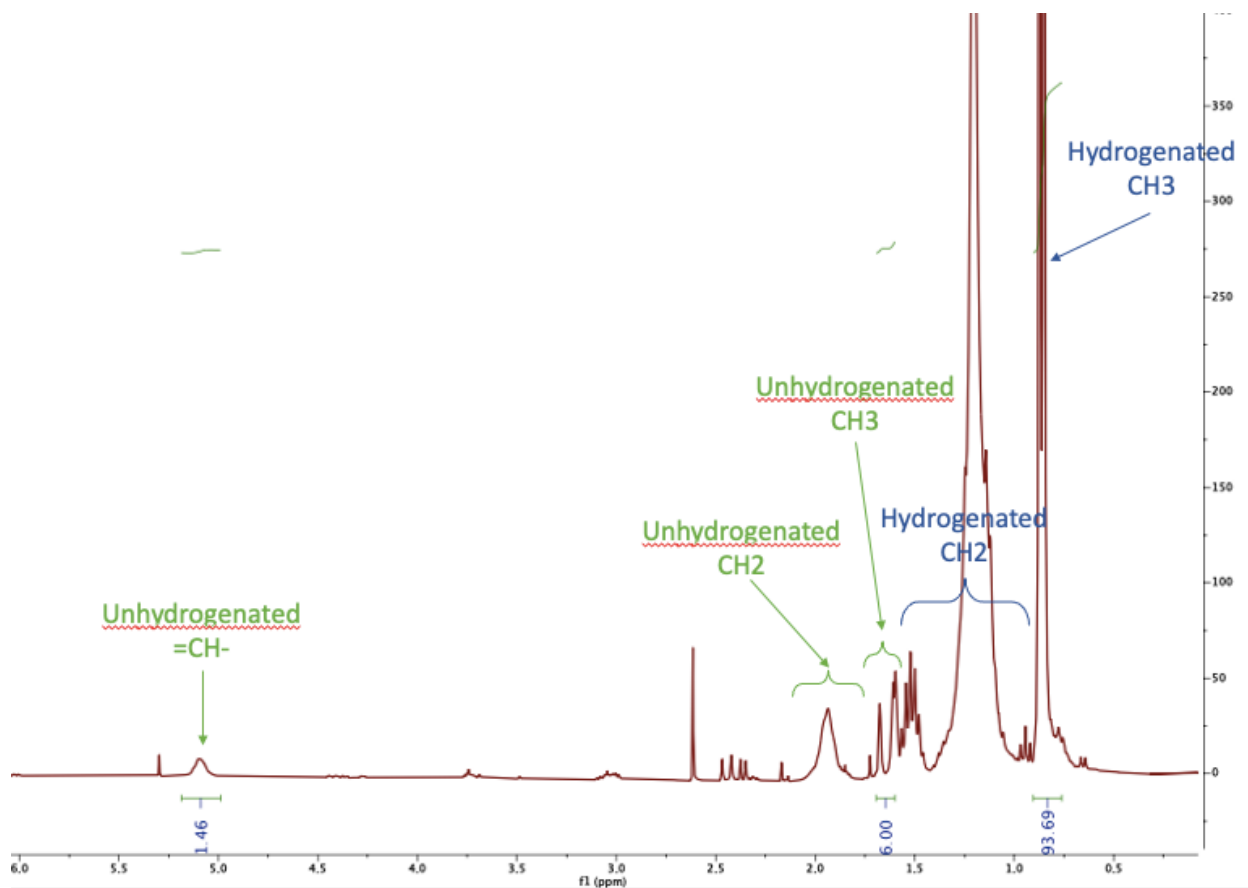


Figure D-5. <sup>1</sup>H NMR (500 MHz) of poly(Myr) in CDCl<sub>3</sub> after 210 min of hydrogenation in semi-batch.

The degree of hydrogenation of poly(Far) is calculated using <sup>1</sup>H NMR as shown in Figure D-6. The protons (9 CH<sub>3</sub> and CH<sub>2</sub>s) at 0.9 ppm and 1 – 1.6 ppm represent saturated poly(Far), where 1,4-addition backbone double bond has been hydrogenated. The doublet at 1.6 ppm represents the 9 CH<sub>3</sub> protons of the unsaturated 1,4-addition backbone double bond, and the peak at 5.1 ppm represents the =CH- proton of the pendant branches of poly(Far). The hydrogenation of the backbone and pendant double bonds is calculated as such

$$HD_{backbone} = \left( 1 - \frac{A_{1.6}}{A_{1.6} + A_{0.9}} \right) \times 100\%$$

$$HD_{pendant} = \left( 1 - \frac{\frac{A_{5.1}}{3}}{\frac{A_{1.6}}{9} + \frac{A_{0.9}}{9}} \right) \times 100\%$$

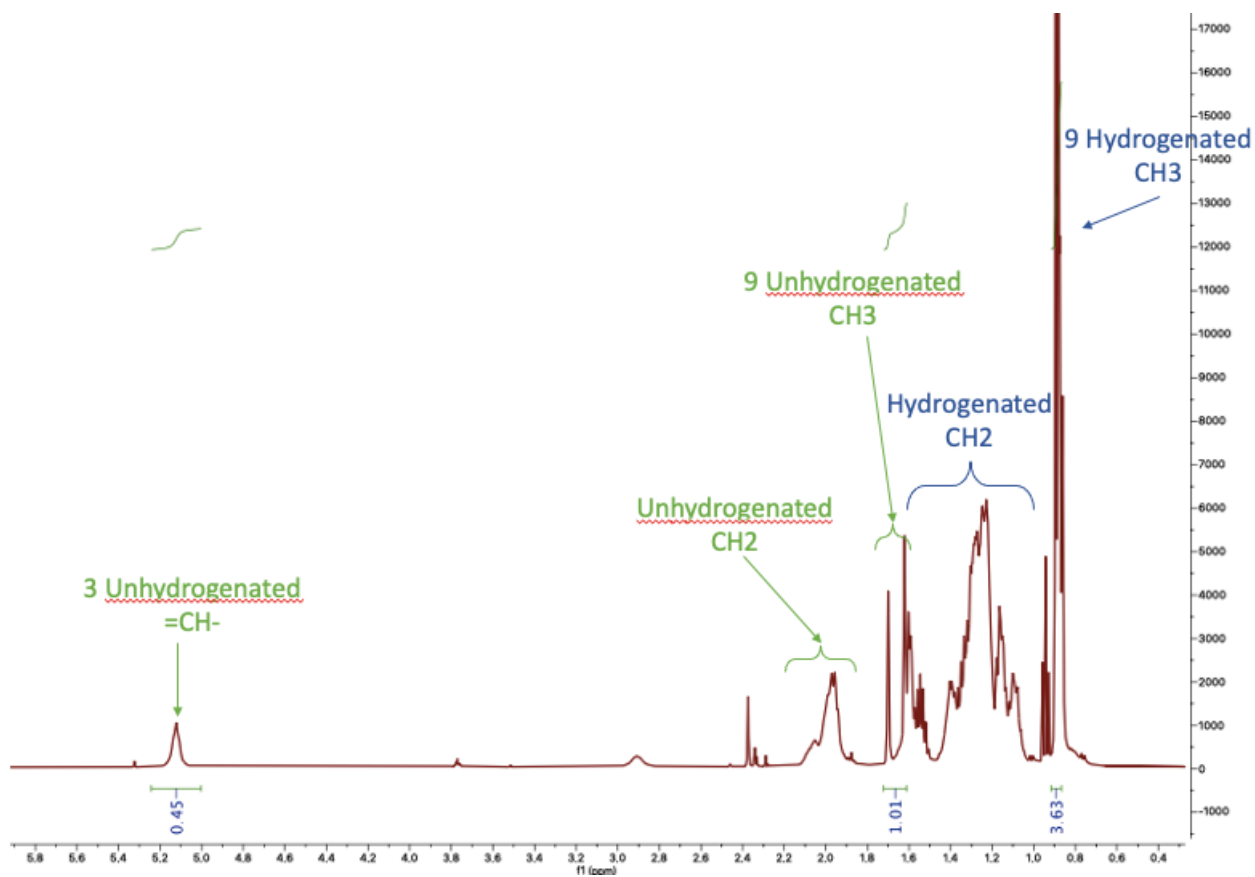


Figure D-6. <sup>1</sup>H NMR (500 MHz) of poly(Far) in CDCl<sub>3</sub> after 240 min of hydrogenation in semi-batch.